frontiers | Research Topics

Perspectives in pharmacological therapy targeting cellular metabolic pathways in respiratory diseases

Edited by
Haiyang Tang, Jie Liu, Na Wang, Peiran Yang
and Dustin Fraidenburg

Published in
Frontiers in Pharmacology

ISSN 1664-8714
ISBN 978-2-8325-3856-2
DOI 10.3389/978-2-8325-3856-2

About Frontiers

Frontiers is more than just an open access publisher of scholarly articles: it is a pioneering approach to the world of academia, radically improving the way scholarly research is managed. The grand vision of Frontiers is a world where all people have an equal opportunity to seek, share and generate knowledge. Frontiers provides immediate and permanent online open access to all its publications, but this alone is not enough to realize our grand goals.

Frontiers journal series

The Frontiers journal series is a multi-tier and interdisciplinary set of open-access, online journals, promising a paradigm shift from the current review, selection and dissemination processes in academic publishing. All Frontiers journals are driven by researchers for researchers; therefore, they constitute a service to the scholarly community. At the same time, the *Frontiers journal series* operates on a revolutionary invention, the tiered publishing system, initially addressing specific communities of scholars, and gradually climbing up to broader public understanding, thus serving the interests of the lay society, too.

Dedication to quality

Each Frontiers article is a landmark of the highest quality, thanks to genuinely collaborative interactions between authors and review editors, who include some of the world's best academicians. Research must be certified by peers before entering a stream of knowledge that may eventually reach the public - and shape society; therefore, Frontiers only applies the most rigorous and unbiased reviews. Frontiers revolutionizes research publishing by freely delivering the most outstanding research, evaluated with no bias from both the academic and social point of view. By applying the most advanced information technologies, Frontiers is catapulting scholarly publishing into a new generation.

What are Frontiers Research Topics?

Frontiers Research Topics are very popular trademarks of the *Frontiers journals series*: they are collections of at least ten articles, all centered on a particular subject. With their unique mix of varied contributions from Original Research to Review Articles, Frontiers Research Topics unify the most influential researchers, the latest key findings and historical advances in a hot research area.

Find out more on how to host your own Frontiers Research Topic or contribute to one as an author by contacting the Frontiers editorial office: frontiersin.org/about/contact

Perspectives in pharmacological therapy targeting cellular metabolic pathways in respiratory diseases

Topic editors

Haiyang Tang — University of Arizona, United States
Jie Liu — Tongji University, China
Na Wang — Tongji University, China
Peiran Yang — Institute of Basic Medical Sciences, Chinese Academy of Medical Sciences and Peking Union Medical College, China
Dustin Fraidenburg — University of Illinois Chicago, United States

Citation

Tang, H., Liu, J., Wang, N., Yang, P., Fraidenburg, D., eds. (2023). *Perspectives in pharmacological therapy targeting cellular metabolic pathways in respiratory diseases*. Lausanne: Frontiers Media SA. doi: 10.3389/978-2-8325-3856-2

Table of contents

frontiers | Frontiers in Pharmacology

TYPE Editorial
PUBLISHED 27 November 2023
DOI 10.3389/fphar.2023.1324586

OPEN ACCESS

EDITED AND REVIEWED BY
Paolo Montuschi,
Catholic University of the Sacred Heart, Italy

*CORRESPONDENCE
Haiyang Tang,
tanghy2008@yahoo.com

RECEIVED 19 October 2023
ACCEPTED 13 November 2023
PUBLISHED 27 November 2023

CITATION
Wang N, Liu J, Yang P, Fraidenburg D and Tang H (2023), Editorial: Perspectives in pharmacological therapy targeting cellular metabolic pathways in respiratory diseases.
Front. Pharmacol. 14:1324586.
doi: 10.3389/fphar.2023.1324586

Editorial: Perspectives in pharmacological therapy targeting cellular metabolic pathways in respiratory diseases

Na Wang[1], Jie Liu[2], Peiran Yang[3], Dustin Fraidenburg[4] and Haiyang Tang[5]*

[1]Department of Pulmonary and Critical Care Medicine, Shanghai East Hospital, Tongji University School of Medicine, Shanghai, China, [2]Key Laboratory of Arrhythmias of the Ministry of Education of China, Department of Cardiovascular Surgery, Research Center for Translational Medicine, Shanghai Heart Failure Research Center, Shanghai East Hospital, Tongji University School of Medicine, Shanghai, China, [3]State Key Laboratory of Respiratory Health and Multimorbidity, Department of Physiology, Institute of Basic Medical Sciences, Chinese Academy of Medical Sciences and School of Basic Medicine, Peking Union Medical College, Beijing, China, [4]Department of Medicine, University of Illinois at Chicago, Chicago, IL, United States, [5]State Key Laboratory of Respiratory Disease, National Clinical Research Center for Respiratory Disease, Guangzhou Institute of Respiratory Health, The First Affiliated Hospital of Guangzhou Medical University, Guangzhou, Guangdong, China

KEYWORDS

respiratory disease, metabolism, metabolic pathway, idiopathic pulmonary fibrosis, acute lung injury, chronic obstructive pulmonary disease, lung infection

Editorial on the Research Topic
Perspectives in pharmacological therapy targeting cellular metabolic pathways in respiratory diseases

Interventions targeting metabolic pathways show promise for innovative therapeutic approaches and disease management. We established a Research Topic, entitled "Perspectives in Pharmacological Therapy Targeting Cellular Metabolic Pathways in Respiratory Diseases" to delve into the most recent advancements in respiratory disease treatment. This Research Topic features contributions from 82 authors with 10 manuscripts and one abstract, along with over 10,000 views and 3,000 article downloads, spanning from basic research to clinical applications. The articles include original research, reviews, bioinformatic analysis, clinical cases, and studies, providing a comprehensive insight on managing various pulmonary diseases, including idiopathic pulmonary fibrosis (IPF), acute lung injury (ALI), lung infections, chronic obstructive pulmonary disease (COPD), pulmonary malignancies, and pulmonary edema.

IPF is a debilitating lung disease characterized by progressive scarring and fibrosis of the lung tissue. Excessive collagen deposition and tissue remodeling are significant hallmarks of IPF (Raghu et al., 2018), both associated with heat shock protein 27 (HSP27) which is a major trigger for epithelial-to-mesenchymal transition (EMT) (Kim et al., 2019). Yoo et al. presented a novel HSP27 inhibitor, NA49, and tested it in radiation and bleomycin-induced pulmonary fibrosis models. NA49 treatment effectively attenuated fibrosis development by hindering NF-κB signaling and EMT. Notably, NA49 caused less DNA damage in human lung epithelial cells compared to previous HSP27 inhibitors. With enhanced pharmacokinetics, treatment with

NA49 stands out as a promising approach in pre-clinical pulmonary fibrosis models. This study presents impressive progress in our pharmacological modulation of HSP27, evolving from antisense oligonucleotides to a new generation of small molecule inhibitors (Wettstein et al., 2013). Regarding the metabolism-immunology interplay in IPF development, Yang et al. performed bioinformatic analysis and differentiated two subtypes with distinct metabolic phenotypes. IPF patients in subtype C1 exhibited less active nucleotide, fatty acid, and amino acid metabolism, correlating with a poorer prognosis than C2. C1 also exhibited increased $CD8^+$ T cell, macrophage, and neutrophil infiltration, alongside upregulated cytokines, chemokines, and TGF-β levels. A diagnostic model comprising nine genes was established. Compound analysis suggested adenosine receptor-targeting meds for C1 and glucose-lactic acid-targeting meds for C2, paving the way for tailored IPF treatments.

Mitochondria, a pivotal cellular organelle, governs numerous metabolic pathways including carbon, lipid and amino acids metabolism. Proper mitochondrial function is imperative for generating essential ATP via oxidative phosphorylation (Sharma et al., 2021), while dysfunctional mitochondria may lead to compromised ATP production and surges in reactive oxygen species (ROS) generation, resulting in overactivated mitophagy (Ornatowski et al., 2020). Tian et al. reported that caffeine effectively attenuates high-altitude pulmonary edema (HAPE) and improves lung function in HAPE rats by enhancing mitochondrial oxidative phosphorylation (OXPHOS) and mitochondrial quality control in AT1 cells. Furthermore, caffeine boosted electron transport chain (ETC.) activity, increasing ATP production and mitochondrial bioenergetics. It also promoted glycolytic enzymes, offering an alternative energy source under hypoxia. Caffeine further enhanced mitophagy via the PINK1/Parkin pathway, facilitating damaged mitochondria disposal. Together, these findings underscore caffeine's potential in alleviating HAPE through the optimization of mitochondrial function and quality control.

Endoplasmic reticulum (ER) stress interacts with metabolic processes through the unfolded protein response (UPR), which monitors protein folding within the ER. The UPR modulates various metabolic pathways, including lipid metabolism, energy homeostasis, inflammation, and cell differentiation (Hetz, 2012). Chang et al. presented the effects of compound B6 on cigarette smoke-induced inflammation and injury in bronchial epithelial cells. The study revealed that B6 mitigated ER stress and inflammation by reducing the expression of BIP, ATF4, and CHOP, suggesting B6 as a potential therapeutic option for COPD-related inflammation and injury. Lou et al. reported Urolithin A (UA) as a prospective treatment for acute lung injury (ALI) induced by lipopolysaccharide in mice. UA exhibited efficacy by enhancing the Keap1-Nrf2/HO-1 pathway, reducing oxidative stress, and ameliorating lung damage, suggesting UA as a potent anti-inflammatory and antioxidant agent in ALI treatment.

Pulmonary infections pose a substantial global health concern, necessitating timely pathogen identification and antibiotic treatment (Magill et al., 2014). Conventional diagnostic approaches often fall short, particularly in the face of multiple infections. In contrast, metagenomic next-generation sequencing (mNGS) has emerged as a commendable leap in clinical microbiology. Han et al. evaluated mNGS for diagnosing pulmonary infections involved 101 participants. The results showed that both Illumina and BGI mNGS platforms outperformed conventional methods in sensitivity, with negligible differences between each platform. This implies that mNGS can enhance pulmonary infection diagnosis by providing earlier pathogen identification, honing treatment precision, and enriching epidemiological insights. The rising incidence and mortality of fungal infections, including pulmonary mycosis, underscore the urgency for the demand of precise diagnosis and efficient treatment (Maitre et al., 2021). Bronchoscopic instillation has been hailed as a novel therapeutic approach for pulmonary mycosis, offering precise local targeting of lesions. However, there has been a lack corroborated clinical data, specific indicators, or parameters gauging the efficacy of this strategy for patients (Lang et al., 2020). Yang et al. conducted a study, involving 80 patients, examined bronchoscopic instillation of amphotericin B. The results showed 72.5% of patients experienced imaging improvements, 77.5% manifested imaging or localized containment of mycosis improvements, and 95% exhibited imaging improvements and containment or fell within the immunotherapy timeframe. This approach demonstrated a commendable success rate coupled with minimal adverse events, spotlighting its potential, particularly for systemic antifungal non-responders or those unable to tolerate it.

Non-small-cell lung cancer (NSCLC) is one of the most common cancers worldwide and causes a vast number of cancer-related deaths (Siegel et al., 2022). SMARCA4, a tumor suppressor gene, is reportedly mutated in approximately 10% of NSCLC patients and associated with poor prognosis (Hodges et al., 2018). While immune checkpoint inhibitors have been used to treat NSCLC, immune-related adverse events can be challenging to manage and may limit the use of these therapeutic agents (Atchley et al., 2021). In their report, Deng et al. shared their experiences regarding a patient with SMARCA4-mutant NSCLC, who developed immune-related pneumonitis during anti-PD-1 treatment and chemotherapy. Switching therapies to corticosteroids and nintedanib, an anti-fibrotic multi-tyrosine kinase inhibitor, led to the patient's recovery and allowed chemotherapy to resume. This study illustrates an interesting strategy of using an anti-fibrotic agent to manage immune-related adverse events and encourages further research on the applications of nintedanib with immune checkpoint inhibitors in NSCLC.

In summary, this Research Topic provides an exhaustive insight into the current state of research related to the diagnosis and management of respiratory diseases. It highlights pioneering therapeutic targets and the emergence of novel pharmaceutical agents in the field. This Research Topic of studies underscores not only the depth of existing knowledge but also illuminates pathways toward new therapeutic strategies. Our aspiration is to catalyze further researches, particularly in translational applications, fostering the evolution of more refined and efficacious strategies to improve patient outcomes in clinical practice.

Author contributions

NW: Writing–original draft, Writing–review and editing. JL: Writing–original draft, Writing–review and editing. PY: Writing–original draft, Writing–review and editing. DF: Writing–review and editing. HT: Supervision, Writing–original draft, Writing–review and editing.

Funding

The author(s) declare that financial support was received for the research, authorship, and/or publication of this article. This work was supported in parts by National Key Research and Development Program of China (2019YFE0119400), Sino German Center Mobility Program (M-0680), Shanghai Rising-Star Program (20QA1408100), Research program of Shenzhen Science and Technology Innovation Committee (JCYJ20220530163601003), the Non-Profit Central Research Institute Fund of the Chinese Academy of Medical Sciences (2021RC310016 to PY), the Chinese Academy of Medical Sciences Innovation Fund for Medical Sciences (2021-I2M-1-001 to PY, and 2022-I2M-JB-003 to PY), and Natural Science Foundation of China (82000055, 82170057, 82270260, 81970234, and 82200060).

Conflict of interest

The authors declare that the research was conducted in the absence of any commercial or financial relationships that could be construed as a potential conflict of interest.

The author(s) declared that they were an editorial board member of Frontiers, at the time of submission. This had no impact on the peer review process and the final decision.

Publisher's note

References

Atchley, W. T., Alvarez, C., Saxena-Beem, S., Schwartz, T. A., Ishizawar, R. C., Patel, K. P., et al. (2021). Immune checkpoint inhibitor-related pneumonitis in lung cancer: real-world incidence, risk factors, and management practices across six health care centers in North Carolina. *Chest* 160 (2), 731–742. doi:10.1016/j.chest.2021.02.032

Hetz, C. (2012). The unfolded protein response: controlling cell fate decisions under ER stress and beyond. *Nat. Rev. Mol. Cell Biol.* 13 (2), 89–102. doi:10.1038/nrm3270

Hodges, H. C., Stanton, B. Z., Cermakova, K., Chang, C. Y., Miller, E. L., Kirkland, J. G., et al. (2018). Dominant-negative SMARCA4 mutants alter the accessibility landscape of tissue-unrestricted enhancers. *Nat. Struct. Mol. Biol.* 25 (1), 61–72. doi:10.1038/s41594-017-0007-3

Kim, J. Y., Jeon, S., Yoo, Y. J., Jin, H., Won, H. Y., Yoon, K., et al. (2019). The hsp27-mediated IkBα-nfκb signaling Axis promotes radiation-induced lung fibrosis. *Clin. cancer Res. official J. Am. Assoc. Cancer Res.* 25 (17), 5364–5375. doi:10.1158/1078-0432.CCR-18-3900

Lang, M., Lang, A. L., Chauhan, N., and Gill, A. (2020). Non-surgical treatment options for pulmonary aspergilloma. *Respir. Med.* 164, 105903. doi:10.1016/j.rmed.2020.105903

Maitre, T., Cottenet, J., Godet, C., Roussot, A., Abdoul Carime, N., Ok, V., et al. (2021). Chronic pulmonary aspergillosis: prevalence, favouring pulmonary diseases and prognosis. *Eur. Respir. J.* 58 (2), 2003345. doi:10.1183/13993003.03345-2020

Magill, S. S., Edwards, J. R., Bamberg, W., Beldavs, Z. G., Dumyati, G., Kainer, M. A., et al. (2014). Multistate point-prevalence survey of health care-associated infections. *N. Engl. J. Med.* 370 (13), 1198–208. doi:10.1056/NEJMoa1306801

Ornatowski, W., Lu, Q., Yegambaram, M., Garcia, A. E., Zemskov, E. A., Maltepe, E., et al. (2020). Complex interplay between autophagy and oxidative stress in the development of pulmonary disease. *Redox Biol.* 36, 101679. doi:10.1016/j.redox.2020.101679

Raghu, G., Remy-Jardin, M., Myers, J. L., Richeldi, L., Ryerson, C. J., Lederer, D. J., et al. (2018). Diagnosis of idiopathic pulmonary fibrosis. An official ATS/ERS/JRS/ALAT clinical practice guideline. *Am. J. Respir. Crit. care Med.* 198 (5), e44–e68. doi:10.1164/rccm.201807-1255ST

Sharma, S., Singh, Y., Sandhir, R., Singh, S., Ganju, L., Kumar, B., et al. (2021). Mitochondrial DNA mutations contribute to high altitude pulmonary edema via increased oxidative stress and metabolic reprogramming during hypobaric hypoxia. *Biochimica biophysica acta Bioenergetics* 1862 (8), 148431. doi:10.1016/j.bbabio.2021.148431

Siegel, R. L., Miller, K. D., Fuchs, H. E., and Jemal, A. (2022). Cancer statistics, 2022. *CA a cancer J. Clin.* 72 (1), 7–33. doi:10.3322/caac.21708

Wettstein, G., Bellaye, P. S., Kolb, M., Hammann, A., Crestani, B., Soler, P., et al. (2013). Inhibition of HSP27 blocks fibrosis development and EMT features by promoting Snail degradation. *FASEB J. official Publ. Fed. Am. Soc. Exp. Biol.* 27 (4), 1549–1560. doi:10.1096/fj.12-220053

frontiers | Frontiers in Pharmacology

TYPE Original Research
PUBLISHED 09 March 2023
DOI 10.3389/fphar.2023.1067402

OPEN ACCESS

EDITED BY
Dustin Fraidenburg,
University of Illinois at Chicago,
United States

REVIEWED BY
Patrick Belvitch,
University of Illinois at Chicago,
United States
Sun Young Park,
Pusan National University, Republic of Korea

*CORRESPONDENCE
Chang Cai,
592396080@qq.com

†These authors have contributed equally to this work

SPECIALTY SECTION
This article was submitted to Respiratory Pharmacology, a section of the journal Frontiers in Pharmacology

RECEIVED 11 October 2022
ACCEPTED 08 February 2023
PUBLISHED 09 March 2023

CITATION
Lou L, Wang M, He J, Yang S, Meng F, Wang S, Jin X, Cai J and Cai C (2023), Urolithin A (UA) attenuates ferroptosis in LPS-induced acute lung injury in mice by upregulating Keap1-Nrf2/HO-1 signaling pathway.
Front. Pharmacol. 14:1067402.
doi: 10.3389/fphar.2023.1067402

Urolithin A (UA) attenuates ferroptosis in LPS-induced acute lung injury in mice by upregulating Keap1-Nrf2/HO-1 signaling pathway

Lejing Lou[1†], Min Wang[1†], Jingjing He[1], Song Yang[1], Fanxi Meng[2], Shijia Wang[1], Xiao Jin[1], Jihao Cai[3] and Chang Cai[1*]

[1]Department of Respiratory and Critical Care Medicine, The First Affiliated Hospital, Wenzhou Medical University, Wenzhou, China, [2]School of Pharmaceutical Science, Wenzhou Medical University, Wenzhou, China, [3]Renji College of Wenzhou Medical University, Wenzhou, China

Acute lung injury (ALI) is a life-threatening disease with high incidence and mortality rates. Urolithin A (UA) is a pomegranate intestinal flora metabolite with anti-inflammatory, antioxidant, and anti-aging properties. Ferroptosis is a critical factor in lipopolysaccharide (LPS)-induced acute lung injury (ALI). However, the link between UA and ferroptosis is unknown. The purpose of this research was to look into the role of UA in regulating LPS-induced ferroptosis in ALI. The current study used LPS to injure two models, one BEAS-2B cell injury model and one ALI mouse model. UA effectively alleviated LPS-induced ALI compared to the LPS group by lowering *in vivo* lung wet/dry weight ratio, reactive oxygen species, and malondialdehyde production, as well as superoxide dismutase, catalase, and glutathione depletion. Furthermore, by increasing GPX4 and SLC7A11 expression and decreasing Fe^{2+} levels, lung histopathological damage, inflammatory cytokine secretion, and ferroptosis levels can be significantly reduced. The Keap1-Nrf2/HO-1 pathway was upregulated by UA, which inhibited LPS-induced ALI and ferroptosis. ML385 inhibited UA's protective effect against LPS-induced ALI. These findings suggested that UA could be a novel potential therapeutic target for ALI.

KEYWORDS

urolithin a, Nrf2, ferroptosis, acute lung injury, LPS

Introduction

The severe respiratory disorder known as acute lung injury (ALI) is characterized by uncontrollable pulmonary edema, oxidative stress (OS), and infiltration of inflammatory cells and has a high mortality rate (Fan et al., 2018). The pathophysiology and pathogenesis of ALI are still not fully elucidated. As ALI is aggravated, acute respiratory distress syndrome (ARDS) may develop (Ware and Matthay, 2000). Currently, there is no effective treatment for ALI that can significantly raise life expectancy and reduce mortality (Beitler et al., 2022; Yaqub et al., 2022). Therefore, uncovering additional information about the pathophysiological and pathogenic mechanisms of ALI and developing efficient therapeutic agents are of great significance.

The type of programmed cell death that is iron-dependent and distinct from apoptosis, which exhibits the features of reactive oxygen species (ROS) accumulation, is called ferroptosis (Dixon et al., 2012). Ferroptosis differs from other types of cell death in terms of both mechanism and phenotype (Xie et al., 2016). Recently, ferroptosis has significantly impacted the frequency of ALI (Liu et al., 2020; Xu et al., 2020; Liu et al., 2021). The levels of ferroptosis markers GPX4 and SLC7A11 significantly decreased while free iron content within bronchial epithelial cells (BECs) in ALI mice increased in the lipopolysaccharide (LPS)-induced ALI mouse model (Liu et al., 2020). However, lung injury was clearly reduced in mice treated with ferroptosis inhibitor (ferrostatin-1), demonstrating the crucial function of ferroptosis in the development and progression of LPS-mediated ALI (Liu et al., 2020). The apoptosis of alveolar epithelial cells (AEC) plays a key role in the progression of ALI (Liu et al., 2022). According to Wang et al. (Wang et al., 2022), the AU-rich element (ARE)-binding factor 1 (AUF1) was found to alleviate cecum ligation and puncture (CLP) -induced ALI by inhibiting alveolar epithelial ferroptosis. Therefore, inhibition of ferroptosis of AECs might serve as the crucial anti-ALI therapeutic target. Ferroptosis has been confirmed as a therapeutic target for acute lung injury in many animal or cellular models of ALI, but the exact mechanisms have not been fully elucidated (Yin et al., 2021).

NRF2 is a crucial regulator of ferroptosis and lipid peroxidation that transcriptionally regulates diverse critical components in the anti-ferroptotic pathway (Dodson et al., 2019). One recent study found that Nrf2 regulates HO-1 and SLC7A11 to suppress ferroptosis, which improved the effect of gut ischemia-reperfusion (IR)-induced ALI (Dong et al., 2020). Qiu and colleagues reported that Nrf2 prevents ALI caused by seawater drowning by inhibiting ferroptosis (Dong et al., 2020). Li and colleagues also reported that panaxydol suppressed ferroptosis in LPS-mediated ALI *via* KEAP1-NRF2/HO-1 pathway (Li et al., 2021). According to Li and colleagues, obacunone promoted Nrf2-mediated antioxidation, reducing ferroptosis in the LPS-mediated ALI (Li et al., 2022). The novel strategy to treat ALI is possible because ferroptosis promotes ALI development while activating Nrf2 can suppress ferroptosis. Therefore, it is essential to investigate the role of Nrf2 activation in ALI-induced ferroptosis and develop inhibitory therapeutic agents.

One of the natural metabolites of ellagitannins and ellagic acid (Cerda et al., 2005), which are abundant in pomegranates, strawberries, and other nuts, is Urolithin A (UA), which is derived from the gut microbiome (D'Amico et al., 2021). Prior research has revealed that UA has different pharmacological properties, including antioxidation (Casedas et al., 2020), anti-inflammation (Larrosa et al., 2010; Singh et al., 2019), neuroprotection (Y. L. Chen et al., 2021), and improved muscle function (Luan et al., 2021). However, it has been unclear what role UA plays in acute lung injury. Recent studies have shown that UA can reduce acetaminophen-mediated liver necrosis and OS by the activation of the Nrf2/ARE pathway (Gao et al., 2022). Through the p62-Keap1-Nrf2 pathway, UA reduced acute kidney injury (AKI) resulting from renal ischemia reperfusion (Zhang et al., 2022). Therefore, it has been hypothesized that UA can ameliorate LPS-mediated ALI by promoting Nrf2-mediated antioxidation.

In this study, we found that UA effectively reduced OS and inflammatory injury caused by ALI. Additionally, UA suppressed ferroptosis and ROS generation caused by LPS *in vitro* and *in vivo*. Our findings showed that UA activated Nrf2 to suppress LPS-mediated inflammation and ferroptosis. Our study also demonstrated that UA is effective in treating ALI and explored the mechanism of inhibiting the effect of ALI-induced ferroptosis.

Materials and methods

Reagents and antibodies

Urolithin A (UA, ≥97% purity) was provided by Sigma-Aldrich (St Louis, MO, United States). ML385 and Erastin were provided by MedChem Express (Monmouth Junction, NJ, United States). Lipopolysaccharides (LPS) were provided by Sigma-Aldrich (St Louis, MO, United States). The anti-Nrf2, anti-GPX4, anti-HO-1, anti-SLC7A11, and anti-NQO1 primary antibodies were provided by Proteintech Group (Wuhan, China). Lamin B and β-actin antibodies were provided by Cell Signaling Technologies (Danvers, MA, United States). 4-HNE used in immunohistochemical (IHC) staining was provided by Abcam (Cambridge, United Kingdom). Reagents for cell culture were provided by Gibco (Grand Island, NY). The Alexa Fluor®488-labeled Goat Anti-Rabbit IgG secondary antibody (H + L), 4′, 6-diamidino-2-phenylindole (DAPI), and cell live/dead staining kits were provided by Yeasen Bio. Inc., (Shanghai, China).

Cell culture and treatment

A human bronchial epithelial cell line BEAS-2B (Procell, Wuhan, China) was cultured in RPMI-1640 containing 1% antibiotics and 10% FBS at 37°C and 5% CO_2. The media was changed every 2-day. At ~ 80%–90% confluence, cells were passaged. In addition, LPS (10ug/mL) treatment of BEAS-2B cells can effectively cause cell damage (J. Li et al., 2022).

Cell viability test

BEAS-2B cells (5×10^3/well) were seeded in 96-well plates and incubated in a 100 μL medium overnight to detect the cytotoxic effect of UA. After that, UA at different concentrations (0, 2.5, 5, 7.5, 1 0, 20, and 40 μM) were used to treat the medium. CCK-8 reagent (10 μL) was added to all the wells after 24/48 h, followed by 1.5 h incubation in the dark. The microplate reader was used to measure the absorbance (OD) at 450 nm.

Animal's model

This study obtained the 8–10-week-old wild-type (WT) male C57BL/6 mice (20–24 g) from the Animal Center of the Chinese Academy of Sciences Shanghai, raised them under SPF-condition, and used them after 1 week of acclimatization. The Animal Ethics Community of the First Affiliated Hospital of Wenzhou Medical

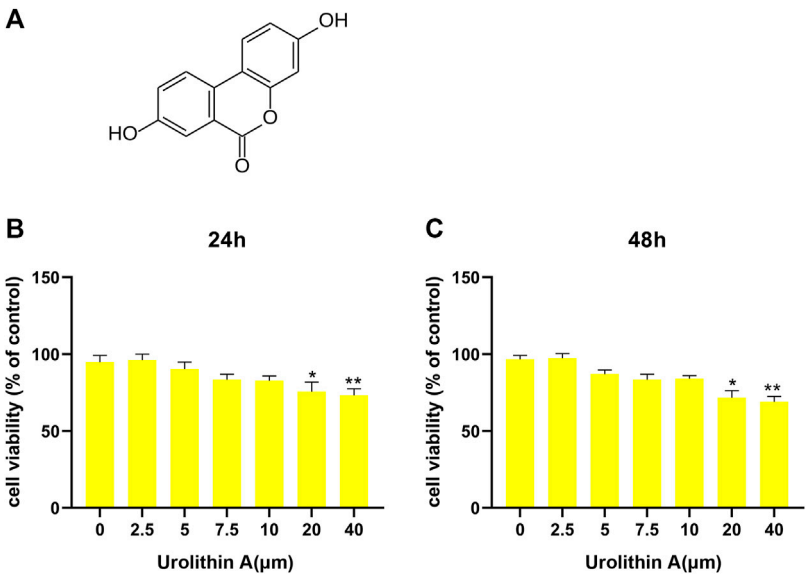

FIGURE 1
Effects of UA treatment on the viability of BEAS-2B cell. **(A)** The molecular formula of Urolithin A (UA). **(B,C)** CCK-8 results of BEAS-2B cells after 24/48 h UA treatments at diverse doses. Results were Shown as mean ± SD. *$p < 0.05$, **$p < 0.01$ in comparison to the control group.

University approved each animal procedure. The mice were randomly divided into five groups: Control, LPS, LPS + UA, LPS + UA + Erastin, and LPS + UA + ML385 groups. Dimethyl sulfoxide (DMSO) was used to dissolve Urolithin A and ML385. ML385 was injected intraperitoneally 30 min before the LPS challenge. Mice were anesthetized and intratracheally injected with 10 mg/kg LPS to induce the LPS-induced ALI model; the same volume of PBS was injected into control mice, while mice of the LPS + UA group were exposed to intraperitoneal injection of 50 mg/kg UA after LPS (10 mg/kg) challenge. The ferroptosis agonist Erastin (15 mg/kg) was mixed with 5% dimethyl sulfoxide (DMSO) and administrated intraperitoneal to mice 1 h before UA administration. Before LPS treatment, 30 mg/kg ML385 was administered to the LPS + UA + ML385 group, followed by UA. Afterward, each mouse was placed in a perpendicular position, followed by slow shaking for a 1-min period to ensure the even distribution of LPS or PBS between bilateral lungs. Each mouse was sacrificed after 24 h of LPS treatment. Subsequently, lung tissues and bronchoalveolar lavage fluid (BALF) were collected.

Western-blot (WB) assay

Cells were lysed in RIPA buffer containing 1% PMSF, and total cellular protein was extracted. In brief, cells were lysed with lysate for a 15-min on ice, followed by 30-min ultracentrifugation at 12,000 rpm at 4 C to obtain cellular protein. The protein content was then detected using the BCA assay kit (Beyotime, Shanghai, China). Later, proteins (40 ng) were separated using AGE, followed by transfer onto the PVDF membrane (Bio-Rad, California, United States). After that, the membrane was blocked for a 1-h with 5% defatted milk, rinsed thrice with TBST (Tris-buffered saline containing Tween-20), cut, and incubated with different primary antibodies overnight at 4°C. After three washes with TBST. The membranes were incubated with a secondary antibody for 1 h at room temperature. Finally, membranes were rinsed three times with TBST before using Chemi DocXRS + imaging system (Bio-Rad) to detect protein blots using the super-sensitive ECL chemiluminescence kit. For quantification, ImageJ software was used.

BALF cell counting, protein concentration, and pro-inflammatory cytokines

The trachea was exposed after the thoracic cavity and neck were opened after the mice were executed. Tracheal intubation was performed, and 1 mL PBS was instilled into the lungs before being aspirated three times with a catheter-connected syringe. BALF was centrifuged for 4 min at 3,000°C at 10 rpm, and the cell precipitate and supernatant were collected separately. After resuspending the cell precipitate in PBS, the total cells were counted using a hematocrit counter. The BCA protein assay kit (Beyotime, Shanghai, China) was used to measure protein contents in BALF according to the manufacturer's instructions. The pro-inflammatory factors TNF-α, IL-1β, and IL-6 were also measured using ELISA kits (Beyotime, Shanghai, China).

Lung wet/dry (W/D) ratio

The whole lung tissue was dissected and washed with PBS solution; after that lung surface was dried using absorbent paper, followed by immediate weighing to obtain wet weight. Afterward, samples were baked in an oven at 55°C for a 48-h before being

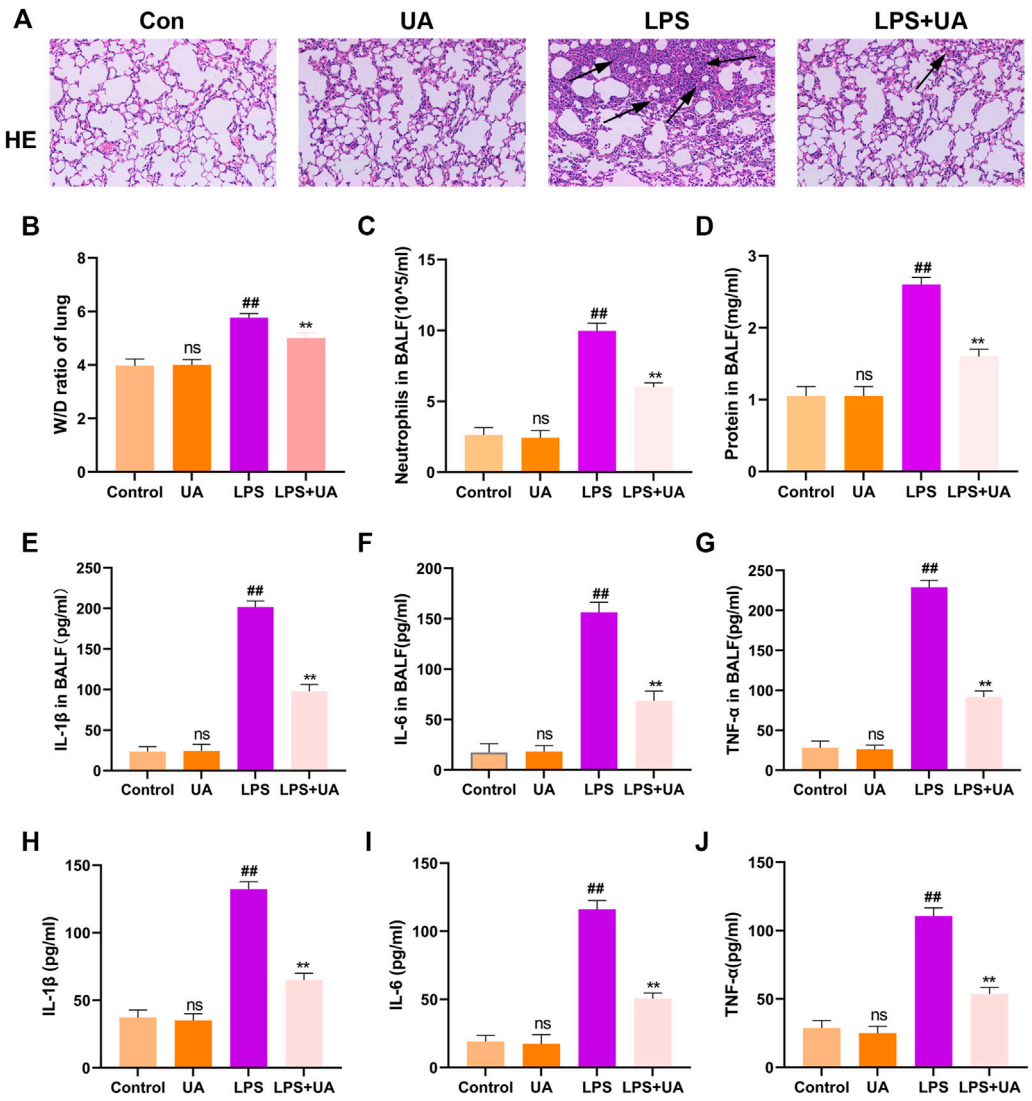

FIGURE 2
Role of Urolithin A (UA) in LPS-mediated ALI in BEAS-2B cells and mice. **(A)** H&E staining images of Lung tissue. **(B)** Lung W/D weight ratio. **(C,D)** Neutrophil number and protein content of the BALF. **(E–G)** TNF-α, IL-1β, and IL-6 expressions in mouse BALF were measured by ELISA assay. **(H–J)** TNF-α, IL-1β, and IL-6 expression in BEAS-2B cells culture supernatant treated with LPS(10 ug/mL) were analyzed through ELISA assay. The results were shown as mean ± SD. ##$p < 0.01$, **$p < 0.01$ in comparison to control and LPS groups, respectively.

weighed to obtain a dry weight. Later, the W/D ratio was determined to assess the severity of tissue edema.

Histopathological evaluation

The Left lung of mice was removed and fixed in 10% neutral formalin for 48 h. Dehydration of lung tissues was accomplished using different concentrations of alcohol, followed by paraffin embedding and sectioning to the 4-μm sections. Thereafter, hematoxylin and eosin (H&E) staining was performed on the obtained sections, and pathological analysis was done using an optical microscope.

Detection of intracellular ROS generation and mitochondrial ROS production

Intracellular were measured using the Reactive Oxygen Species Assay Kits as directed by the manufacturer (Beyotime, Shanghai, China). Briefly, cells were incubated with fresh DMEM medium containing 10 μM DCFH-DA at 37°C for 30 min. Then the cells were washed twice with PBS and resuspended in cold PBS for flow cytometry analysis. Mitochondrial ROS levels in appropriately treated BEAS-2B cells were determined by staining with MitoSox according to the manufacturer's instructions (Thermo Fisher Scientific). A fluorescence microscope was used to examine stained cells (Olympus Life Science; Tokyo, Japan).

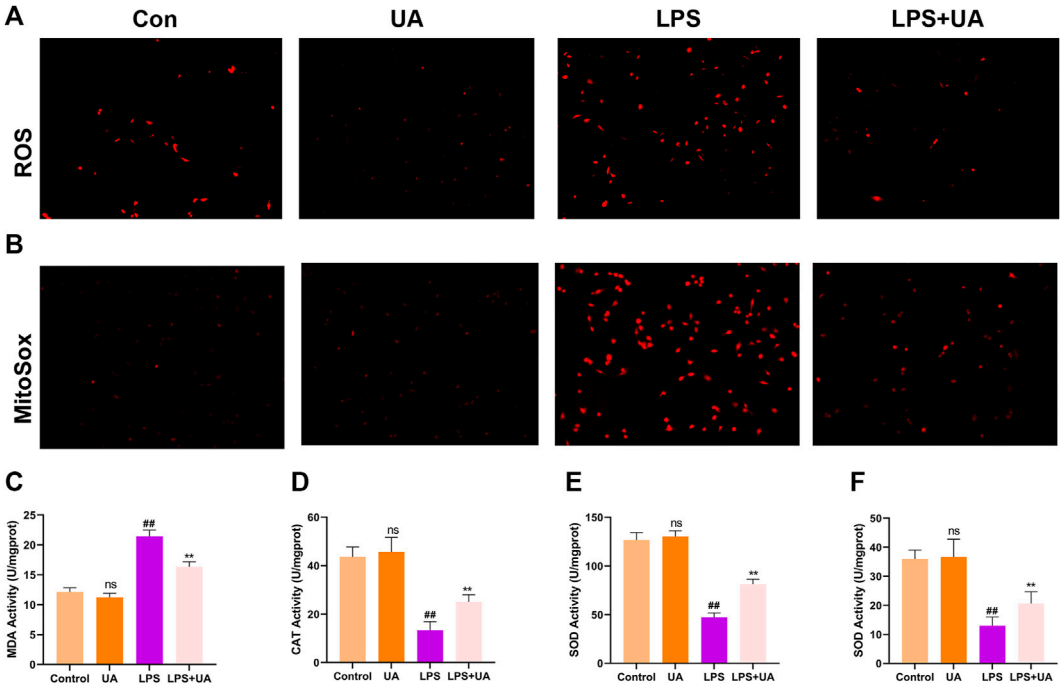

FIGURE 3
Effects of Urolithin A (UA) on LPS-mediated OS in ALI. **(A)** Typical images showed the ROS level in BEAS-2B cells. **(B)** Typical images showed MitoSox in BEAS-2B cells. **(C–F)** MDA, CAT, GSH, and SOD activities in the mouse lung tissues. All data were shown as mean ± SD. ##$p < 0.01$, **$p < 0.01$ in comparison to control and LPS groups, respectively.

Quantification of MDA, GSH-Px, SOD, and CAT activities

Following the sacrifice of the mouse, the right lung tissue was dissected. Later, extraction buffer was added to the lung tissue homogenates. Finally, the levels of SOD, MDA, CAT, and GSH-Px were determined using commercial assay kits (Jiancheng Biotechnology, Nanjing, China) as directed by the manufacturer.

Fe^{2+} detection

Cell lysate (200 μL/well) was rinsed with PBS twice and then put on shaking for 2 h. After that, standard and mix A dilutions were completed per specific protocols (Abcam (Cambridge, United Kingdom). Samples from different groups were combined and incubated at 60°C for 1 h. The sample was cooled and centrifuged. 30 μL of iron ion detection agent was added to the samples, and all the samples were incubated for 30 min at room temperature. Thereafter, each well of the 96 well-plate was added with solution (200 μL), and the OD value was measured at 550 nm. Finally, iron ion content was determined, and a standard curve was drawn.

Immunofluorescence (IF) staining

Cell sections were rinsed with PBS (three times)and fixed for 30-min using 4% paraformaldehyde (PFA), followed by another 3-min treatment using 0.3% Triton X-100. Then sections were washed with PBS (three times), and 10% BSA was added to seal cells for a 30-min, followed by overnight incubation with primary antibodies (1:200) at 4°C. Next day, fluorescent secondary antibodies (1:300) were added to cells and incubated in the dark for a 60-min at room temperature, followed by 8-min DAPI (1:4,000) staining before fluorescence microscopy (Olympus Life Science; Tokyo, Japan). All codomain computations were performed in five separate experiments, each with 50 cells. The images were demonstrated using Adobe Photoshop 6.0. Individuals blinded to the treatments determined fluorescence intensities using Image J software (Bethesda, United States).

Immunohistochemical (IHC) staining

Lung tissues were fixed in 4% PFA, embedded in paraffin, and cut into 4-μm sections. The sections were dewaxed with xylene before being rehydrated with gradient ethanol. Sections were treated with 3% hydrogen peroxide to block endogenous peroxidase activity, and non-specific binding was inactivated with 10% goat serum. Then, sections were incubated overnight with anti-4-HNE, anti-GPX4 and anti- Nrf2 antibodies at 4°C, followed by 1-h incubation with HRP-labeled secondary antibodies at 37 °C. By adding a fresh DAB reaction mixture, color rendering was observed. The sections were dehydrated and sealed after being counterstained with hematoxylin. Finally, each section was photographed using a light microscope. The blinded observers quantified the rate of positive cells in each section. Five mice from each group were employed for the quantitative assessment.

10.3389/fphar.2023.1067402

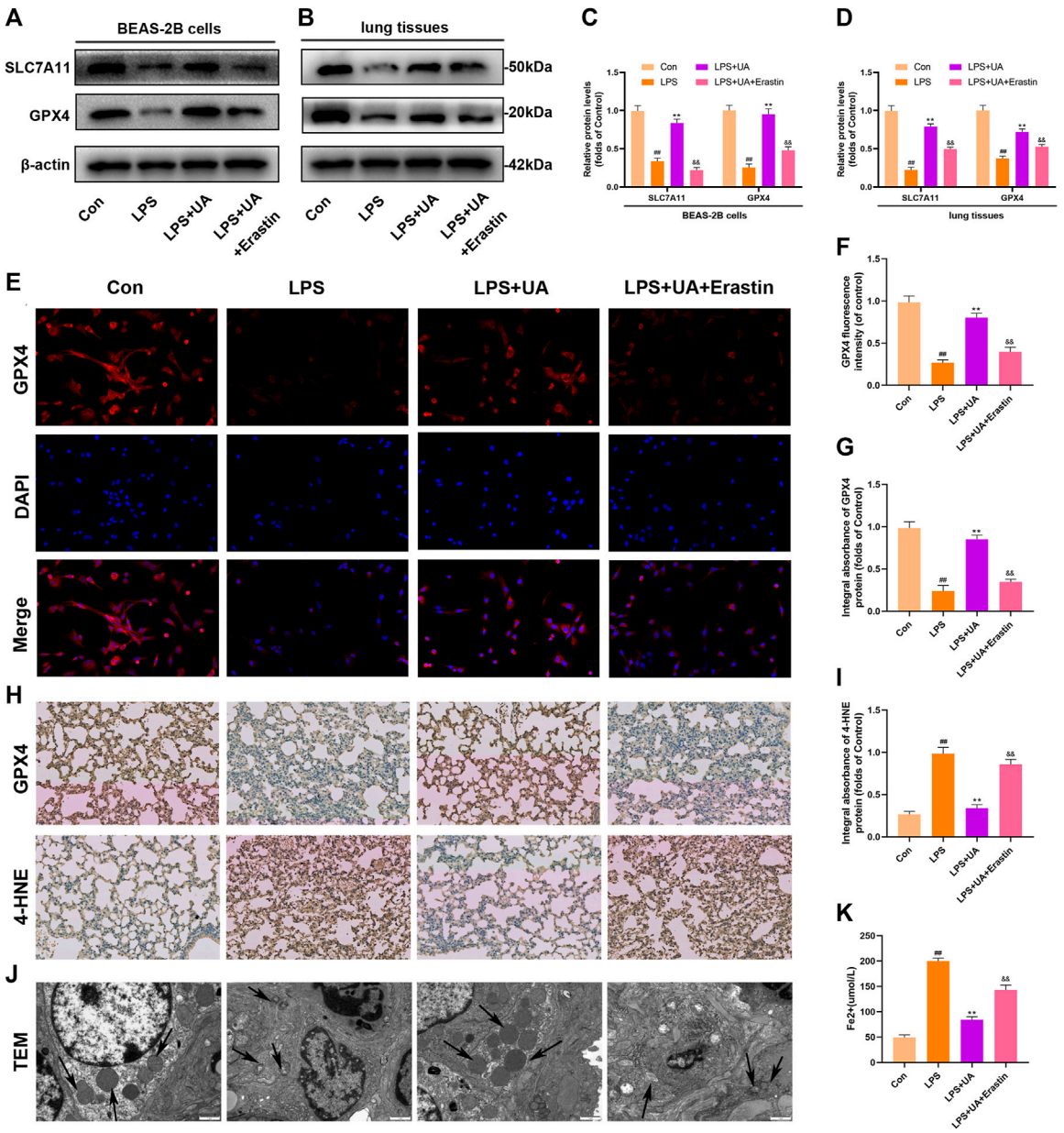

FIGURE 4
Role of UA in Ferroptosis during LPS-mediated injury *in vitro* and *in vivo*. **(A,C)** Levels of SLC7A11 and GPX4 in BEAS-2B cells were measured. **(B,D)** Quantification of SLC7A11 and GPX4 levels in lung tissues. **(E,F)** Representative immunofluorescence images of GPX4 in BEAS-2B cells. **(G–I)** IHC images for GPX4 and 4-HNE expression in lung tissues. **(J)** Fe^{2+} expression in BEAS-2B cells. **(K)** TEM imaged showed ferroptosis of lung tissues. The results were represented by mean ± SD. ## $p < 0.01$, ** $p < 0.01$, &&$p < 0.01$ in comparison with control, LPS and LPS + UA groups, separately.

Transmission electron microscopy (TEM)

To fix lung tissues, 2.5% glutaraldehyde with 0.05 M sodium cacodylate buffer (pH 7.2) was added and incubated at 25°C for a 2-h. Additionally, 2% OsO4 with 0.1 M sodium cacodylate buffer was added for 2-h fixation, and 1% aqueous uranyl acetate was added for 18-h fixation. Following ethanol dehydration, samples were embedded in Epon 812 and collected in ultrathin sections onto the copper grids. Later, Lead citrate and uranyl acetate were added to examine the sections with a Tecnai G2 spirit BioTwin transmission electron microscope (FEI Company, Hillsboro, Oregon).

Molecular docking (MD)

For MD analysis to determine the Nrf2/UA start structure for subsequent treatment, Discovery Studio 3.1 was used. The crystal structures of the Nrf2/Keap1 complex were obtained from the Protein Data Bank database (PDB ID: 1X2R). The minimum

10.3389/fphar.2023.1067402

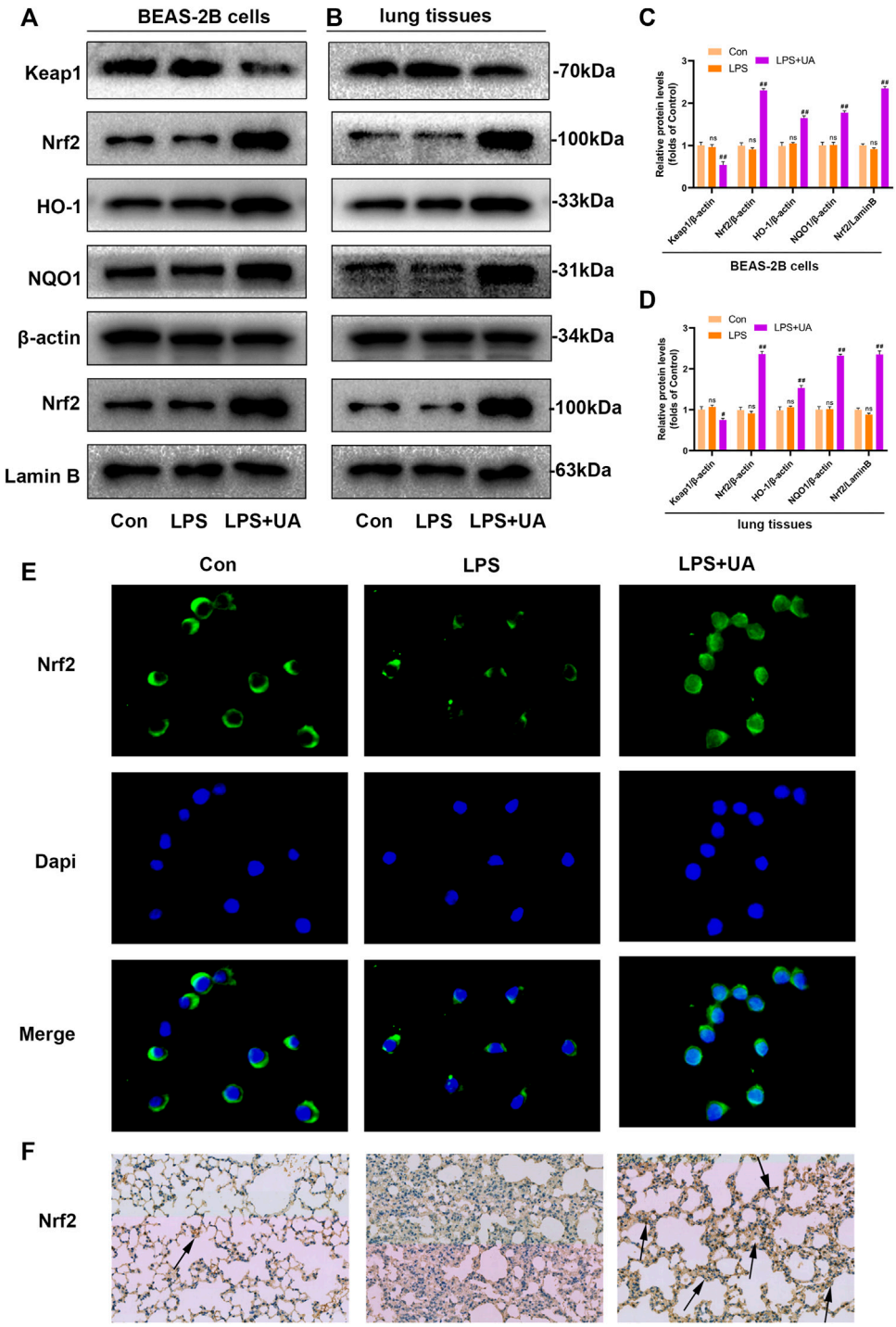

FIGURE 5
Urolithin A (UA) increased Nrf2 expression in LPS-mediated BEAS-2B cells and ALI models. **(A,C)** Quantification of Keap1, Nrf2, HO1, and NQO1 levels in BEAS-2B cells. **(B,D)** Quantification of Keap1, Nrf2, HO1, and NQO1 levels within lung tissues. **(E)** Representative immunofluorescence images showed Nrf2 in BEAS-2B cells. **(F)** Typical IHC images showed the Nrf2 in lung tissues. The results were represented by mean ± SD. ## $p < 0.01$ and ns in comparison to LPS and control groups, respectively.

energy conformations for MD were established using default parameters, and PyMoL (version 1.7.6) was adopted for treatment. The molecular structures of Nrf2-Keap1 and UA's were generated for MD analysis using AutoDockTools (version 1.5.6). PyMoL was used to view the final images in 3D.

Statistical analysis

The statistical analysis was done using GraphPad Prism 8 software. Results were represented by mean ± SD. The Kruskal-Wallis test was used to determine lung injury scores

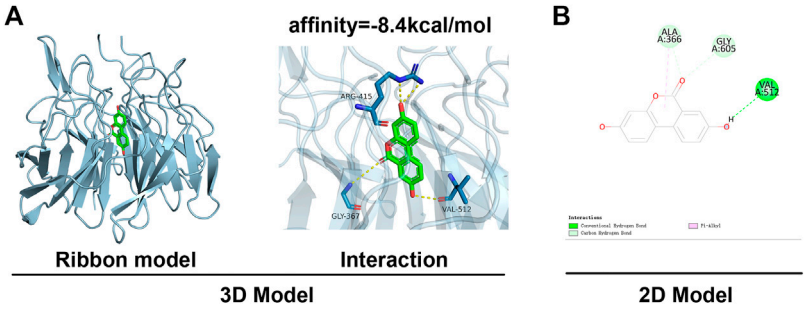

FIGURE 6
MD analysis showed that UA binds to Nrf2. **(A)** Ribbon and space-filling models of UA with Nrf2-Keap1 complex. **(B)** 2D binding models of UA with Nrf2-Keap1 complex.

across several groups. Multiple groups were compared using One-way ANOVA, and the statistical significance level was $p < 0.05$.

Results

Cytotoxic effect of UA on BEAS-2B Cells

UA had the molecular formula of C13H8O4, as shown in Figure 1A. For assessing UA's cytotoxic effect on BEAS-2B cells, UA (2.5, 5, 7.5, 10, 20, 40 μM) was added to treat cells for 24/48 h. Then cell viability was measured using CCK-8 assay. Consequently, 24/48-h of 20 μM UA treatment reduced cell viability, whereas no cytotoxic effect of UA was seen at the dose of 0–10 μM (Figures 1B, C). Thus 10 μM was selected to be used as content in later experiments.

Treatment with UA inhibited inflammatory responses and alleviated LPS-mediated injuries in BEAS-2B Cells and ALI mice

H&E was added to stain mouse lung tissues for pathological analysis, and the effectiveness of UA in preventing LPS-induced ALI was analyzed. Compared to the control group, Mouse lung tissues from the LPS-mediated ALI model group showed distinct and specific pathological alterations, including decreased alveolar cavity, alveolar wall edema and congestion, and significant infiltration of inflammatory cells. Compared to the LPS-mediated ALI model group, the lung tissue structure of LPS + UA animals was nearly normal (Figure 2A). Lung W/D ratio and protein leakage in BALF were also used to determine edema severity, and LPS-mediated W/D ratio and protein content significantly increased as compared to the control group. In contrast, UA significantly reduced protein leakage and lung edema (Figures 2B, D).

In the mouse model, LPS treatment significantly increased neutrophil count compared to the control group, but UA treatment efficiently suppressed the LPS-mediated increase in neutrophil count (Figure 2C). Additionally, an ELISA assay was performed to measure the level of TNF-α, IL-1β, and IL-6 in BALF to analyze the effect of UA on LPS-mediated inflammatory responses. Our results suggested that UA effectively reduced the levels of TNF-α, IL-1β, and IL-6 (Figures 2E–G). According to the above *in-vivo* results, this study explored the role of UA treatment in inhibiting LPS-mediated inflammatory responses in BEAS-2B cells. In BEAS-2B cells, LPS treatment significantly increased the level of IL-1β, TNF-α, and IL-6, while UA significantly reduced LPS-induced IL-1β, IL-6, and TNF-α generation, as shown in Figures 2H–J.

Treatment with UA reduced oxidative stress during LPS-mediated injuries to BEAS-2B Cells and ALI mice

This study analyzed the role of UA treatment in suppressing LPS-mediated OS *in vitro* and *in vivo* since Oxidative damage significantly promoted LPS-mediated ALI; We wanted to see if pretreatment with UA could prevent LPS-induced oxidative stress. Intracellular ROS and mitochondrial ROS can respond to a certain extent to the level of oxidative stress (L. Chen et al., 2020). The result shows that UA treatment significantly decreased LPS-induced ROS accumulation and mitochondrial ROS production in BEAS-2B cells (Figures 3A, B). MDA is a significant marker of OS, whereas SOD, CAT, and GSH-Px are significant markers of anti-OS. MDA contents in mice treated with UA significantly decreased compared to those in the LPS group (Figure 3C). Additionally, UA reversed CAT, SOD, and GSH-Px activities; however, after LPS treatment, these activities were decreased (Figures 3D–F). In BEAS-2B cells and ALI animals, UA thus decreased oxidative stress during LPS-mediated injury.

UA suppressed ferroptosis and reduced LPS-mediated BEAS-2B injury and ALI

Ferroptosis results from lipid peroxidation and iron deposition, leading to mitochondrial contraction. The ferroptosis level in Lung

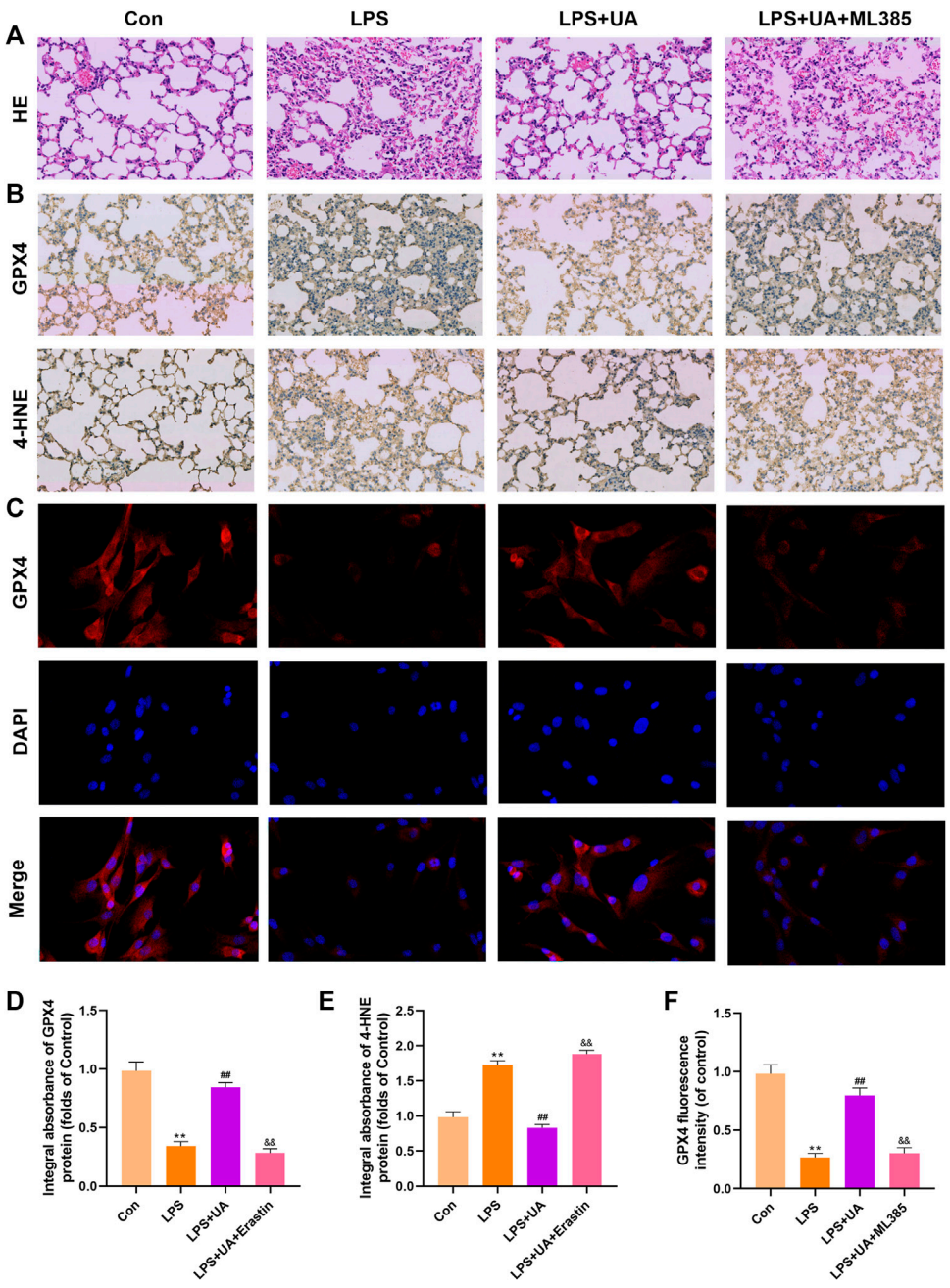

FIGURE 7
Urolithin A (UA) inhibited ferroptosis by activating Nrf2. **(A)** Typical images showed the H&E staining in lung tissue. **(B,D,E)** A typical IHC image showed the GPX4 and 4-HNE expression in lung tissues. **(C,F)** Typical IF images showed GPX4 expression in BEAS-2B cells. The results were represented by mean ± SD. ## $p < 0.01$, ** $p < 0.01$, && $p < 0.01$ in comparison to control, LPS and LPS + UA groups, respectively.

tissue was evaluated by using the contents of 4-HNE, GPX4, SLC7A11, and Fe^{2+} in the LPS-mediated ALI model. UA treatment increased SLC7A11 and GPX4 in lung tissues and BEAS-2B cells compared to the LPS group (Figures 4A–D). The results of immunofluorescence evaluation of GPX4 and Fe^{2+} levels in BEAS-2B cells were consistent with WB results (Figures 4E, F, K). Additionally, SLC7A11 and GPX4 levels were increased in UA-treated BEAS-2B cells and mouse lung tissues (Supplementary Figures S4A–D). GPX4 expression significantly declined, while 4-HNE expression significantly increased in the LPS group, accompanied by distinct mitochondrial contraction (a typical morphological characteristics of ferroptosis) as shown by IHC staining and TEM analysis. Based on the above results, UA might reduce LPS-mediated ALI by suppressing ferroptosis

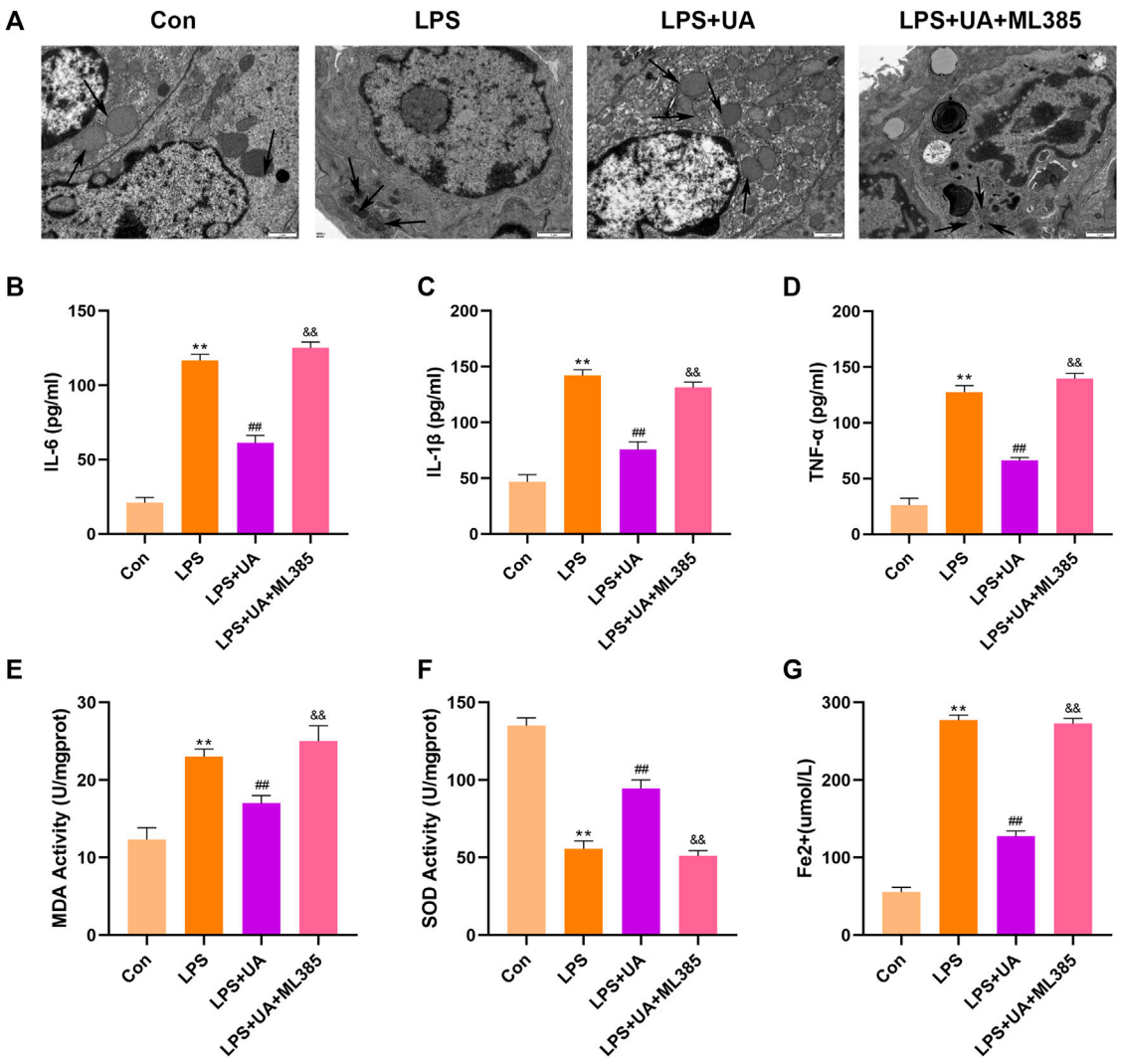

FIGURE 8
Urolithin A (UA) inhibited ferroptosis by activating Nrf2. **(A)** Typical TEM images showed ferroptosis in the lung tissues. **(B–D)** TNF-α, IL-1β, and IL-6 concentrations in the supernatants BEAS-2B cells. **(E,F)** SOD and MDA activities in lung tissues. **(G)** Fe^{2+} expression in BEAS-2B cells. The results were represented by mean ± SD. ## $p < 0.01$, ** $p < 0.01$, &&$p < 0.01$ in comparison to control, LPS and LPS + UA groups, respectively.

(Figures 4G–J). Erastin is a putative activator for ferroptosis and can activate rapid, non-apoptotic, and oxidative cell death. As shown in Figure 4, Erastin was able to counteract UA's inhibition of the ferroptosis in lung tissues and BEAS-2B cells. These findings suggested that UA ameliorated LPS-mediated injuries in BEAS-2B cells and ALI by inhibiting ferroptosis.

UA Increased Keap1-Nrf2/HO-1 pathway in LPS-mediated BEAS-2B cells and ALI mice

Nrf2 has been identified as the activator of the antioxidant response element (ARE) and an important transcription factor (TF) that regulates the antioxidant stress response. To evaluate the effect of UA on LPS-induced injuries in BEAS-2B cells and ALI, WB, IF, and IHC assays were carried out to analyze Nrf2 expression and distribution. UA treatment enhanced the degradation of Keap1, and nuclear import and expression of Nrf2. Besides this, the downstream genes NQO1 and HO-1 also showed significant up-regulation, which indicated that UA's protection on LPS-mediated ALI was possibly associated with increased Nrf2 expression (Figures 5–D). The IF and IHC results of Nrf2 level in BEAS-2B cells and mouse lung tissue are consistent with WB results (Figures 5E, F). In addition, consistent with the above results, the Keap1/Nrf2-HO-1 signaling pathway was activated in UA-treated BEAS-2B cells and mouse lung tissues (Supplementary Figures S4A–D). These findings suggested that UA Increased Keap1-Nrf2/HO-1 pathway in LPS-mediated BEAS-2B Cells and ALI Mice.

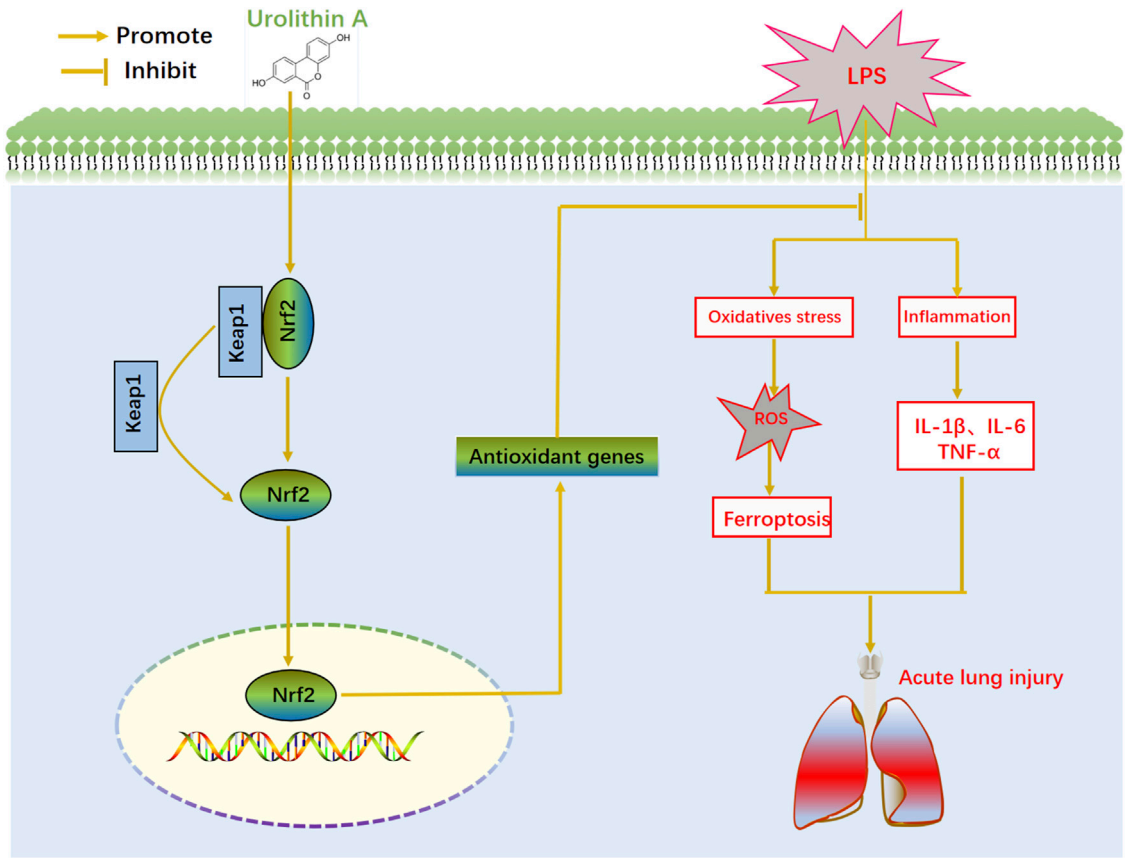

FIGURE 9
Schematic illustration of effect of UA in LPS-induced ALL.

Molecular docking interaction of UA with Nrf2-Keap1

This study was done by using *in silico* MD to analyze the effect of UA on the activation of Nrf2. The binding affinity was found to be −8.4 kcal $mol^{-1,}$ and UA showed favorable embedding into the Keap1 structural domain that interacted with Nrf2 in Figure 6A, with local interaction images showing a hydrogen bond between UA and ALA366 residue was formed. Moreover, the 2D model clearly showed the formation of massive hydrophobic bonds between TF and diverse surrounding residues, namely, ALA 366, GLY 605, and VAL 512. The results indicated a strong affinity between UA and Keap1-Nrf2 complex protein.

UA suppressed ferroptosis by activating Nrf2

To confirm how UA works to protect against ALI by activating Nrf2. Mice were pretreated with the Nrf2 inhibitor (ML385) at a dose of 30 mg/kg for 2 h, and BEAS-2B cells were treated with 5 μm ML385 for a period of 24 h, as described earlier, followed by UA treatment. Figure 7, 8 showed that ML385 significantly decreased UA's ability to protect against inflammatory response, ferroptosis, and OS. Consequently, Nrf2 has a critical effect on the development of LPS-mediated ALI. In addition, Nrf2 activation by UA may help to decrease OS and inflammation, while suppressing ferroptosis in LPS-mediated BEAS-2B injury and ALI.

Discussion

ALI/ARDS induces serious pulmonary diseases, pulmonary presentation of multiple organ dysfunction syndromes (MODS), as well as uncontrollable, self-amplified lung inflammation (Ferguson et al., 2012; Matthay et al., 2020). The major pathogenic mechanism of ALI/ARDS is uncontrolled lung or systemic inflammation (Janz and Ware, 2013). Among inpatients, ALI results in annual mortality of 4%, while that is 10% among intensive care unit (ICU) cases (Bellani et al., 2016). Despite the fact that numerous medicines have been investigated. There is currently no effective pharmaceutical treatment for ALI/ARDS that can significantly increase life quality and lower mortality (Ortiz-Diaz et al., 2013; Fan et al., 2018). In this regard, developing novel therapeutic agents to treat ALI/ARDS is necessary. Our results showed that UA efficiently promoted Keap1-Nrf2/HO-1 signaling pathways while suppressing ferroptosis, suggesting that it might be the potential anti-ALI therapeutic agent.

UA is an intestinal metabolite produced by ellagic acid-rich foods such as pomegranates, walnuts, and berries. It is known for

various biological activities, such as anti-inflammatory and antioxidant properties (Espin et al., 2013; Wong et al., 2021). However, due to differences in gut microbiota composition between individuals, the amount of UA produced in bodies can vary significantly (Selma et al., 2017). Some populations do not even produce UA due to a lack of corresponding gut microbiota. Therefore, proper UA dosage is required in light of its safety and beneficial effects (Lin et al., 2020). Despite this, the role of UA in ALI is unknown. The current study analyzed the effect of UA on LPS-mediated ALI. Therefore, UA treatment significantly reduced the LPS-mediated pathological changes, edema, inflammation, and oxidative stress in the lungs.

The regulated form of necrosis known as ferroptosis is brought on by iron toxicity, plasma membrane damage, and lipid peroxidation (Berke et al., 2021). Ferroptosis is extensively suggested to promote ALI development (Dong et al., 2020; Li et al., 2020; Liu et al., 2020; Qiu et al., 2020). UA has been widely implicated in oxidative stress and lipid peroxidation (Casedas et al., 2020). In our study, we investigated the impact of ferroptosis on LPS-mediated ALI. As a result, ferroptosis developed in LPS-induced ALI, and UA significantly decreased LPS-induced ferroptosis. Erastin is an experimentally verified drug for inducing ferroptosis (Sehm et al., 2016; Roh et al., 2017). The ferroptosis-inducing small molecule erastin significantly decreased GSH expression in cells, thereby promoting ferroptosis, lipid peroxidation, and loss of protective GPX4 expression. Interestingly, UA reversed this effect, suggesting that it might be used as a treatment because it protects by inhibiting LPS-mediated ferroptosis.

This study also analyzed the mechanisms related to UA's effect on LPS-mediated ALI. According to a recent study, UA inhibited hepatotoxicity caused by acetaminophen by increasing OS and activating Nrf2(Gao et al., 2022). It is now known that Nrf2 plays a key role in regulating antioxidant defense, which is also related to several cell death pathways (Kaminskyy and Zhivotovsky, 2014; Dodson et al., 2019). The most important transcriptional regulators in anti-ferroptotic pathways include Nrf2(Kerins and Ooi, 2018). It is also a crucial element in regulating ferroptosis and lipid peroxidation. Nrf2 is activated by electrophilic modification of KEAP1, which inhibits ferroptosis and lipid peroxidation and negatively regulates Nrf2 Normally, Nrf2 shows the cytoplasmic location, which can connect to Keap1 and maintain a low level of Nrf2 expression (Dinkova-Kostova et al., 2017). When stimulated externally, Nrf2 will be dissociated from Keap1, enters the nucleus, activates downstream molecule HO-1, increases the expression of SOD, CAT, and GSH, and defends against oxidative stress (Kensler et al., 2007; Niso-Santano et al., 2010; Gong and Yang, 2020; Zhao et al., 2021). An increasing body of evidence pointed out that numerous therapeutic agents inhibit ferroptosis by activating the Nrf2. For instance, obacunone boosted Nrf2-mediated antioxidant responses to reduce ferroptosis in LPS-mediated ALI increase (J. Li et al., 2022). Leonurine also reduced ferroptosis in the cisplatin-mediated AKI by activating the Nrf2 pathway (Hu et al., 2022). By stimulating Nrf2, TBHQ reduced ferroptosis' effect on 5-fluorouracil-mediated intestinal mucositis and damage to intestinal epithelial cells (Deng et al., 2021). In this study, UA treatment led to Keap1-Nrf2/HO-1 pathways activation in LPS-induced acute lung injury ferroptosis, while inhibiting the Keap1-Nrf2/HO-1 pathways significantly abolished trehalose's function in suppressing ferroptosis. As a result, UA reduced the ferroptosis and inflammation in LPS-mediated ALI by activating Keap1-Nrf2/HO-1 pathways. UA, the novel agonist for Nrf2, inhibited OS resulting from LPS-mediated ALI, which may become the candidate therapeutic target for ALI.

However, this study has some limitations. In addition to BEAS-2B cells, *in vivo* protective effects of UA on endothelial cells and macrophages may have other cytoprotective modalities. Finally, the current study is limited to animal models and *in vitro* studies, and there is no clinical evidence. More comprehensive and in-depth scientific studies will be required to further investigate the relationship between UA and iron death in ALI and provide a theoretical foundation for clinical work.

Conclusion

In summary, UA significantly reduced histopathological changes, W/D weight ratio, inflammatory cell infiltration, and protected from LPS-mediated mouse ALI. UA increased the level of antioxidants in lung tissues while reducing LPS-mediated ferroptosis by activating Keap1-Nrf2/HO-1 pathway; thus, protecting from LPS-mediated ALI (Figure 9). This study suggested that UA can be potentially used to prevent ALI, offering exciting prospective applications.

Data availability statement

The original contributions presented in the study are included in the article/Supplementary Material, further inquiries can be directed to the corresponding author.

Ethics statement

The animal study was reviewed and approved by the Animal Care and Use Committee of Wenzhou Medical University.

Author contributions

LL and MW wrote the manuscript. JH, FM, and SY are responsible for collecting tissue samples and other animal experiments. SW, XJ, and JC are participated in analyzing the data. CC is responsible for designing the entire experimental procedure and revising the experimental manuscript.

Acknowledgments

The authors gratefully acknowledge the financial support by The General Program (Key Program, Major Research Plan) of the National Natural Science Foundation of China under Grant No. 81470225, as well as the Basic Science Foundation of Wenzhou City under project No. Y2020003.

Conflict of interest

The authors declare that the research was conducted in the absence of any commercial or financial relationships that could be construed as a potential conflict of interest.

Publisher's note

All claims expressed in this article are solely those of the authors and do not necessarily represent those of their affiliated organizations, or those of the publisher, the editors and the reviewers. Any product that may be evaluated in this article, or claim that may be made by its manufacturer, is not guaranteed or endorsed by the publisher.

Supplementary material

The Supplementary Material for this article can be found online at: https://www.frontiersin.org/articles/10.3389/fphar.2023.1067402/full#supplementary-material

References

Beitler, J. R., Thompson, B. T., Baron, R. M., Bastarache, J. A., Denlinger, L. C., Esserman, L., et al. (2022). Advancing precision medicine for acute respiratory distress syndrome. *Lancet Respir. Med.* 10 (1), 107–120. doi:10.1016/S2213-2600(21)00157-0

Bellani, G., Laffey, J. G., Pham, T., Fan, E., Brochard, L., Esteban, A., et al. (2016). Epidemiology, patterns of care, and mortality for patients with acute respiratory distress syndrome in intensive care units in 50 countries. *JAMA* 315 (8), 788–800. doi:10.1001/jama.2016.0291

Berke, I. M., Jain, E., Yavuz, B., McGrath, T., Chen, L., Silva, M. J., et al. (2021). NF-κB-mediated effects on behavior and cartilage pathology in a non-invasive loading model of post-traumatic osteoarthritis. *Osteoarthr. Cartil.* 29 (2), 248–256. doi:10.1016/j.joca.2020.10.008

Casedas, G., Les, F., Choya-Foces, C., Hugo, M., and Lopez, V. (2020). The metabolite urolithin-A ameliorates oxidative stress in neuro-2a cells, becoming a potential neuroprotective agent. *Antioxidants (Basel)* 9 (2), 177. doi:10.3390/antiox9020177

Cerda, B., Periago, P., Espin, J. C., and Tomas-Barberan, F. A. (2005). Identification of urolithin a as a metabolite produced by human colon microflora from ellagic acid and related compounds. *J. Agric. Food Chem.* 53 (14), 5571–5576. doi:10.1021/jf050384i

Chen, L., Hu, S. L., Xie, J., Yan, D. Y., Weng, S. J., Tang, J. H., et al. (2020). Proanthocyanidins-mediated Nrf2 activation ameliorates glucocorticoid-induced oxidative stress and mitochondrial dysfunction in osteoblasts. *Oxid. Med. Cell Longev.* 2020, 9102012. doi:10.1155/2020/9102012

Chen, Y. L., Yan, D. Y., Wu, C. Y., Xuan, J. W., Jin, C. Q., Hu, X. L., et al. (2021). Maslinic acid prevents IL-1β-induced inflammatory response in osteoarthritis via PI3K/AKT/NF-κB pathways. *J. Cell Physiol.* 236 (3), 1939–1949. doi:10.1002/jcp.29977

D'Amico, D., Andreux, P. A., Valdes, P., Singh, A., Rinsch, C., and Auwerx, J. (2021). Impact of the natural compound urolithin A on health, disease, and aging. *Trends Mol. Med.* 27 (7), 687–699. doi:10.1016/j.molmed.2021.04.009

Deng, S., Wu, D., Li, L., Li, J., and Xu, Y. (2021). TBHQ attenuates ferroptosis against 5-fluorouracil-induced intestinal epithelial cell injury and intestinal mucositis via activation of Nrf2. *Cell Mol. Biol. Lett.* 26 (1), 48. doi:10.1186/s11658-021-00294-5

Dinkova-Kostova, A. T., Kostov, R. V., and Canning, P. (2017). Keap1, the cysteine-based mammalian intracellular sensor for electrophiles and oxidants. *Arch. Biochem. Biophys.* 617, 84–93. doi:10.1016/j.abb.2016.08.005

Dixon, S. J., Lemberg, K. M., Lamprecht, M. R., Skouta, R., Zaitsev, E. M., Gleason, C. E., et al. (2012). Ferroptosis: An iron-dependent form of nonapoptotic cell death. *Cell* 149 (5), 1060–1072. doi:10.1016/j.cell.2012.03.042

Dodson, M., Castro-Portuguez, R., and Zhang, D. D. (2019). NRF2 plays a critical role in mitigating lipid peroxidation and ferroptosis. *Redox Biol.* 23, 101107. doi:10.1016/j.redox.2019.101107

Dong, H., Qiang, Z., Chai, D., Peng, J., Xia, Y., Hu, R., et al. (2020). Nrf2 inhibits ferroptosis and protects against acute lung injury due to intestinal ischemia reperfusion via regulating SLC7A11 and HO-1. *Aging (Albany NY)* 12 (13), 12943–12959. doi:10.18632/aging.103378

Espin, J. C., Larrosa, M., Garcia-Conesa, M. T., and Tomas-Barberan, F. (2013). Biological significance of urolithins, the gut microbial ellagic acid-derived metabolites: the evidence so far. *Evid. Based Complement. Altern. Med.* 2013, 270418. doi:10.1155/2013/270418

Fan, E., Brodie, D., and Slutsky, A. S. (2018). Acute respiratory distress syndrome: Advances in diagnosis and treatment. *JAMA* 319 (7), 698–710. doi:10.1001/jama.2017.21907

Ferguson, N. D., Fan, E., Camporota, L., Antonelli, M., Anzueto, A., Beale, R., et al. (2012). The berlin definition of ARDS: An expanded rationale, justification, and supplementary material. *Intensive Care Med.* 38 (10), 1573–1582. doi:10.1007/s00134-012-2682-1

Gao, Z., Yi, W., Tang, J., Sun, Y., Huang, J., Lan, T., et al. (2022). Urolithin A protects against acetaminophen-induced liver injury in mice via sustained activation of Nrf2. *Int. J. Biol. Sci.* 18 (5), 2146–2162. doi:10.7150/ijbs.69116

Gong, Y., and Yang, Y. (2020). Activation of nrf2/AREs-mediated antioxidant signalling, and suppression of profibrotic TGF-β1/smad3 pathway: A promising therapeutic strategy for hepatic fibrosis - a review. *Life Sci.* 256, 117909. doi:10.1016/j.lfs.2020.117909

Hu, J., Gu, W., Ma, N., Fan, X., and Ci, X. (2022). Leonurine alleviates ferroptosis in cisplatin-induced acute kidney injury by activating the Nrf2 signalling pathway. *Br. J. Pharmacol.* 179 (15), 3991–4009. doi:10.1111/bph.15834

Janz, D. R., and Ware, L. B. (2013). Biomarkers of ALI/ARDS: pathogenesis, discovery, and relevance to clinical trials. *Semin. Respir. Crit. Care Med.* 34 (4), 537–548. doi:10.1055/s-0033-1351124

Kaminskyy, V. O., and Zhivotovsky, B. (2014). Free radicals in cross talk between autophagy and apoptosis. *Antioxid. Redox Signal* 21 (1), 86–102. doi:10.1089/ars.2013.5746

Kensler, T. W., Wakabayashi, N., and Biswal, S. (2007). Cell survival responses to environmental stresses via the Keap1-Nrf2-ARE pathway. *Annu. Rev. Pharmacol. Toxicol.* 47, 89–116. doi:10.1146/annurev.pharmtox.46.120604.141046

Kerins, M. J., and Ooi, A. (2018). The roles of NRF2 in modulating cellular iron homeostasis. *Antioxid. Redox Signal* 29 (17), 1756–1773. doi:10.1089/ars.2017.7176

Larrosa, M., Gonzalez-Sarrias, A., Yanez-Gascon, M. J., Selma, M. V., Azorin-Ortuno, M., Toti, S., et al. (2010). Anti-inflammatory properties of a pomegranate extract and its metabolite urolithin-A in a colitis rat model and the effect of colon inflammation on phenolic metabolism. *J. Nutr. Biochem.* 21 (8), 717–725. doi:10.1016/j.jnutbio.2009.04.012

Li, Y., Cao, Y., Xiao, J., Shang, J., Tan, Q., Ping, F., et al. (2020). Inhibitor of apoptosis-stimulating protein of p53 inhibits ferroptosis and alleviates intestinal ischemia/reperfusion-induced acute lung injury. *Cell Death Differ.* 27 (9), 2635–2650. doi:10.1038/s41418-020-0528-x

Li, J., Lu, K., Sun, F., Tan, S., Zhang, X., Sheng, W., et al. (2021). Panaxydol attenuates ferroptosis against LPS-induced acute lung injury in mice by Keap1-Nrf2/HO-1 pathway. *J. Transl. Med.* 19 (1), 96. doi:10.1186/s12967-021-02745-1

Li, J., Deng, S. H., Li, J., Li, L., Zhang, F., Zou, Y., et al. (2022). Obacunone alleviates ferroptosis during lipopolysaccharide-induced acute lung injury by upregulating Nrf2-dependent antioxidant responses. *Cell Mol. Biol. Lett.* 27 (1), 29. doi:10.1186/s11658-022-00318-8

Lin, J., Zhuge, J., Zheng, X., Wu, Y., Zhang, Z., Xu, T., et al. (2020). Urolithin A-induced mitophagy suppresses apoptosis and attenuates intervertebral disc degeneration via the AMPK signaling pathway. *Free Radic. Biol. Med.* 150, 109–119. doi:10.1016/j.freeradbiomed.2020.02.024

Liu, P., Feng, Y., Li, H., Chen, X., Wang, G., Xu, S., et al. (2020). Ferrostatin-1 alleviates lipopolysaccharide-induced acute lung injury via inhibiting ferroptosis. *Cell Mol. Biol. Lett.* 25, 10. doi:10.1186/s11658-020-00205-0

Liu, X., Wang, L., Xing, Q., Li, K., Si, J., Ma, X., et al. (2021). Sevoflurane inhibits ferroptosis: A new mechanism to explain its protective role against lipopolysaccharide-induced acute lung injury. *Life Sci.* 275, 119391. doi:10.1016/j.lfs.2021.119391

Liu, X., Zhang, J., and Xie, W. (2022). The role of ferroptosis in acute lung injury. *Mol. Cell Biochem.* 477 (5), 1453–1461. doi:10.1007/s11010-021-04327-7

Luan, P., D'Amico, D., Andreux, P. A., Laurila, P. P., Wohlwend, M., Li, H., et al. (2021). Urolithin A improves muscle function by inducing mitophagy in muscular dystrophy. *Sci. Transl. Med.* 13 (588), eabb0319. doi:10.1126/scitranslmed.abb0319

Matthay, M. A., Arabi, Y. M., Siegel, E. R., Ware, L. B., Bos, L. D. J., Sinha, P., et al. (2020). Phenotypes and personalized medicine in the acute respiratory distress syndrome. *Intensive Care Med.* 46 (12), 2136–2152. doi:10.1007/s00134-020-06296-9

Niso-Santano, M., Gonzalez-Polo, R. A., Bravo-San Pedro, J. M., Gomez-Sanchez, R., Lastres-Becker, I., Ortiz-Ortiz, M. A., et al. (2010). Centro de Investigacion biomedica en red sobre enfermedades, NActivation of apoptosis signal-regulating kinase 1 is a key factor in paraquat-induced cell death: modulation by the nrf2/trx axis. *Free Radic. Biol. Med.* 48 (10), 1370–1381. doi:10.1016/j.freeradbiomed.2010.02.024

Ortiz-Diaz, E., Festic, E., Gajic, O., and Levitt, J. E. (2013). Emerging pharmacological therapies for prevention and early treatment of acute lung injury. *Semin. Respir. Crit. Care Med.* 34 (4), 448–458. doi:10.1055/s-0033-1351118

Qiu, Y. B., Wan, B. B., Liu, G., Wu, Y. X., Chen, D., Lu, M. D., et al. (2020). Nrf2 protects against seawater drowning-induced acute lung injury via inhibiting ferroptosis. *Respir. Res.* 21 (1), 232. doi:10.1186/s12931-020-01500-2

Roh, J. L., Kim, E. H., Jang, H., and Shin, D. (2017). Aspirin plus sorafenib potentiates cisplatin cytotoxicity in resistant head and neck cancer cells through xCT inhibition. *Free Radic. Biol. Med.* 104, 1–9. doi:10.1016/j.freeradbiomed.2017.01.002

Sehm, T., Fan, Z., Ghoochani, A., Rauh, M., Engelhorn, T., Minakaki, G., et al. (2016). Sulfasalazine impacts on ferroptotic cell death and alleviates the tumor microenvironment and glioma-induced brain edema. *Oncotarget* 7 (24), 36021–36033. doi:10.18632/oncotarget.8651

Selma, M. V., Beltran, D., Luna, M. C., Romo-Vaquero, M., Garcia-Villalba, R., Mira, A., et al. (2017). Isolation of human intestinal bacteria capable of producing the bioactive metabolite isourolithin A from ellagic acid. *Front. Microbiol.* 8, 1521. doi:10.3389/fmicb.2017.01521

Singh, R., Chandrashekharappa, S., Bodduluri, S. R., Baby, B. V., Hegde, B., Kotla, N. G., et al. (2019). Enhancement of the gut barrier integrity by a microbial metabolite through the Nrf2 pathway. *Nat. Commun.* 10 (1), 89. doi:10.1038/s41467-018-07859-7

Wang, H., Zhang, B., Li, R., Chen, J., Xu, G., Zhu, Y., et al. (2022). KIAA1199 drives immune suppression to promote colorectal cancer liver metastasis by modulating neutrophil infiltration. *Hepatology* 76 (4), 967–981. doi:10.1002/hep.32383

Ware, L. B., and Matthay, M. A. (2000). The acute respiratory distress syndrome. *N. Engl. J. Med.* 342 (18), 1334–1349. doi:10.1056/NEJM200005043421806

Wong, T. L., Strandberg, K. R., Croley, C. R., Fraser, S. E., Nagulapalli Venkata, K. C., Fimognari, C., et al. (2021). Pomegranate bioactive constituents target multiple oncogenic and oncosuppressive signaling for cancer prevention and intervention. *Semin. Cancer Biol.* 73, 265–293. doi:10.1016/j.semcancer.2021.01.006

Xie, Y., Hou, W., Song, X., Yu, Y., Huang, J., Sun, X., et al. (2016). Ferroptosis: process and function. *Cell Death Differ.* 23 (3), 369–379. doi:10.1038/cdd.2015.158

Xu, Y., Li, X., Cheng, Y., Yang, M., and Wang, R. (2020). Inhibition of ACSL4 attenuates ferroptotic damage after pulmonary ischemia-reperfusion. *FASEB J.* 34 (12), 16262–16275. doi:10.1096/fj.202001758R

Yaqub, N., Wayne, G., Birchall, M., and Song, W. (2022). Recent advances in human respiratory epithelium models for drug discovery. *Biotechnol. Adv.* 54, 107832. doi:10.1016/j.biotechadv.2021.107832

Yin, X., Zhu, G., Wang, Q., Fu, Y. D., Wang, J., and Xu, B. (2021). Ferroptosis, a new insight into acute lung injury. *Front. Pharmacol.* 12, 709538. doi:10.3389/fphar.2021.709538

Zhang, Y., Liu, M., Zhang, Y., Tian, M., Chen, P., Lan, Y., et al. (2022). Urolithin A alleviates acute kidney injury induced by renal ischemia reperfusion through the p62-Keap1-Nrf2 signaling pathway. *Phytother. Res.* 36 (2), 984–995. doi:10.1002/ptr.7370

Zhao, M., Wang, S., Zuo, A., Zhang, J., Wen, W., Jiang, W., et al. (2021). HIF-1α/JMJD1A signaling regulates inflammation and oxidative stress following hyperglycemia and hypoxia-induced vascular cell injury. *Cell Mol. Biol. Lett.* 26 (1), 40. doi:10.1186/s11658-021-00283-8

frontiers | Frontiers in Pharmacology

TYPE Original Research
PUBLISHED 16 March 2023
DOI 10.3389/fphar.2023.1118143

OPEN ACCESS

EDITED BY
Haiyang Tang,
University of Arizona, United States

REVIEWED BY
Yongchun Shen,
Sichuan University, China
Raffaele Campisi,
Azienda Ospedaliera Universitaria
Policlinico G. Rodolico-San Marco, Italy

*CORRESPONDENCE
Ting Yang,
dryangting@qq.com
Chen Wang,
cyh-birm@263.net

†These authors have contributed equally to this work and share first authorship

SPECIALTY SECTION
This article was submitted to Respiratory Pharmacology, a section of the journal Frontiers in Pharmacology

RECEIVED 07 December 2022
ACCEPTED 20 February 2023
PUBLISHED 16 March 2023

CITATION
Fan G, Wang D, Wu S, Li D, Ren X, Dong F, Huang K, Chen Y, Zhang H, Wang C and Yang T (2023), Better response to Tanreqing injection in frequent acute exacerbation of chronic obstructive pulmonary disease (AECOPD) patients—Real-world evidence from a nationwide registry (ACURE) study. *Front. Pharmacol.* 14:1118143. doi: 10.3389/fphar.2023.1118143

Better response to Tanreqing injection in frequent acute exacerbation of chronic obstructive pulmonary disease (AECOPD) patients—Real-world evidence from a nationwide registry (ACURE) study

Guohui Fan[1†], Dingyi Wang[1†], Sinan Wu[1†], Demin Li[2], Xiaoxia Ren[3], Fen Dong[1], Kewu Huang[4], Yahong Chen[5], Hongchun Zhang[2], Chen Wang[3*] and Ting Yang[3*]

[1]Department of Clinical Research and Data Management, Center of Respiratory Medicine, China-Japan Friendship Hospital, National Center for Respiratory Medicine, Institute of Respiratory Medicine, Chinese Academy of Medical Sciences, National Clinical Research Center for Respiratory Diseases, Beijing, China, [2]Department of Traditional Chinese Medicine for Pulmonary Diseases, Center of Respiratory Medicine, China-Japan Friendship Hospital, National Center for Respiratory Medicine, Institute of Respiratory Medicine, Chinese Academy of Medical Sciences, National Clinical Research Center for Respiratory Diseases, Beijing, China, [3]Department of Pulmonary and Critical Care Medicine, Center of Respiratory Medicine, China-Japan Friendship Hospital, National Center for Respiratory Medicine, Institute of Respiratory Medicine, Chinese Academy of Medical Sciences, National Clinical Research Center for Respiratory Diseases, Beijing, China, [4]Beijing Key Laboratory of Respiratory and Pulmonary Circulation Disorders, Department of Pulmonary and Critical Care Medicine, Beijing Chao-Yang Hospital, Capital Medical University, Beijing Institute of Respiratory Medicine, Beijing, China, [5]Department of Respiratory and Critical Care Medicine, Peking University Third Hospital, Beijing, China

Objective: Our aim was to systematically investigate the efficacy of Tanreqing (TRQ) injection on in-hospital outcomes among inpatients with frequent or infrequent AECOPD.

Methods: In this ongoing, nationwide multicenter registry designed to investigate clinical characteristics, management, and prognoses of Chinese patients admitted for AECOPD in real-world settings, we collected characteristics, comorbidities, in-hospital prognoses, and information on the COPD assessment test (CAT) questionnaire, PEACE questionnaire, and modified British Medical Research Council (mMRC) questionnaire from each enrolled patient. Frequent AECOPD was determined as being admitted to the hospital ≥1 time or visiting the emergency room (ER) ≥ 2 times due to AECOPD within a year. A propensity match method and univariable and multivariable regression models were performed to analyze the efficacy of TRQ on clinical outcomes for inpatients with frequent AECOPD.

Results: A total of 4135 inpatients were involved in the analysis, including 868 administered with TRQ and 3267 not administered with TRQ. After propensity score match, among those administered with TRQ, 493 had frequent AECOPD and 358 had infrequent AECOPD. A significant reduction of CAT score at discharge (TRQ median 12, IQR 8.0–16.0; non-TRQ median 13, IQR 9.0–18.0, $p = 0.0297$), a lower rate of ICU admission (TRQ 0.8% vs. non-TRQ 2.6%, $p = 0.0191$), and a shorter length of stay (LOS) (TRQ median 11, IQR 9.0–14.0; non-TRQ median 11, IQR

8.0–14.0, $p = 0.004$) were observed in the TRQ group, compared with the non-TRQ group among frequent AECOPD patients. In the subgroup analysis, for those with a PEACE score >7 on admission, TRQ contributed to a significantly lower CAT score at discharge ($p = 0.0084$) and a numerically lower ICU admission rate with a marginal statistical significance. Among those with phlegm-heat symptom complex on admission ≥2, a lower CAT score at discharge and a lower ICU admission were also observed in the TRQ group.

Conclusion: TRQ injection had better efficacy in patients with frequent AECOPD in reducing ICU admission and alleviating respiratory symptoms, especially for those with higher severity on admission or more phlegm-heat symptoms.

KEYWORDS

Tanreqing injection, frequent AECOPD, comparative study, real-world, efficacy

Introduction

Chronic obstructive pulmonary disease (COPD) is characterized by chronic irreversible airflow limitation, and its high prevalence and mortality continue to lead to a heavy disease burden globally (GBD Chronic Respiratory Disease Collaborators, 2020; Global strategy for the diagnosis and management and prevention of chronic obstructive pulmonary disease, 2022). In China, the prevalence of COPD was 8.6%, and it was estimated that there were nearly 100 million patients among those over 20 years old in 2015.

Acute exacerbation of COPD (AECOPD) is an acute event where a worsening of respiratory symptoms beyond normal daily variations occurs, resulting in the need for a change in therapy (Wang et al., 2018). AECOPD is thought to be caused by complex interactions between the human body, pathogens, and the external environment, which leads to an increase in the inflammatory burden, and it is associated with increased airway and systemic inflammation and physiological changes (Wedzicha and Terence, 2007). Frequent exacerbation increases hospitalization and promotes disease progression, thus negatively impacting the management of COPD. A large cohort study revealed that AECOPD frequency in a single year predicts long-term AECOPD rate. Increasing frequency and severity of AECOPD is associated with the risk of death (Rothnie et al., 2018). The GOLD report uses a threshold of two or more acute exacerbations in the previous year, or at least one hospital admission related to acute exacerbation to identify individuals at a high risk of future events (Ouaalaya et al., 2020). Patients who have frequent exacerbations have higher mortality, worse quality of life, more future exacerbation events, and faster FEV1 decline than those with infrequent exacerbations (0–1/time per year) (Seemungal et al., 2000; Wedzicha et al., 2013; Mullerova et al., 2014). These patients also have an increased airway inflammation, which contributes to a higher risk of hospital admission and disease progression (Seemungal et al., 2000).

The management of AECOPD includes short-acting inhaled bronchodilators, systemic corticosteroids, antibiotics, oxygen therapy, and mechanical ventilation if required (Ko et al., 2016). Some clinical trials have evaluated the efficacy and safety of Chinese medicine injections for AECOPD patients and proved their effectiveness in inhibiting inflammation, regulating immune function, and alleviating symptoms (Li et al., 2010; Hu et al., 2021). Tanreqing (TRQ), an injectable prescription from traditional Chinese medicine with functions of clearing the heart, detoxifying, and resolving phlegm has been approved to treat acute respiratory infection (National Medical Products Administration, China, Number Z20030054). Several randomized clinical trials (RCTs) with limited sample sizes demonstrated the efficacy of TRQ for the treatment of AECOPD and severe pneumonia (Wang et al., 2020; Hu et al., 2021; Chen et al., 2022). However, the effectiveness of TRQ on frequent AECOPD in real-world applications has never been discussed. In our study, we conducted an analysis among AECOPD inpatients who were prescribed TRQ injection using the propensity score match (PSM) method, compared with those who did not use TRQ, to systematically investigate its efficacy on in-hospital outcomes of frequent or infrequent AECOPD.

Materials and methods

Study design and participants

Our study analyzed data from the acute exacerbation of chronic obstructive pulmonary disease inpatient registry (ACURE) study. The ACURE study is an ongoing, nationwide multicenter registry designed to investigate clinical characteristics, management, and prognoses of Chinese patients admitted for AECOPD in real-world settings (ClinicalTrials. gov identifier: NCT02657525). It started on 1 September 2017 and planned to recruit 7600 in-hospital AECOPD patients with a 3-year follow-up. The protocol and phase 1 results of the registry have been previously described (Pei et al., 2020; Liang et al., 2021). The study was approved by the ethics committee of China-Japan Friendship Hospital (No. 2015-88) and informed consent was obtained from all involved participants. The study was conducted in accordance with the Declaration of Helsinki.

Measurements and outcomes

For each patient, a baseline survey was conducted within 1–3 days after hospitalization to collect information on medical history, physical examination, and inpatient diagnosis. During the hospital stay, the COPD assessment test (CAT) questionnaire, PEACE questionnaire (consisting of eight questions assessing daily variance of COPD symptoms, i.e., dyspnea, purulent sputum,

sputum volume, upper respiratory tract infection, fever, wheezing, cough, and breath rate), modified British Medical Research Council (mMRC) questionnaire, medical examinations, laboratory tests, and treatments were recorded. Comorbidities including respiratory diseases, cardiovascular diseases, metabolic diseases (diabetes and osteoporosis), and digestive diseases, as well as malignancies other than lung cancer, peripheral arterial disease, venous thromboembolism, cerebrovascular disease, anxiety/depression, musculoskeletal dysfunction, chronic kidney disease, etc., were recorded.

During hospitalization, treatment (including the application of TRQ) and auxiliary examination results including laboratory and lung function tests were recorded if available. All auxiliary examinations were conducted at local sites, and the results were uploaded to the database by investigators. If laboratory data were unavailable during hospitalization, the most recent results within 3 days before admission were used for imputation. If multiple tests were conducted after admission, the earliest one was used. The severity of airflow limitation was classified into four grades based on the 2017 Global Initiative for Chronic Obstructive Lung Disease (GOLD) report: GOLD 1 (forced expiratory volume in one second [FEV1]% predicted ≥80), GOLD 2 (50 ≤ FEV1% predicted <80), GOLD 3 (30 ≤ FEV1% predicted <50), and GOLD 4 (FEV1% predicted <30) (Global strategy for the diagnosis and management and prevention of chronic obstructive pulmonary disease, 2017). Total direct costs were calculated in US dollars using the average exchange rate in 2019 (one US dollar was equivalent to 6.90 yuan).

Patients were divided into "frequent AECOPD" if they were admitted to the hospital ≥1 time or visited the emergency room (ER) ≥ 2 times due to AECOPD within a year and "infrequent AECOPD" if they were never admitted to the hospital or visited the emergency room (ER) < 2 times due to AECOPD, according to the GOLD report (Global strategy for the diagnosis and management and prevention of chronic obstructive pulmonary disease, 2017). According to the theory of traditional Chinese medicine, patients were defined as having "phlegm and heat" syndrome if they had ≥ two of the following symptoms: fever, pharyngalgia, purulent sputum, and sputum over 50 mL/day. Those without a single of the above symptoms were defined as having "no phlegm and heat" syndrome.

The primary outcome was a PEACE score at discharge (Zheng et al., 2008). The secondary outcomes were ICU admission, the change of CAT score at discharge, mMRC dyspnea grade at discharge, length of hospitalization, and total cost of hospitalization.

Statistical analysis

Baseline patient characteristics were expressed in terms of descriptive statistics. Categorical variables were summarized as frequency (percentage). Continuous variables were presented as mean (standard deviation, SD) or median (interquartile range, IQR). p values were calculated by students' t-test, χ^2 test, or Fisher exact test where appropriate.

A propensity score was estimated by logistic regression to determine the probability of TRQ treatment of each patient conditionally on observed covariates. Based on the propensity score, we performed 2:1 match-to-match patients who were not administered with TRQ to those who were on a range of ±0.0001 to ± 0.1. The match started with the range of ± 0.0001, and those who were matched were extracted from the database and excluded from the following ranges. If more than two patients who were not administered TRQ were detected, only two of them were selected randomly. Variables involved in the propensity score estimation included age, drug therapy, PEACE score at admission, mMRC score at admission, hospitalization frequency, diagnosis as COPD for the first time, cor pulmonale, non-drug therapy, cough frequency, expectoration, and fever. The propensity score matches were performed in the analyses between frequent AECOPD and infrequent AECOPD, PEACE score >7 and ≤7 on admission, phlegm-heat symptom complex ≥2 and <2 on admission, or phlegm-heat symptom complex ≥1 and <1 on admission. Univariable and multivariable analyses of the efficacy of TRQ on clinical outcomes for inpatients with frequent AECOPD were performed by the logistic regression model or general linear model to investigate the efficacy of TRQ. In the multivariable model, covariates including age, drug therapy, PEACE score at admission, mMRC score at admission, hospitalization frequency, diagnosis as COPD for the first time, cor pulmonale, non-drug therapy, cough frequency, expectoration, and fever were adjusted.

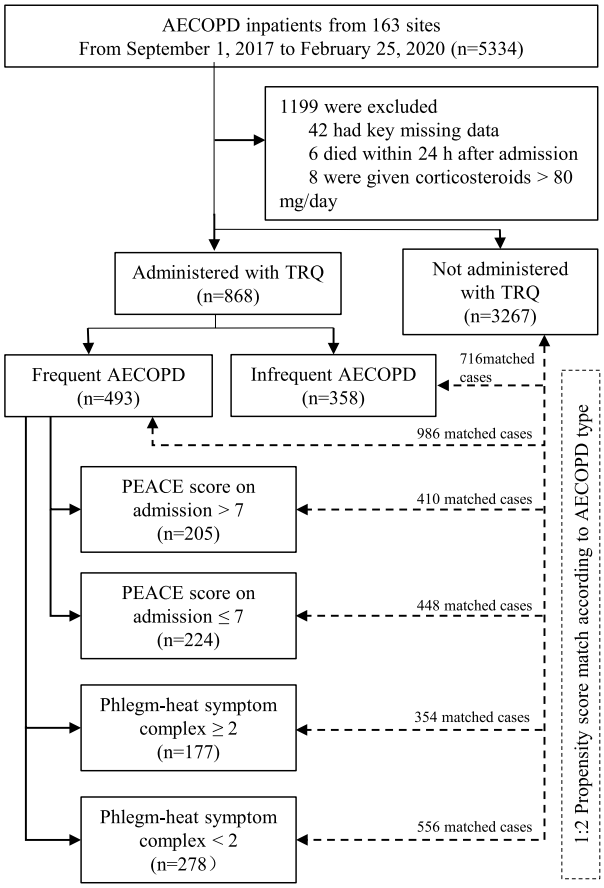

FIGURE 1
Flowchart of this study. Abbreviations: COPD, chronic obstructive pulmonary disease; AECOPD, acute exacerbation of COPD; TRQ, Tanreqing injection.

TABLE 1 Characteristics of inpatients with frequent AECOPD or Infrequent AECOPD before propensity score match.

Characteristics	Frequent AECOPD				Infrequent AECOPD			
	Total	TRQ	Without TRQ	p	Total	TRQ	Without TRQ	p
	N = 2179	N = 505	N = 1674		N = 1956	N = 363	N = 1593	
Age, years	70.8 (64.8, 77.5)	71.0 (65.1, 77.1)	70.6 (64.7, 77.6)	0.788	69.3 (62.8, 76.0)	69.6 (62.9, 75.6)	69.2 (62.7, 76.1)	0.7567
Male	1747 (80.2)	397 (78.6)	1350 (80.6)	0.3156	1425 (72.9)	277 (76.3)	1148 (72.1)	0.1009
BMI, Kg/m^2	21.8 (19.5, 24.2)	21.8 (19.4, 24.2)	21.8 (19.5, 24.2)	0.9525	22.0 (19.7, 24.5)	22.0 (19.6, 24.2)	22.0 (19.8, 24.6)	0.1882
Smoking				0.9971				0.6736
Current smoking	406 (18.6)	94 (18.6)	312 (18.6)		556 (28.4)	105 (28.9)	451 (28.3)	
Never smoking	706 (32.4)	163 (32.3)	543 (32.4)		685 (35.0)	120 (33.1)	565 (35.5)	
Quit smoking	1067 (49.0)	248 (49.1)	819 (48.9)		715 (36.6)	138 (38.0)	577 (36.2)	
Pulmonary thromboembolism	10 (0.5)	3 (0.6)	7 (0.4)	0.6189	4 (0.2)	0 (0.0)	4 (0.3)	0.1998
Pulmonary artery hypertension	99 (4.5)	28 (5.5)	71 (4.2)	0.2177	41 (2.1)	8 (2.2)	33 (2.1)	0.8738
Hypertension	720 (33.0)	160 (31.7)	560 (33.5)	0.4587	628 (32.1)	106 (29.2)	522 (32.8)	0.1889
Myocardial infarction	367 (16.8)	81 (16.0)	286 (17.1)	0.5822	300 (15.3)	44 (12.1)	256 (16.1)	0.0595
Cor pulmonale	525 (24.1)	143 (28.3)	382 (22.8)	0.0113	243 (12.4)	50 (13.8)	193 (12.1)	0.3873
Bronchiectasia	189 (8.7)	54 (10.7)	135 (8.1)	0.0658	131 (6.7)	24 (6.6)	107 (6.7)	0.9423
Non-drug therapy	1036 (47.5)	270 (53.5)	766 (45.8)	0.0024	451 (23.1)	91 (25.1)	360 (22.6)	0.3133
Drug therapy	1492 (68.5)	349 (69.1)	1143 (68.3)	0.7252	689 (35.2)	134 (36.9)	555 (34.8)	0.4552
Regular inhaled corticosteroid	100/178 (56.2)	35/61 (57.4)	65/117 (55.6)	0.8162	28/53 (52.8)	3/8 (37.5)	25/45 (55.6)	0.3449
Regular oral corticosteroid	24/94 (25.5)	8/33 (24.2)	16/61 (26.2)	0.833	6/40 (15.0)	4/11 (36.4)	2/29 (6.9)	0.0278
Inhaled corticosteroids	178 (8.2)	61 (12.1)	117 (7.0)	0.0003	53 (2.7)	8 (2.2)	45 (2.8)	0.5108
Inhaled bronchial dilator	444 (20.4)	125 (24.8)	319 (19.1)	0.0053	179 (9.2)	37 (10.2)	142 (8.9)	0.4457
PEACE at admission	7.0 (6.0, 9.0)	8.0 (6.0, 9.0)	7.0 (6.0, 9.0)	0.0038	7.0 (5.0, 9.0)	7.0 (6.0, 9.0)	7.0 (5.0, 8.0)	<.0001
CAT at admission	21.0 (16.0, 26.0)	21.0 (17.0, 25.0)	21.0 (16.0, 26.0)	0.924	19.0 (14.0, 24.0)	19.0 (15.0, 24.0)	19.0 (14.0, 24.0)	0.2091
mMRC at admission	3.0 (2.0, 3.0)	3.0 (2.0, 3.0)	3.0 (2.0, 3.0)	0.8024	3.0 (2.0, 3.0)	3.0 (2.0, 3.0)	3.0 (2.0, 3.0)	0.0166
Diagnosed with COPD for the first time	147 (6.7)	21 (4.2)	126 (7.5)	0.0082	1127 (57.6)	190 (52.3)	937 (58.8)	0.0242
Hospitalization frequency due to AECOPD	2.0 (1.0, 2.0)	2.0 (1.0, 2.0)	2.0 (1.0, 2.0)	0.5266	0.0 (0.0, 0.0)	0.0 (0.0, 0.0)	0.0 (0.0, 0.0)	1.000

(Continued on following page)

10.3389/fphar.2023.1118143

TABLE 1 (*Continued*) Characteristics of inpatients with frequent AECOPD or Infrequent AECOPD before propensity score match.

Characteristics	Frequent AECOPD				Infrequent AECOPD			
	Total	TRQ	Without TRQ	p	Total	TRQ	Without TRQ	p
	N = 2179	N = 505	N = 1674		N = 1956	N = 363	N = 1593	
Cough frequency				0.0084				0.0324
All day	1074 (49.3)	241 (47.7)	833 (49.8)		962 (49.2)	195 (53.7)	767 (48.1)	
Continuously	256 (11.7)	75 (14.9)	181 (10.8)		255 (13.0)	53 (14.6)	202 (12.7)	
No cough	35 (1.6)	2 (0.4)	33 (2.0)		39 (2.0)	3 (0.8)	36 (2.3)	
Occasionally	814 (37.4)	187 (37.0)	627 (37.5)		700 (35.8)	112 (30.9)	588 (36.9)	
Amount of sputum				0.046				0.0036
<50 mL	1300 (59.7)	282 (55.8)	1018 (60.8)		1146 (58.6)	188 (51.8)	958 (60.1)	
≥50 mL	879 (40.3)	223 (44.2)	656 (39.2)		810 (41.4)	175 (48.2)	635 (39.9)	
Purulent sputum	1069 (49.1)	258 (51.1)	811 (48.4)	0.2978	837 (42.8)	158 (43.5)	679 (42.6)	0.7539
Fever	347 (15.9)	101 (20.0)	246 (14.7)	0.0043	278 (14.2)	65 (17.9)	213 (13.4)	0.0255
Pharyngalgia	181 (8.3)	50 (9.9)	131 (7.8)	0.1385	140 (7.2)	26 (7.2)	114 (7.2)	0.9967
pH	7.4 (7.4, 7.4)	7.4 (7.4, 7.4)	7.4 (7.4, 7.4)	0.0038	7.4 (7.4, 7.4)	7.4 (7.4, 7.4)	7.4 (7.4, 7.4)	0.1243
PaO_2 (mmHg)	43.5 (38.0, 52.0)	43.7 (38.0, 52.0)	43.0 (38.1, 51.0)	0.6548	42.0 (37.6, 48.0)	42.0 (37.8, 48.0)	42.0 (37.5, 48.0)	0.7088
PaO_2 (mmHg)	73.0 (61.6, 89.6)	73.0 (61.8, 87.8)	75.0 (61.0, 94.0)	0.0651	72.1 (63.0, 85.9)	74.0 (64.2, 88.0)	72.0 (62.8, 85.0)	0.0745
High sensitivity C reactive protein, mg/dl	5.0 (1.2, 15.3)	5.0 (1.3, 16.0)	4.4 (0.8, 13.1)	0.0366	3.8 (0.9, 11.6)	2.6 (0.6, 10.0)	4.1 (1.0, 11.8)	0.0601
≥3, mg/dl	795/1297 (61.3)	608/965 (63.0)	187/332 (56.3)	0.0311	666/1220 (54.6)	111/231 (48.1)	555/989 (56.1)	0.0266
PCT, ng/ml	0.1 (0.0, 0.1)	0.1 (0.0, 0.1)	0.1 (0.0, 0.1)	0.3479	0.1 (0.0, 0.1)	0.1 (0.0, 0.1)	0.1 (0.0, 0.1)	0.7028
≥0.1, ng/ml	480/1266 (37.9)	351/952 (36.9)	129/314 (41.1)	0.1821	438/1173 (37.3)	76/225 (33.8)	362/948 (38.2)	0.2191
White blood cell count, $\times 10^9$/L	7.2 (5.7, 9.7)	7.2 (5.6, 9.7)	7.5 (5.8, 9.9)	0.0559	7.2 (5.7, 9.2)	7.1 (5.8, 9.2)	7.2 (5.7, 9.2)	0.9683
Neutrophils, %	72.0 (63.0, 80.3)	71.8 (63.0, 80.1)	73.0 (63.3, 80.9)	0.2839	69.1 (60.0, 78.3)	70.6 (59.9, 78.5)	69.0 (60.0, 78.3)	0.4635
Lymphocyte, %	16.8 (10.2, 24.0)	17.0 (10.3, 24.0)	16.4 (9.7, 23.8)	0.3638	18.7 (11.3, 27.0)	18.2 (11.1, 26.9)	19.0 (11.3, 27.0)	0.3586
Aspartate aminotransferase, U/L	19.1 (15.4, 26.0)	19.1 (15.4, 26.0)	19.1 (15.2, 26.0)	0.8056	20.0 (15.8, 26.0)	19.0 (15.0, 24.0)	20.0 (16.0, 26.4)	0.0093
>40, U/L	169/2067 (8.2)	122/1572 (7.8)	47/495 (9.5)	0.2195	129/1886 (6.8)	19/352 (5.4)	110/1534 (7.2)	0.2346

Note. Data were expressed as n (%) or median (interquartile range), where appropriate. *p* values were calculated by the Mann-Whitney *U* test, Chi-square test, or Fisher exact test, where appropriate. Abbreviations: COPD, chronic obstructive pulmonary disease; AECOPD, acute exacerbation of COPD; TRQ, tanreqing injection; BMI, body mass index; CAT, the COPD assessment test; mMRC, modified British medical research council; PCT, procalcitonin.

10.3389/fphar.2023.1118143

TABLE 2 Treatment and clinical outcomes of inpatients with frequent AECOPD or Infrequent AECOPD after propensity score match.

Characteristics	Frequent AECOPD				Infrequent AECOPD			
	Total	TRQ	Without TRQ	p	Total	TRQ	Without TRQ	p
	N = 1479	N = 493	N = 986		N = 1074	N = 358	N = 716	
PEACE at discharge	3.0 (2.0, 4.0)	3.0 (2.0, 4.0)	3.0 (2.0, 4.0)	0.4074	3.0 (2.0, 4.0)	3.0 (2.0, 4.0)	3.0 (2.0, 4.0)	0.6681
PEACE difference	−4.0 (−6.0, −3.0)	−4.0 (−6.0, −3.0)	−4.0 (−6.0, −3.0)	0.321	−5.0 (−6.0, −3.0)	−5.0 (−6.0, −3.0)	−5.0 (−6.0, −3.0)	0.3576
CAT at discharge	13.0 (9.0, 17.0)	12.0 (8.0, 16.0)	13.0 (9.0, 18.0)	0.0297	10.0 (8.0, 14.0)	10.0 (7.5, 14.0)	10.0 (8.0, 15.0)	0.3198
mMRC at discharge	2.0 (1.0, 2.0)	2.0 (1.0, 2.0)	2.0 (1.0, 2.0)	0.2772	1.0 (1.0, 2.0)	1.0 (1.0, 2.0)	1.0 (1.0, 2.0)	0.7438
mMRC difference	−1.0 (−2.0, 0.0)	−1.0 (−2.0, 0.0)	−1.0 (−2.0, 0.0)	0.5614	−1.0 (−2.0, −1.0)	−1.0 (−2.0, 0.0)	−1.0 (−2.0, −1.0)	0.9162
length of hospital stay, days	11.0 (9.0, 14.0)	11.0 (9.0, 14.0)	11.0 (8.0, 14.0)	0.004	10.0 (8.0, 13.0)	10.0 (8.0, 13.0)	10.0 (8.0, 12.0)	0.2043
Death or worsening in the hospital	8 (0.5)	2 (0.4)	6 (0.6)	0.6074	2 (0.2)	1 (0.3)	1 (0.1)	0.6271
ICU admission	30/1478 (2.0)	4/492 (0.8)	26/986 (2.6)	0.0191	17 (1.6)	3 (0.8)	14 (2.0)	0.1667
Oxygen support				0.7970				0.9644
No oxygen support	169 (11.4)	58 (11.8)	111 (11.3)		240 (22.3)	80 (22.3)	160 (22.3)	
Tube/mask	1129 (76.3)	382 (77.5)	747 (75.8)		773 (72.0)	259 (72.3)	514 (71.8)	
HFNC	15 (1.0)	4 (0.8)	11 (1.1)		5 (0.5)	1 (0.3)	4 (0.6)	
NPPV	160 (10.8)	47 (9.5)	113 (11.5)		52 (4.8)	17 (4.7)	35 (4.9)	
IPPV	6 (0.4)	2 (0.4)	4 (0.4)		4 (0.4)	1 (0.3)	3 (0.4)	
Total cost of hospitalization (USD)	1504.9 (1078.1, 2118.2)	1459 (1060.9, 2022.2)	1517.3 (1087, 2175.2)	0.0821	1350.6 (985.4, 1956.8)	1337.6 (990.1, 2000.1)	1359.4 (976.4, 1950.2)	0.9473
Antibiotics	1378/1478 (93.2)	465/493 (94.3)	913/985 (92.7)	0.2394	1002/1073 (93.4)	347/358 (96.9)	655/715 (91.6)	0.001
Systemic Corticosteroid	1192/1478 (80.6)	391/493 (79.3)	801/985 (81.3)	0.3565	834/1073 (77.7)	275/358 (76.8)	559/715 (78.2)	0.6121

Note. The exchange rate of RMB was 6.9 yuan to the US dollar. Data were expressed as n (%) or median (interquartile range), where appropriate. *p* values were calculated by the Mann-Whitney *U* test, Chi-square test, or Fisher exact test, where appropriate. Abbreviations: COPD, chronic obstructive pulmonary disease; AECOPD, acute exacerbation of COPD; TRQ, tanreqing injection; CAT, the COPD assessment test; mMRC, modified British medical research council; ICU, intensive care unit; HFNC, high-flow nasal cannula oxygen therapy; NPPV, non-invasive positive pressure ventilation; IPPV, invasive positive pressure ventilation.

10.3389/fphar.2023.1118143

TABLE 3 Univariable and multivariable analyses of the efficacy of TRQ on clinical outcomes for inpatients with frequent AECOPD.

Outcomes		Univariable		Multivariable	
		OR/β (95% CI)	P	OR/β (95% CI)	P
PEACE at discharge		−0.08 (−0.25,0.10)	0.3829	−0.08 (−0.23,0.08)	0.3532
CAT at discharge		−0.90 (−1.56,-0.25)	0.0070	−0.90 (−1.53,−0.27)	0.0050
mMRC at discharge		−0.06 (−0.17,0.04)	0.2381	−0.06 (−0.15,0.03)	0.1821
PEACE difference		−0.09 (−0.33,0.15)	0.4655	−0.08 (−0.23,0.08)	0.3532
mMRC difference		−0.06 (−0.17,0.04)	0.2152	−0.06 (−0.15,0.03)	0.1821
length of hospital stay (days, log-transformed)		0.04 (−0.02,0.09)	0.1701	0.04 (−0.01,0.09)	0.1577
Death or worsening in the hospital	Non-TRQ	Reference		Reference	
	TRQ	0.67 (0.13–3.31)	0.6185	0.74 (0.14–3.83)	0.7218
ICU admission	Non-TRQ	Reference		Reference	
	TRQ	0.30 (0.11–0.87)	0.0269	0.30 (0.10–0.87)	0.0267
NPPV	Non-Tanreqing	Ref		Ref	
	Tanreqing	0.81 (0.57–1.17)	0.2614	0.85 (0.58–1.24)	0.4005
Total cost of hospitalization (USD, log-transformed)		0.01 (−0.07,0.09)	0.8257	0.01 (−0.07,0.09)	0.7748

Note. The exchange rate of RMB was 6.9 yuan to the US dollar. OR (95% CI) and β (95% CI) were estimated by logistic regression models or general linear models, respectively. In the multivariable model, TRQ was adjusted for covariates including age, drug therapy, PEACE score at admission, mMRC score at admission, hospitalization frequency, diagnosis as COPD for the first time, cor pulmonale, non-drug therapy, cough frequency, expectoration, and fever.

Abbreviations: COPD, chronic obstructive pulmonary disease; AECOPD, acute exacerbation of COPD; TRQ, tanreqing injection; CAT, the COPD assessment test; mMRC, modified British medical research council; ICU, intensive care unit; NPPV, non-invasive positive pressure ventilation; OR, odds ratio; 95% CI, 95% confidence interval.

All tests were two-sided and were considered statistically significant at a p-value of <0.05. All analyses were performed using SAS 9.4 software (Cary, NC, United States).

Results

Baseline characteristics

As is shown in the flow chart of this study, 5334 AECOPD inpatients were enrolled from 153 sites between 1 September 2017 and 25 February 2020. After excluding 1199 inpatients, 4135 inpatients were involved in the analysis, including 868 administered with TRQ and 3267 not administered with TRQ. After propensity score match, among those administered with TRQ, 493 had frequent AECOPD and 358 had infrequent AECOPD (Figure 1).

Among frequent AECOPD patients (n = 2179), those who have been prescribed TRQ (n = 505) had a significantly higher rate of cor pulmonale, cough, a larger amount of sputum, fever, and lower C-reactive protein (CRP) level on admission. The PEACE scores were higher among the TRQ group, compared with the non-TRQ group (TRQ median 8.0, interquartile range [IQR] 6.0–9.0 vs. non-TRQ median 7.0, IQR 6.0–9.0, p = 0.0038), indicating that those injected with TRQ had more severe symptoms on admission. Similar results were revealed among the infrequent AECOPD patients (Table 1). After the propensity match, the demographic and baseline characteristics were balanced between TRQ and non-TRQ groups in patients with frequent AECOPD or infrequent AECOPD (Supplementary Table S1).

Treatment and clinical outcomes after PSM

After the propensity score match, a significant reduction of CAT score at discharge (TRQ median 12, IQR 8.0–16.0; non-TRQ median 13, IQR 9.0–18.0, p = 0.0297), a lower rate of ICU admission (TRQ 0.8% Vs. non-TRQ 2.6%, p = 0.0191), and a shorter length of stay (LOS) (TRQ median 11 days, IQR 9.0–14.0; non-TRQ median 11 days, IQR 8.0–14.0, p = 0.004) were observed in the TRQ group, compared with the non-TRQ group among frequent AECOPD patients. Treatment and clinical outcomes including PEACE at discharge, PEACE difference, mMRC at discharge, mMRC difference, death or worsened cases, cost, antibiotics, and systemic corticosteroid were compared between TRQ and non-TRQ groups among frequent AECOPD patients. No significant difference in outcomes was shown in infrequent AECOPD patients (Table 2). After adjusting for covariates, the TRQ group was independently associated with a lower CAT score at discharge (β −0.90, 95% confidence interval [95% CI] −1.53 to −0.27, p = 0.0050) and lower ICU admission (odds ratio [OR] 0.30, 95% CI 0.10–0.87, p = 0.0050) (Table 3).

Subgroup analysis after PSM

To further analyze the potential of susceptible patients treated with TRQ, a series of subgroup analyses were conducted among frequent AECOPD inpatients with PEACE scores >7 or ≤7 on admission and different phlegm-heat symptom complex. As shown in Table 4 and supplementary table 2, among those with PEACE score >7 on

TABLE 4 Subgroup analyses on treatment and clinical outcomes of inpatients with frequent AECOPD after propensity match.

Characteristics	Total	TRQ	Without TRQ	p	Total	TRQ	Without TRQ	p
PEACE on admission	>7				≤7			
	N = 615	N = 205	N = 410		N = 672	N = 224	N = 448	
PEACE at discharge	4.0 (3.0, 4.0)	4.0 (3.0, 4.0)	4.0 (3.0, 4.0)	0.3084	3.0 (2.0, 4.0)	3.0 (2.0, 4.0)	3.0 (2.0, 4.0)	0.4652
CAT at discharge	13.0 (10.0, 18.0)	12.0 (8.5, 16.0)	13.0 (10.0, 19.0)	0.0084	12.0 (9.0, 17.0)	12.0 (8.0, 16.0)	12.0 (9.0, 17.0)	0.0921
PEACE difference	−6.0 (−7.0, −4.0)	−6.0 (−7.0, −4.0)	−5.0 (−7.0, −4.0)	0.5022	−3.0 (−4.0, −2.0)	−3.0 (−4.0, −2.0)	−3.0 (−4.0, −2.0)	0.4585
mMRC at discharge	2.0 (1.0, 2.0)	2.0 (1.0, 2.0)	2.0 (1.0, 2.0)	0.361	1.0 (1.0, 2.0)	1.0 (1.0, 2.0)	1.5 (1.0, 2.0)	0.3015
mMRC difference	−1.0 (−2.0, −1.0)	−1.0 (−2.0, −1.0)	−1.0 (−2.0, −1.0)	0.5721	−1.0 (−1.0, 0.0)	−1.0 (−1.0, 0.0)	−1.0 (−1.0, 0.0)	0.5021
length of hospital stay, days	12.0 (9.0, 15.0)	12.0 (10.0, 15.0)	12.0 (9.0, 15.0)	0.2145	10.0 (8.0, 13.0)	11.0 (9.0, 13.0)	10.0 (8.0, 13.0)	0.0112
Total cost of hospitalization (USD)	1652.8 (1175.9, 2406.4)	1607.0 (1140.9, 2211.8)	1690.7 (1197.3, 2530.5)	0.1570	1362.2 (1013.2, 1898.8)	1354.4 (996.3, 1738.3)	1366.4 (1017.2, 1993.2)	0.2520
Death or worsening in the hospital	6 (1.0)	1 (0.5)	5 (1.2)	0.3558	2 (0.3)	1 (0.4)	1 (0.2)	0.6269
ICU admission	17 (2.8)	2 (1.0)	15 (3.7)	0.0557	8/671 (1.2)	1/223 (0.4)	7/448 (1.6)	0.1739
Oxygen support				0.2748				0.2175
No oxygen support	58 (9.4)	20 (9.8)	38 (9.3)		96 (14.3)	30 (13.4)	66 (14.7)	
Tube/mask	474 (77.1)	163 (79.5)	311 (75.9)		507 (75.4)	166 (74.1)	341 (76.1)	
HFNC	8 (1.3)	1 (0.5)	7 (1.7)		4 (0.6)	2 (0.9)	2 (0.4)	
NPPV	72 (11.7)	21 (10.2)	51 (12.4)		63 (9.4)	24 (10.7)	39 (8.7)	
IPPV	3 (0.5)	0 (0.0)	3 (0.7)		2 (0.3)	2 (0.9)	0 (0.0)	
Antibiotics	587/614 (95.6)	194/205 (94.6)	393/409 (96.1)	0.4073	612 (91.1)	209 (93.3)	403 (90.0)	0.1513
Corticosteroid	511/614 (83.2)	168/205 (82.0)	343/409 (83.9)	0.5499	540 (80.4)	176 (78.6)	364 (81.3)	0.41
Phlegm-heat symptom complex on admission	≥2				<2			
	N = 531	N = 177	N = 354		N = 834	N = 278	N = 556	
PEACE at discharge	3.0 (2.0, 4.0)	3.0 (2.0, 4.0)	3.0 (3.0, 4.0)	0.3992	3.0 (2.0, 4.0)	3.0 (2.0, 4.0)	3.0 (2.0, 4.0)	0.6273
CAT at discharge	13.0 (9.0, 17.0)	12.0 (8.0, 16.0)	13.0 (9.0, 18.0)	0.0145	12.0 (9.0, 17.0)	12.0 (9.0, 17.0)	12.0 (9.0, 18.0)	0.6000
PEACE difference	−6.0 (−7.0, −4.0)	−6.0 (−7.0, −4.0)	−5.0 (−7.0, −4.0)	0.2391	−4.0 (−5.0, −2.0)	−4.0 (−5.0, −2.0)	−4.0 (−5.0, −2.0)	0.8013
mMRC at discharge	2.0 (1.0, 2.0)	2.0 (1.0, 2.0)	2.0 (1.0, 2.0)	0.0676	2.0 (1.0, 2.0)	2.0 (1.0, 2.0)	2.0 (1.0, 2.0)	0.5671
mMRC difference	−1.0 (−2.0, −1.0)	−1.0 (−2.0, −1.0)	−1.0 (−2.0, 0.0)	0.06	−1.0 (−2.0, 0.0)	−1.0 (−2.0, 0.0)	−1.0 (−2.0, 0.0)	0.4352

(Continued on following page)

10.3389/fphar.2023.1118143

TABLE 4 (*Continued*) Subgroup analyses on treatment and clinical outcomes of inpatients with frequent AECOPD after propensity match.

Phlegm-heat symptom complex on admission	≥2			<2			
	N = 531	N = 177	N = 354		N = 834	N = 278	N = 556	
length of hospital stay, days	11.0 (9.0, 15.0)	12.0 (10.0, 15.0)	11.0 (9.0, 15.0)	0.3357	11.0 (9.0, 14.0)	11.0 (9.0, 14.0)	11.0 (8.0, 13.0)	0.0413
Total cost of hospitalization (USD)	1616.8 (1172.8, 2274.5)	1652.0 (1239.2, 2264.2)	1585.8 (1159.7, 2275.4)	0.5277	1415.3 (1011.3, 2013.3)	1331.5 (978.7, 1801.3)	1485.7 (1023.5, 2136.8)	0.0126
Death or worsening in the hospital	3 (0.6)	0 (0.0)	3 (0.8)	0.1182	6 (0.7)	2 (0.7)	4 (0.7)	1.0000
ICU admission	5 (0.9)	0 (0.0)	5 (1.4)	0.0434	23/833 (2.8)	4/277 (1.4)	19/556 (3.4)	0.1015
Oxygen support				0.5143				0.3974
No oxygen support	52 (9.8)	20 (11.3)	32 (9.0)		97 (11.6)	35 (12.6)	62 (11.2)	
Tube/mask	420 (79.1)	135 (76.3)	285 (80.5)		627 (75.2)	214 (77.0)	413 (74.3)	
HFNC	6 (1.1)	2 (1.1)	4 (1.1)		8 (1.0)	2 (0.7)	6 (1.1)	
NPPV	51 (9.6)	20 (11.3)	31 (8.8)		98 (11.8)	25 (9.0)	73 (13.1)	
IPPV	2 (0.4)	0 (0.0)	2 (0.6)		4 (0.5)	2 (0.7)	2 (0.4)	
Antibiotics	500/530 (94.3)	168/177 (94.9)	332/353 (94.1)	0.6847	766 (91.8)	263 (94.6)	503 (90.5)	0.0396
Corticosteroid	436/530 (82.3)	145/177 (81.9)	291/353 (82.4)	0.8835	673 (80.7)	219 (78.8)	454 (81.7)	0.3209

Note. The phlegm-heat symptom complex includes fever, pharyngalgia, expectoration, and purulent sputum. Data were expressed as n (%) or median (interquartile range), where appropriate. *p* values were calculated by the Mann-Whitney *U* test, Chi-square test, or Fisher exact test, where appropriate. Abbreviations: COPD, chronic obstructive pulmonary disease; AECOPD, acute exacerbation of COPD; TRQ, tanreqing injection; CAT, the COPD assessment test; mMRC, modified British medical research council; ICU, intensive care unit; HFNC, high-flow nasal cannula oxygen therapy; NPPV, non-invasive positive pressure ventilation; IPPV, invasive positive pressure ventilation.

10.3389/fphar.2023.1118143

admission, TRQ contributed to a significantly lower CAT score at discharge (TRQ median 12.0, IQR 8.5–16.0; non-TRQ median 13.0, median 10.0–19.0, $p = 0.0084$) and numerically lower ICU admission rate with marginal statistical significance (TRQ 1.0%; non-TRQ 3.7%, $p = 0.0557$). Among those with phlegm-heat symptom complex on admission ≥2, lower CAT score at discharge and lower ICU admission were also observed in the TRQ group ($p = 0.0145$ and 0.0434, respectively); among those with phlegm-heat symptom complex on admission <2, TRQ contributed to the lower total cost of hospitalization ($p = 0.0126$) (Table 4). The treatment of TRQ may prolong the length of hospital stay in patients with phlegm-heat symptom complex on admission ≥1 ($p = 0.0271$) but still be effective in lowering CAT score at discharge among those without any phlegm-heat symptom complex ($p = 0.0438$) (Supplementary Table S2).

Discussion

This was a real-world, national wide, multi-center registry study investigating the efficacy of TQR injection in the treatment of AECOPD Patients. In this study, we found TRQ was effective in lowering CAT score at discharge and ICU admission rate, especially for those with phlegm-heat symptom complex on admission ≥2 and PEACE score >7 on admission among frequent AECOPD patients. For those with infrequent AECOPD, the efficacy is to be further explored. The results of our study provided robust support to the real-world evidence on the clinical use of TRQ and clues for the future investigation of mechanisms of TRQ.

In traditional Chinese medicine, COPD is placed in the same category as cough, dyspnea, and lung distention. Patients with AECOPD often have a series of symptoms of exacerbated cough, increased amounts of sputum, purulent sputum, and fever belonging to the Chinese medicine syndrome of phlegm-heat congestion of the lungs. For such a syndrome, the common treatment principle is clearing the heat and dissipating the phlegm (Li et al., 2010). TRQ consists of Scutellariae radix (SR, *Scutellaria baicalensis* Georgi), bear bile powder (BBP, Selenaretos thibetanus Cuvier), Cornu Caprae Hicus (CCH, Naemorhedus goral Hardwicke), Lonicerae japonicae flos (LJF, *Lonicera japonica* Thunb.), and Forsythiae fructus (FF, *Forsythia suspensa* (Thunb.) Vahl), and it is in accordance with the formulation of Tanreqing injection for treating syndromes including fever, cough, and expectoration (Han et al., 2022).

In our study, TRQ injection was effective in frequent AECOPD inpatients instead of infrequent patients. Frequent and infrequent AECOPD has been recently considered as different phenotypes: patients with frequent exacerbations may have increased airway inflammation in a stable state. More frequent exacerbations were associated with greater impairment in health status, a history of gastroesophageal reflux, and an elevated white-cell count (Hurst et al., 2010).

Modern pharmacological studies have found that Scutellaria baicalensis contained in TRQ injection has antioxidant, free radical scavenging, anti-infection, and antiviral effects; bear gall has anti-infective, sedative, and antispasmodic effects; goat horn has a strong antipyretic effect; honeysuckle contains chlorogenic acid and isochlorogenic acid, which has broad-spectrum antibacterial effect (Jiao et al., 2019). Moreover, laboratory studies showed that effective constituents of TRQ injection promoted the anti-inflammation progress in AECOPD patients. TRQ may improve lung function by inhibiting airway mucus hypersecretion and alleviating airway obstruction and inflammatory injury. Its action pathway may include inhibiting MAPK/NF-κB, which regulates IL-10 and TNF-α release, as well as regulating MUC5AC mRNA expression, which attenuates airway inflammation, airway damage, and mucus hypersecretion (Han et al., 2022). Several clinical studies have suggested that TRQ can regulate cytokines in AECOPD patients, reduce the activation and recruitment of neutrophils and other inflammatory cells in the respiratory tract, slow down the inflammatory process, and promote patient recovery (Yang et al., 2014; Yong et al., 2015). In our study, inpatients with frequent AECOPD were with significantly higher inflammation levels, compared to those with infrequent AECOPD. The drug reaction of TRQ may be influenced by inflammation status, but more studies are needed to verify this finding.

Patients with frequent AECOPD were known for risk factors such as a long time of COPD diagnosis, a larger amount of daily sputum production, higher mMRC score, lower predicted FEV1, and hospitalization during the previous year (Le Rouzic et al., 2018). Our study was consistent with previous findings and also found that inpatients with frequent AECOPD had a higher rate of death, ICU admission, and systemic corticosteroid use, compared with those with infrequent AECOPD. This indicated that among frequent AECOPD patients, antibiotic resistance may be common and inflammation status of the host has been changed for long-term, high-dose corticosteroids as well. As a classic traditional Chinese medicine, TRQ functions in the regulation of homeostasis and rebalance, thus contributing to the recovery of frequent AECOPD, especially for those with more than two phlegm-heat symptoms on admission.

Our study has some limitations. Firstly, we lacked data on biomarkers in our study, making it difficult to analyze the efficacy of TRQ combined with inflammation status. Secondly, the information on the use of antibiotics was missing. Patients with frequent or infrequent AECOPD may be administered with different grades of antibiotics and have different drug resistance statuses, which possibly impacts the course of treatment, length of hospital stay, and clinical outcomes as well. Thirdly, the follow-up data on rehospitalization were temporarily unavailable, therefore we were unable to evaluate the long-term efficacy of TRQ. However, our study revealed that the short-term efficacy was significant and provided important clues for future studies.

Conclusion

TRQ injection had better efficacy in patients with frequent AECOPD in reducing ICU admission and alleviating respiratory symptoms, especially for those with higher severity on admission or more phlegm-heat symptoms. TRQ may have the potential to improve the long-term prognosis of AECOPD, but more studies are needed to verify this.

Data availability statement

The raw data supporting the conclusion of this article will be made available by the authors, without undue reservation.

Ethics statement

The studies involving human participants were reviewed and approved by the ethics committee of China-Japan Friendship Hospital (No. 2015-88). The patients/participants provided their written informed consent to participate in this study.

Author contributions

GF, DW, and SW had full access to all the data in this study, conceived the analysis, and took responsibility for the integrity and accuracy of the analysis. Concept and design: GF, DW, SW, FD, KH, YC, HZ, CW, and TY. Data collection and management: GF, DW, KH, FD, YC, HZ, CW, and TY. Statistical analysis: GF and DW. Drafting of the manuscript: GF and DW. All authors: Clinical interpretation of results, critical revision of the manuscript for intellectual content, agreement on the journal to which the manuscript should be submitted, approval of the final manuscript to be submitted, and agreement to be accountable for the contents of the manuscript.

Funding

National High Level Hospital Clinical Research Funding (2022-NHLHCRF-LX-01-01-01); CAMS Innovation Fund for Medical Sciences (2021-I2M-1-049); Respiratory Disease Clinical Research Public Welfare Program of China Song Qingling Foundation (2018MZFC-032). The funders of the study had no role in study design, data collection and management, data analysis, data interpretation, writing of the manuscript, and the decision to submit the manuscript for publication.

Acknowledgments

The authors thank all participants, staff, and investigators involved in the ACURE from all participating sites for their efforts in providing and collecting the data used in this study.

Conflict of interest

The authors declare that the research was conducted in the absence of any commercial or financial relationships that could be construed as a potential conflict of interest.

Publisher's note

All claims expressed in this article are solely those of the authors and do not necessarily represent those of their affiliated organizations, or those of the publisher, the editors and the reviewers. Any product that may be evaluated in this article, or claim that may be made by its manufacturer, is not guaranteed or endorsed by the publisher.

Supplementary material

The Supplementary Material for this article can be found online at: https://www.frontiersin.org/articles/10.3389/fphar.2023.1118143/full#supplementary-material

References

Chen, X., Kang, F., Lai, J., Deng, X., Guo, X., and Liu, S. (2022). Comparative effectiveness of phlegm-heat clearing Chinese medicine injections for AECOPD: A systematic review and network meta-analysis. *J. Ethnopharmacol.* 292, 115043. doi:10.1016/j.jep.2022.115043

GBD Chronic Respiratory Disease Collaborators (2020). Prevalence and attributable health burden of chronic respiratory diseases, 1990–2017: A systematic analysis for the global burden of disease study 2017. *Lancet Respir. Med.* 8 (6), 585–596.

Global strategy for the diagnosis, management and prevention of chronic obstructive pulmonary disease (2017). Global initiative for chronic obstructive lung disease (GOLD) committees. Available at: https://goldcopd.org/wp-content/uploads/2017/02/wms-GOLD-2017-FINAL.pdf (*Accessed December 1, 2018*).

Global strategy for the diagnosis, management and prevention of chronic obstructive pulmonary disease (2022). Global initiative for chronic obstructive lung disease (GOLD) committees. Available at: https://goldcopd.org/wp-content/uploads/2021/12/GOLD-REPORT-2022-v1.1-22Nov2021_WMV.pdf (*Accessed November 3, 2022*).

Han, X. X., Tian, Y. G., Liu, X. F., Zhao, D., Du, X. H., Dong, H. R., et al. (2022). Network pharmacology combined with pharmacodynamics revealed the anti-inflammatory mechanism of Tanreqing capsule against acute-exacerbation chronic obstructive pulmonary disease. *Sci. Rep.* 12 (1), 13967. doi:10.1038/s41598-022-18326-1

Hu, H., Ji, Z., Qiang, X., Liu, S., Sheng, X., Chen, Z., et al. (2021). Chinese medical injections for acute exacerbation of chronic obstructive pulmonary disease: A network meta-analysis. *Int. J. Chron. Obstruct Pulmon Dis.* 16, 3363–3386. doi:10.2147/COPD.S335579

Hurst, J. R. V. J., Anzueto, A., Locantore, N., Müllerova, H., Tal-Singer, R., Miller, B., et al. (2010). Susceptibility to exacerbation in chronic obstructive pulmonary disease. *N. Engl. J. Med.* 363 (12), 1128–1138. doi:10.1056/NEJMoa0909883

Jiao, W. U., Wang, C., Hai-Chuan, Y. U., Pharmacy, S. O., and XmjcjoETMF, U. (2019). *Chemical constituents and pharmacological effect of Lonicerae japonicae flos.*

Ko, F. W., Chan, K. P., Hui, D. S., Goddard, J. R., Shaw, J. G., Reid, D. W., et al. (2016). Acute exacerbation of COPD. *Respirology* 21 (7), 1152–1165. doi:10.1111/resp.12780

Le Rouzic, O., Roche, N., Cortot, A. B., Tillie-Leblond, I., Masure, F., Perez, T., et al. (2018). Defining the "frequent exacerbator" phenotype in COPD: A hypothesis-free approach. *Chest* 153 (5), 1106–1115. doi:10.1016/j.chest.2017.10.009

Li, W., Mao, B., Wang, G., Wang, L., Chang, J., Zhang, Y., et al. (2010). Effect of Tanreqing Injection on treatment of acute exacerbation of chronic obstructive pulmonary disease with Chinese medicine syndrome of retention of phlegm and heat in Fei. *Chin. J. Integr. Med.* 16 (2), 131–137. doi:10.1007/s11655-010-0131-y

Liang, C., Mao, X., Niu, H., Huang, K., Dong, F., Chen, Y., et al. (2021). Characteristics, management and in-hospital clinical outcomes among inpatients with acute exacerbation of chronic obstructive pulmonary disease in China: Results from the phase I data of ACURE study. *Int. J. Chron. Obstruct Pulmon Dis.* 16, 451–465. doi:10.2147/COPD.S281957

Mullerova, H., Shukla, A., Hawkins, A., and Quint, J. (2014). Risk factors for acute exacerbations of COPD in a primary care population: A retrospective observational cohort study. *BMJ Open* 4 (12), e006171. doi:10.1136/bmjopen-2014-006171

Ouaalaya, E. H., Falque, L., Dupis, J. M., Sabatini, M., Bernady, A., Nguyen, L., et al. (2020). Susceptibility to frequent exacerbation in COPD patients: Impact of the exacerbations history, vaccinations and comorbidities? *Respir. Med.* 169, 106018. doi:10.1016/j.rmed.2020.106018

Pei, Z., Sun, Y., Wang, S., Chen, Y., Yang, T., Huang, K., et al. (2020). Estimating mortality among inpatients with acute exacerbation of chronic obstructive pulmonary disease using registry data. *NPJ Prim. Care Respir. Med.* 30 (1), 28. doi:10.1038/s41533-020-0186-y

Rothnie, K. J., Mullerova, H., Smeeth, L., and Quint, J. K. (2018). Natural history of chronic obstructive pulmonary disease exacerbations in a general practice-based population with chronic obstructive pulmonary disease. *Am. J. Respir. Crit. Care Med.* 198 (4), 464–471. doi:10.1164/rccm.201710-2029OC

Seemungal, T. A. D. G., Bhowmik, A., Jeffries, D. J., and Wedzicha, J. A. (2000). Time course and recovery of exacerbations in patients with chronic obstructive pulmonary disease. *Am. J. Respir. Crit. Care Med.* 161 (5), 1608–1613. doi:10.1164/ajrccm.161.5.9908022

Wang, C., Xu, J., Yang, L., Xu, Y., Zhang, X., Bai, C., et al. (2018). Prevalence and risk factors of chronic obstructive pulmonary disease in China (the China pulmonary health [CPH] study): A national cross-sectional study. *Lancet* 391 (10131), 1706–1717. doi:10.1016/S0140-6736(18)30841-9

Wang, L., Fan, Y., Xu, J., Deng, H., Geng, C., and Jia, B. (2020). The efficacy and safety of tanreqing injection combined with Western medicine for severe pneumonia: A protocol for systematic review and meta-analysis. *Med. Baltim.* 99 (35), e22010. doi:10.1097/MD.0000000000022010

Wedzicha, J. A. B. S., Allinson, J. P., and Donaldson, G. C. (2013). Mechanisms and impact of the frequent exacerbator phenotype in chronic obstructive pulmonary disease. *BMC Med.* 14 (11), 181. doi:10.1186/1741-7015-11-181

Wedzicha, J. A., and Terence, A. S. (2007). COPD exacerbations: Defining their cause and prevention. *Lancet* 370 (9589), 786–796. doi:10.1016/S0140-6736(07)61382-8

Yang, J., Chen, X. X., Huang, F., Sun, S. Y., and Stomatology, D. (2014). *Effect of LPS on expression of TLR4 and the downstream cytokines in PDLCs*.

Yong, D. U., Jie, Z. J., and HejcjoN, W. (2015). *Study of influence of Tanreqing injection on serum high-sensitivity C-reactive protein and procalcitonin of patients with acute exacerbation of chronic obstructive pulmonary disease*.

Zheng, J. P., Kang, J., Huang, S. G., Chen, P., Yao, W. Z., Yang, L., et al. (2008). Effect of carbocisteine on acute exacerbation of chronic obstructive pulmonary disease (PEACE study): A randomised placebo-controlled study. *Lancet* 371 (9629), 2013–2018. doi:10.1016/S0140-6736(08)60869-7

frontiers | Frontiers in Pharmacology

TYPE Original Research
PUBLISHED 04 April 2023
DOI 10.3389/fphar.2023.1155414

OPEN ACCESS

EDITED BY
Na Wang,
Tongji University, China

REVIEWED BY
Bhaskar Saha,
University of New Mexico, United States
Qiuhua Yang,
Augusta University, United States
Changwen Deng,
Tongji University, China

*CORRESPONDENCE
Zhilong Jia,
jiazhilong@plagh.org
Xiaojing Zhao,
xjingzhao@126.com
Kunlun He,
kunlunhe@plagh.org

†These authors have contributed equally to this work

SPECIALTY SECTION
This article was submitted to Respiratory Pharmacology, a section of the journal Frontiers in Pharmacology

RECEIVED 31 January 2023
ACCEPTED 23 March 2023
PUBLISHED 04 April 2023

CITATION
Tian L, Jia Z, Yan Y, Jia Q, Shi W, Cui S, Chen H, Han Y, Zhao X and He K (2023), Low-dose of caffeine alleviates high altitude pulmonary edema *via* regulating mitochondrial quality control process in AT1 cells.
Front. Pharmacol. 14:1155414.
doi: 10.3389/fphar.2023.1155414

Low-dose of caffeine alleviates high altitude pulmonary edema *via* regulating mitochondrial quality control process in AT1 cells

Liuyang Tian[1,2,3†], Zhilong Jia[3,4*†], Yan Yan[5], Qian Jia[3,5], Wenjie Shi[6], Saijia Cui[5], Huining Chen[5], Yang Han[2,3,5], Xiaojing Zhao[3,5*] and Kunlun He[2,3,1*]

[1]School of Medicine, Nankai University, Tianjin, China, [2]Medical Big Data Research Center, Medical Innovation Research Division of Chinese PLA General Hospital, Beijing, China, [3]National Engineering Research Center for Medical Big Data Application Technology, Chinese PLA General Hospital, Beijing, China, [4]Center for Artificial Intelligence in Medicine, Medical Innovation Research Division of Chinese PLA General Hospital, Beijing, China, [5]Research Center for Translational Medicine, Medical Innovation Research Division of Chinese PLA General Hospital, Beijing, China, [6]Technical Research Centre for Prevention and Control of Birth Defects, Medical Innovation Research Division of Chinese PLA General Hospital, Beijing, China

Backgrounds: High-altitude pulmonary edema (HAPE) is a life-threatening disease without effective drugs. Caffeine is a small molecule compound with antioxidant biological activity used to treat respiratory distress syndrome. However, it is unclear whether caffeine plays a role in alleviating HAPE.

Methods: We combined a series of biological experiments and label-free quantitative proteomics analysis to detect the effect of caffeine on treating HAPE and explore its mechanism *in vivo* and *in vitro*.

Results: Dry and wet weight ratio and HE staining of pulmonary tissues showed that the HAPE model was constructed successfully, and caffeine relieved pulmonary edema. The proteomic results of mice lungs indicated that regulating mitochondria might be the mechanism by which caffeine reduced HAPE. We found that caffeine blocked the reduction of ATP production and oxygen consumption rate, decreased ROS accumulation, and stabilized mitochondrial membrane potential to protect AT1 cells from oxidative stress damage under hypoxia. Caffeine promoted the PINK1/parkin-dependent mitophagy and enhanced mitochondrial fission to maintain the mitochondria quality control process.

Conclusion: Low-dose of caffeine alleviated HAPE by promoting PINK1/parkin-dependent mitophagy and mitochondrial fission to control the mitochondria quality. Therefore, caffeine could be a potential treatment for HAPE.

Abbreviations: HAPE, High-altitude pulmonary edema; AHAI, Acute high altitude illness; HIF-1α, hypoxia-inducible factor-1α; VEGF, vascular endothelial growth factor; ROS, reactive oxygen species; RDS, respiratory distress syndrome; UPLC, ultra-performance liquid chromatography; LFQ, label-free quantitation; DEPs, differentially expressed proteins; GO, Gene Ontology; KEGG, Kyoto Encyclopedia of Genes and Genomes; AT1, Type I alveolar epithelial; FBS, Fetal bovine serum; OCR, oxygen consumption rate; ECAR, extracellular acidification rate; 2-DG, 2-deoxy-D-glucose; MMP, mitochondrial membrane potential; PCA, Principal component analysis; DRP1, dynamin related protein 1; PGC-1α, peroxisome proliferator-activated receptor-γ coactivator-1-α.

KEYWORDS

caffeine, high altitude pulmonary edema (HAPE), mitochondrial, mitochondrial quality control, proteomics

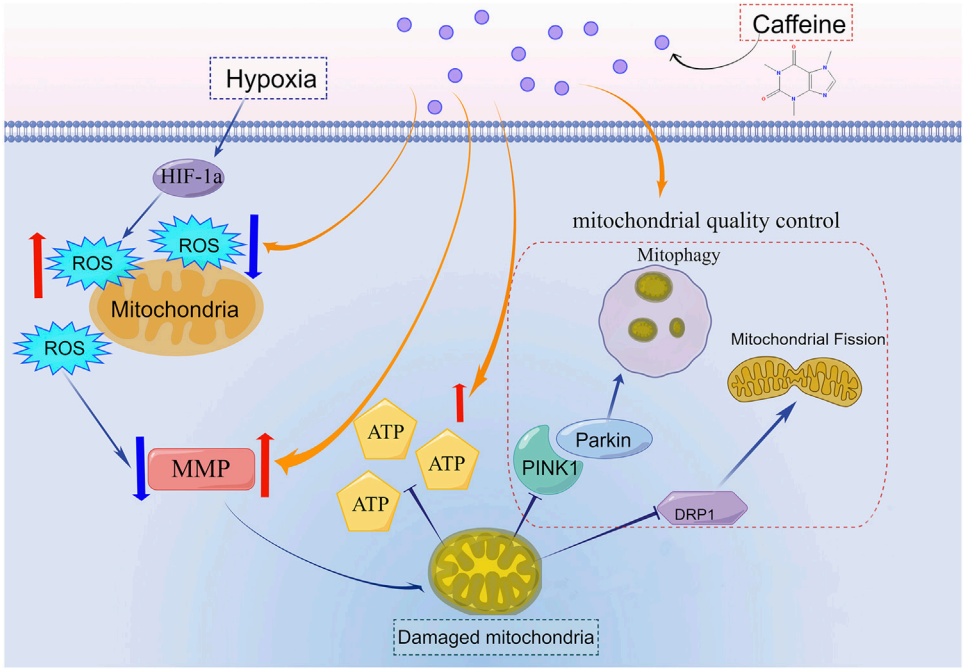

GRAPHICAL ABSTRACT

Highlights

- Caffeine alleviated high altitude pulmonary edema *in vivo*.
- Caffeine reduced oxidative stress and stabilized mitochondrial morphology in AT1 cells under hypoxia.
- Caffeine alleviated HAPE by regulating the PINK1/Parkin-mediated mitophagy, mitochondrial fission, and mitochondrial biogenesis to maintain the quality control of mitochondria.

1 Introduction

Acute high altitude illness (AHAI) frequently occurs when a person ascends to a high altitude of more than 2500 m (m), which is hypoxic, hypobaric, and ultraviolet intensive (Khodaee et al., 2016). The incidence of AHAI is approximately 50%–85% for unacclimatized individuals at 4500–5500 m (Hackett et al., 1976). High altitude pulmonary edema (HAPE) is a severe subtype of AHAI, which is characterized by pulmonary edema, dyspnea, lung moist rales, cyanosis, dry cough with exertion, and pink frothy sputum (Swenson and Bartsch, 2021). The mortality rate of individuals with untreated HAPE is approximately 50% (Yanamandra et al., 2019). The typical pathogenesis of HAPE is pulmonary edema caused by excessive pulmonary vasoconstriction and abnormally high pulmonary pressures (Sharma Kandel et al., 2020). In the guidelines for prevention and treatment of acute altitude illness, acetazolamide, nifedipine, sildenafil, salmeterol, and dexamethasone are drugs used for the prevention of HAPE; acetazolamide, a diuretic, and dexamethasone are drugs used for the treatment of HAPE. However, the effectiveness of these therapies was unsatisfactory (Luks et al., 2019; Luks and Hackett, 2022). The plateau environment is a natural hypoxic environment. Hypoxia induces reactive oxygen species (ROS) accumulation and leads to oxidative stress damage in multiple diseases, such as inflammation (McGarry et al., 2018), cardiovascular disease (Giussani et al., 2014), and lung damage (Tuleta et al., 2016). Hence, inhibiting oxidative stress damage has the potential to protect the lungs from damage, holding the promise of treating HAPE.

Caffeine is a natural methylxanthine occurring in several beverages, such as coffee, tea, and cola, which is often used to fight fatigue and boost energy levels (Szlapinski et al., 2023). Caffeine has both pro-oxidative stress and anti-oxidative stress properties depending upon the dosage. Min et al. reported that intake of 10 mM caffeine causes mitochondrial dysfunction and increases oxidative stress by decreasing the level of phosphoethanolamine (PE) (Min et al., 2020). While several studies reviewed that a low dose of caffeine (10 μM) can protect several tissues from hypoxic damage by inhibiting oxidative stress damage (Ikram et al., 2020; Marte et al., 2020; Barrea et al., 2021). Such as, reducing renal fibrosis (Nilnumkhum et al., 2019), promoting neonatal neuronal survival (Li et al., 2019), and alleviating ultraviolet-induced skin senescence (Li et al., 2018).

Recent studies have revealed that caffeine is widely used to treat respiratory distress syndrome (RDS) in premature infants and improve the prognosis (Ren et al., 2015; Ines et al., 2021; Elmowafi et al., 2022). The leading cause of RDS is increased pulmonary capillary permeability caused by inflammation and endothelial dysfunction (Millar et al., 2016). The antioxidant is essential in protecting human pulmonary artery endothelial cells against excessive permeability, alleviating acute

RDS (Li et al., 2020). HAPE has similar symptoms and pathological changes as RDS. However, there are no reports on whether caffeine plays a role in alleviating HAPE.

In this study, we found that a low dose of caffeine neutralized oxidative stress damage in AT1 cells by upregulating the expression of multiple genes involved in mitochondrial dynamics and mitophagy under hypoxic conditions. Caffeine promoted the PINK1/parkin-dependent mitophagy and mitochondrial fission to control the mitochondria quality both *in vivo* and *in vitro*. Moreover, we also found that pulmonary congestion and alveolar structural destruction caused by hypoxia were alleviated by caffeine in the lungs. Collectively, our results indicated that caffeine could be a potential treatment for HAPE.

2 Materials and methods

2.1 Animal care

Eight-week-old male C57BL/6 mice were purchased from SPF (Beijing) Biotechnology (Beijing, China). Animals were fed under conditions of constant humidity (50% ± 5%), temperature (23°C ± 2°C), and illumination (12 h light/dark cycles). All animal experiments were conducted following the National Institutes of Health's Guide for the Care and Use of Laboratory Animals (NIH publication No. 80–23, revised in 1996). The Animal Ethics Committee of the Chinese PLA General Hospital (SQ2020030) approved all experimental procedures involving animals.

2.2 Mice and caffeine treatment

Mice were divided into three groups randomly (n = 6 in each) which received: (1) Control group (Con); (2) Mice were exposed to hypobaric hypoxic conditions for 3 days (Hypoxia group, Hypo); To construct the mice models of high altitude pulmonary edema, we exposed mice to a hypobaric hypoxic chamber for 3 days, which referred to our previous studies and reported methods (Ni et al., 2014; Tian et al., 2021). (3) Mice were exposed to hypobaric hypoxic conditions 3 days, and given caffeine intervention by oral gavage caffeinated water (Velazquez et al., 2020; Szlapinski et al., 2023) (Caffeine from Sigma–Aldrich, St. Louis, MO, U.S., 0.2 g/kg/d, dose volume of 10 mL/kg/d body weight) (Hypoxia + caffeine group, Hypo + Caf). The human equivalent dose based on body surface area (Km value for humans = 37 and for mice weighing 25 g = 3) was 2.5 mg/kg/day (Nair and Jacob, 2016), which was approximately 1-2 cups of canned coffee or specialty espresso (McGuire, 2014). The hypobaric hypoxic environment was constructed to simulate a 5,500-m-high atmospheric environment using a FLYDWC50-1C hypobaric hypoxic cabin (Guizhou Fenglei Air Ordnance LTD., Guizhou, China).

2.3 HE staining

The lung specimens were fixed in 4% paraformaldehyde overnight, embedded in paraffin, and sectioned into 6 μm thick slices. Tissue sections were stained with hematoxylin for 5 min and eosin for 3 min. HE-stained sections were analyzed using an optical microscope (Nikon, Japan).

2.4 Dry and wet weight ratio of lung

The pulmonary dry and wet weight ratio reveals the severity of pulmonary edema. To calculate the dry/wet ratio, we weighed the whole left lung at the initial removal and after drying it in an oven at a temperature of 160°C for 72 h.

2.5 LC-MS analysis

Liquid chromatography-tandem mass spectrometry (LC-MS) was carried out as described previously (Goldman et al., 2019). Briefly, cells or lungs were sonicated three times on ice using a high-intensity ultrasonic processor (Scientz, China) in the lysis buffer. Then the proteins were digested by trypsin. The peptides were subjected to NSI source followed by tandem mass spectrometry (MS) in Q Exactive TM Plus (ThermoFisher Scientific, U.S.) coupled online to the ultra-performance liquid chromatography (UPLC). The proteomic experiments of lungs were finished by the ptm-biolab (Hangzhou, China). The proteomic experiments of AT1 cells were completed by Metware Biotechnology Co. (Wuhan, China). The resulting LC-MS data were processed using the Maxquant search engine (v.1.5.2.8). The minimum score for modified peptides was set at> 40, and FDR was <1%. The LFQ (label-free quantitation) intensity was mean-based scaled per protein in all the samples, which was used in the downstream analysis.

2.6 Differential expression analysis

The analysis of differentially expressed proteins (DEPs) was implemented through the Limma package in the R language. The DEPs are defined as $|\log FC|>1.5$ and p-value < 0.05. Proteins with logFC >1.5 are defined as upregulated proteins. Proteins with LogFC < −1.5 are defined as downregulated proteins.

2.7 GO annotation

Gene Ontology (GO) is a major bioinformatics initiative to unify the representation of genes and gene product attributes across all species (Ashburner et al., 2000). Gene Ontology (GO) annotation proteome was derived from the UniProt-GOA database (http://www.ebi.ac.uk/GOA/). Proteins were classified by Gene Ontology annotation based on three categories: biological process, cellular component, and molecular function.

2.8 KEGG pathway annotation

The Kyoto Encyclopedia of Genes and Genomes (KEGG) database were used to annotate protein pathways (Kanehisa et al., 2021). Firstly, using KEGG online service tool KAAS to annotate the protein's KEGG database description and then mapping the annotation result on the KEGG pathway database using KEGG online service tool KEGG mapper.

2.9 Enrichment of pathway analysis

The KEGG database was used to identify enriched pathways by a two-tailed Fisher's exact test to test the enrichment of the DEPs against all identified proteins. The pathway with a p-value <0.05 was considered significant.

2.10 Protein-protein interaction network

All DEPs were searched against the STRING database version 11.5 for protein-protein interactions (Szklarczyk et al., 2021). We fetched all interactions that had a confidence score ≥0.7 (high confidence) and visualized the interaction network using Cytoscape String App (Doncheva et al., 2019). The significant modules with a score ≥5 were screened out *via* MCODE.

2.11 The construction of the cell model

Type I alveolar epithelial (AT1) cells were purchased from Beijing Qianzhao Xinye Biology Science and Technology Company (Beijing, China). Cells were cultured in DMEM with 10% Fetal bovine serum (FBS) and 1% antibiotics (Penicillin and Streptomycin). The hypoxic model cells were constructed by exposure to 1% O_2 for 24 h, according to the pathological hypoxic cell model construction (McKeown, 2014).

2.12 Cell activity measurements

AT1 cells were seeded in the 96-well plate at 8000 cells/100 ul/well. The CCK-8 solution (Cell Counting Kit-8, Coolaber, Beijing) was added to each well according to the manufacturer's instructions. Plates were incubated at 37°C and measured the absorbance at 450 nm using a microplate reader (BioTek, U.S.). The concentration of 0 μM, 5 μM, 10 μM, 15 μM, 20 μM, 40 μM, and 80 μM caffeine were co-cultured with cells, and the optimum concentration was calculated.

2.13 Mitochondrial real-time ATP rate assay

AT1 cells were inoculated in a 24-well cell culture plate and incubated at 37°C with 5% CO_2 overnight. The following compounds were injected into the cell culture medium: oligomycin (1.5 μM), a mixture of rotenone (0.5 μM) and antimycin A (0.5 μM). The oxygen consumption rate (OCR) and extracellular acidification rate (ECAR) were measured by Seahorse XFe/XF24 Analyzers (Agilent Technologies, U.S.) according to instructions.

2.14 Mitochondrial Mito Stress Test kit assay

AT1 Cells were inoculated in a 24-well cell culture plate and incubated at 37°C with 5% CO_2 overnight. The following compounds were injected into the cell culture medium: oligomycin (1.0 μM), FCCP (1.0 μM), and a mix of rotenone and antimycin A (0.5 μM)) to measure ATP production, maximal respiration, and non-mitochondrial respiration, respectively.

2.15 Mitochondrial glycolysis rate assay

AT1 Cells were inoculated in a 24-well cell culture plate and incubated at 37°C with 5% CO_2 overnight. The following compounds were injected into the cell culture medium: a mixture of rotenone (0.5 μM) and antimycin A (0.5 μM), and 2-deoxy-D-glucose (2-DG, 500 mM). The proton efflux rate (PER) and glycolytic rate were measured by Seahorse XFe/XF24 Analyzers (Agilent Technologies, U.S.) according to instructions.

2.16 Determination of reactive oxygen species (ROS) in the cytoplasm and mitochondria

The CellROX™ Deep Red reagent is a novel fluorogenic probe for measuring cellular oxidative stress which is to be fluorescent upon oxidation by reactive oxygen species. The cytoplasmic ROS was measured using CellROX® Deep Red Reagent according to the manufacturer's instructions (CellROX® Oxidative Stress Reagents (C10422), ThermoFisher Scientific, U.S.). To detect the mitochondrial superoxide, we used the MitoSOX which could selectively detect the superoxide in the mitochondria of live cells (Kalyanaraman et al., 2012; Forman et al., 2015) (MitoSOX™ Red mitochondrial superoxide indicator (M36008), ThermoFisher Scientific, U.S.). Briefly, cells were incubated with the CellROX®/MitoSOX Reagent at a final concentration of 5/10 μM for 30 min at 37°C, then removed medium and washed cells three times with PBS. The cells were supplemented with an antifade mounting medium with DAPI. Images were acquired using the OLYMPUS FV1000 inverted confocal microscope (Japan).

2.17 Determination of mitochondrial membrane potential

The mitochondrial membrane potential (MMP) was measured using JC-1 (5′,6,6′-tetrachloro-1,1′,3,3′-tetraethylbenzimidazolylcarbocyanine iodide), which exhibits potential-dependent accumulation in mitochondria according to the manufacture instruction (MitoProbe™ JC-1 Assay Kit (M34152), ThermoFisher Scientific, U.S.). The JC-1 dye loading solution was diluted into a final concentration of 2 μM. Then, the cells were co-incubated with JC-1 dye at 37°C with 5% CO2 for 30 min. Then the medium was removed and cells were washed three times with PBS. The cells were supplemented with an antifade mounting medium with DAPI. Images were acquired using the OLYMPUS FV1000 inverted confocal microscope (Japan).

2.18 Immunofluorescence

For confocal immunofluorescence analysis, cells were fixed in 4% formaldehyde for 10 min, then permeated in 0.2% Triton X-100 for 5 min and blocked in 3% BSA for 2 h. The incubation condition was as follows: CoraLite®488-conjugated

TOM20 Monoclonal antibody (CL488-66777, Proteintech, China, 1:200 dilution), CoraLite®594-conjugated LAMP1 Monoclonal antibody (CL594-67300, Proteintech, China, 1:200 dilution), MTCO2 Mouse Monoclonal Antibody (A-6404, ThermoFisher Scientific, U.S., 1:200 dilution) and Parkin Polyclonal Antibody (PA5-13399, ThermoFisher Scientific, U.S., 1:50 dilution) at 4°C over-night. After being washed three times with TBST, the cells were co-incubated with/without fluor-conjugated goat anti-rabbit secondary antibody (red) (SA00013-4, Proteintech, China, 1: 200 dilution) and fluor-conjugated goat anti-mouse secondary antibody (green) (SA00013-1, Proteintech, China, 1: 200 dilution). The cells were supplemented with an antifade mounting medium with DAPI. Images were acquired using the OLYMPUS FV1000 inverted confocal microscope (Japan). Mitophagy was measured by the co-expression fluorescence of yellow dots (LAMP1 and Tom20 overlay) per field.

2.19 Transmission electron microscopy

The freshly harvested cells were processed as described previously (Labuschagne et al., 2019). The sections with a thickness of 70 nm were observed under an HT7800 transmission electron microscope (Hitachi, HT7800).

2.20 Isolation of mitochondria

Mitochondria were isolated by a mitochondrial isolation kit (Mitochondrial extraction Kit (SM0020), Beijing Solarbio Science & Technology Company, China). Briefly, the AT1 cells were washed three times with PBS and collected after centrifugation at 800 *g* for 10 min 500 μL lysis buffer was added to resuspend the cells. Then the cells were ground 30–40 times in a 0°C ice bath in a small-capacity glass homogenizer. Cell debris and nuclei were removed by centrifugation at 1000 *g* for 5 min, 4°C. And mitochondrial fractions were collected by centrifugation at 12,000 g for 15 min, 4°C.

2.21 Quantitative real-time PCR

AT1 cells were collected and washed 3 times with PBS. Trizol reagents were added to dissociate nucleoproteins (TRIzol™ (15596026), ThermoFisher Scientific, U.S.). Total RNA was extracted following the manufacturer's protocol. Then the total RNA was reversed into cDNA (GoTaq® qPCR Master Mix (A6001), Promega, U.S.). Quantitative RT-PCR analysis was actualized by Bio-Rad CFX96 Real-Time PCR Detection System (Bio-Rad, U.S.). The sequences of primers used in this study are listed in Supplementary Table S3.

2.22 Western blotting

The protein lysates were prepared in RIPA buffer and phenylmethylsulfonyl fluoride (Merck Millipore, U.S.). The concentration of protein was measured by the BCA assay (NO.23225, ThermoFisher Scientific, U.S.). The quality of 20 μg proteins was loaded per condition. Proteins were separated by 4%–20% SDS-polyacrylamide gel electrophoresis and then transferred to nitrocellulose membranes. The membranes were incubated in 5% milk for 2 h before incubation with primary antibodies at 4°C overnight. Primary antibodies were as follows: Platelet-type phosphofructokinase (PFKP, 8164, 1:1000 dilution), Pyruvate kinasem1/2 (PKM1/2, 3106, 1: 1000 dilution), Tom20 (42406, 1:1000 dilution), LC3A/B (4108, 1: 1000 dilution), PINK1(4946, 1:1000 dilution), Parkin (L211, 1: 1000 dilution), Bnip3L (12396, 1:1000 dilution) and FUNDC1 (49240, 1:1000 dilution) were purchased from Cell Signaling Technology (U.S.). DRP1 (ab56788, 1:1000 dilution) and Hexokinase II (ab209847, 1:1000 dilution), ACTIN (ab6276, 1:1000 dilution) were purchased from Abcam (U.S.). Glucose-6-phosphate isomerase protein (GPI, PA5-97517) and P-Ser65-Parkin (Ser65) (p-Parkin, PA5-114616) were purchased from ThermoFisher Scientific (U.S.), Tim23 (67535-1-Ig, 1:4000 dilution), PGC1α (66369-1-Ig, 1:10000 dilution) were purchased from Proteintech (China). After being washed three times with TBST, the membranes were incubated with corresponding secondary antibodies (1:5000 dilution) and visualized using the instrument Amersham imager 600 (GE Healthcare Life Sciences, U.S.). The relative levels of individual proteins to control ACTB/VDAC were analyzed by ImageJ software (Madison, WI, U.S.).

2.23 Statistical analysis

Results were represented by means ± S.D. Statistical analyses were performed using GraphPad Prism 8.0 Software (GraphPad Software Inc., America). The choice of statistical tests for pairwise comparisons was made based on whether the data satisfies a normal distribution and/or equal variance tests. For normally distributed continuous variables, an independent sample *t*-test was used for statistical significance between two experimental groups. Otherwise, a Mann-Whitney U test was deployed. *p*-value (p) < 0.05 was considered statistically significant.

3 Results

3.1 Caffeine alleviates HAPE might by regulating mitochondrial OXPHOS

To examine the effect of caffeine on alleviating HAPE, we conducted multi-level biological assays and bioinformatic analysis *in vivo and in vitro*. The schematic overview of our experimental workflow was shown in Figure 1. We found that pulmonary congestion and alveolar structural destruction were severe after hypobaric hypoxia intervention, but caffeine attenuated these changes (Figure 2A). Compared with the control group, the dry and wet weight ratio (D/W weight ratio) significantly declined in the Hypo group (16% reduction, $p = 0.0001$, Figure 2B), suggesting severe pulmonary edema. Notably, caffeine neutralized the decrease in the dry and wet weight ratio (16% increase, $p = 0.0004$, Figure 2B) and relieved pulmonary edema. To explore the mechanism of caffeine in alleviating HAPE, we performed label-free quantitative proteomics for the mice lungs to search for crucial proteins. We detected 64,300 unique peptides from 3,105,702 MS spectra (Supplementary

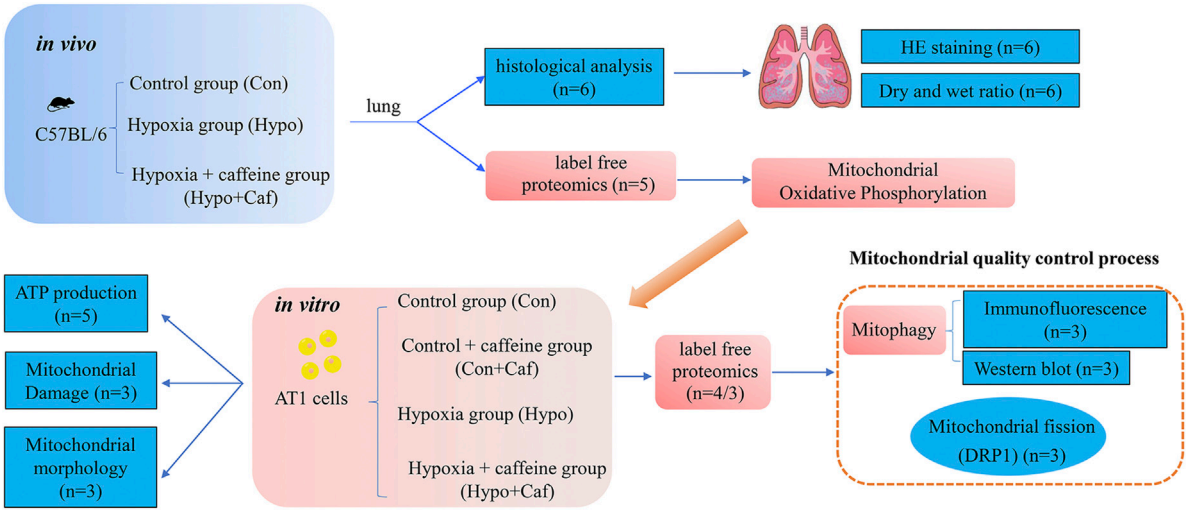

FIGURE 1
The schematic overview of the experimental workflow. We designed three groups, consisting of control, hypoxia and hypoxia + caffeine groups for *in vivo* mice experiments. Via histological and proteomics analysis of pulmonary tissues, we tested the function of caffeine for HAPE at the tissue level and discovered mitochondria probably involved in preventing HAPE. Then, we designed four groups (control group, control + caffeine group, hypoxia and hypoxia + caffeine group) in the *in vitro* AT1 cell-based experiments to detail the function of mitochondria in HAPE *via* mitochondrial oxidative phosphorylation, ROS synthesis, mitochondrial membrane potential, mitochondrial morphology, mitochondrial fission and proteomics analysis, identifying key mitophagy proteins and pathway.

Figure S1A). Principal component analysis (PCA) with all the identified proteins could be separated between the Con group, Hypo group, and Hypo + Caf group (Figure 2C). The PCA results also validated that our model construction was successful. We found 327 DEPs between Hypo and Control groups and 93 DEPs between Hypo + Caf and Hypo groups (Supplementary Figure S1B; Supplementary Table S1). The heatmap with hierarchical clustering of DEPs between the Hypo + Caf group and the Hypo group showed a clear separation (Figure 2D). The subcellular location of these DEPs varied greatly, and mitochondria were the organelle with the greatest difference. 16% of upregulated DEPs in the Hypo group compared with the Con group were located in the mitochondria (Supplementary Figure S1C), and 17% of downregulated DEPs in the Hypo + Caf group compared with the Hypo group were located in the mitochondria (Figure 2E). Volcano plots with the labeled top 20 DEPs were shown (Figure 2F; Supplementary Figure S1D). Notably, we found multi-subunit genes of mitochondria, such as Ndufs1, Ndufa10, Ndufb8, and Atp6ap1 (Figure 2F). Gene Ontology (GO) enrichment analysis revealed that the downregulated DEPs between Hypo + Caf and Hypo groups were significantly enriched in cellular respiration, mitochondrial respiratory complexes and NADH dehydrogenase oxidative phosphorylation (Figure 2H; Supplementary Figure S1E–G). The enriched KEGG pathways of DEPs between the Hypo and Hypo + Caf groups showed that the most significantly downregulated pathway was oxidative phosphorylation (Figure 2G). In detail, hypoxia upregulated the expression of oxidative phosphorylation pathway-associated proteins, and caffeine maintained its normal levels (Figure 2H). The mRNA expressions of the mitochondrial oxidative phosphorylation genes were decreased by caffeine in hypoxia (Supplementary Figure S2B). Hence, we concluded that the mechanism of caffeine alleviating HAPE may be through the regulation of the mitochondrial oxidative phosphorylation pathway.

3.2 Effects of caffeine on mitochondrial ATP metabolism

Mitochondria are the powerhouses of animal cells. To explore the effects of caffeine on mitochondrial bioenergetics, we measured energy metabolism phenotypes using AT1 cells, which cover more than 95% of the internal surface of the lung (Eaton et al., 2009). One of the functions of AT1 cells is the reabsorption of excess lining fluid from the alveolar surface (Baloglu et al., 2020). The effect of cell viability was detected by the CCK8 assay. Hypoxia decreased cell viability, and caffeine increased cell viability in a dose-dependent manner. We found that caffeine at 10–20 μM significantly increased the cell viability of AT1 cells, and 15 μM caffeine was the optimum concentration (Supplementary Figure S2A).

The total ATP production was composed of mitochondrial oxidative phosphorylation-produced ATP (mitoATP) and glycolysis-produced ATP (glycoATP). The mitoATP and glycoATP were calculated by measuring the oxygen consumption rate (OCR) and extracellular acidification rate (ECAR), separately (Supplementary Figures S2C,D). The total ATP was decreased in hypoxia, but reversed by caffeine (Figure 3A). The mitoATP dramatically decreased in hypoxia, and caffeine mitigated the decrease in the Hypo + Caf group (Figure 3B). The glycoATP was significantly increased in hypoxia, and caffeine amplified this change (Figure 3C). Cell Mito Stress Test was detected to explore the mitochondrial activity (Figure 3D). Hypoxia decreased basal respiration, but caffeine did not affect it (Supplementary Figure S2E). The maximal and ATP production respiration decreased in hypoxia, and caffeine reversed these changes (Figures 3E,F). GlycoATP production is almost four times of mitoATP in hypoxia (Figure 3A). As a result, glycolysis becomes the primary source of ATP synthesis in hypoxic conditions. To determine the rate of glycolysis, we measured the glycolytic rate and maximum

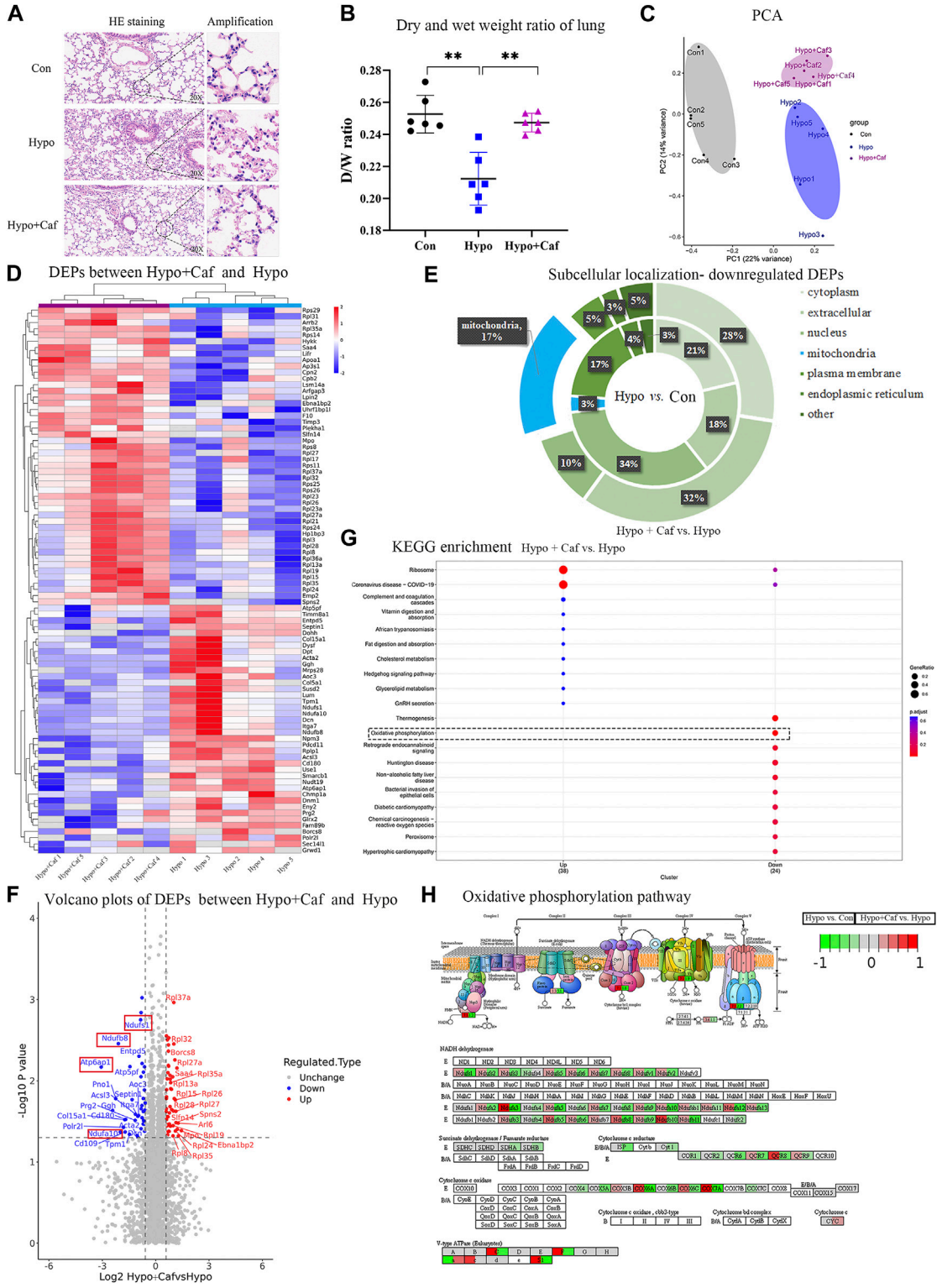

FIGURE 2
Caffeine alleviates HAPE by acting on mitochondria. **(A)** Images of hematoxylin and eosin–stained lung tissues. Hypoxia led to pulmonary congestion and alveolar structural destruction, but caffeine suppressed these damages. **(B)** Dry and wet weight ratio of lung. The dry and wet weight ratio of lung dramatically declines in Hypo group, suggesting the successful mice model of pulmonary edema model. Caffeine neutralized the decrease in dry and wet weight ratio. **(C)** Principal component analysis of 15 samples based on the expression of all the proteins. These proteins could clearly separate the three groups from each other. **(D)** Heatmap of DEPs between Hypo and Hypo + Caf groups. The hierarchical clustering showed a clear separation of the two groups. **(E)** Subcellular localization of downregulated proteins. The internal ring refers to the subcellular localization ratio of DEPS between Hypo and Con group, while the external ring refers to the subcellular localization ratio of DEPS between Hypo + Caf and Hypo group. 3% of proteins localized to mitochondria (shown in blue) were downregulated in hypoxia. 17% of proteins localized to mitochondria were downregulated by

(*Continued*)

FIGURE 2 (Continued)
caffeine in hypoxic condition. **(F)** Volcano map of DEPs between Hypo group and Hypo + Caf group. The top 20 DEPs were labeled and contained multiple mitochondrial subunits (red box), such as Ndufs1, Ndufa10, Ndufb8 and Atp6ap1. **(G)** KEGG pathway enrichment of DEPs between Hypo group and Hypo + Caf group. The most significantly downregulated pathway by caffeine was oxidative phosphorylation (dashed box). **(H)** The DEPs in oxidative phosphorylation pathway. Hypoxia upregulated the expression of proteins in the oxidative phosphorylation pathway (the left side of the box), and the addition of caffeine decreased the expression of these proteins (the right side of the box) to maintain their normal levels. $^{**}p < 0.01$.

glycolytic capacity using Seahorse XF Glycolytic Rate Assay (Figure 3G). The basal glycolysis and the compensatory glycolysis were increased in hypoxia compared to the control, and caffeine further amplified the increase (Figures 3H,I). The expressions of rate-limiting enzymes in glycolysis were detected by Western blot (Figure 3J). Compared with normoxia, hypoxia increased the expression of HK2, GPI, PFKP, and PKM1/2, and caffeine amplified the increased degree of PFKP and PKM1/2 (Figures 3K–N). These findings suggest that caffeine increased the glycolytic capacity to supply energy in hypoxia.

3.3 Caffeine reduces mitochondrial damage triggered by hypoxia

To determine whether caffeine repaired the mitochondria damage caused by hypoxia, we detected the production of ROS and the changes in MMP. Previous studies have shown that damaged mitochondria will increase ROS production, decrease MMP and injure ATP synthesis (Labuschagne et al., 2019). We found that hypoxia significantly increased both the cytoplasmic ROS production and mitochondrial ROS production, but caffeine reduced the cytoplasmic and mitochondrial ROS accumulation (Figures 4A–D). MMP is a crucial parameter for evaluating mitochondrial function. MMP depolarization indicates cells become less healthy (Sakamuru et al., 2016). Oxidative stress damage caused the depolarization of MMP and further aggravated mitochondrial dysfunction. We found MMP got significantly depolarized in hypoxia, while caffeine maintained the normal MMP (Figures 4E,F). These results suggested that mitochondrial damage and oxidative stress triggered by hypoxia could be relieved by caffeine.

3.4 Caffeine reduces oxidative stress and stabilizes mitochondrial morphology

We found abnormally shaped mitochondria in the Hypo group compared to the typical conformation seen in the Con group in the transmission electron microscopy analysis (Figure 4G). Notably, mitochondria in the Hypo group showed more apparent cristae rarefication and swelling, wherein mitochondrial ultrastructure was severely disorganized. Caffeine normalized the damaged mitochondrial conformation in hypoxia (Figure 4G). While the number of mitochondria per high-power field showed no difference in each group (Figure 4H). We also found that Hypoxia increased the degradation of mitochondrial membrane proteins Tom20 and Tim23 (Figures 4I–K), reflecting the mitochondrial damage (Narendra et al., 2008). But caffeine attenuated the degradation (Figures 4I–K). These results indicated that caffeine protected the morphology and maintained the health of mitochondria.

3.5 Mechanism of the mitochondrial protective effects of caffeine

To investigate the mechanism of caffeine protective effects on mitochondria, we further implemented the label-free quantitative proteomics analysis in AT1 cells. We detected 104729 peptides and 7571 proteins (Supplementary Figure S3A). PCA showed that the three groups were separated, and the Hypo + Caf group was closer to the Con group. (Supplementary Figure S3B). 821 DEPs between the Hypo and Con groups and 687 DEPs between the Hypo + Caf and Hypo groups were detected (Supplementary Figure S3C; Supplementary Table S1). The volcano map of DEPs was shown, and the top 20 DEPs were labeled (Figure 5D; Supplementary Figure S3D). For these top 20 DEPs, we found that caffeine could markedly reverse the gene regulation induced by hypoxia. 60% of upregulated DEPs in hypoxia were decreased by caffeine, and 40% of downregulated DEPs in hypoxia were increased by caffeine (Figure 5D; Supplementary Figure S3D). The heatmap with hierarchical clustering demonstrated that the Hypo + Caf group was close to the Con group instead of the Hypo group (Figure 5A). Mfuzz clustering analysis revealed four clusters consisting of 98, 358, 402, and 224 quantified proteins, respectively (Figure 5B). Proteins in cluster 2 were downregulated in hypoxia but increased in Hypo + Caf group. In this cluster, oxidative phosphorylation was highly enriched (Figure 5C). Proteins in cluster 3 were upregulated in hypoxia but decreased in the Hypo + Caf group. The HIF-1a signaling pathway, ECM receptor interaction, and folate biosynthesis were enriched in cluster 3 (Figure 5C). From these clustering results, we found several pathways associated with energy metabolism and mitochondrial functions. The GO analysis of the upregulated DEPs between the Hypo + Caf and Hypo groups was significantly enriched in the ribosome (Supplementary Figure S3F), mitochondria (Figure 5E), and constituent of ribosome (Supplementary Figure S3G). Eight significant modules of DEPs were visualized *via* the Cytoscape MCODE app (Figure 5F), and the mitochondria-associated oxidative phosphorylation and mitophagy were marked. The suppressive oxidative phosphorylation manifests mitochondrial impairment (Brunetti et al., 2021), and mitophagy is one of the mechanisms to remove damaged mitochondria (Shan et al., 2019). We found that the upregulated KEGG pathway enriched the mitophagy pathway between the Hypo + Caf and Hypo groups (Supplementary Figure S3G). Most proteins in the mitophagy pathway were upregulated by caffeine could increase the expression of these proteins in hypoxia (Figure 5G). Therefore, we hypothesized that caffeine reduced mitochondrial damage in hypoxia by regulating mitophagy.

10.3389/fphar.2023.1155414

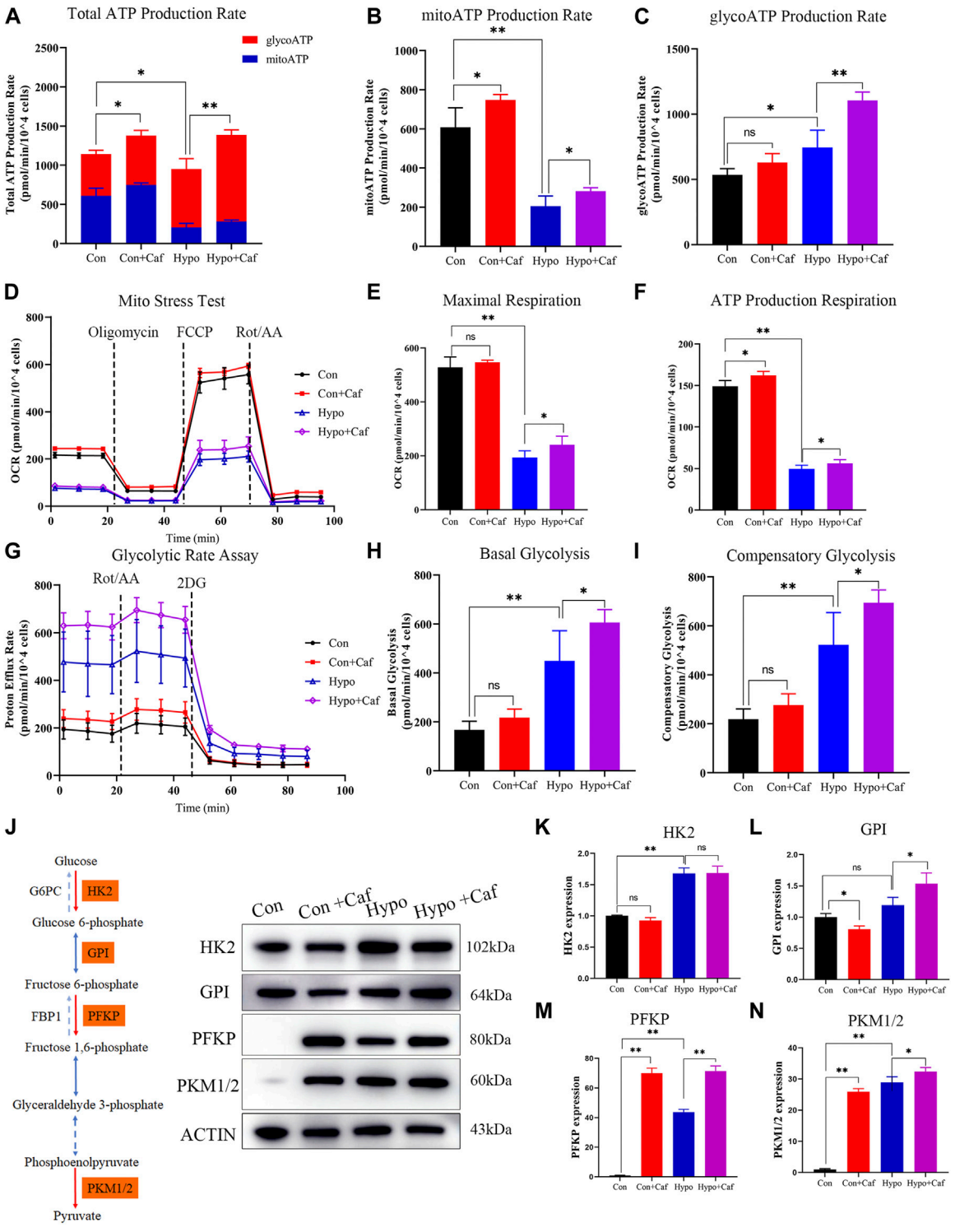

FIGURE 3
Effects of caffeine on mitochondrial ATP production. **(A–C)** The total ATP produced by mitochondrial oxidative phosphorylation and glycolysis. Caffeine increased the total ATP production in normoxia (Con + Caf group vs. Con group) and hypoxia (Hypo + Caf group vs. Hypo group). **(B)** Rate of ATP production produced by mitochondrial oxidative phosphorylation. The mitoATP production rate dramatically decreased in hypoxia, and caffeine can mitigate the decrease in the Hypo + Caf group. **(C)** Rate of ATP production produced by glycolysis. We found a significant increase in glycoATP production rate in hypoxia, and caffeine significantly amplified this change. **(D)** The OCR was measured using Seahorse XF Cell Mito Stress Test. **(E)** Maximal respiration and **(F)** ATP production respiration of the Mito Stress Test was calculated. Hypoxia decreased the maximal and ATP production respiration, and caffeine reversed these changes. **(G)** The rate of cellular glycolysis. By measuring the proton efflux rate, we calculated the rate of glycolysis. **(H)** The basal glycolysis and **(I)** the compensatory glycolysis of mitochondria were calculated. Hypoxia caused the accumulation of basal and compensatory glycolysis, and caffeine significantly amplified these changes. **(J–N)** The representative Western blot images and summarized data of rate-limiting enzymes in glycolysis. ACTB was used as an internal reference. *$p < 0.05$, **$p < 0.01$.

10.3389/fphar.2023.1155414

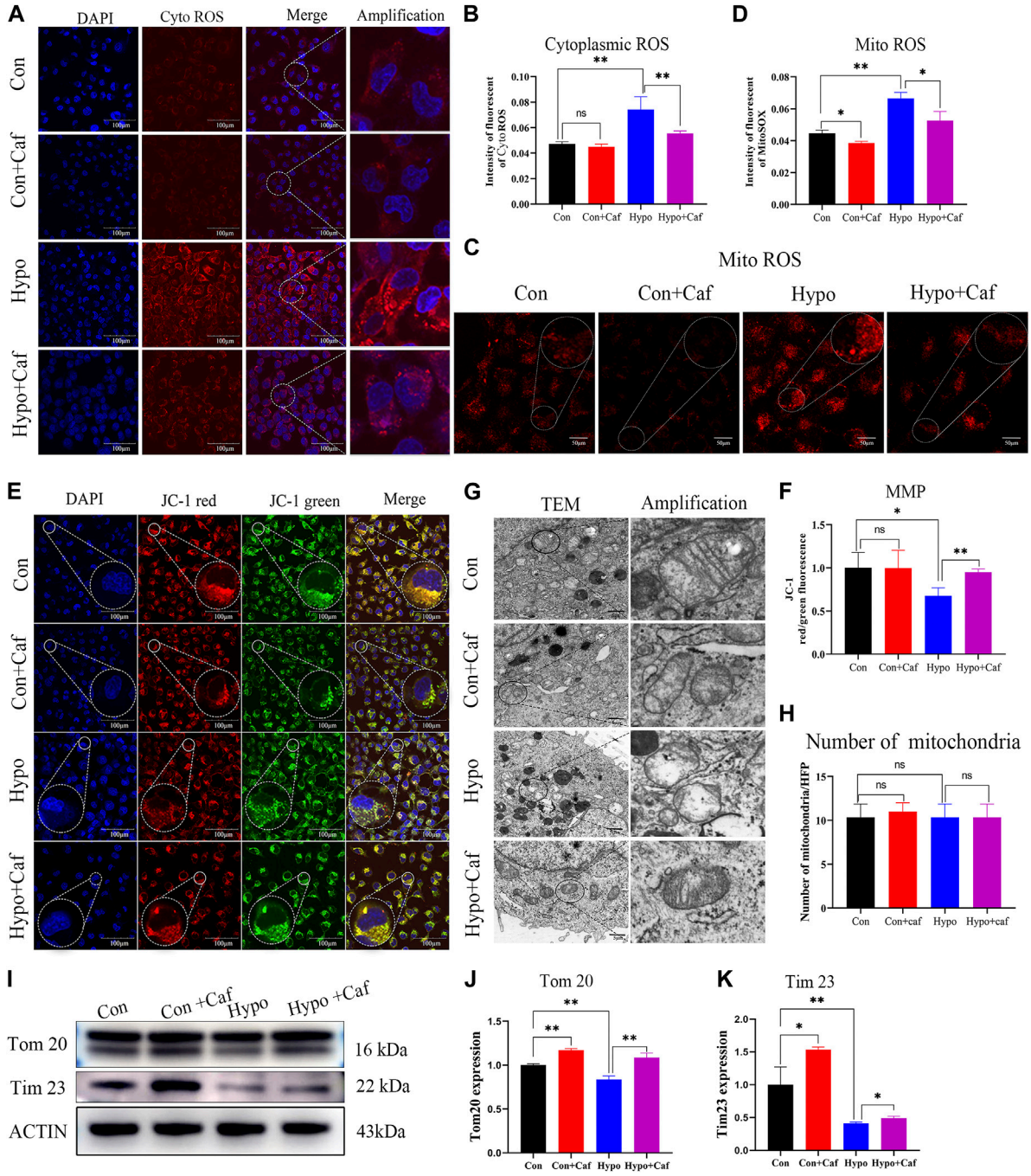

FIGURE 4
Caffeine reduces mitochondrial damage triggered by hypoxia and maintain mitochondrial morphology. **(A, B)** Confocal microscopy images of cytoplasmic ROS production (scale bars, 100 μm). The cytoplasmic ROS was measured using a fluorogenic probe (red), and the nucleus was marked by DAPI staining (blue). The intensity of fluorescent ROS was calculated by ImageJ software. Hypoxia caused a substantial increase in ROS production, but caffeine suppressed this ROS accumulation. **(C, D)** Confocal microscopy images of mitochondrial ROS production (scale bars, 50 μm). The mitochondrial ROS was detected by MitoSOX™ Red mitochondrial superoxide indicator. Hypoxia caused a significant increase in mitochondrial ROS production, but caffeine suppressed this ROS accumulation. **(E, F)** Confocal microscopy images of MMP (scale bars, 100 μm). MMP was measured using JC-1 reagent. The intensity of fluorescent of MMP. MMP is indicated by a ratio of the red/green fluorescence intensity. MMP decreased in hypoxia, while most mitochondria still have normal MMP in the caffeine group. **(G)** Representative transmission electron microscopy images of mitochondria at magnification 12000. Scale bars represent 5 μm. Mitochondria in the Hypo group showed more apparent cristae rarefication and swelling, wherein mitochondrial ultrastructure was severely disorganized. Caffeine can recover the conformation of mitochondria into normal in hypoxia. **(H)** The number of mitochondria per high-power field in each group. The number of mitochondria per field was counted and showed no difference in each group. **(I–K)** Representative Western blot images and summarized data of Tom20 and Tim23. ACTB was used as an internal reference. *$p < 0.05$, **$p < 0.01$.

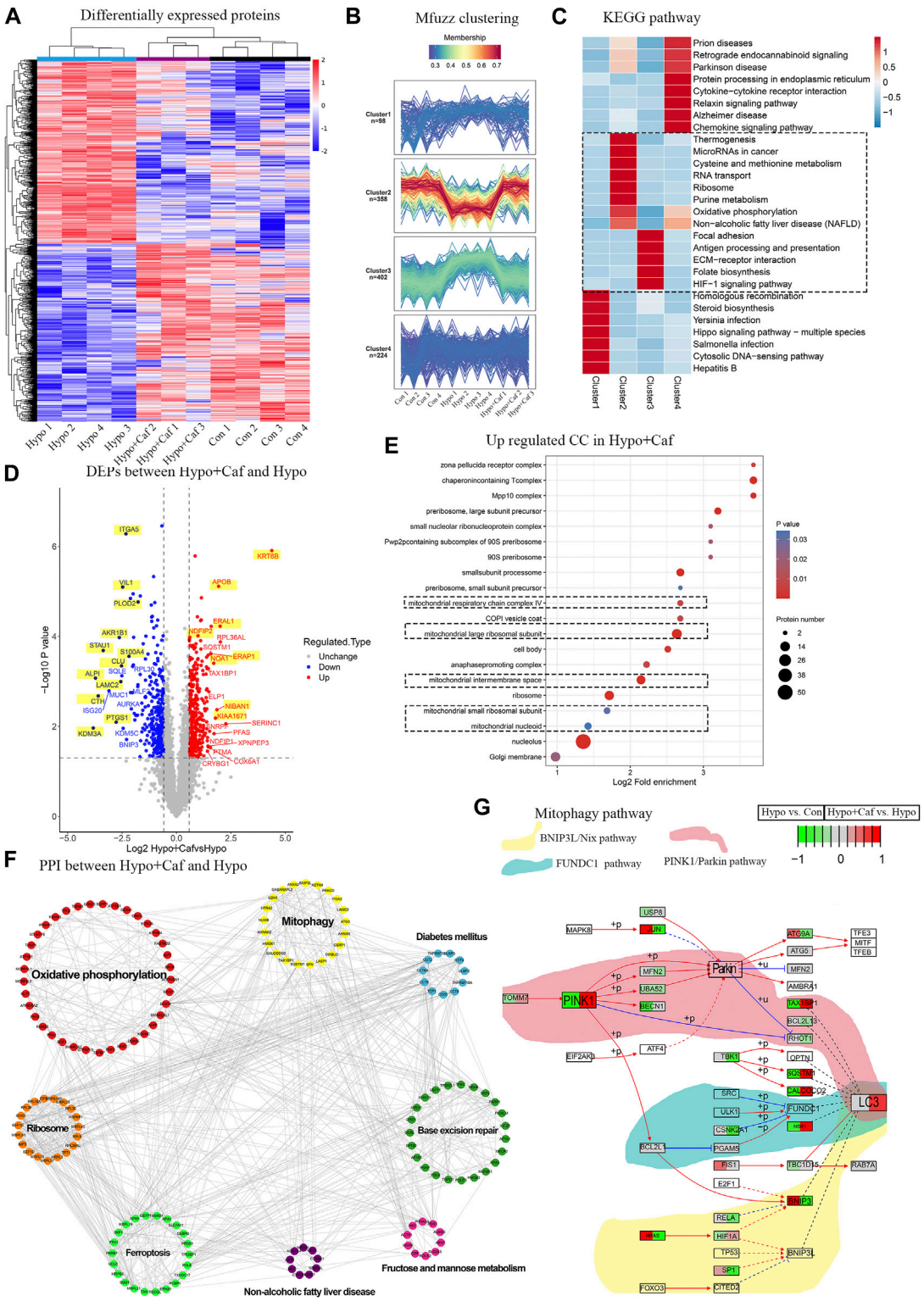

FIGURE 5
Mechanism of the mitochondrial protective effect of caffeine. **(A)** Heatmap of the quantitative proteomics. The heatmap with hierarchical clustering demonstrated Hypo + Caf group was closed to the Control group instead of the Hypo group, and caffeine could essentially recover the expression changes of the DEPs induced by hypoxia, indicating caffeine could relieve the damage caused by hypoxia. One sample in the Hypo + Caf group was removed due to the quality control of the proteomic data. **(B)** Mfuzz clustering analysis of DEPs. Mfuzz clustering analysis revealed four groups of proteins consisting of 10898, 541358, 428 402, and 431 224 quantified proteins, respectively. **(C)** The enrichment KEGG pathways of four clusters. Proteins in cluster 2 were downregulated in the Hypo group but increased in the Hypo + Caf group. In this cluster, oxidative phosphorylation was highly enriched. Proteins in cluster 3 were upregulated in the Hypo group but decreased in the Hypo + Caf group. The HIF-1a signaling pathway, ECM receptor interaction, thiamine metabolism, folate biosynthesis, protein digestion, and absorption were enriched in cluster 3. **(D)** Volcano map of DEPs between
(*Continued*)

FIGURE 5 (Continued)
Hypo group and Hypo + Caf group. For these top 20 DEPS, we found that 60% of upregulated DEPs by hypoxia were decreased by caffeine, and 40% of downregulated DEPs by hypoxia were increased by caffeine. Co-regulated DEPs labeled with a yellow background color. **(E)** The cellular compound of GO enrichment analysis of the upregulated DEPs between Hypo + Caf group and Hypo group. The cellular component of the upregulated DEPs between the Hypo + Caf group and Hypo group were significantly enriched in mitochondria (dashed box). **(F)** Protein interaction network of DEPs between Hypo + Caf group and Hypo group. Eight significant modules of DEPs were visualized *via* the Cytoscape MCODE app, and the mitochondria-associated oxidative phosphorylation and mitophagy were revealed. **(G)** The specific expression level of DEPs in the mitophagy pathway. Most proteins in the mitophagy pathway were downregulated in the Hypo group (the left side of the box), but caffeine could increase the expression of these proteins in hypoxia (the right side of the box).

3.6 Caffeine mediated the mitochondrial quality control process

As damaged mitochondria need to be cleared, we next detected whether caffeine contributes to the clearing of low-quality mitochondria, which are known to be removed through multiple ways, such as cell apoptosis, autophagy, mitophagy and mitocytosis (Pickles et al., 2018; An et al., 2021; Jiao et al., 2021; Song et al., 2021). Mitophagy is a particular form of autophagy to clear the damaged mitochondria and maintains cell homeostasis (Li et al., 2018). We examined the immunofluorescence colocalization analysis of mitochondria and lysosomes. Mitochondria displayed a regular uniform network in the control group (Figure 6A, green fluorescence). While hypoxia resulted in mitochondria fragmentation and increased colocalization of mitochondria and lysosomes (red fluorescence), which reflected increased mitophagy (yellow fluorescence) (Figure 6A). The yellow fluorescence was intensive in the Hypo + Caf group (Figure 6A). The quantification of colocalization showed that caffeine enhanced the colocalization of Tom20 and LAMP1 (Figure 6B), which suggested that caffeine improved mitophagy in hypoxia. LC3 is a mammalian autophagosome with two isoforms, LC3-I and LC3-II. The conversion of the cytosolic-associated protein LC3-I to the membrane-bound LC3-II form is an important indicator of autophagosome activation. Therefore, the detection of LC3-II can be used to evaluate autophagosome formation (Bjorkoy et al., 2009). Western blot analysis showed that the expression level of LC3-II was significantly increased at the early stage of hypoxia treatment (24 h) and then gradually decreased (48 h). Caffeine treatment amplified the changes in LC3-II expression levels under hypoxic conditions. (Figures 6C,D). In addition, P62 was integrated into the formed autophagosome and degraded in autolysosomes, which was another common marker to study autophagic flux (Bjorkoy et al., 2009). The protein expression of p62 was decreased in hypoxia, suggesting enhanced autophagy. Compared with the Hypo group, caffeine further aggravated P62 degradation in hypoxia (Figure 6C; Figure 6E). Chloroquine (CQ) was an inhibitor of the fusion of autophagosomes and lysosomes, was used to further investigate the role of caffeine in the induction of mitophagy. We found that the enhanced autophagic flux induced by caffeine was inhibited by CQ (Figure 6C), which suggested that caffeine increased mitophagy by promoting autophagolysosome degradation.

Given the three classic pathways in mitophagy, we detected the expression of essential proteins in these pathways. BCL2/adenovirus E1B interacting protein 3 like (BNIP3L/Nix), a mitochondrial protein, plays a critical role in mitophagy (Fu et al., 2020). BNIP3L-mediated mitophagy is activated by HIF-1a in hypoxia (Lin Q. et al., 2021). BNIP3L protein showed low-level expression in normoxia and significantly increased in hypoxia. In comparison, we found that caffeine did not affect the expression of BNIP3L (Figures 6F,G). The second pathway is the PINK1/Parkin-dependent mitophagy pathway, which is the primary mechanism of mitochondrial membrane depolarization-induced mitophagy (Poole and Macleod, 2021). We found that hypoxia increased the expression of the total PINK1(t-PINK) and mitochondrial PINK1(m- PINK), and caffeine enlarged the degree of increase in hypoxia. Parkin is auto-inhibited and requires activation by PINK1, which phosphorylates Ser65 in the ubiquitin domain (Tan et al., 2022). The mitochondrial Parkin (m- Parkin) and phosphorylated Parkin (pParkin) were increased in hypoxia, and caffeine magnified this increased degree (Figures 6F,G), suggesting caffeine enhanced the PINK1/Parkin pathway in hypoxia. PARKIN phosphorylation is a signal to activate its E3 ligase activity, which leads to the ubiquitination of the VDAC, TOM20, COXII, MFNs, and multiple other mitochondrial membrane proteins to label the damaged mitochondria for mitophagy (Narendra et al., 2008). We found that damaged mitochondria, marked by parkin puncta (Saha et al., 2022), showed degradation of COXII protein under hypoxia and caffeine treatment (Supplementary Figure S4). The total FUNDC1 (t-FUNDC1) expression decreased in hypoxia, but caffeine did not affect its expression in hypoxia. The expression of mitochondrial FUNDC1 (m- FUNDC1) was slightly reduced in normoxia by caffeine but showed no difference in hypoxia (Figures 6F,G). Most changes in protein expression levels were consistent with quantitative proteomics results and proved the stability of the results (Figure 5G). These findings suggested that mitophagy was increased in hypoxia, which was further amplified by caffeine *via* the PINK1/Parkin pathway.

Excessive mitophagy decreased the number of mitochondria and impaired ATP production. But the number of mitochondria did not lessen in the Hypo + Caf group (Figures 4I–K). This indicated that there must be other mechanisms to regulate the number of mitochondria by caffeine. Previous studies reveal that fission underlies both proliferation and degradation of mitochondria (Kleele et al., 2021). Thus, we hypothesized whether caffeine also regulated mitochondrial fission in hypoxia to maintain the mitochondria quantity. To verify this conjecture, we detected the expression of dynamin-related protein 1 (DRP1), which is the signature protein of mitochondrial fission. The expression of the total DRP1 (t- DRP1) was decreased in hypoxia, while caffeine could significantly increase its expression. The expression of mitochondrial DRP1 (m- DRP1) was increased under hypoxic conditions, which was amplified by caffeine (Figures 6F,G). Peroxisome proliferator-activated receptor-γ coactivator-1-α (PGC-1α) is a master indicator of mitochondrial biogenesis (Li et al., 2017). The expression of PGC1α was increased in hypoxia, which was amplified by caffeine (Figures 6F,G). We next explored the mitophagy and mitochondrial fission markers in mice models. Consistently with the result in AT1 cells, the expression of PINK, pParkin (S65), LC3II, and DRP1 of lungs was

10.3389/fphar.2023.1155414

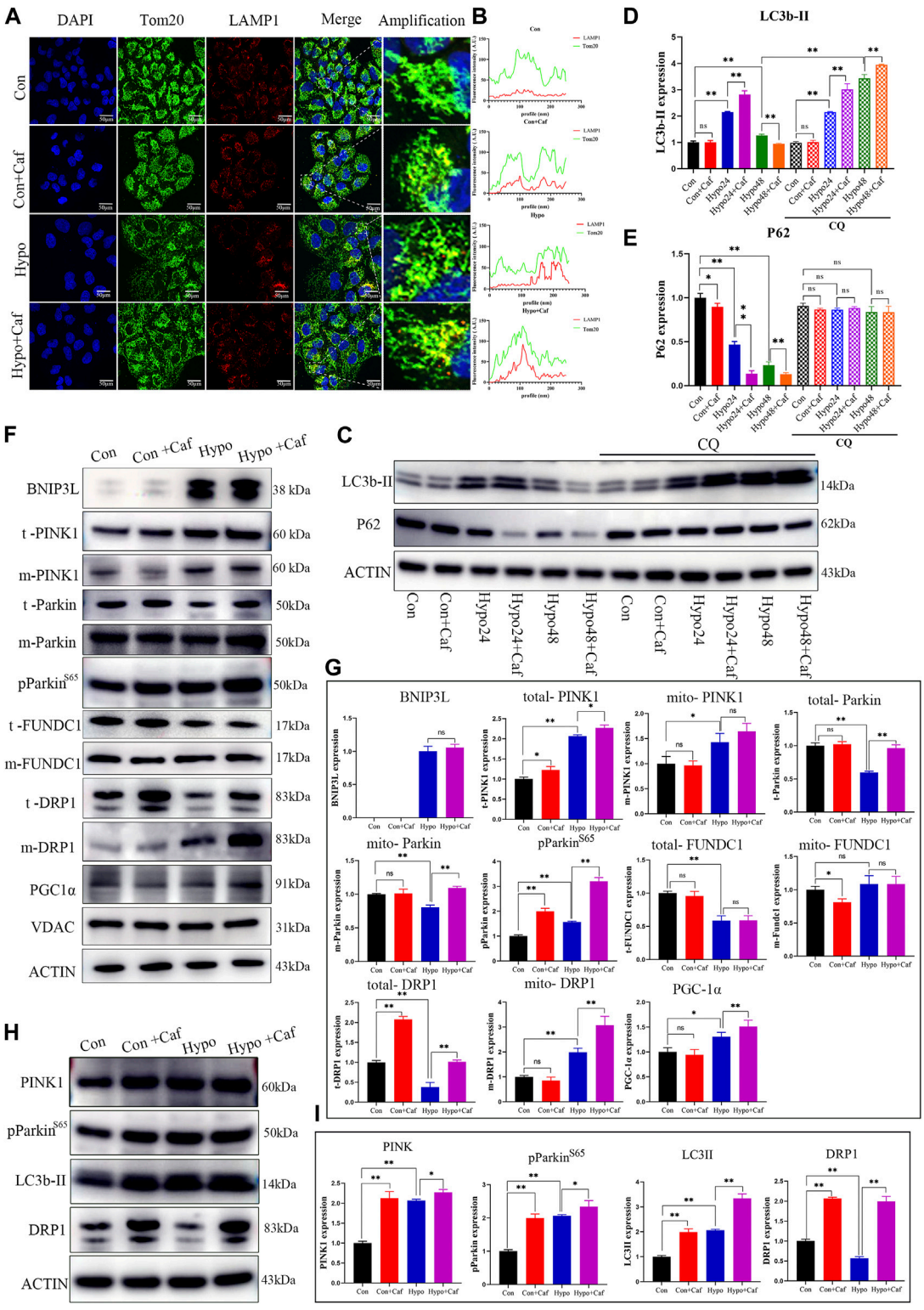

FIGURE 6
Caffeine mediated mitochondrial quality control process. **(A, B) (A)** The fluorescence images showed the colocalization of mitochondria (green fluorescence) and lysosomes (red fluorescence). The merged fluorescence (yellow) reflected mitophagy, and caffeine increased mitophagy in hypoxia. (Scale bars, 100 μm). **(B)** Quantification of colocalization. **(C–E)** Representative Western blot images and summarized data of LC3b-II and P62 following hypoxic treatment for 24h/48 h in the absence or presence of chloroquine (50 μM). LC3-II was significantly increased at the early stage of hypoxia treatment (24 h) and then gradually decreased (48 h), while caffeine further amplified the LC3-II changes. P62 protein expression level was downregulated in hypoxia, and caffeine enlarged the degree of decrease. CQ blocked the role of caffeine in the enhanced autophagic flux. **(F, G)** Representative Western blot images and summarized data of BNIP3L, t- PINK, m- PINK, t- Parkin, m- Parkin, pParkin (S65), t- FUNDC1, m- FUNDC1, t- DRP1, m- DRP1and PGC1α in AT1 cells. VDAC was the internal reference of mitochondrial membrane proteins, and ACTB was the internal reference of total proteins. **(H, I)** Representative Western blot images and summarized data of PINK, pParkin (S65), LC3II, and DRP1 proteins of lungs. ACTB was used as an internal reference.

also upregulated by caffeine, especially in hypoxia (Figures 6H,I). These results indicated that caffeine mediated mitochondrial quality control by activating mitophagy, mitochondrial biogenesis, and mitochondrial fission to mitigate the damage caused by hypoxia.

4 Discussion

High altitude pulmonary edema (HAPE) as one of the severe sub-type of high altitude illness is considered a life-threatening disease (Swenson and Bartsch, 2012; Wang Y. et al., 2022), but the effectiveness of current therapies was unsatisfactory (Luks et al., 2019; Luks and Hackett, 2022). Caffeine is a small molecule compound with biological activity, which can be used to treat respiratory distress syndrome (Ines et al., 2021; Elmowafi et al., 2022). HAPE has similar pathological changes to respiratory distress syndrome, but there is no report on whether caffeine plays a role in alleviating HAPE. In our study, we found that a low dose of caffeine could relieve HAPE through mediating the mitochondrial quality control to reduce oxidative stress in AT1 cells.

Through a series of experiments and bioinformatics analysis, we demonstrated that caffeine alleviates HAPE might by regulating the mitochondrial oxidative phosphorylation (OXPHOS) pathway. Previous studies show that caffeine could enhance OXPHOS to increase mitochondrial bioenergetics, promoting the necessary energy supply for brain recovery (Goncalves et al., 2020). We found that caffeine neutralized the ATP reduction and significantly increased the glycolytic capacity of AT1 cells in hypoxia. Mammalian cells normally require molecular oxygen to produce ATP as an energy source through the OXPHOS of mitochondria. However, under hypoxic conditions, the energy source is mainly provided by glycolysis (Wang D. et al., 2022). Tibetan chickens are well-adapted to hypoxia, showing decreased oxygen consumption rates and increased glycolysis to enable adaptation to hypoxia compared with dwarf-laying chickens (Tang et al., 2021). We found that caffeine significantly increased ATP production, especially GlycoATP production, under hypoxic conditions. The expressions of rate-limiting enzymes in glycolysis, such as PFKP and PKM1/2, were upregulated by caffeine. These results revealed that caffeine maintained an adequate energy supply by promoting glycolysis under hypoxic conditions in AT1 cells.

The accumulation of ROS caused by hypoxia leads to oxidative stress damage, disruption of mitochondrial structure and mitochondrial permeability transition (Bugger and Pfeil, 2020; Chowdhury et al., 2020; Sreedhar et al., 2020). We found that caffeine reduced the production of cytoplasmic ROS and mitochondrial ROS induced by hypoxia. MMP plays an important role in maintaining mitochondrial stability, and MMP depolarization induced by oxidative stress can induce cell apoptosis (Yang et al., 2019; Lin B. et al., 2021). We found decreased MMP and swelled mitochondria in hypoxia, but caffeine suppressed the MMP depolarization and recovered the typical morphological characteristics of mitochondria.

Caffeine alleviated hypoxic damage in HAPE by regulating mitochondrial quality control. To maintain the quality of mitochondria, cells must remove the damaged mitochondria in multiple ways, such as cell apoptosis, autophagy, mitophagy, and mitocytosis (Gao et al., 2021; Hyttinen et al., 2021; Jiao et al., 2021). What is the mechanism by which caffeine maintains the mitochondrial function under hypoxia? The label-free quantitative proteomics of AT1 cells indicated that caffeine promoted mitophagy. Mitophagy is a particular form of autophagy that clears the damaged mitochondria to maintain cell homeostasis (Li et al., 2018; Onishi et al., 2021). We explored the expression of proteins in three classic mitophagy pathways and found that caffeine enhanced the PINK1/Parkin-dependent mitophagy. But excessive mitophagy will cause insufficient numbers of mitochondria and decreased cellular resistance to injury due to energy shortage (Wu et al., 2020). We found no lessen in the number of mitochondria in the hypoxic and caffeine-treated groups. Hence, we detected the expression of signature proteins of mitochondrial fission (DRP1) and mitochondrial biogenesis (PGC-1α) to explore the effect of caffeine on mitochondrial fission and biogenesis. Indeed, caffeine upregulated the expression of DRP1and PGC1α, indicating the upregulation of mitochondrial fission and biogenesis. Collectively, we found that caffeine maintained mitochondrial quality control by regulating the PINK1/Parkin-dependent mitophagy, mitochondrial fission, and biogenesis.

5 Conclusion

In conclusion, we found that low-dose of caffeine could relieve pulmonary edema in hypobaric hypoxia *in vivo*. Caffeine attenuated hypoxia-induced mitochondrial damage by reducing oxidative stress and restoring mitochondrial morphology *in vitro*. Caffeine maintained the mitochondria quality control by enhancing the PINK1/Parkin-dependent mitophagy, promoting mitochondrial fission and biogenesis under hypoxic conditions. Furthermore, our results suggest that caffeine alleviated HAPE *via* regulating mitochondrial dynamics in AT1 cells, but further research is needed to determine whether a low dose of caffeine can increase mitochondrial turnover in other types of alveoli cells.

Data availability statement

The raw proteomic data analyzed in this study are available at iProX with the corresponding dataset identifier PXD034002 (https://www.iprox.cn/page/project.html?id=IPX0004468000).

Ethics statement

The animal study was reviewed and approved by The Animal Ethics Committee of the Chinese PLA General Hospital (SQ2020030) approved all experimental procedures involving animals.

Author contributions

KH and XZ conceived and designed the experiments. LT, YY and QJ performed the *in vivo* experiments. LT, SC, and HC performed the *in vitro* experiments. LT, WS and YH performed the collation and analysis of proteomics data. LT drafted the manuscript. ZJ performed supervision of the bioinformatic section, data interpretation and manuscript edit. All authors critically revised the manuscript for important intellectual content. All authors approved the final version of the manuscript.

Funding

This work was supported by the Science and Technology Innovation Special Zone (grant number 19-163-12-ZD-037-003-02) and the National Natural Sciences Foundation of China (grant number 82001994 and 31701155). The funders had no role in study design, data collection and analysis, decision to publish, or preparation of the manuscript.

Conflict of interest

The authors declare that the research was conducted in the absence of any commercial or financial relationships that could be construed as a potential conflict of interest.

Publisher's note

Supplementary material

The Supplementary Material for this article can be found online at: https://www.frontiersin.org/articles/10.3389/fphar.2023.1155414/full#supplementary-material

References

An, H., Zhou, B., and Ji, X. (2021). Mitochondrial quality control in acute ischemic stroke. *J. Cereb. Blood Flow. Metab.* 41 (12), 3157–3170. doi:10.1177/0271678X211046992

Ashburner, M., Ball, C. A., Blake, J. A., Botstein, D., Butler, H., Cherry, J. M., et al. (2000). Gene ontology: Tool for the unification of biology. The gene Ontology consortium. *Nat. Genet.* 25 (1), 25–29. doi:10.1038/75556

Baloglu, E., Nonnenmacher, G., Seleninova, A., Berg, L., Velineni, K., Ermis-Kaya, E., et al. (2020). The role of hypoxia-induced modulation of alveolar epithelial Na(+)- transport in hypoxemia at high altitude. *Pulm. Circ.* 10, 50–58. doi:10.1177/2045894020936662

Barrea, L., Vetrani, C., Caprio, M., El Ghoch, M., Frias-Toral, E., Mehta, R. J., et al. (2021). Nutritional management of type 2 diabetes in subjects with obesity: An international guideline for clinical practice. *Crit. Rev. Food Sci. Nutr.* 2021, 1–13. doi:10.1080/10408398.2021.1980766

Bjorkoy, G., Lamark, T., Pankiv, S., Overvatn, A., Brech, A., and Johansen, T. (2009). Monitoring autophagic degradation of p62/SQSTM1. *Methods Enzymol.* 452, 181–197. doi:10.1016/S0076-6879(08)03612-4

Brunetti, D., Dykstra, W., Le, S., Zink, A., and Prigione, A. (2021). Mitochondria in neurogenesis: Implications for mitochondrial diseases. *Stem Cells* 39 (10), 1289–1297. doi:10.1002/stem.3425

Bugger, H., and Pfeil, K. (2020). Mitochondrial ROS in myocardial ischemia reperfusion and remodeling. *Biochim. Biophys. Acta Mol. Basis Dis.* 1866 (7), 165768. doi:10.1016/j.bbadis.2020.165768

Chowdhury, A. R., Zielonka, J., Kalyanaraman, B., Hartley, R. C., Murphy, M. P., and Avadhani, N. G. (2020). Mitochondria-targeted paraquat and metformin mediate ROS production to induce multiple pathways of retrograde signaling: A dose-dependent phenomenon. *Redox Biol.* 36, 101606. doi:10.1016/j.redox.2020.101606

Doncheva, N. T., Morris, J. H., Gorodkin, J., and Jensen, L. J. (2019). Cytoscape StringApp: Network analysis and visualization of proteomics data. *J. Proteome Res.* 18 (2), 623–632. doi:10.1021/acs.jproteome.8b00702

Eaton, D. C., Helms, M. N., Koval, M., Bao, H. F., and Jain, L. (2009). The contribution of epithelial sodium channels to alveolar function in health and disease. *Annu. Rev. Physiology* 71 (1), 403–423. doi:10.1146/annurev.physiol.010908.163250

Elmowafi, M., Mohsen, N., Nour, I., et al. (2022). Prophylactic versus therapeutic caffeine for apnea of prematurity: A randomized controlled trial. *J. Matern. Fetal Neonatal Med.* 35 (25), 6053–6061. doi:10.1080/14767058.2021.1904873

Forman, H. J., Augusto, O., Brigelius-Flohe, R., Dennery, P. A., Kalyanaraman, B., Ischiropoulos, H., et al. (2015). Even free radicals should follow some rules: A guide to free radical research terminology and methodology. *Free Radic. Biol. Med.* 78, 233–235. doi:10.1016/j.freeradbiomed.2014.10.504

Fu, Z. J., Wang, Z. Y., Xu, L., Chen, X. H., Li, X. X., Liao, W. T., et al. (2020). HIF-1α-BNIP3-mediated mitophagy in tubular cells protects against renal ischemia/reperfusion injury. *Redox Biol.* 36, 101671. doi:10.1016/j.redox.2020.101671

Gao, H., Liu, Z., Xu, W., Wang, Q., Zhang, C., Ding, Y., et al. (2021). Pterostilbene promotes mitochondrial apoptosis and inhibits proliferation in glioma cells. *Sci. Rep.* 11 (1), 6381. doi:10.1038/s41598-021-85908-w

Giussani, D. A., Niu, Y., Herrera, E. A., Richter, H. G., Camm, E. J., Thakor, A. S., et al. (2014). Heart disease link to fetal hypoxia and oxidative stress. *Adv. Exp. Med. Biol.* 814, 77–87. doi:10.1007/978-1-4939-1031-1_7

Goldman, A. R., Beer, L. A., Tang, H. Y., Hembach, P., Zayas-Bazan, D., and Speicher, D. W. (2019). Proteome analysis using gel-LC-MS/MS. *Curr. Protoc. Protein Sci.* 96 (1), e93. doi:10.1002/cpps.93

Goncalves, D. F., Tassi, C. C., Amaral, G. P., Stefanello, S. T., Dalla Corte, C. L., Soares, F. A., et al. (2020). Effects of caffeine on brain antioxidant status and mitochondrial respiration in acetaminophen-intoxicated mice. *Toxicol. Res. (Camb)* 9 (5), 726–734. doi:10.1093/toxres/tfaa075

Hackett, P. H., Rennie, D., and Levine, H. D. (1976). The incidence, importance, and prophylaxis of acute mountain sickness. *Lancet* 2 (7996), 1149–1155. doi:10.1016/s0140-6736(76)91677-9

Hyttinen, J., Blasiak, J., Tavi, P., and Kaarniranta, K. (2021). Therapeutic potential of PGC-1α in age-related macular degeneration (AMD) - the involvement of mitochondrial quality control, autophagy, and antioxidant response. *Expert Opin. Ther. Targets* 25 (9), 773–785. doi:10.1080/14728222.2021.1991913

Ikram, M., Park, T. J., Ali, T., and Kim, M. O. (2020). Antioxidant and neuroprotective effects of caffeine against alzheimer's and Parkinson's disease: Insight into the role of nrf-2 and A2AR signaling. *Antioxidants (Basel)* 9 (9), 902. doi:10.3390/antiox9090902

Ines, F., Hutson, S., Coughlin, K., Hopper, A., Banerji, A., Uy, C., et al. (2021). Multicentre, randomised trial of preterm infants receiving caffeine and less invasive surfactant administration compared with caffeine and early continuous positive airway pressure (CaLI trial): Study protocol. *BMJ Open* 11 (1), e038343. doi:10.1136/bmjopen-2020-038343

Jiao, H., Jiang, D., Hu, X., Du, W., Ji, L., Yang, Y., et al. (2021). Mitocytosis, a migrasome-mediated mitochondrial quality-control process. *Cell.* 184 (11), 2896–2910 e13. doi:10.1016/j.cell.2021.04.027

Kalyanaraman, B., Darley-Usmar, V., Davies, K. J. A., Dennery, P. A., Forman, H. J., Grisham, M. B., et al. (2012). Measuring reactive oxygen and nitrogen species with fluorescent probes: Challenges and limitations. *Free Radic. Biol. Med.* 52 (1), 1–6. doi:10.1016/j.freeradbiomed.2011.09.030

Kanehisa, M., Furumichi, M., Sato, Y., Ishiguro-Watanabe, M., and Tanabe, M. (2021). Kegg: Integrating viruses and cellular organisms. *Nucleic Acids Res.* 49 (D1), D545–D551. doi:10.1093/nar/gkaa970

Khodaee, M., Grothe, H. L., Seyfert, J. H., and VanBaak, K. (2016). Athletes at high altitude. *Sports Health* 8 (2), 126–132. doi:10.1177/1941738116630948

Kleele, T., Rey, T., Winter, J., Zaganelli, S., Mahecic, D., Perreten Lambert, H., et al. (2021). Distinct fission signatures predict mitochondrial degradation or biogenesis. *Nature* 593 (7859), 435–439. doi:10.1038/s41586-021-03510-6

Labuschagne, C. F., Cheung, E. C., Blagih, J., Domart, M. C., and Vousden, K. H. (2019). Cell clustering promotes a metabolic switch that supports metastatic colonization. *Cell. Metab.* 30 (4), 720–734 e5. doi:10.1016/j.cmet.2019.07.014

Li, H. L., Zaghloul, N., Ahmed, I., Omelchenko, A., Firestein, B. L., Huang, H., et al. (2019). Caffeine inhibits hypoxia-induced nuclear accumulation in HIF-1α and promotes neonatal neuronal survival. *Exp. Neurol.* 317, 66–77. doi:10.1016/j.expneurol.2019.01.014

Li, P. A., Hou, X., and Hao, S. (2017). Mitochondrial biogenesis in neurodegeneration. *J. Neurosci. Res.* 95 (10), 2025–2029. doi:10.1002/jnr.24042

Li, W., Long, L., Yang, X., Tong, Z., Southwood, M., King, R., et al. (2020). Circulating BMP9 protects the pulmonary endothelium during inflammation-induced lung injury in mice. *Am. J. Respir. Crit. Care Med.* 203 (11), 1419–1430. doi:10.1164/rccm.202005-1761OC

Li, Y. F., Ouyang, S. H., Tu, L. F., Wang, X., Yuan, W. L., Wang, G. E., et al. (2018). Caffeine protects skin from oxidative stress-induced senescence through the activation of autophagy. *Theranostics* 8 (20), 5713–5730. doi:10.7150/thno.28778

Lin, B., Liu, Y., Zhang, X., Fan, L., Shu, Y., and Wang, J. (2021). Membrane-activated fluorescent probe for high-fidelity imaging of mitochondrial membrane potential. *ACS Sens.* 6 (11), 4009–4018. doi:10.1021/acssensors.1c01390

Lin, Q., Li, S., Jiang, N., Jin, H., Shao, X., Zhu, X., et al. (2021). Inhibiting NLRP3 inflammasome attenuates apoptosis in contrast-induced acute kidney injury through the upregulation of HIF1A and BNIP3-mediated mitophagy. *Autophagy* 17 (10), 2975–2990. doi:10.1080/15548627.2020.1848971

Luks, A. M., Auerbach, P. S., Freer, L., Grissom, C. K., Keyes, L. E., McIntosh, S. E., et al. (2019). Wilderness medical society clinical practice guidelines for the prevention and treatment of acute altitude illness: 2019 update. *Wilderness Environ. Med.* 30 (4S), S3–S18. doi:10.1016/j.wem.2019.04.006

Luks, A. M., and Hackett, P. H. (2022). Medical conditions and high-altitude travel. *N. Engl. J. Med.* 386 (4), 364–373. doi:10.1056/NEJMra2104829

Ma, J., Chen, T., Wu, S., Yang, C., Bai, M., Shu, K., et al. (2019). iProX: an integrated proteome resource. *Nucleic Acids Res.* 47 (D1), D1211–D1217. doi:10.1093/nar/gky869

Marte, L., Boronat, S., Garcia-Santamarina, S., Ayte, J., Kitamura, K., and Hidalgo, E. (2020). Identification of ubiquitin-proteasome system components affecting the degradation of the transcription factor Pap1. *Redox Biol.* 28, 101305. doi:10.1016/j.redox.2019.101305

McGarry, T., Biniecka, M., Veale, D. J., and Fearon, U. (2018). Hypoxia, oxidative stress and inflammation. *Free Radic. Biol. Med.* 125, 15–24. doi:10.1016/j.freeradbiomed.2018.03.042

McGuire, S. (2014). *Caffeine in food and dietary supplements: Examining safety-workshop summary*. Washington, DC: The National Academies Press.

McKeown, S. R. (2014). Defining normoxia, physoxia and hypoxia in tumours-implications for treatment response. *Br. J. Radiol.* 87 (1035), 20130676. doi:10.1259/bjr.20130676

Millar, F. R., Summers, C., Griffiths, M. J., Toshner, M. R., and Proudfoot, A. G. (2016). The pulmonary endothelium in acute respiratory distress syndrome: Insights and therapeutic opportunities. *Thorax* 71 (5), 462–473. doi:10.1136/thoraxjnl-2015-207461

Min, H., Youn, E., Kim, J., Son, S. Y., Lee, C. H., and Shim, Y. H. (2020). Effects of phosphoethanolamine supplementation on mitochondrial activity and lipogenesis in a caffeine ingestion *Caenorhabditis elegans* model. *Nutrients* 12 (11), 3348. doi:10.3390/nu12113348

Nair, A. B., and Jacob, S. (2016). A simple practice guide for dose conversion between animals and human. *J. Basic Clin. Pharm.* 7 (2), 27–31. doi:10.4103/0976-0105.177703

Narendra, D., Tanaka, A., Suen, D. F., and Youle, R. J. (2008). Parkin is recruited selectively to impaired mitochondria and promotes their autophagy. *J. Cell. Biol.* 183 (5), 795–803. doi:10.1083/jcb.200809125

Ni, Q., Shao, Y., Wang, Y. Z., Jing, Y. H., and Zhang, Y. C. (2014). Impact of high altitude on the hepatic fatty acid oxidation and synthesis in rats. *Biochem. Biophys. Res. Commun.* 446 (2), 574–579. doi:10.1016/j.bbrc.2014.03.001

Nilnumkhum, A., Kanlaya, R., Yoodee, S., and Thongboonkerd, V. (2019). Caffeine inhibits hypoxia-induced renal fibroblast activation by antioxidant mechanism. *Cell. Adh Migr.* 13 (1), 260–272. doi:10.1080/19336918.2019.1638691

Onishi, M., Yamano, K., Sato, M., Matsuda, N., and Okamoto, K. (2021). Molecular mechanisms and physiological functions of mitophagy. *EMBO J.* 40 (3), e104705. doi:10.15252/embj.2020104705

Pickles, S., Vigie, P., and Youle, R. J. (2018). Mitophagy and quality control mechanisms in mitochondrial maintenance. *Curr. Biol.* 28 (4), R170–R185. doi:10.1016/j.cub.2018.01.004

Poole, L. P., and Macleod, K. F. (2021). Mitophagy in tumorigenesis and metastasis. *Cell. Mol. Life Sci.* 78 (8), 3817–3851. doi:10.1007/s00018-021-03774-1

Ren, J., Ding, X., and Greer, J. J. (2015). Ampakines enhance weak endogenous respiratory drive and alleviate apnea in perinatal rats. *Am. J. Respir. Crit. Care Med.* 191 (6), 704–710. doi:10.1164/rccm.201410-1898OC

Saha, B., Salemi, M., Williams, G. L., Oh, S., Paffett, M. L., Phinney, B., et al. (2022). Interactomic analysis reveals a homeostatic role for the HIV restriction factor TRIM5α in mitophagy. *Cell. Rep.* 39 (6), 110797. doi:10.1016/j.celrep.2022.110797

Sakamuru, S., Attene-Ramos, M. S., and Xia, M. (2016). Mitochondrial membrane potential assay. *Methods Mol. Biol.* 1473, 17–22. doi:10.1007/978-1-4939-6346-1_2

Shan, S., Shen, Z., Zhang, C., Kou, R., Xie, K., and Song, F. (2019). Mitophagy protects against acetaminophen-induced acute liver injury in mice through inhibiting NLRP3 inflammasome activation. *Biochem. Pharmacol.* 169, 113643. doi:10.1016/j.bcp.2019.113643

Sharma Kandel, R., Mishra, R., Gautam, J., Alaref, A., Hassan, A., and Jahan, N. (2020). Patchy vasoconstriction versus inflammation: A debate in the pathogenesis of high altitude pulmonary edema. *Cureus* 12 (9), e10371. doi:10.7759/cureus.10371

Song, J., Herrmann, J. M., and Becker, T. (2021). Quality control of the mitochondrial proteome. *Nat. Rev. Mol. Cell. Biol.* 22 (1), 54–70. doi:10.1038/s41580-020-00300-2

Sreedhar, A., Aguilera-Aguirre, L., and Singh, K. K. (2020). Mitochondria in skin health, aging, and disease. *Cell. Death Dis.* 11 (6), 444. doi:10.1038/s41419-020-2649-z

Swenson, E. R., and Bartsch, P. (2012). High-altitude pulmonary edema. *Compr. Physiol.* 2 (4), 2753–2773. doi:10.1002/cphy.c100029

Swenson, E. R., and Bartsch, P. (2021). The search for a model of high-altitude pulmonary oedema must continue. *Acta Physiol. (Oxf)* 231 (1), e13485. doi:10.1111/apha.13485

Szklarczyk, D., Gable, A. L., Nastou, K. C., Lyon, D., Kirsch, R., Pyysalo, S., et al. (2021). The STRING database in 2021: Customizable protein-protein networks, and functional characterization of user-uploaded gene/measurement sets. *Nucleic Acids Res.* 49 (D1), D605–D612. doi:10.1093/nar/gkaa1074

Szlapinski, S. K., Charrette, A., Guthrie, N., and Hilmas, C. J. (2023). Paraxanthine safety and comparison to caffeine. *Front. Toxicol.* 5, 1117729. doi:10.3389/ftox.2023.1117729

Tan, H. W. S., Lu, G., Dong, H., Cho, Y. L., Natalia, A., Wang, L., et al. (2022). A degradative to secretory autophagy switch mediates mitochondria clearance in the absence of the mATG8-conjugation machinery. *Nat. Commun.* 13 (1), 3720. doi:10.1038/s41467-022-31213-7

Tang, Q., Ding, C., Xu, Q., Bai, Y., Xu, Q., Wang, K., et al. (2021). Mitochondrial fusion potentially regulates a metabolic change in Tibetan chicken embryonic brain during hypoxia. *Front. Cell. Dev. Biol.* 9, 585166. doi:10.3389/fcell.2021.585166

Tian, L., Jia, Z., Xu, Z., Shi, J., Zhao, X., and He, K. (2021). Transcriptional landscape in rat intestines under hypobaric hypoxia. *PeerJ* 9, e11823. doi:10.7717/peerj.11823

Tuleta, I., Stockigt, F., Juergens, U. R., Pizarro, C., Schrickel, J. W., Kristiansen, G., et al. (2016). Intermittent hypoxia contributes to the lung damage by increased oxidative stress, inflammation, and disbalance in protease/antiprotease system. *Lung* 194 (6), 1015–1020. doi:10.1007/s00408-016-9946-4

Velazquez, A. M., Roglans, N., Bentanachs, R., Gene, M., Sala-Vila, A., Lazaro, I., et al. (2020). Effects of a low dose of caffeine alone or as part of a green coffee extract, in a rat dietary model of lean non-alcoholic fatty liver disease without inflammation. *Nutrients* 12 (11), 3240. doi:10.3390/nu12113240

Wang, D., Liu, F., Yang, W., Sun, Y., Wang, X., Sui, X., et al. (2022). Meldonium ameliorates hypoxia-induced lung injury and oxidative stress by regulating platelet-type phosphofructokinase-mediated glycolysis. *Front. Pharmacol.* 13, 863451. doi:10.3389/fphar.2022.863451

Wang, Y., Huang, X., Peng, F., Han, H., Gu, Y., Liu, X., et al. (2022). Association of variants m.T16172C and m.T16519C in whole mtDNA sequences with high altitude pulmonary edema in Han Chinese lowlanders. *BMC Pulm. Med.* 22 (1), 72. doi:10.1186/s12890-021-01791-1

Wu, J., Yang, Y., Gao, Y., Wang, Z., and Ma, J. (2020). Melatonin attenuates anoxia/reoxygenation injury by inhibiting excessive mitophagy through the MT2/SIRT3/FoxO3a signaling pathway in H9c2 cells. *Drug Des. Devel Ther.* 14, 2047–2060. doi:10.2147/DDDT.S248628

Yanamandra, U., Sharma, M., Katoch, D., Yanamandra, S., Bhattachar, S. A., Gupta, A., et al. (2019). High-altitude pulmonary oedema: Newer treatment modalities for an age-old problem. *Indian J. Med. Res.* 149 (6), 778–782. doi:10.4103/ijmr.IJMR_1981_17

Yang, F., Pei, R., Zhang, Z., Liao, J., Yu, W., Qiao, N., et al. (2019). Copper induces oxidative stress and apoptosis through mitochondria-mediated pathway in chicken hepatocytes. *Toxicol Vitro* 54, 310–316. doi:10.1016/j.tiv.2018.10.017

frontiers | Frontiers in Pharmacology

TYPE Original Research
PUBLISHED 17 April 2023
DOI 10.3389/fphar.2023.1164633

OPEN ACCESS

EDITED BY
Jie Liu,
Tongji University, China

REVIEWED BY
Yi Li,
Tianjin Chest Hospital, China
Ke Wang,
First Affiliated Hospital of Guangxi University of Chinese Medicine, China

*CORRESPONDENCE
Yubao Wang,
yubaowang2020@hotmail.com,
Jing Feng,
zyyhxkfj@126.com

†These authors have contributed equally to this work and share first authorship

RECEIVED 13 February 2023
ACCEPTED 03 April 2023
PUBLISHED 17 April 2023

CITATION
Han S, Zhao Z, Yang L, Huang J, Wang Y and Feng J (2023), The performance of metagenomic next-generation sequencing in diagnosing pulmonary infectious diseases using authentic clinical specimens: The Illumina platform versus the Beijing Genomics Institute platform.
Front. Pharmacol. 14:1164633.
doi: 10.3389/fphar.2023.1164633

The performance of metagenomic next-generation sequencing in diagnosing pulmonary infectious diseases using authentic clinical specimens: The Illumina platform versus the Beijing Genomics Institute platform

Shuangyu Han†, Zhan Zhao†, Lei Yang, Jie Huang, Yubao Wang* and Jing Feng*

Department of Respiratory and Critical Care Medicine, Tianjin Medical University General Hospital, Tianjin, China

Introduction: Metagenomic next-generation sequencing (mNGS) has been increasingly used to detect infectious organisms and is rapidly moving from research to clinical laboratories. Presently, mNGS platforms mainly include those from Illumina and the Beijing Genomics Institute (BGI). Previous studies have reported that various sequencing platforms have similar sensitivity in detecting the reference panel that mimics clinical specimens. However, whether the Illumina and BGI platforms provide the same diagnostic performance using authentic clinical samples remains unclear.

Methods: In this prospective study, we compared the performance of the Illumina and BGI platforms in detecting pulmonary pathogens. Forty-six patients with suspected pulmonary infection were enrolled in the final analysis. All patients received bronchoscopy, and the specimens collected were sent for mNGS on the two different sequencing platforms.

Results: The diagnostic sensitivity of the Illumina and BGI platforms was notably higher than that of conventional examination (76.9% vs. 38.5%, $p < 0.001$; 82.1% vs. 38.5%, $p < 0.001$; respectively). The sensitivity and specificity for pulmonary infection diagnosis were not significantly different between the Illumina and BGI platforms. Furthermore, the pathogenic detection rate of the two platforms were not significantly different.

Conclusion: The Illumina and BGI platforms exhibited similar diagnostic performance for pulmonary infectious diseases using clinical specimens, and both are superior to conventional examinations.

KEYWORDS

metagenomic next-generation sequencing, Illumina, BGI, conventional examination, pulmonary infection

1 Introduction

Pulmonary infections cause significant morbidity and mortality annually worldwide, leading to various complications such as empyema, pleural effusion, and lung abscess (Magill et al., 2014). Pulmonary infections are immune-mediated lung diseases caused by various microbial pathogens, including fungi, bacteria, viruses, atypical pathogens, and parasites. Early recognition and verification of the pathogen and treatment with appropriate antibiotics are critical to improving outcomes in pulmonary infections. Conversely, delays could lead to disease worsening and a greater risk of death. For an extended period, detection of pathogenic bacteria has mainly relied on conventional examination (CE), such as smears, culture, immunological tests, and polymerase chain reaction (PCR).

Sputum samples, fiber bronchoscope brush biopsies, bronchoalveolar lavage fluids (BALF), and endobronchial biopsies are the most common respiratory specimen types. However, one problem in detecting pathogens is that conventional pathogen detection methods are time-consuming because an infectious disease may be caused by a wide range of pathogens, which must be checked individually. Another limitation is that antibiotic treatment significantly reduces the diagnostic efficacy in the culture, and the pathogens in some infectious diseases cannot be detected. Moreover, given the notable drawbacks of CE, treatment decisions are largely more empirical, particularly the emergence of mixed infection and multidrug-resistant bacteria, making further treatment difficult. Therefore, a novel pathogen detection method for improved detection and precise treatment is urgently required.

Metagenomic next-generation sequencing (mNGS) technology has been used to identify the etiology of infection and potential pathogens, including viruses, parasites, bacteria, and fungi, using high-throughput sequencing without the need to isolate and cultivate individual isolates. In the fields of clinical microbiology, compared with CE methods, mNGS has shown significant advantages, including unbiased detection, high throughput sequencing, and relatively rapid turnaround; it takes only approximately 24 h on a basic NGS workflow, which includes sample/library preparation, sequencing, data analysis, and reporting. Consequently, the mNGS technology shows evident advantages in clinical utility with its rapid identification of pathogens and simultaneous detection of multiple pathogens. It is widely used to complement CE methods and has been increasingly applied in clinical and public health settings.

NGS technology has increasingly developed, and different sequencing platforms have been applied for mNGS of clinical samples. Among the numerous available sequencing platforms, second generation sequencing technologies, such as the platforms provided by Illumina and the Beijing Genomics Institute (BGI), are the most commonly used (Jerome et al., 2019; Zhou et al., 2019; Chen L et al., 2020; Chen P et al., 2020; Yan et al., 2020; Liu et al., 2021; Zhao et al., 2021). However, few studies have determined whether choosing different sequencing platforms significantly affects clinical diagnosis; hence, selecting an appropriate sequencing platform remains a challenge for clinical laboratories and clinicians. Previous studies have reported that various sequencing platforms have similar sensitivity in detecting reference panels that mimic clinical specimens (Liu et al., 2021). However, the reference samples may not precisely represent clinical specimens. To address this issue, we investigated the diagnostic accuracy of the BGI and Illumina platforms by detecting clinical specimens simultaneously to aid clinicians in interpreting the diagnostic results of different platforms, which helps to guide treatment decisions. We attempted to evaluate the advantages of mNGS for detecting pathogens and the difference between the Illumina and BGI platforms in terms of their diagnostic performance for pulmonary infectious diseases.

2 Materials and methods

2.1 Study design and patient population

This prospective, observational, single-center study was conducted in the Respiratory Department of the General Hospital of Tianjin Medical University, China, from December 2018 to July 2019. The major inclusion criteria were as follows: 1) patients with suspected pulmonary infection who exhibited typical clinical symptoms of pulmonary infection, such as cough, fever, expectoration, and respiratory failure, and laboratory data and radiographic manifestations of pneumonia; 2) patients that agreed to undergo bronchoscopy and mNGS testing; 3) both specimens and the detection process passed mNGS quality control; and 4) patients with complete medical records. Patients with incomplete medical records and no mNGS results were excluded. A total of 46 patients admitted to the hospital with suspected pneumonia were analyzed (Figure 1).

2.2 Specimen collection and processing

The specimens collected included transbronchial lung biopsy (6–10 pieces, each weighing approximately 4–6 g) and BALF. Furthermore, fiber bronchoscope brush biopsies of patients with suspected pulmonary infection were collected using bronchoscopy performed according to standard procedures (Meyer et al., 2012).

Samples from three different categories were collected from most patients; only one or two samples were collected in some patients because of long-term bronchoscopy intolerance or difficulty in obtaining specimens. Subsequently, the lung biopsy specimens were sent to histopathology laboratories within 2 h, and dehydration, paraffin embedding, slicing, special pathological staining (including hematoxylin-eosin (HE) staining, Ziehl–Neelsen acid-fast staining, hexamine silver staining), and pathological examination were carried out. The BALF samples were used for fungal and bacterial culture, galactomannan (GM) test, and GeneXpert MTB/RIF (Xpert) assays for diagnosing tuberculosis (TB). The remaining lung biopsy specimens, BALF, and brush biopsies were divided into two parts and sent to the BGI and Illumina for mNGS. Other CEs, including sputum culture, serum GM test, β-1,3-glucans test (G-test), and cryptococcal capsular antigen serology detection, were also performed. For cytomegalovirus (CMV) and Ebstein-Barr virus (EBV) detection in blood, quantitative real-time polymerase chain reaction (qRT-PCR) was conducted.

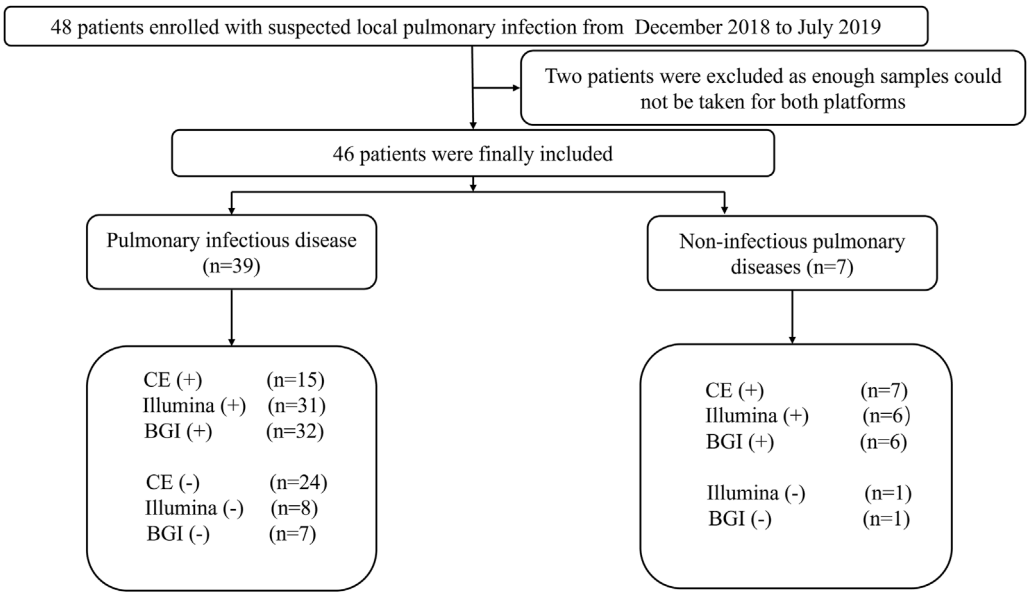

FIGURE 1
Flow chart depicting the enrollment of patients in this study. CE, conventional examination; BGI, Beijing Genomics Institute.

2.3 mNGS on two sequencing platforms and data analysis

2.3.1 BGI platform

DNA was extracted from lung biopsy specimens, BALF, and brush biopsy samples using the TIANamp Micro DNA Kit (DP316; TIANGEN BIOTECH, Beijing, China) following the manufacturer's standard procedures. The Agilent 2100 equipment (Agilent Technologies, Santa Clara, CA, United States) was used for quality control of the DNA libraries. Libraries that passed quality control were sequenced using the BGISEQ-50 platform (Jeon et al., 2014a). To obtain high-quality sequencing data, low-quality and short (length <35 bp) reads were removed. Computational subtraction databases of human host sequences were mapped to the human reference genome (GRCh38 downloaded from NCBI: ftp://ftp.ncbi.nlm.nih.gov/genomes/on December 2013) using the Burrows-Wheeler alignment (BWA) tool (version 0.7.17-r1188, http://biobwa.sourceforge.net/) (Li et al., 2009). Microbial reads were classified using Kraken2 (version 2.1.2). The classification reference databases were downloaded from NCBI (ftp://ftp.ncbi.nlm.nih.gov/genomes/). RefSeq contains more than 4,000 viral genomes, nearly 3,000 bacterial genomes, over 200 clinically prevalent fungi, as well as 140 disease-related parasites.

2.3.2 Illumina platform

DNA from lung samples including lung biopsy specimens, BALF, and brush biopsies was extracted using the TIANamp Micro DNA kit (DP316; Tiangen Biotech, Beijing, China). The extracted DNA was amplified into 200–300 bp fragments, and a DNA library was constructed by terminal overnight repair and PCR amplification of extracted DNA. The libraries were sequenced on the Illumina MiniSeq platform (Illumina) (Gu et al., 2019). Additionally, read quality was determined using FASTQC. High-quality sequencing data were retained, while short (<35 bp), low-complexity, and low-quality reads were removed, followed by computational subtraction of human sequences using the BWA tool. Reads were aligned to the GRCh38 human reference genome using BWA (version. 0.7.17-r1188). Finally, the remaining reads were aligned to the Microbial Genome Database. Microbial reads were classified using Kraken2 (version 2.1.2). The classification reference databases were downloaded from NCBI (ftp://ftp.ncbi.nlm.nih.gov/genomes/). RefSeq contains 4192 whole-genome sequence of viral taxa, 3233 bacterial genomes or scaffolds, 265 fungi related to human infection, and 274 parasites associated with human diseases.

2.4 Diagnostic criteria

Owing to the lack of standard methods for interpreting mNGS results and the diversity of reported parameters among different sequencing platforms, we used previously published standards (Petrucelli et al., 2020; Xie et al., 2021). The interpretation criteria were as follows: 1) a relative abundance of bacteria and fungi at the genus level (excluding *Mycobacterium tuberculosis*) greater than 30%; 2) sample considered positive for *M. tuberculosis* when at least one read aligned to the reference genome at the genus or species level, and 3) a pathogen considered to be positively detected using a traditional detection method and the mNGS reads number more than 50 (Li et al., 2018). An extensive literature search showed that for identifying pathogens of pulmonary infection, the normal skin flora and microbes in the oral cavity or respiratory tract must be excluded. The final clinical mNGS diagnosis results were determined by combining the original mNGS results and the clinical symptoms of the patients, which were analyzed thoroughly by three

TABLE 1 Baseline characteristics of the patients (N = 46).

	Total patients' group [n (%)]
Sex	
Male	26 (56.52)
Female	20 (43.48)
Age (years) (mean ± SD)	40.96 ± 19.40
<40	22 (47.83)
40–70	22 (47.83)
≥70	2 (4.34)
Sample type (mNGS)	
BALF	42 (91.30)
Lung tissue	34 (73.91)
Brush	34 (73.91)
Chest computed tomography (CT)	
Bilateral	26 (56.52)
Unilateral	20 (43.48)
Immunocompromised status	
Immunocompromised	33 (71.73)
Acute Lymphocytic Leukemia	14 (30.43)
Acute Myeloid Leukemia	10 (21.74)
Myelodysplastic Syndrome	2 (4.35)
Multiple Myeloma	2 (4.35)
Aplastic Anemia	2 (4.35)
Non-Hodgkin's lymphoma	1 (2.17)
Systemic Lupus Erythematosus	1 (2.17)
Idiopathic Thrombocytopenia	1 (2.17)
Non-immunocompromised	13 (28.26)

experienced physicians. CE pathogenic diagnosis was performed if at least one of the following criteria was satisfied: 1) positive culture results of the sputum, lung tissue, BALF, or transbronchial needle aspiration; 2) positive GeneXpert TB result of lung tissue sample DNA, sputum, or BALF; 3) presence of pathogens or granulomas related to infections, detected with Ziehl–Neelsen, HE, Grocott's methenamine silver, and periodic acid-Schiff staining for examination of tissue pathology; or 4) CMV/EBV DNA levels >1,000 copies/mL in the blood detected using qRT-PCR were considered CMV/EBV positive.

Immunosuppression status was defined as the concurrent use of an immunosuppressive agent for hematologic or solid malignancy, ongoing severe cytopenia, solid organ transplantation, or hematopoietic stem cell transplantation (Zachariah et al., 2020).

2.5 Statistical analysis

Statistical analysis was performed using SPSS 28.0. Count data are expressed as the percentage of the number of cases (n%). Associations between groups were determined using two-by-two contingency tables. Sensitivity (Se), specificity (Sp), negative predictive value (NPV), and positive predictive value (PPV) are presented with their 95% confidence intervals (CIs). Comparisons were performed using the McNemar test and Cochran's Q test. $p < 0.05$ was considered significant.

3 Results

3.1 Baseline characteristics of patients

In total, 46 patients with suspected pulmonary infection were enrolled in the final analysis (Figure 1). Their baseline characteristics are shown in Table 1. Twenty (43.48%) patients were female, and 26 (56.52%) were male. The mean age was 40.96 ± 19.40 years. Thirty-three (71.73%) patients had an immunosuppressed status. Furthermore, all patients underwent bronchoscopy. The main samples obtained during bronchoscopy were BALF (42 cases, 91.30%), bronchoscopy lung biopsy tissue (34 cases, 73.91%), protected specimen brush (34 cases, 73.91%), and lymph node biopsy (2 cases, 4.34%). Amongst the 46 patients, 39 (84.78%) were diagnosed with pulmonary infection, and seven (15.22%) showed no clinical evidence of pulmonary infection (non-infectious pulmonary disease, Figure 1).

A number of patients were infected with the following pathogens: 1) fungi (13 cases, 33.3%), including *Aspergillus*, *Rhizopus*, *Cryptococcus*, and *Pneumocystis jirovecii*; 2) bacteria (9 cases, 23.08%), including *Streptococcus pneumoniae*, *Haemophilus influenzae*, *Pseudomonas aeruginosa*, *Nocardiopsis*, *Moraxella osloensis*, *Escherichia coli*, and *Staphylococcus*; 3) viruses (9 cases, 23.08%), including Epstein-Barr virus, *human* respiratory syncytial virus, *human parvovirus B19*, *Torque teno virus*, *human adenovirus*, and *human parainfluenza virus*; and 4) mixed infection (8 cases, 20.51%), including co-infection with *Aspergillus* and *M. tuberculosis*, *Cryptococcus* and *Nocardia*; Enterobacteriaceae, *K. pneumoniae*, *Mycoplasma pneumoniae*, and *Mucor circinelloides*; and Cytomegalovirus and *M. tuberculosis* (Figure 2A).

Most patients (31/39, 79.49%) received empirical antibiotic therapy during hospitalization. Among patients with fungal, bacterial, viral, and mixed infections, antibiotics were used in 12 of 13 cases (92.31%), 5 of 9 cases (55.56%), 6 of 9 cases (66.67%), and 8 of 8 cases (100%), respectively (Figure 2B).

3.2 Comparison of CE and mNGS (Illumina vs. BGI) in the diagnosis of pulmonary infection

Among the 39 patients with identified pathogens, 15 (38.46%) cases were diagnosed using CE, 31 (79.49%) using only the Illumina platform, and 32 (82.05%) using only the BGI platform (Figure 1). Twenty-seven (69.23%) cases were diagnosed using both the Illumina and BGI platforms, 4 (10.25%) cases using only the Illumina platform, and 5 (12.82%) cases using only the BGI platform (Figure 3). Furthermore, three (7.69%) cases were not detected by both platforms (Figure 3). Among the seven patients with non-infectious pulmonary disease, six (85.71%) cases were diagnosed using both the Illumina and BGI platforms, and seven (100%) cases were diagnosed using CE (Figure 1).

The performance of the two mNGS platforms and CE in diagnosing suspected pulmonary infection is shown in Table 2.

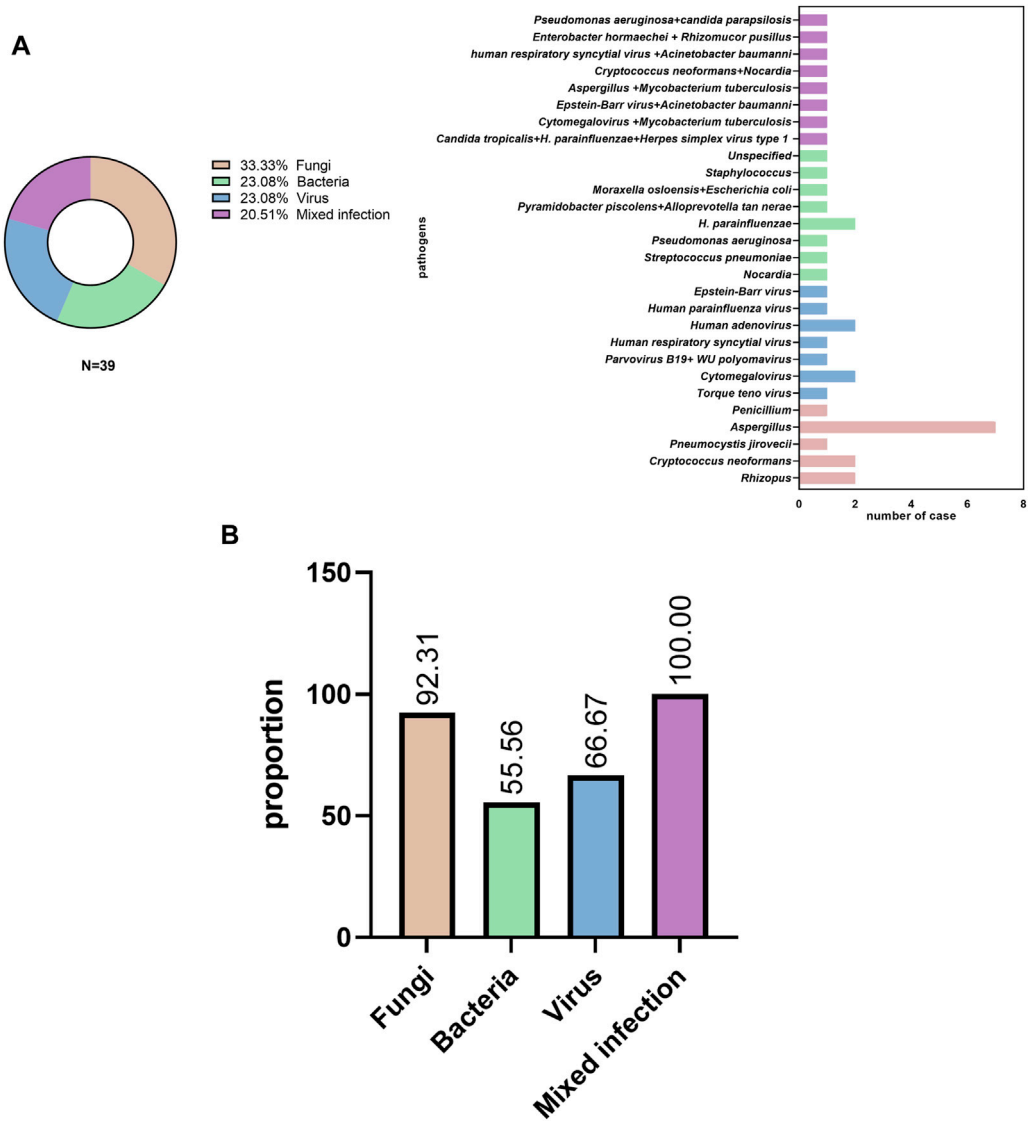

FIGURE 2
Pathogen distribution **(A)** in pulmonary infectious disease and **(B)** initial empiric antibiotic treatment.

The Se, Sp, PPV, and NPV of the Illumina platform were 76.9% (95% CI: 64.46–89.23), 85.7% (95% CI: 48.71–97.42), 96.8% (95% CI: 88.43–99.46), and 40% (95% CI: 21.38–67.40), respectively. Meanwhile, those of the BGI platform were 82.1% (95% CI: 67.33–91.02), 85.7% (95% CI: 48.71–97.42), 97.0% (95% CI: 84.68–99.47), and 46.2% (95% CI: 23.22–70.84), respectively. Furthermore, those of CE were 38.5% (95% CI: 24.89–54.10), 100% (95% CI: 64.58–100.0), 100% (95% CI: 79.62–100), and 22.6% (95% CI: 11.39–39.81), respectively. The Se of the Illumina and BGI platforms were significantly higher than that of the CE (76.9% vs. 38.5%, $p < 0.05$; 82.1% vs. 38.5%, $p < 0.05$); however, the Se of the three methods did not have significant difference (100% vs. 85.7%, $p > 0.05$). In addition, the Se and Sp of the two platforms showed no significant difference (76.9% vs. 82.1%, $p > 0.05$; 85.7% vs. 85.7%, $p > 0.05$).

3.3 Comparison of the diagnostic performance between CE and the mNGS platforms (Illumina vs. BGI)

We further compared the detection rates of the Illumina and BGI platforms and CE in the 39 patients with pulmonary infections (Cochran Q = 20.222, $p < 0.001$) (Figure 4). The detection rate of CE was significantly inferior to that of the Illumina and BGI platforms ($p < 0.001$). No significant difference was observed between the detection rates of the Illumina and BGI platforms ($p > 0.05$) (Figure 4).

We compared the diagnostic performance of the Illumina and BGI platforms in detecting bacterial, fungal, viral, and mixed infections. Of the nine pulmonary bacterial infection cases, five were detected using Illumina and eight using BGI ($p = 0.39$). Of the 13 fungal infections, 10 were detected using Illumina and 10 using BGI ($p > 0.99$). Eight of

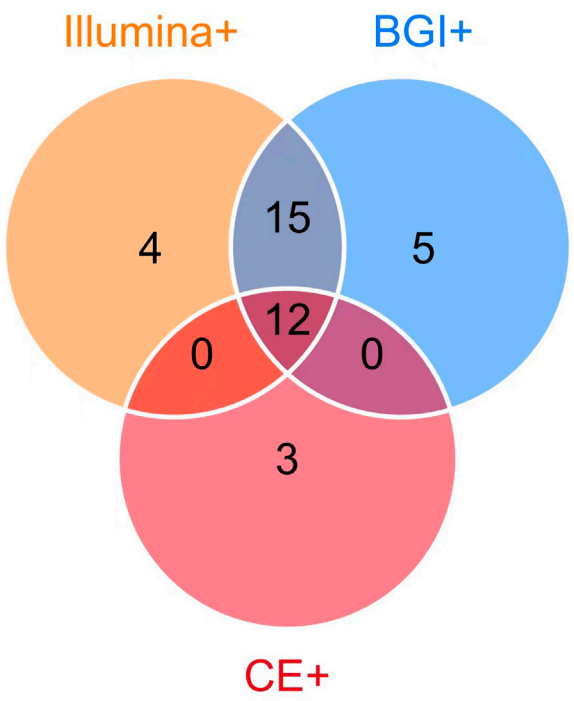

FIGURE 3
Comparison of pathogens detected using mNGS (Illumina and BGI platforms) and CE. Among the 39 patients with identified pathogens, 15 (38.46%) were diagnosed using CE (pink circle) and 3 (7.69%) using CE only; 36 (92.31%) were diagnosed using mNGS, 32 (82.05%) using the BGI platform (blue circle), 31 (79.49%) using the Illumina platform (orange circle), 12 (30.77%) using mNGS and CE (the overlap of pink, orange, blue circle). The 27 patients (69.23%) were diagnosed using the Illumina and BGI platforms (overlap between orange and blue circle Illumina and BGI platforms), 4 (10.25%) using only the Illumina platform, and 5 (12.82%) using only the BGI platform.

the nine pulmonary virus infections were detected using Illumina, while seven were detected using BGI ($p > 0.99$). Lastly, seven of the eight mixed infections were detected using Illumina, and six were detected using BGI ($p > 0.99$) (Figure 5).

4 Discussion

In the present study, the most commonly detected pathogens were bacteria, viruses, fungi, and mixed infections. The Se of the Illumina and BGI platforms was significantly higher than that of the CE. A previous study found that mNGS had higher Se and Sp than CE (Cai et al., 2020). However, our findings were consistent with those of other published studies (Li et al., 2018; Wang et al., 2019; Huang et al., 2020). These discrepancies may have been caused by the low sample size of our study.

Furthermore, we found that both the Illumina and BGI platforms had a high detection rate of pulmonary infection compared to CE. These results are consistent with those of a previous study (Miao et al., 2018; Zhao et al., 2021). In the present study, nine patients were diagnosed with bacterial infection (Figure 2A); amongst them, only 22.22% (2/9) were identified using CE. One representative case was diagnosed with lymph node bacterial infection by pathology of massive neutrophil infiltration. Another case was diagnosed with *P. aeruginosa* infection detected using BALF culture. However, these findings differ substantially from those of a prior report in which compared with mNGS, the traditional culture method identified the vast majority (74%) of bacterium-associated pneumonia (Toma et al., 2014). We consider that the lower positive culture rate in this study may be related to the initial empiric antibiotic treatment (Figure 2B).

Furthermore, in this study, the Illumina and BGI platforms offer numerous advantages in detecting *Aspergillus* infection, which is consistent with a previous study (Gu et al., 2021; Yang et al., 2021). We found that both the Illumina and BGI platforms detected *Aspergillus* infection in 100% (7/7) of patients diagnosed, and only 28.57% (2/7) of such cases were detected using a serological GM test (not a significant difference). Moreover, a previous study identified immunocompromised status as a risk factor associated with fungal and bacterial co-infection (Zhao et al., 2021). Among the eight cases of mixed pulmonary infection confirmed in the present study, eight (100%) had immunosuppressed status, seven (87.50%) mixed infections were diagnosed with the Illumina platform, and six (87.50%) were diagnosed as mixed infections using the BGI platform ($p > 0.05$). Unsurprisingly, some pathogens were not detected using CE in the eight mixed infections.

It is worth mentioning that two cases were diagnosed with TB. A patient (P12) was diagnosed with co-infection with *Aspergillus* and *M. tuberculosis*, and another patient (P30) was diagnosed with co-infection with Cytomegalovirus and *M. tuberculosis*. *M. tuberculosis* was detected using the TB GENE XPERT test of BALF and mNGS. The result is consistent with that of previous studies (Zhou et al., 2019; Xu et al., 2022), which showed that two platforms had a similar detection ability for *M. tuberculosis* when compared with TB GENE XPERT. However, because of the small sample sizes, these studies

TABLE 2 Comparison of the sensitivity and specificity between the mNGS platforms (BGI and Illumina platform) and conventional examinations.

Method	% sensitivity	% specificity	% PPV	% NPV
CE	38.5 (24.89–54.10)	100 (64.58–100.0)	100 (79.62–100)	22.6 (11.39–39.81)
Illumina	76.9[a] (64.46–89.23)	85.7[a] (48.71–97.42)	96.8[b] (88.43–99.46)	40[b] (21.38–67.40)
BGI	82.1[a,c] (67.33–91.02)	85.7[a,c] (48.71–97.42)	97.0[c] (84.68–99.47)	46.2[c] (23.22–70.84)

Data are presented as percent and 95% confidence interval. PPV, positive predictive value; NPV, negative predictive value; mNGS, metagenomic next-generation sequencing; CE, conventional examination. $p < 0.05$ was considered statistically significant.
[a]Compared to CE, $p < 0.001$.
[b]Compared to CE, $p > 0.05$.
[c]Compared to Illumina, $p > 0.05$.

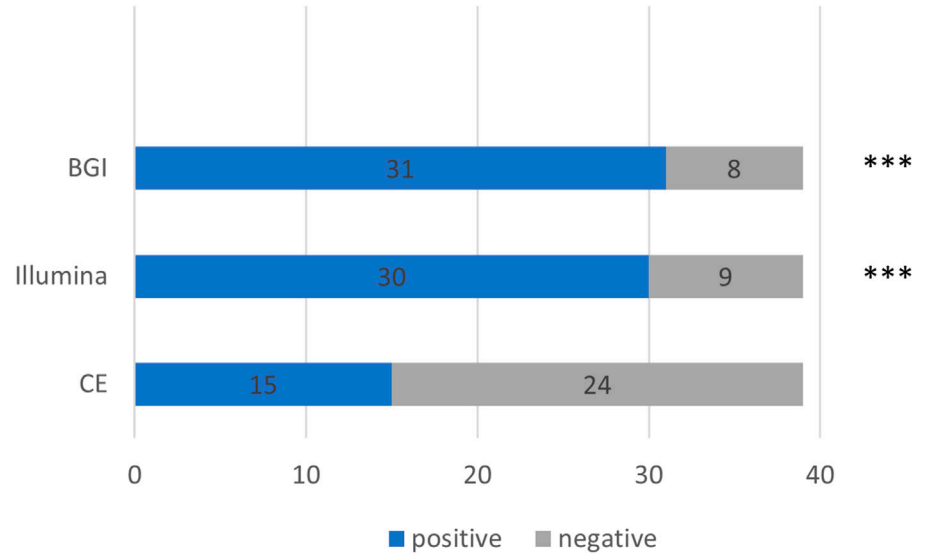

FIGURE 4
Comparison between the pathogenic detection rates of CE and the mNGS platforms (Illumina and BGI). ***$p < 0.001$, compared with CE. The x-axis represents the number of cases, while the y-axis represents the detection methods. CE, conventional examinations.

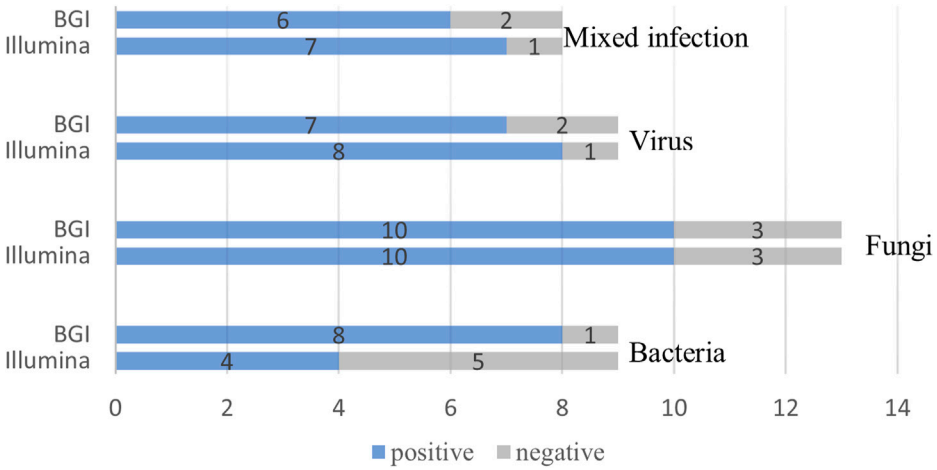

FIGURE 5
Comparison of the Illumina and BGI platforms in detecting different pathogens. No significant difference was observed between the two platforms ($p > 0.05$). The number of positive samples (x-axis) for pairwise Illumina and BGI platforms is plotted against the bacteria, fungi, virus and mixed infection groups (y-axis).

had limited power to detect effects; therefore, more evidence is needed.

CE is recommended as an auxiliary or necessary detection method for microorganisms. Three cases (P01, P03, and P41) diagnosed with cryptococcal infection, *Penicillium* infection, and bacterial lymphadenitis were detected using CE in our study. The pathogen causing pulmonary infection was unknown in one patient (P41) who was diagnosed based on histopathological examination, which showed an abundant infiltration of neutrophils.

The mNGS can theoretically report all pathogens with known genome sequences. This also means that microbial contamination in the human body will confuse doctors or affect clinical decisions (Pragman et al., 2018). Owing to the lack of standardization, defining a "positive" or "negative" infection can be difficult, thereby complicating the process of interpretation and comparisons of mNGS results. Moreover, the cost of mNGS is relatively high, which may also affect its clinical application.

Illumina sequencers are characterized by sequencing-by-synthesis technology, which includes solid-phase amplification and a cyclic reversible termination process, which confers high coverage, generating very deep data and short reads with high accuracy. However, the major shortcomings of Illumina are the long run times and the low throughput (Jerome et al., 2019; Chen L et al., 2020). Meanwhile, the BGISEQ-50 platform is based on

sequencing-by-ligation technology, which consists of combinatorial probe-anchor synthesis and DNA nanoballs. It has a short sequencing time, high output, and low cost; however, short read lengths are produced (Zhou et al., 2019; Chen P et al., 2020; Yan et al., 2020). In our study, we explored whether the samples from patients sequenced using different platforms yield the same diagnosis, which commonly confuses physicians. We found no difference in the pathogenic detection rate of the Illumina and BGI platforms (Figure 5). Thus, we can choose either of the two platforms, which does not significantly affect the clinical diagnosis. This study is helpful to clinicians selecting platforms of mNGS.

Our study has certain limitations. One is the small sample size. However, although experienced senior clinicians made a clinical judgment, no unified criteria are available for detecting pathogens using mNGS. Furthermore, distinguishing between pathogenic and colonizing microorganisms is still a challenge. Moreover, 79.49% of patients were given empirical antimicrobic treatment before pathogen detection, which might decrease the rate of obtaining positive results from the culture. CE methods of virus detection are limited in our laboratory, which may decrease the rate of virus detection to some extent.

In summary, the sensitivity of both the Illumina and BGI platforms in pulmonary infection pathogen detection were notably higher than that of CE. Furthermore, with the combination of CE and clinician experience, this technology will become a promising tool for diagnosing infectious diseases and developing a tailored therapy. Moreover, the Illumina and BGI platforms had similar performances in the diagnosis of pulmonary infectious diseases. Thus, for clinicians, the choice of sequencing platform has a less influence on clinical diagnosis. However, considerable work still needs to be done in interpreting the mNGS results.

Data availability statement

The data presented in the study are deposited in the NCBI. The accession number is PRJNA942244.

Ethics statement

The studies were reviewed and approved by the Ethics Review Committee of Tianjin Medical University General Hospital. All participants provided written informed consent for this study.

Author contributions

Conceptualization and writing—review and editing, YW, JF; data analysis and interpretation and writing—original draft preparation, SH; data analysis and writing—original draft preparation, ZZ; writing—review and editing, JH, LY. All authors have read and approved the final version and contributed significantly to this manuscript.

Funding

This research was supported by grants from the National Natural Science Foundation of China (81970083, 81270144, 81570084, 30800507 and 82170097 to JF), the National Science and Technology Major Project of China (No. 2018ZX10305409-001-001), the National Key Technology R&D Program, China (2015BAI12B00 to JF), and the Tianjin Key Medical Discipline (Specialty) Construction Project (TJYXZDXK-008A).

Acknowledgments

We gratefully acknowledge the contribution of the respiratory endoscopy team of Tianjin Medical University General Hospital.

Conflict of interest

The authors declare that the research was conducted in the absence of any commercial or financial relationships that could be construed as a potential conflict of interest.

Publisher's note

References

Cai, Y., Fang, X., Chen, Y., Huang, Z., Zhang, C., Li, W., et al. (2020). Metagenomic next generation sequencing improves diagnosis of prosthetic joint infection by detecting the presence of bacteria in periprosthetic tissues. *Int. J. Infect. Dis.* 96, 573–578. doi:10.1016/j.ijid.2020.05.125

Chen, L., Liu, W., Zhang, Q., Xu, K., Ye, G., Wu, W., et al. (2020). RNA based MNGS approach identifies a novel human coronavirus from two individual pneumonia cases in 2019 wuhan outbreak. *Emerg. Microbes Infect.* 9, 313–319. doi:10.1080/22221751.2020.1725399

Chen, P., Sun, W., and He, Y. (2020). Comparison of metagenomic next-generation sequencing technology, culture and GeneXpert MTB/RIF assay in the diagnosis of tuberculosis. *J. Thorac. Dis.* 12, 4014–4024. doi:10.21037/jtd-20-1232

Gu, W., Deng, X., Lee, M., Sucu, Y. D., Arevalo, S., Stryke, D., et al. (2021). Rapid pathogen detection by metagenomic next-generation sequencing of infected body fluids. *Nat. Med.* 27, 115–124. doi:10.1038/s41591-020-1105-z

Gu, W., Miller, S., and Chiu, C. Y. (2019). Clinical Metagenomic Next-Generation Sequencing for Pathogen Detection. *Annu. Rev. Pathol.: Mech. Dis.* 14 (1), 319–338. doi:10.1146/annurev-pathmechdis-012418-012751

Huang, J., Jiang, E., Yang, D., Wei, J., Zhao, M., Feng, J., et al. (2020). Metagenomic next-generation sequencing versus traditional pathogen detection in the diagnosis of peripheral pulmonary infectious lesions. *Infect. Drug Resist.* 13, 567–576. doi:10.2147/IDR.S235182

Jeon, Y. J., Zhou, Y., Li, Y., Guo, Q., Chen, J., Quan, S., et al. (2014a). The Feasibility Study of Non-Invasive Fetal Trisomy 18 and 21 Detection with Semiconductor Sequencing Platform. *PloS one.* 9 (10), e110240. doi:10.1371/journal.pone.0110240

Jerome, H., Taylor, C., Sreenu, V. B., Klymenko, T., Filipe, A. D. S., Jackson, C., et al. (2019). Metagenomic next-generation sequencing Aids the diagnosis of viral infections in febrile returning travellers. *J. Infect.* 79, 383–388. doi:10.1016/j.jinf.2019.08.003

Li, H., and Durbin, R. (2009). Fast and accurate short read alignment with Burrows–Wheeler transform. *Bioinform.* 25 (14), 1754–1760. doi:10.1093/bioinformatics/btp324

Li, H., Gao, H., Meng, H., Wang, Q., Li, S., Chen, H., et al. (2018). Detection of pulmonary infectious pathogens from lung biopsy tissues by metagenomic next-generation sequencing. *Front. Cell. Infect. Microbiol.* 8, 205. doi:10.3389/fcimb.2018.00205

Liu, D., Zhou, H., Xu, T., Yang, Q., Mo, X., Shi, D., et al. (2021). Multicenter assessment of shotgun metagenomics for pathogen detection. *EBiomedicine* 74, 103649. doi:10.1016/j.ebiom.2021.103649

Magill, S. S., Edwards, J. R., Bamberg, W., Beldavs, Z. G., Dumyati, G., Kainer, M. A., et al. (2014). Multistate point-prevalence survey of health care–associated infections. *N. Engl. J. Med.* 370, 1198–1208. doi:10.1056/NEJMoa1306801

Meyer, K. C., Raghu, G., Baughman, R. P., Brown, K. K., Costabel, U., du Bois, R. M., et al. (2012). An official American Thoracic Society clinical practice guideline: The clinical utility of bronchoalveolar lavage cellular analysis in interstitial lung disease. *Am. J. Respir. Crit. Care Med.* 185, 1004–1014. doi:10.1164/rccm.201202-0320ST

Miao, Q., Ma, Y., Wang, Q., Pan, J., Zhang, Y., Jin, W., et al. (2018). Microbiological diagnostic performance of metagenomic next-generation sequencing when applied to clinical practice. *Clin. Infect. Dis.* 67, S231–S240. doi:10.1093/cid/ciy693

Petrucelli, M. F., Abreu, M. H., Cantelli, B. A. M., Segura, G. G., Nishimura, F. G., Bitencourt, T. A., et al. (2020). Epidemiology and diagnostic perspectives of dermatophytoses. *J. Fungi (Basel).* 6, 310. doi:10.3390/jof6040310

Pragman, A. A., Lyu, T., Baller, J. A., Gould, T. J., Kelly, R. F., Reilly, C. S., et al. (2018). The lung tissue microbiota of mild and moderate chronic obstructive pulmonary disease. *Microbiome* 6, 7. doi:10.1186/s40168-017-0381-4

Toma, I., Siegel, M. O., Keiser, J., Yakovleva, A., Kim, A., Davenport, L., et al. (2014). Single-molecule long-read 16S sequencing to characterize the lung microbiome from mechanically ventilated patients with suspected pneumonia. *J. Clin. Microbiol.* 52, 3913–3921. doi:10.1128/JCM.01678-14

Wang, J., Han, Y., and Feng, J. (2019). Metagenomic next-generation sequencing for mixed pulmonary infection diagnosis. *BMC Pulm. Med.* 19, 252. doi:10.1186/s12890-019-1022-4

Xie, G., Zhao, B., Wang, X., Bao, L., Xu, Y., Ren, X., et al. (2021). Exploring the clinical utility of metagenomic next-generation sequencing in the diagnosis of pulmonary infection. *Infect. Dis. Ther.* 10, 1419–1435. doi:10.1007/s40121-021-00476-w

Xu, P., Yang, K., Yang, L., Wang, Z., Jin, F., Wang, Y., et al. (2022). Next-generation metagenome sequencing shows superior diagnostic performance in acid-fast staining sputum smear-negative pulmonary tuberculosis and non-tuberculous mycobacterial pulmonary disease. *Front. Microbiol.* 13, 898195. doi:10.3389/fmicb.2022.898195

Yan, L., Sun, W., Lu, Z., and Fan, L. (2020). Metagenomic next-generation sequencing (MNGS) in cerebrospinal fluid for rapid diagnosis of tuberculosis meningitis in HIV-negative population. *Int. J. Infect. Dis.* 96, 270–275. doi:10.1016/j.ijid.2020.04.048

Yang, L., Song, J., Wang, Y., and Feng, J. N. D. (2021). Metagenomic next-generation sequencing for pulmonary fungal infection diagnosis: Lung biopsy versus bronchoalveolar lavage fluid. *Infect. Drug Resist.* 14, 4333–4359. doi:10.2147/IDR.S333818

Zachariah, P., Johnson, C. L., Halabi, K. C., Ahn, D., Sen, A. I., Fischer, A., et al. (2020). Epidemiology, clinical features, and disease severity in patients with coronavirus disease 2019 (COVID-19) in a Children's Hospital in New York City, New York. *JAMA Pediatr.* 174, 202430. doi:10.1001/jamapediatrics.2020.2430

Zhao, Z., Song, J., Yang, C., Yang, L., Chen, J., Li, X., et al. (2021). Prevalence of fungal and bacterial co-infection in pulmonary fungal infections: A metagenomic next generation sequencing-based study. *Front. Cell. Infect. Microbiol.* 11, 749905. doi:10.3389/fcimb.2021.749905

Zhou, X., Wu, H., Ruan, Q., Jiang, N., Chen, X., Shen, Y., et al. (2019). Clinical evaluation of diagnosis efficacy of active *Mycobacterium tuberculosis* complex infection via metagenomic next-generation sequencing of direct clinical samples. *Front. Cell. Infect. Microbiol.* 9, 351. doi:10.3389/fcimb.2019.00351

frontiers | Frontiers in Pharmacology

TYPE Case Report
PUBLISHED 04 May 2023
DOI 10.3389/fphar.2023.1177329

OPEN ACCESS

EDITED BY
Peiran Yang,
Chinese Academy of Medical Sciences and Peking Union Medical College, China

REVIEWED BY
Haibo Li,
China-Japan Friendship Hospital, China
Li Li,
Shanghai Baoshan Hospital of Integrated Traditional Chinese and Western Medicine, China

*CORRESPONDENCE
Xiaoping Zhu,
dfyyky@tongji.edu.cn

†These authors have contributed equally to this work

RECEIVED 01 March 2023
ACCEPTED 24 April 2023
PUBLISHED 04 May 2023

CITATION
Deng C, Deng G and Zhu X (2023), Case Report: Nintedanib for immune-related pneumonitis triggered by anti-PD-1 treatment in a patient with SMARCA4-mutant NSCLC: a case report. *Front. Pharmacol.* 14:1177329. doi: 10.3389/fphar.2023.1177329

Case Report: Nintedanib for immune-related pneumonitis triggered by anti-PD-1 treatment in a patient with SMARCA4-mutant NSCLC: a case report

Changwen Deng†, Ganxiu Deng† and Xiaoping Zhu*

Department of Respiratory and Critical Care Medicine, Shanghai East Hospital, Tongji University School of Medicine, Tongji University, Shanghai, China

SMARCA4-mutant lung cancer accounts for approximately 10% of non-small-cell lung cancers (NSCLCs), has few effective treatments, and has been associated with a poor prognosis. Our case report describes a 73-year-old man who was diagnosed with SMARCA4-mutant advanced lung adenocarcinoma. Routine driver gene mutation screening was negative, and tumor tissue immunohistochemistry analysis showed the absence of the BRG1 protein (encoded by SMARCA4). In addition to the standard chemotherapy regimens, programmed cell death protein 1 (PD-1) inhibitors were administered. After three cycles of combination therapy, the focus of the primary lung tumor shrunk evidently, but radiological interstitial abnormalities emerged in the basal and subpleural areas of the bilateral lungs. The patient's clinical condition deteriorated and he was diagnosed with immune checkpoint inhibitor (ICI)-associated pneumonia. Thus, the combination regimen was discontinued, corticosteroid therapy was administered according to guidelines, and nintedanib was added, given that interstitial abnormalities were observed on chest computed tomography (CT). Following the above treatment, the patient's condition improved, the standard chemotherapy regimen was restarted, and nintedanib treatment was maintained. The patient's clinical condition continued to improve, and follow-up CT showed significant resolution of the interstitial abnormalities and stabilization of the primary tumor lesion. In summary, we report the case of a patient with SMARCA4-mutant NSCLC, which is generally considered to be associated with a poor prognosis owing to a lack of effective treatments. The patient responded favorably to initial combination therapy with ICIs, although he subsequently developed immune-related adverse events. We also found that nintedanib, a multitargeted anti-fibrotic agent, was beneficial for the treatment of immune-related lung injury and showed potential anti-tumor effects.

KEYWORDS

SMARCA4-mutant, NSCLC, immune checkpoint inhibitors, nintedanib, case report

Introduction

Non-small-cell lung cancer (NSCLC) accounts for 80%–85% of lung cancers and is one of the most common cancers in the world as well as a leading cause of cancer-related deaths (Siegel et al., 2022). Historically, cytotoxic chemotherapy has been the primary treatment option. Owing to the growing depth of cancer biology knowledge and identification of carcinogenic driving genes over the past decade, personalized targeted therapy has become the first-line treatment for patients with NSCLC (Tan and Tan, 2022). However, owing to the lack of targetable gene mutations and presence of drug resistance in some patients, targeted therapy is not suitable for all patients. In recent years, immunotherapy based on immune checkpoint inhibitors (ICIs), including programmed death receptor and ligand 1 (PD-1 and PD-L1) inhibitors, has gradually shifted to first-line therapy and has been found to significantly prolong the survival of patients with advanced NSCLC (Reck et al., 2022). Despite significant improvements, several challenges remain associated with ICI therapy, such as an initial failure response that can be attributed to potential low inherent immunogenicity in certain patients and the development of acquired resistance over time despite an initial promising response (Passaro et al., 2022). Furthermore, increasing evidence has described the acute or chronic clinical toxicities, namely, immune-related adverse events (irAEs), that are associated with the use of these agents.

An increasing number of studies have shown that NSCLCs are associated with cancerous mutations along with non-carcinogenic factors, such as loss of tumor suppressor gene function or abnormalities in the tumor microenvironment (Altorki et al., 2019; Skoulidis and Heymach, 2019). SMARCA4, which encodes the tumor suppressor and transcriptional acting factor BRG1, is a subunit of the switch/sucrose non-fermentable (SWI/SNF) chromatin remodeling complex (Mittal and Roberts, 2020). Through changing the topology of DNA-nucleosomes to regulate gene activity/expression, SMARCA4 is involved in a variety of cellular functions, such as proliferation, differentiation, and DNA repair (Mardinian et al., 2021). SMARCA4 mutations are found in a variety of cancers, including lung cancer, colon adenocarcinoma, bladder urothelial carcinoma, and invasive breast ductal carcinoma, and have been reported in approximately 10% of NSCLCs (Hodges et al., 2018). NSCLC with SMARCA4 deficiency is associated with poor clinical outcomes, and an effective treatment has not been determined (Orvis et al., 2014). Recent studies have suggested that ICIs may show a promising therapeutic response in cancers with SWI/SNF complex mutations (Abou Alaiwi et al., 2020).

Case presentation

A 73-year-old man who presented with a history of blood-stained sputum for 3 weeks was admitted to Shanghai East Hospital with no fever, chest pain, dyspnea, abdominal pain, or nausea. The patient had a smoking history of approximately 50 pack-years. A chest computed tomography (CT) scan in April 2022 showed a mass

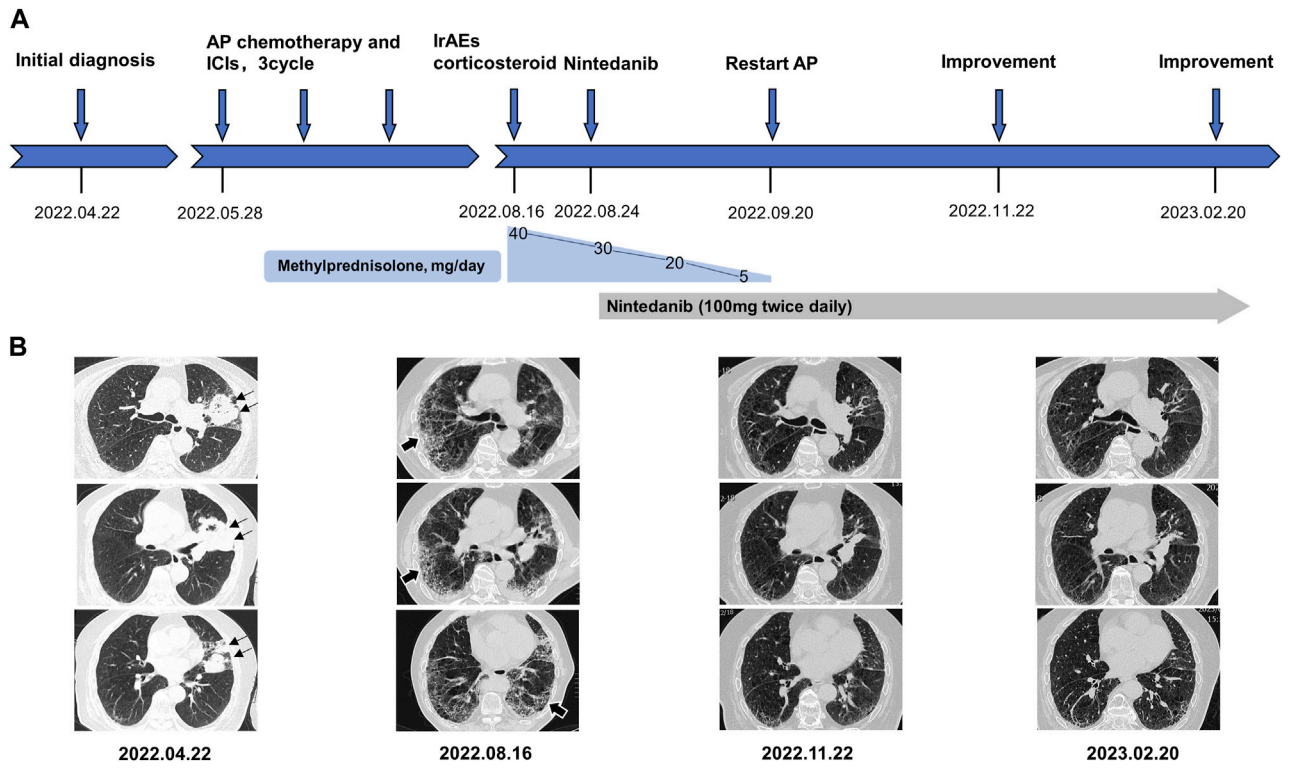

FIGURE 1
(A) refers to the timeline of the patient. **(B)** shows a series of representative different section of chest CT image changes over time. Black thin arrows indicate primary tumor lesion in left upper lung. Black thick arrows indicate immune checkpoint inhibitors-associated pneumonia in bilateral lung. AP chemotherapy, pemetrexed plus carboplatin chemotherapy. irAEs, immune-related adverse events.

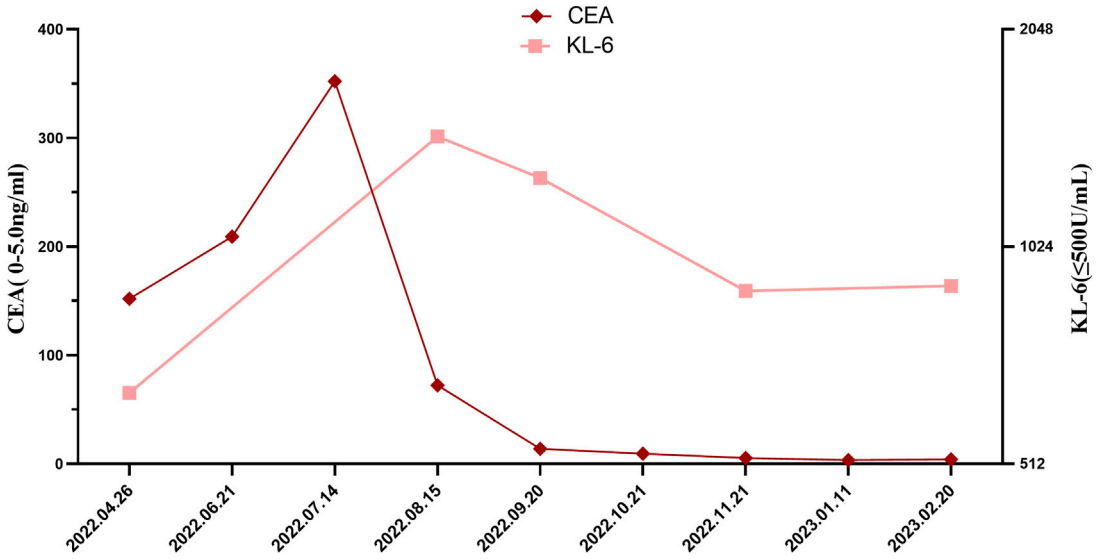

FIGURE 2
Changes in serum CEA and KL-6 levels through the clinical course. CEA, Carcinoma Embryonic Antigen, KL-6, Krebs von den Lungen-6.

in the lingual segment of the upper lobe of the left lung, with a cavity and mediastinal lymph node enlargement (Figure 1). On 28 April 2022, the patient underwent endobronchial ultrasound (EBUS) under general anesthesia, and the enlarged lymph nodes were subjected to needle biopsy.

The pathological result of the biopsy specimens indicated poorly differentiated adenocarcinoma, and immunohistochemical staining showed the following: CK(+), CK7(+), TTF1(−), NapsinA(−), BRG1(−), INI1(+), Calretinin(−), WT-1(−), Ki-67(+, 50%), PD-1(lymphocyte +, 10%), PD-L1(polyclonal EIL3N), tumor cell (+) <1%. No driver gene alterations were found in a routine nine-gene mutation test (*EGFR*, *KRAS*, *BRAF*, *HER2*, *NRAS*, *PIK3CA*, *ALK*, *ROS1*, and *RET*). The patient was eventually diagnosed with stage T3N3M0, IIIc left upper lung adenocarcinoma.

After exclusion of a series of contraindications, the patient began combination therapy with AP chemotherapy (pemetrexed disodium; 500 mg/m^2, day 1, every 3 weeks) plus carboplatin (AUC 5–6, day 1, every 3 weeks) and camrelizumab (anti-PD-1, 2 mg/kg, every 3 weeks) on 28 May 2022 (Figure 1A). When preparing for the fourth round of combined therapy on 16 August 2022, the chest CT scan suggested a large shrinkage of the primary tumor lesion, but additional interstitial abnormalities in the bilateral basal and subpleural lungs were observed (Figure 1B), along with respiratory distress. The combined treatment was discontinued, oxygen inhalation was initiated, and methylprednisolone (40 mg/day) was added (Figure 1A). The laboratory tests revealed no abnormalities in white blood cell count and C-reactive protein level, but a dramatic elevation of serum tumor markers (carcinoma embryonic antigen; CEA: 72.3 ng/mL [0–5 ng/mL] and Krebs von den Lungen-6; KL-6: 1454 U/mL [0–200 ng/mL]) was observed (Figure 2). The patient was diagnosed with grade 3 camrelizumab-related pneumonitis based on the above findings. Owing to acute dyspnea, bronchoscopy was not performed. After 1 week of corticosteroid therapy, the patient reported no significant symptom alleviation. We then decided to deliver nintedanib (100 mg twice/day), given the fibrosis-like finding on chest CT. After 1 month of corticosteroid treatment combined with nintedanib, the interstitial changes in the chest imaging findings of the patient improved (Figure 1B). Since the tumor treatment needed to be continued, carboplatin plus pemetrexed chemotherapy was restarted on 22 September 2022 and was maintained with nintedanib. During the next 4 months of follow-up, the clinical condition of the patient further improved, with stabilization of the interstitial abnormality and primary tumor lesion (Figure 1) and with significant reductions in serum CEA and KL-6 levels (Figure 2).

Discussion

The BRG1 protein encoded by SMARCA4, located on chromosome 19q13, is one of two SWI/SNF complex heterodimer catalytic subunits with ATPase activity (Mittal and Roberts, 2020). The SWI/SNF complex consists of three subunits: ATP enzyme catalytic subunit SMARCA4 (BRG1)/SMARCA2 (BRM); highly conserved core subunits SMARCB1 (encoding INI1 protein), SMARCC1, and SMARCC2; and functional specific helper subunits PBRM1 and ARID1A (Mittal and Roberts, 2020). In this patient, the immunohistochemical staining of the tumor tissue showed an absence of BRG1 expression, which indicated *SMARCA4* deletion, and the positive expression of the INI protein was also consistent with the highly conserved characteristics of *SMARCB1*. SMARCA4 has a variety of biological functions that are involved in regulating gene expression, differentiation, and transcription via chromatin remodeling. *SMARCA4* mutations are found in a variety of cancers, including 10% of NSCLCs (Hodges et al., 2018).

In terms of clinical features, most patients with BRG1-deficient NSCLC are smokers (Dagogo-Jack et al., 2020; Schoenfeld et al., 2020; Alessi et al., 2021) and usually diagnosed at an advanced stage. Prior immunohistochemistry (IHC) results have shown that more than 80% of NSCLC tumors can be classified as an adenocarcinoma, although a portion do not express thyroid transcription factor-1 (TTF-1), which is a specific adenocarcinoma marker (Dagogo-Jack et al., 2020). This finding is consistent with the pathological results of our patient. In NSCLCs, *SMARCA4* is rarely co-mutated with certain targeted driver oncogenes, such as *EGFR*, *ALK*, *MET*, *ROS1*, and *RET*, but more frequently co-occurs with other gene mutations, including *KRAS*, *TP53*, *STK11*, and *KEAP1* (Dagogo-Jack et al., 2020; Schoenfeld et al., 2020; Alessi et al., 2021). In our case, a routine nine-oncogene screen was negative, resulting in ineligibility for targeted therapy. The relationship between *SMARCA4* mutations and lung cancer prognosis has attracted increasing attention. A retrospective study of advanced NSCLCs found that patients with the *SMARCA4*-mutation type were associated with shorter overall survival than the wild-type group, and survival was the worst in the BRG1-del group (Schoenfeld et al., 2020; Alessi et al., 2021). Furthermore, patients with BRG1-deficient NSCLCs respond poorly to conventional platinum-based chemotherapy (Bell et al., 2016). This type of cancer is characterized by a lack of targetable mutated genes, insensitivity to chemotherapy, few treatment options, and poor prognosis.

In our case, the patient's clinical symptoms and primary tumor lesions improved in the early period after receiving combination therapy with ICIs. Several studies have shown that ICI-related immunotherapy can improve the prognosis of patients with *SMARCA4*-mutant NSCLC (Abou Alaiwi et al., 2020; Dagogo-Jack et al., 2020; Schoenfeld et al., 2020). Naito et al. (2019) reported a patient with SMARCA4-deficient NSCLC without targeted driver gene mutations and negative PD-L1 expression who presented a sustained response to nivolumab as a fourth-line treatment. This suggests that ICIs may be a potential promising strategy for such patients, despite their frequent negative expression of PD-L1. Mechanistically, the benefit of this strategy may be related to an elevated tumor burden (Dagogo-Jack et al., 2020; Schoenfeld et al., 2020) and the immune cell infiltration of tumor tissues (Abou Alaiwi et al., 2020). However, other studies have shown no significant correlation between ICIs and improved clinical outcomes in *SMARCA*4-mutant NSCLC (Alessi et al., 2021; Liu et al., 2021). Notably, ICIs showed poor therapeutic effects in these patients, especially in those with *KRAS* co-mutations. The main reasons for the contradictory findings among these studies are that most of the evidence was obtained from retrospective studies and case reports with small sample sizes. The identification of the potential mechanism underlying ICI therapy in *SMARCA4*-mutant NSCLC, such as tumor mutation burden and immune cell infiltration in the tumor microenvironment, may be important for stratifying patients with *SMARCA4*-mutant NSCLC who will benefit from ICIs.

ICIs are revolutionary in the treatment of cancer, especially advanced cancers, and have gradually become the core pillar of cancer therapy. However, with wide clinical application, ICIs have been associated with an increasing number of immune-related adverse events (irAEs) owing to their unique mechanism of action. IrAEs can involve almost all organ systems (Postow et al., 2018), and their onset varies widely, ranging from a few days to several months after administration. Although most of the toxicity is mild and reversible, 0.3%–1.3% of irAEs remain lethal (Postow et al., 2018; Moey et al., 2020), such as immune-associated pneumonia, which is one of the major sources of ICI morbidity and mortality. The most common clinical manifestations are dry cough, dyspnea, and oxygen desaturation. Typical imaging findings include bilateral ground-glass opacities, while other imaging findings include interstitial and organized pneumonia (Wang et al., 2018). More than 85% of patients with pneumonia respond to glucocorticoids and ICI discontinuation, although radiological findings persist for at least 1–2 years in some patients (Johnson et al., 2019).

In this case, the patient developed irAEs approximately 3 months after the initial anti-PD-1 therapy, and chest CT showed bilateral basal and subpleural reticular abnormalities, which improved after treatment with steroids and ICI discontinuation. During the treatment of irAEs, the patients was also administered nintedanib, which was based on the bilateral basement subpleural interstitial changes in CT findings and dramatically increased KL-6 levels.

Nintedanib, an oral multitargeted intracellular tyrosine kinase inhibitor (TKI), has been widely used in the treatment of idiopathic pulmonary fibrosis (IPF). Recently, it has been approved for use in other chronic interstitial lung diseases with fibrotic phenotypes, because it has been found to significantly reduce the annual decline rate of forced vital capacity in multiple well-designed clinical trials (Richeldi et al., 2014; Flaherty et al., 2019; Wells et al., 2020). However, its role in immune-associated pneumonia remains unclear. Fang et al. (2020) found that nintedanib had a significant effect on targeted therapy-related interstitial pneumonia and provided a promising strategy for patients who are not candidates for corticosteroid therapy. Another study reported that nintedanib plus corticosteroids prevented pneumonitis induced by atezolizumab, a PD-L1 inhibitor, in patients with IPF and NSCLC (Yamakawa et al., 2019). Mechanistically, nintedanib can reduce the pulmonary complications of PD-L1 inhibitors and enhance ICI efficacy by promoting vascular normalization, increasing immune cell infiltration and activation in tumors and upregulating MHC-I and PD-L1 expression on the tumor cell surface (Tu et al., 2022). The clinical symptoms in our patient did not improve significantly in the first week after corticosteroid use and ICI withdrawal. When nintedanib was added, the clinical symptoms began to show continuous improvement, and serial chest CT scans showed significant improvement of the pulmonary lesion, which enabled follow-up opportunities to restart anti-tumor treatment.

KL-6 is an extracellular domain epitope of mucins MUC1 and MUC16 and is mainly expressed by alveolar type II epithelial cells and bronchial epithelial cells (Hirasawa et al., 1997). KL-6 is a potential serum biomarker for the diagnosis and prognosis of pulmonary fibrosis (Ohshimo et al., 2014; Hamai et al., 2016). In this patient, KL-6 levels increased dramatically after the development of irAEs, which was associated with interstitial trends, and decreased during nintedanib treatment, which was consistent with radiological improvement.

In addition to its good performance in the treatment of pulmonary fibrosis, nintedanib, originally developed as an anti-neoplastic drug, plays a role in anti-tumor activity because of its

multitargeted functions. A multiple phase 3 clinical trial (LUME-Lung 1) in patients with recurrent advanced NSCLC (Reck et al., 2014) revealed that nintedanib combined with docetaxel is an effective second-line treatment, especially for patients with adenocarcinoma. A meta-analysis (Popat et al., 2017) also reported that nintedanib plus docetaxel performed well as second-line treatment and showed better performance in the lower PD-L1 expression group, altogether supporting its clinical use. In our patient, his clinical condition stabilized after restarting chemotherapy and continuing nintedanib, and the primary tumor lesion also stabilized on follow-up CT.

Our study has several limitations. The patient did not undergo testing for *SMARCA4*, despite the nine routine oncogene screening. The *SMARCA4* mutation was identified based on IHC results for the loss of BRG1 expression, although the latter is encoded by *SMARCA4*. In addition to tumor lesions and intestinal abnormalities, the chest CT showed signs of emphysema, which suggested that this patient may have chronic obstructive pulmonary disease (COPD) owing to his long smoking history. However, the patient did not complete lung function tests during the COVID-19 epidemic. Owing to the comorbidities of COPD, the patient was more likely to experience dyspnea at the time of irAEs. This also reminds us of the need for close monitoring in a clinical setting when faced with such patients.

Conclusion

NSCLC with *SMARCA4* mutations has a poor prognosis and few treatment options. ICI-related immunotherapy may have potential benefits for this type of cancer, but its side effects should be closely monitored. Nintedanib, a anti-fibrotic agent, has shown promising efficacy in the treatment of irAEs and has also been found to have potentially promising anti-tumor effects. The potential synergistic effect of antifibrotic drugs in the treatment of tumors opens up a new therapeutic approach for related complicated diseases with poor prognosis.

Data availability statement

The original contributions presented in the study are included in the article/supplementary material, further inquiries can be directed to the corresponding author.

Ethics statement

Written informed consent was obtained from the individual(s) for the publication of any potentially identifiable images or data included in this article.

Author contributions

XZ and CD conceived the case report and reviewed the article. GD wrote the original draft and prepared the case data. CD collected and analyzed clinical data. All authors approved the final manuscript.

Funding

The study was funded by grants from the National Natural Science Foundation of China, No. 82072576.

Acknowledgments

We thank the patient who participated in this study for his cooperation.

Conflict of interest

The authors declare that the research was conducted in the absence of any commercial or financial relationships that could be construed as a potential conflict of interest.

Publisher's note

References

Abou Alaiwi, S., Nassar, A. H., Xie, W., Bakouny, Z., Berchuck, J. E., Braun, D. A., et al. (2020). Mammalian SWI/SNF complex genomic alterations and immune checkpoint blockade in solid tumors. *Cancer Immunol. Res.* 8 (8), 1075–1084. doi:10.1158/2326-6066.CIR-19-0866

Alessi, J. V., Ricciuti, B., Spurr, L. F., Gupta, H., Li, Y. Y., Glass, C., et al. (2021). SMARCA4 and other SWItch/sucrose NonFermentable family genomic alterations in NSCLC: Clinicopathologic characteristics and outcomes to immune checkpoint inhibition. *J. Thorac. Oncol.* 16 (7), 1176–1187. doi:10.1016/j.jtho.2021.03.024

Altorki, N. K., Markowitz, G. J., Gao, D., Port, J. L., Saxena, A., Stiles, B., et al. (2019). The lung microenvironment: An important regulator of tumour growth and metastasis. *Nat. Rev. Cancer* 19 (1), 9–31. doi:10.1038/s41568-018-0081-9

Bell, E. H., Chakraborty, A. R., Mo, X., Liu, Z., Shilo, K., Kirste, S., et al. (2016). SMARCA4/BRG1 is a novel prognostic biomarker predictive of cisplatin-based chemotherapy outcomes in resected non-small cell lung cancer. *Clin. Cancer Res.* 22 (10), 2396–2404. doi:10.1158/1078-0432.CCR-15-1468

Dagogo-Jack, I., Schrock, A. B., Kem, M., Jessop, N., Lee, J., Ali, S. M., et al. (2020). Clinicopathologic characteristics of BRG1-deficient NSCLC. *J. Thorac. Oncol.* 15 (5), 766–776. doi:10.1016/j.jtho.2020.01.002

Fang, W., Huang, Y., Gan, J., He, B., and Zhang, L. (2020). Nintedanib effect in osimertinib-induced interstitial pneumonia. *J. Thorac. Oncol.* 15 (3), e34–e35. doi:10.1016/j.jtho.2019.09.086

Flaherty, K. R., Wells, A. U., Cottin, V., Devaraj, A., Walsh, S. L. F., Inoue, Y., et al. (2019). Nintedanib in progressive fibrosing interstitial lung diseases. *N. Engl. J. Med.* 381 (18), 1718–1727. doi:10.1056/nejmoa1908681

Hamai, K., Iwamoto, H., Ishikawa, N., Horimasu, Y., Masuda, T., Miyamoto, S., et al. (2016). Comparative study of circulating MMP-7, CCL18, KL-6, SP-A, and SP-D as disease markers of idiopathic pulmonary fibrosis. *Dis. Markers* 2016, 4759040. doi:10.1155/2016/4759040

Hirasawa, Y., Kohno, N., Yokoyama, A., Inoue, Y., Abe, M., and Hiwada, K. (1997). KL-6, a human MUC1 mucin, is chemotactic for human fibroblasts. *Am. J. Respir. Cell Mol. Biol.* 17 (4), 501–507. doi:10.1165/ajrcmb.17.4.2253

Hodges, H. C., Stanton, B. Z., Cermakova, K., Chang, C. Y., Miller, E. L., Kirkland, J. G., et al. (2018). Dominant-negative SMARCA4 mutants alter the accessibility landscape of tissue-unrestricted enhancers. *Nat. Struct. Mol. Biol.* 25 (1), 61–72. doi:10.1038/s41594-017-0007-3

Johnson, D. B., Taylor, K. B., Cohen, J. V., Ayoubi, N., Haugh, A. M., Wang, D. Y., et al. (2019). Anti-PD-1-Induced pneumonitis is associated with persistent imaging abnormalities in melanoma patients. *Cancer Immunol. Res.* 7 (11), 1755–1759. doi:10.1158/2326-6066.CIR-18-0717

Liu, L., Ahmed, T., Petty, W. J., Grant, S., Ruiz, J., Lycan, T. W., et al. (2021). SMARCA4 mutations in KRAS-mutant lung adenocarcinoma: A multi-cohort analysis. *Mol. Oncol.* 15 (2), 462–472. doi:10.1002/1878-0261.12831

Mardinian, K., Adashek, J. J., Botta, G. P., Kato, S., and Kurzrock, R. (2021). SMARCA4: Implications of an altered chromatin-remodeling gene for cancer development and therapy. *Mol. Cancer Ther.* 20 (12), 2341–2351. doi:10.1158/1535-7163.MCT-21-0433

Mittal, P., and Roberts, C. W. M. (2020). The SWI/SNF complex in cancer - biology, biomarkers and therapy. *Nat. Rev. Clin. Oncol.* 17 (7), 435–448. doi:10.1038/s41571-020-0357-3

Moey, M. Y. Y., Gougis, P., Goldschmidt, V., Johnson, D. B., Lebrun-Vignes, B., Moslehi, J., et al. (2020). Increased reporting of fatal pneumonitis associated with immune checkpoint inhibitors: A WHO pharmacovigilance database analysis. *Eur. Respir. J.* 55 (6), 2000038. doi:10.1183/13993003.00038-2020

Naito, T., Umemura, S., Nakamura, H., Zenke, Y., Udagawa, H., Kirita, K., et al. (2019). Successful treatment with nivolumab for SMARCA4-deficient non-small cell lung carcinoma with a high tumor mutation burden: A case report. *Thorac. Cancer* 10 (5), 1285–1288. doi:10.1111/1759-7714.13070

Ohshimo, S., Ishikawa, N., Horimasu, Y., Hattori, N., Hirohashi, N., Tanigawa, K., et al. (2014). Baseline KL-6 predicts increased risk for acute exacerbation of idiopathic pulmonary fibrosis. *Respir. Med.* 108 (7), 1031–1039. doi:10.1016/j.rmed.2014.04.009

Orvis, T., Hepperla, A., Walter, V., Song, S., Simon, J., Parker, J., et al. (2014). BRG1/SMARCA4 inactivation promotes non-small cell lung cancer aggressiveness by altering chromatin organization. *Cancer Res.* 74 (22), 6486–6498. doi:10.1158/0008-5472.CAN-14-0061

Passaro, A., Brahmer, J., Antonia, S., Mok, T., and Peters, S. (2022). Managing resistance to immune checkpoint inhibitors in lung cancer: Treatment and novel strategies. *J. Clin. Oncol.* 40 (6), 598–610. doi:10.1200/JCO.21.01845

Popat, S., Mellemgaard, A., Reck, M., Hastedt, C., and Griebsch, I. (2017). Nintedanib plus docetaxel as second-line therapy in patients with non-small-cell lung cancer of adenocarcinoma histology: A network meta-analysis vs new therapeutic options. *Future Oncol. Lond Engl.* 13 (13), 1159–1171. doi:10.2217/fon-2016-0493

Postow, M. A., Sidlow, R., and Hellmann, M. D. (2018). Immune-related adverse events associated with immune checkpoint blockade. *N. Engl. J. Med.* 378 (2), 158–168. doi:10.1056/NEJMra1703481

Reck, M., Kaiser, R., Mellemgaard, A., Douillard, J. Y., Orlov, S., Krzakowski, M., et al. (2014). Docetaxel plus nintedanib versus docetaxel plus placebo in patients with previously treated non-small-cell lung cancer (LUME-Lung 1): A phase 3, double-blind, randomised controlled trial. *Lancet Oncol.* 15 (2), 143–155. doi:10.1016/S1470-2045(13)70586-2

Reck, M., Remon, J., and Hellmann, M. D. (2022). First-line immunotherapy for non–small-cell lung cancer. *J. Clin. Oncol.* 40 (6), 586–597. doi:10.1200/jco.21.01497

Richeldi, L., du Bois, R. M., Raghu, G., Azuma, A., Brown, K. K., Costabel, U., et al. (2014). Efficacy and safety of Nintedanib in idiopathic pulmonary fibrosis. *N. Engl. J. Med.* 370 (22), 2071–2082. doi:10.1056/nejmoa1402584

Schoenfeld, A. J., Bandlamudi, C., Lavery, J. A., Montecalvo, J., Namakydoust, A., Rizvi, H., et al. (2020). The genomic landscape of SMARCA4 alterations and associations with outcomes in patients with lung cancer. *Clin. Cancer Res.* 26 (21), 5701–5708. doi:10.1158/1078-0432.CCR-20-1825

Siegel, R. L., Miller, K. D., Fuchs, H. E., and Jemal, A. (2022). Cancer statistics, 2022. *CA Cancer J. Clin.* 72 (1), 7–33. doi:10.3322/caac.21708

Skoulidis, F., and Heymach, J. V. (2019). Co-occurring genomic alterations in non-small-cell lung cancer biology and therapy. *Nat. Rev. Cancer* 19 (9), 495–509. doi:10.1038/s41568-019-0179-8

Tan, A. C., and Tan, D. S. W. (2022). Targeted therapies for lung cancer patients with oncogenic driver molecular alterations. *J. Clin. Oncol.* 40 (6), 611–625. doi:10.1200/JCO.21.01626

Tu, J., Xu, H., Ma, L., Li, C., Qin, W., Chen, X., et al. (2022). Nintedanib enhances the efficacy of PD-L1 blockade by upregulating MHC-I and PD-L1 expression in tumor cells. *Theranostics* 12 (2), 747–766. doi:10.7150/thno.65828

Wang, D. Y., Salem, J. E., Cohen, J. V., Chandra, S., Menzer, C., Ye, F., et al. (2018). Fatal toxic effects associated with immune checkpoint inhibitors: A systematic review and meta-analysis. *JAMA Oncol.* 4 (12), 1721–1728. doi:10.1001/jamaoncol.2018.3923

Wells, A. U., Flaherty, K. R., Brown, K. K., Inoue, Y., Devaraj, A., Richeldi, L., et al. (2020). Nintedanib in patients with progressive fibrosing interstitial lung diseases-subgroup analyses by interstitial lung disease diagnosis in the INBUILD trial: A randomised, double-blind, placebo-controlled, parallel-group trial. *Lancet Respir. Med.* 8 (5), 453–460. doi:10.1016/S2213-2600(20)30036-9

Yamakawa, H., Oba, T., Ohta, H., Tsukahara, Y., Kida, G., Tsumiyama, E., et al. (2019). Nintedanib allows retreatment with atezolizumab of combined non-small cell lung cancer/idiopathic pulmonary fibrosis after atezolizumab-induced pneumonitis: A case report. *BMC Pulm. Med.* 19 (1), 156. doi:10.1186/s12890-019-0920-9

frontiers | Frontiers in Pharmacology

TYPE Original Research
PUBLISHED 18 May 2023
DOI 10.3389/fphar.2023.1173961

OPEN ACCESS

EDITED BY
Na Wang,
Tongji University, China

REVIEWED BY
Huihui Zeng,
Central South University, China
Yongchun Shen,
Sichuan University, China
Changwen Deng,
Tongji University, China

*CORRESPONDENCE
Yubao Wang,
yubaowang2020@hotmail.com
Jing Feng,
zyyhxkfj@126.com

†These authors have contributed equally to this work and share first authorship

RECEIVED 25 February 2023
ACCEPTED 02 May 2023
PUBLISHED 18 May 2023

CITATION
Yang C, Wang G, Zhan W, Wang Y and Feng J (2023), The identification of metabolism-related subtypes and potential treatments for idiopathic pulmonary fibrosis.
Front. Pharmacol. 14:1173961.
doi: 10.3389/fphar.2023.1173961

The identification of metabolism-related subtypes and potential treatments for idiopathic pulmonary fibrosis

Changqing Yang[1†], Guixin Wang[2,3†], Wenyu Zhan[1], Yubao Wang[1*] and Jing Feng[1*]

[1]Respiratory Department, Tianjin Medical University General Hospital, Tianjin, China, [2]Tianjin Institute of Urology, Second Hospital of Tianjin Medical University, Tianjin, China, [3]Department of Urology, Second Hospital of Tianjin Medical University, Tianjin, China

Background: Idiopathic pulmonary fibrosis (IPF) is caused by aberrant repair because of alveolar epithelial injury and can only be effectively treated with several compounds. Several metabolism-related biomolecular processes were found to be involved in IPF. We aimed to identify IPF subtypes based on metabolism-related pathways and explore potential drugs for each subtype.

Methods: Gene profiles and clinical information were obtained from the Gene Expression Omnibus (GEO) database (GSE70867 and GSE93606). The enrichment scores for 41 metabolism-related pathways, immune cells, and immune pathways were calculated using the Gene Set Variation Analysis (GSVA) package. The ConsensusClusterPlus package was used to cluster samples. Novel modules and hub genes were identified using weighted correlation network analysis (WGCNA). Receiver operating characteristic (ROC) and calibration curves were plotted, and decision curve analysis (DCA) were performed to evaluate the model in the training and validation cohorts. A connectivity map was used as a drug probe.

Results: Two subtypes with significant differences in prognosis were identified based on the metabolism-related pathways. Subtype C1 had a poor prognosis, low metabolic levels, and a unique immune signature. CDS2, LCLAT1, GPD1L, AGPAT1, ALDH3A1, LAP3, ADH5, AHCYL2, and MDH1 were used to distinguish between the two subtypes. Finally, subtype-specific drugs, which can potentially treat IPF, were identified.

Conclusion: The aberrant activation of metabolism-related pathways contributes to differential prognoses in patients with IPF. Collectively, our findings provide novel mechanistic insights into subtyping IPF based on the metabolism-related pathway and potential treatments, which would help clinicians provide subtype-specific individualized therapeutic management to patients.

KEYWORDS

idiopathic pulmonary fibrosis, subtype, metabolism, prognosis, treatment, drug

1 Introduction

Idiopathic pulmonary fibrosis (IPF) is a chronic respiratory disease characterized by the destruction of healthy pulmonary tissue, which is replaced by fibrotic remodeling (Richeldi et al., 2017). The incidence and mortality of IPF have increased worldwide, placing a considerable burden on society (Hutchinson et al., 2014; Maher et al., 2021). The prognosis of IPF is poor, with a 5-year survival rate of 31% (Khor et al., 2020) although some patients may live longer (Lederer and Martinez, 2018). Thus, there is an urgent need to identify the heterogeneity of IPF prognosis and develop precise therapies.

Metabolomics has recently become a popular topic for researchers exploring health conditions in humans (Surendran et al., 2022). Metabolomics has reportedly helped elucidate the pathological mechanism of IPF (Roque and Romero, 2021; Gonzalez-Garcia et al., 2022; Wygrecka et al., 2023). Several studies have demonstrated that lipidomic markers can be used to diagnose IPF, indicating their involvement in lipid metabolism (Yan et al., 2017; Rindlisbacher et al., 2018). Metabolic pathways related to energy consumption, such as the tricarboxylic acid cycle, are accelerated in the lungs of patients with IPF (Kang et al., 2016; Zhao et al., 2017). Similar results have been obtained in mouse models, demonstrating that metabolic pathways are involved in IPF pathogenesis (Xie et al., 2015; Chung et al., 2019). Based on these findings, researchers have explored possible treatments. Small molecule-mediated 8-oxoguanine DNA glycosylase-1 (OGG1) inhibition has a potential role in pulmonary fibrosis and a modulatory effect on metabolic syndromes (Tanner et al., 2023). Zhu et al. (2021) reported that drug-targeted iron metabolism could inactivate fibroblasts and attenuate pulmonary fibrosis. However, as a call for personalized management based on treatable traits (Amati et al., 2023), few studies have focused on distinguishing IPF to provide individualized metabolic therapies. Therefore, stratification of metabolic characteristics is potentially suitable for identifying the subtypes of candidate treatments for patients with IPF.

Accordingly, we aimed to classify patients into subtypes based on their metabolism-related pathways that significantly alter the prognosis. Furthermore, we investigated the hub genes to further aid in distinguishing between the two subtypes. Finally, putative drugs for precise treatment of different subtypes were probed.

2 Materials and methods

2.1 Data collection and processing

Gene expression data and related clinical information were extracted from the Gene Expression Omnibus (GEO) database (Supplementary Tables S1 and S2). The GSE70867 dataset was used for training analysis, and normalized gene profiles were mapped using the GPL14550 and GPL17077 probes. The GSE93606 dataset was used for validation analysis, and normalized gene profiles were mapped using GPL11532 probes. Patients in these datasets were diagnosed with IPF by matching their survival-related information. Survival status was defined as death as the positive endpoint and was censored as the negative endpoint. After removing the batch effect using the SVA R package (Johnson et al., 2007), the gene expression data were collected for further analysis. Subsequent analyses were performed using R version 4.1.3 and online tools.

2.2 Metabolism-related subtyping

Metabolism-related pathway gene sets were obtained using gene set enrichment analysis (GSEA) (Mootha et al., 2003; Subramanian et al., 2005). Single-sample GSEA (ssGSEA) was performed on the training and validation cohorts to calculate the enriched fraction of each pathway in the different samples using the GSVA R package (Barbie et al., 2009). A total of 41 metabolism-related pathways were used to construct a consistency matrix using the ConsensusClusterPlus R package (Wilkerson and Hayes, 2010). The PAM algorithm was selected to perform 100 bootstraps, each of which ensured an 80% involvement of the original dataset. The k-values of the clusters ranged from 2 to 6. After classification, the view was mapped using the uniform manifold approximation and projection (UMAP) method to reduce the space dimension. The Kaplan–Meier method was used to calculate the median survival time, and survival comparisons between different subtypes were performed using the log-rank test, with p-values <0.05 considered significant.

2.3 Immune-related analysis

Enriched fractions for immune pathways and cells were obtained for each sample using ssGSEA. The immune-related data were obtained from published literature (Charoentong et al., 2017). The Wilcoxon rank-sum test was used to assess the differences in immune cell infiltration and immune pathway enrichment between metabolism-related subtypes. Pearson's correlation analysis was performed to visualize the relationships between the metabolic and immune pathways in each subtype.

2.4 Weighted gene co-expression network analysis

Weighted gene co-expression network analysis (WGCNA) (Langfelder and Horvath, 2008; 2012) was performed on 143 samples using 1,723 metabolism-related genes obtained from GSEA. An independence power value of approximately 0.85–0.9 was set to construct an unsigned topology matrix with a minimum of 30 genes and a maximum of 0.75 similarities between each module. Module–trait relationship analysis was then performed to calculate the correlation between each module and the features of the subtype. Module gene enrichment analysis was performed using Metascape (https://metascape.org/) (Zhou et al., 2019), and enrichment terms were significant at p-values <0.01. Hub genes were identified using Molecular Complex Detection (MCODE) (Bader and Hogue, 2003) in Metascape, and visualization was performed using Cytoscape (Shannon et al., 2003).

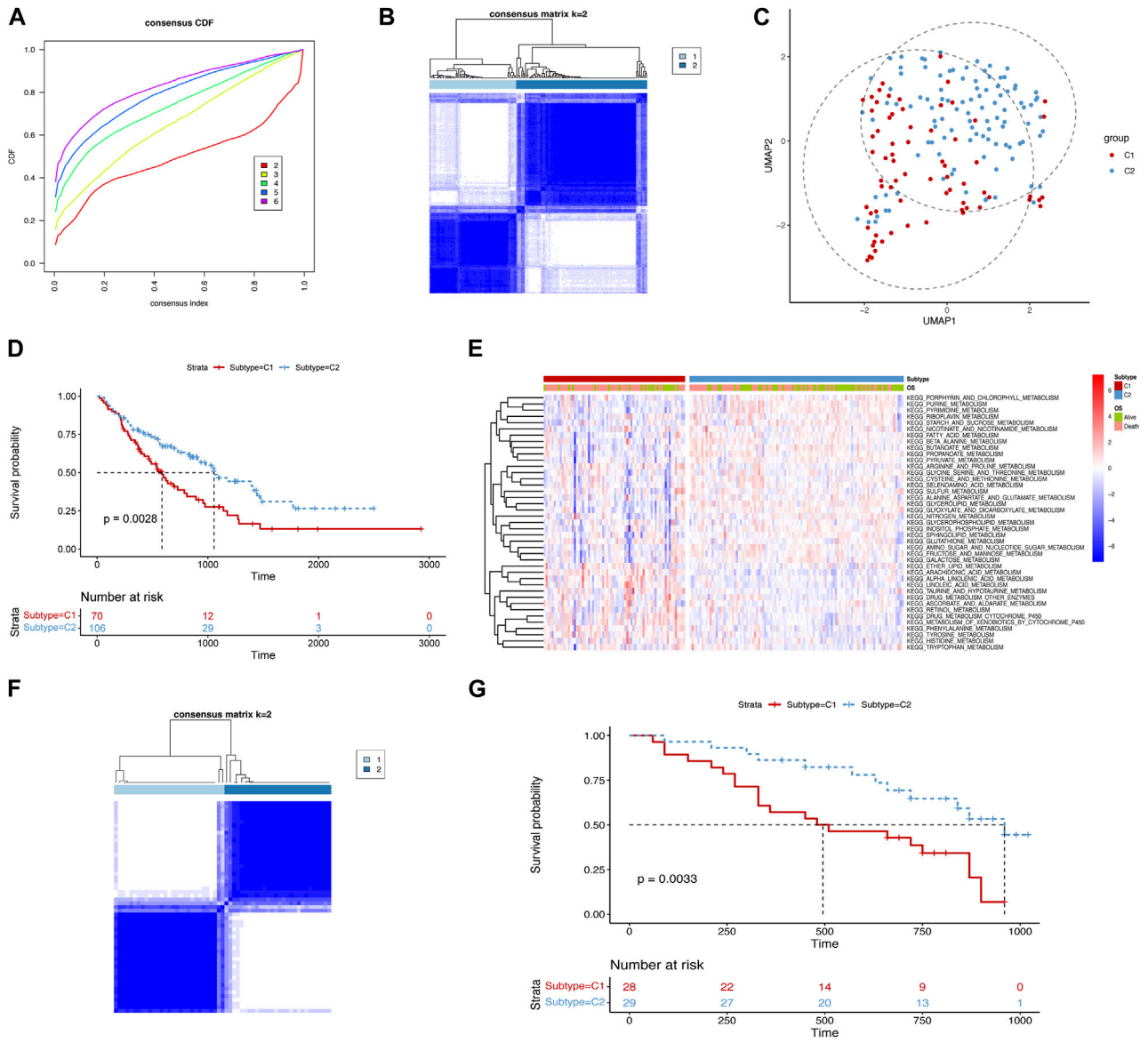

FIGURE 1
identification of metabolism-related subtypes of IPF. **(A)** Cumulative distribution function curves of the training cohort. **(B)** Sample clustering heatmap of the training cohort. **(C)** Uniform manifold approximation and projection (UMAP) plot for the two subtypes in the training cohort. **(D)** Kaplan–Meier curves displaying the overall survival of the two subtypes in the training cohort (median survival time of subtype C1: 586 days and C2: 1,055 days). **(E)** Heatmap of the differential enrichment scores of metabolism-related pathways for the two subtypes in the training cohort. **(F)** Sample clustering heatmap of the validation cohort. **(G)** Kaplan–Meier curves depicting the overall survival of the two subtypes in the validation cohort (median survival time of subtype C1: 495 days and C2: 960 days).

2.5 Diagnostic efficiency analysis of hub genes

Logistic regression was used to construct a model with hub genes to better predict the metabolism-related subtypes. A receiver operating characteristic (ROC) curve was constructed using the ROC R package (Sing et al., 2005) to assess the discriminatory ability of the model. A calibration curve was applied to assess the predictive accuracy of the model using the bootstrap method with 1,000 re-samplings (Van Calster et al., 2019). The Hosmer–Lemeshow (HL) test was added to the calibration curve, which recognized a *p*-value >0.05 as a good model fitting and calibration. The decision curve analysis (DCA) was applied to assess the clinical applicability of the model (Vickers and Elkin, 2006). The training and validation cohorts were subjected to these analyses.

2.6 Connectivity map analysis

To explore potential drugs for different subtypes, a Connectivity Map (CMap) (https://clue.io/) was used for drug identification. The L1000 method was used to identify perturbations in the mechanism

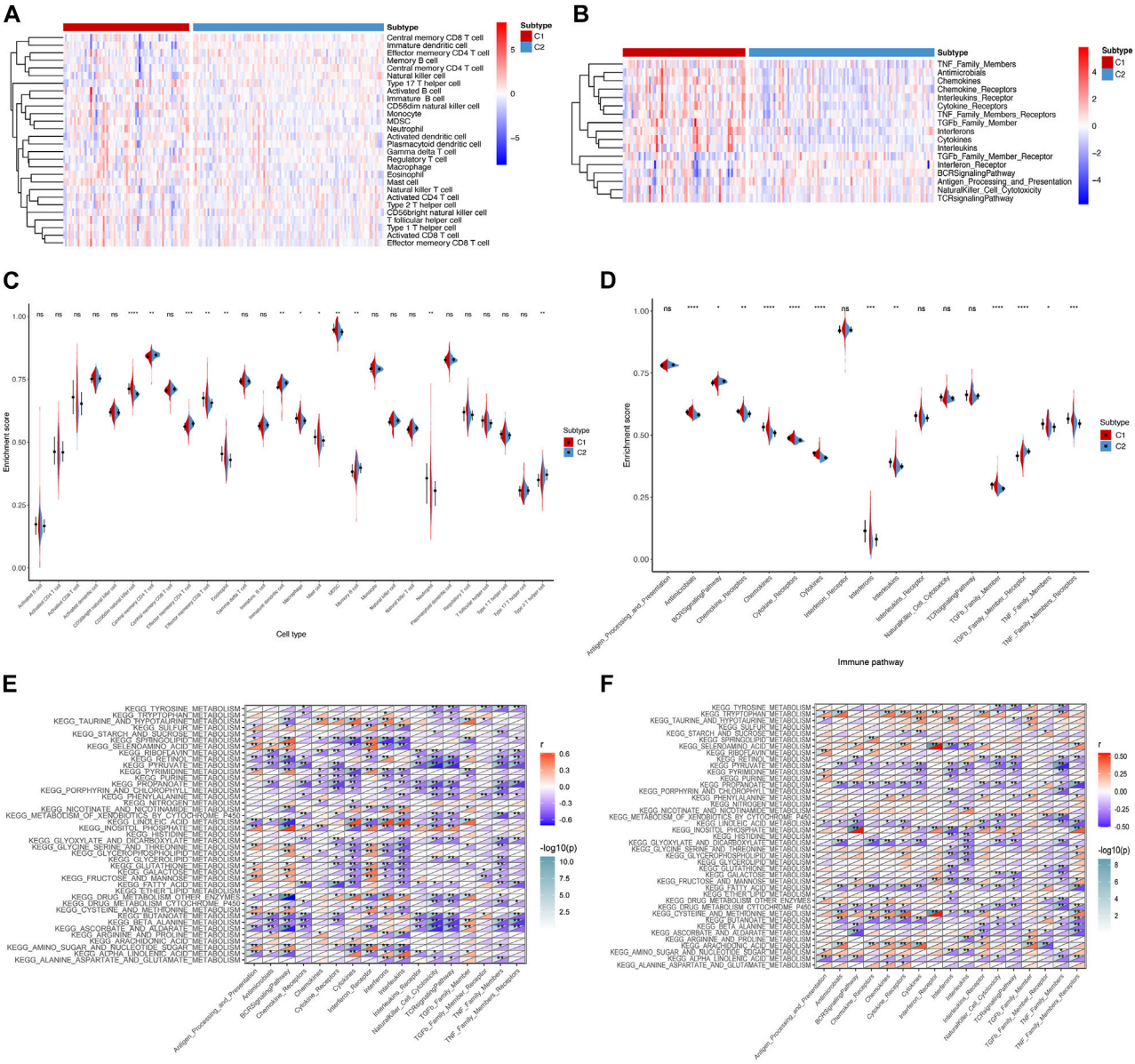

FIGURE 2
Immune landscape of metabolism-related subtypes in IPF. **(A)** Heatmap and **(C)** violin plots of differential enrichment scores of the immune cell signatures of the two subtypes. **(B)** Heatmap and **(D)** violin plots of differential enrichment scores of immune pathway categories of the two subtypes. Correlation between metabolism-related and immune pathways in **(E)** subtype C1 and **(F)** subtype C2. *$p < 0.05$, **$p < 0.01$, ***$p < 0.001$, ****$p < 0.0001$; ns, no significance.

of action (MoA) or biological functions caused by drug treatment of cells, which helped assess the possibility of drug application for different subtypes (Subramanian et al., 2017).

3 Results

3.1 The identification of the metabolism-related subtypes

To better understand metabolism-related mechanisms in IPF, we calculated the scores of the metabolism-related pathways using ssGSEA in both the training and validation cohorts (Supplementary Tables S3 and S4). Based on the 41 metabolism-related pathways, we chose k = 2 to cluster the samples into two subtypes (Figures 1A,B). We then used UMAP to project the samples into a two-dimensional space, and subtype C1 was distinguished from C2 (Figure 1C). By constructing a survival analysis, we observed that subtype C1 had a significantly shorter survival time than C2 (Figure 1D). To provide an overview of the differences between the two subtypes, we generated a heatmap showing the landscape of the metabolism-related pathway enrichment (Figure 1E). Considering all enrichments, subtype C1 exhibited a lower

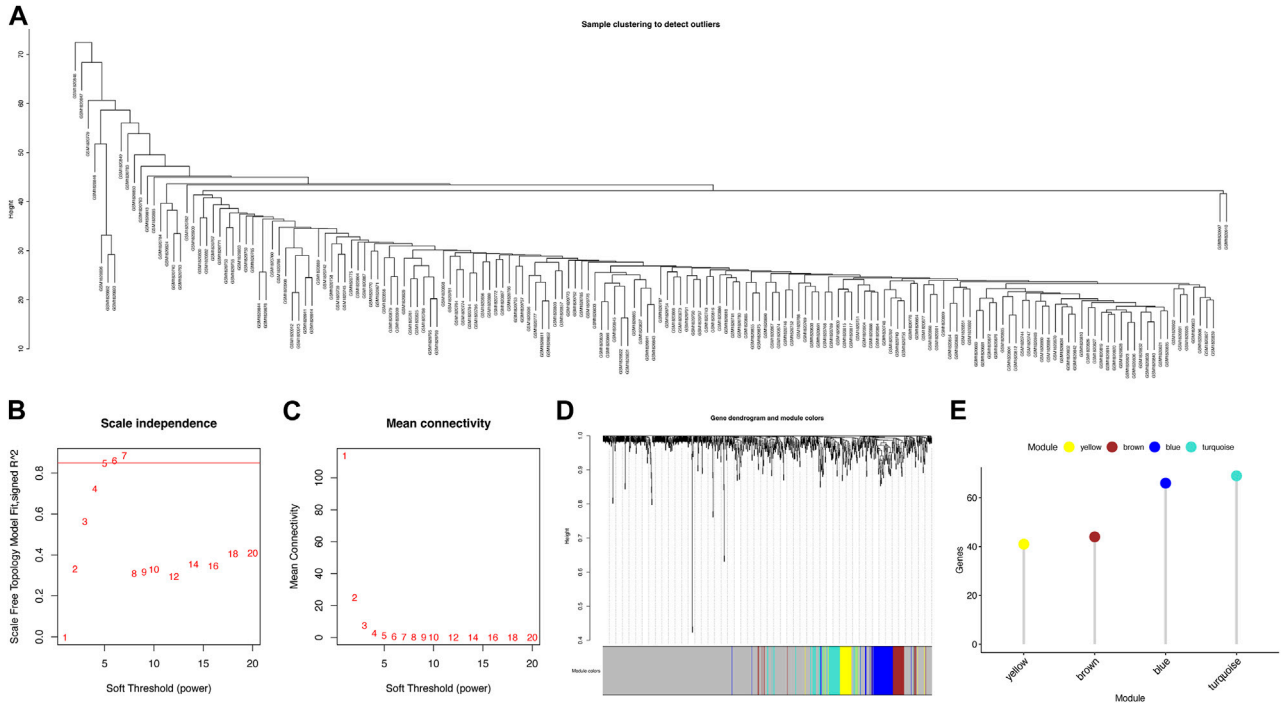

FIGURE 3
Identification of metabolism-related gene modules. **(A)** Sample clustering. **(B)** Scale-free fit index for various soft-thresholding powers. **(C)** Mean connectivity for various soft-thresholding power values. **(D)** Dendrogram of metabolism-related genes clustered using the one-step method. **(E)** Gene numbers for each module.

degree of metabolism than C2. In the validation cohort, we used the same parameters to cluster the samples into two subtypes (Figure 1F). Consistent with the results in the training cohort, the metabolism-related subtypes were significantly different in the validation cohort (Figure 1G). These results indicate that metabolic heterogeneity exists in IPF, which manifests differently according to metabolic status and can consistently distinguish the prognosis of patients in different cohorts.

3.2 Immune analysis of metabolism-related subtypes

Given that immune dysregulation plays a role in IPF (Shenderov et al., 2021), we compared the immune landscapes of the two subtypes. We analyzed immune cell infiltration and the immune pathway enrichment using a heatmap (Figures 2A,B) and a corresponding violin plot (Figures 2C,D). We observed that effector memory $CD8^+$ T cells, macrophages, and neutrophils showed increased infiltration in subtype C1 than in C2. Moreover, the antimicrobials, chemokines, cytokines, and transforming growth factor beta (TGF-β) family members were more enriched in subtype C1 than in subtype C2. Based on these findings, we examined the correlation between metabolic and immune pathways to investigate the potential crosstalk in each subtype (Figures 2E,F). We observed more negative correlations between metabolic and immune pathways in subtype C1 than in subtype C2. Collectively, our results suggest that the immune signature differs between the IPF subtypes C1 and C2, indicating differences in the immune microenvironment.

3.3 Identification of novel modules and hub genes

To investigate the key genes in the metabolism-related subtypes, we performed WGCNA. First, we used a hierarchical clustering algorithm to cluster the samples using an average calculation (Figure 3A). To obtain a balance between independence and connectivity, we chose six participants to create a scale-free network (Figures 3B,C) based on which a topological matrix was constructed. We obtained yellow, brown, blue, and turquoise modules, each of which contained clustered genes (Figures 3D,E). To identify the key genes, we first analyzed the module-trait relationships for modules and subtypes (Figure 4A). The turquoise and yellow modules (Supplementary Tables S5 and S6) exhibited apparent differences in their correlations with subtypes. Both were positively correlated with subtype C2 and negatively correlated with subtype C1, indicating that patients with a higher fraction of the two modules were more likely to have subtype C2. The smaller the fraction of the two modules, the more likely it was for the possible subtype to be C1. Notably, both the turquoise and yellow modules were highly enriched in lipid-related metabolism (Figures 4B,C). We then detected the hub genes in each correlated module using the MCODE algorithm (Figures 4D,E). Thus, we identified the hub genes CDS2, LCLAT1, GPD1L, AGPAT1,

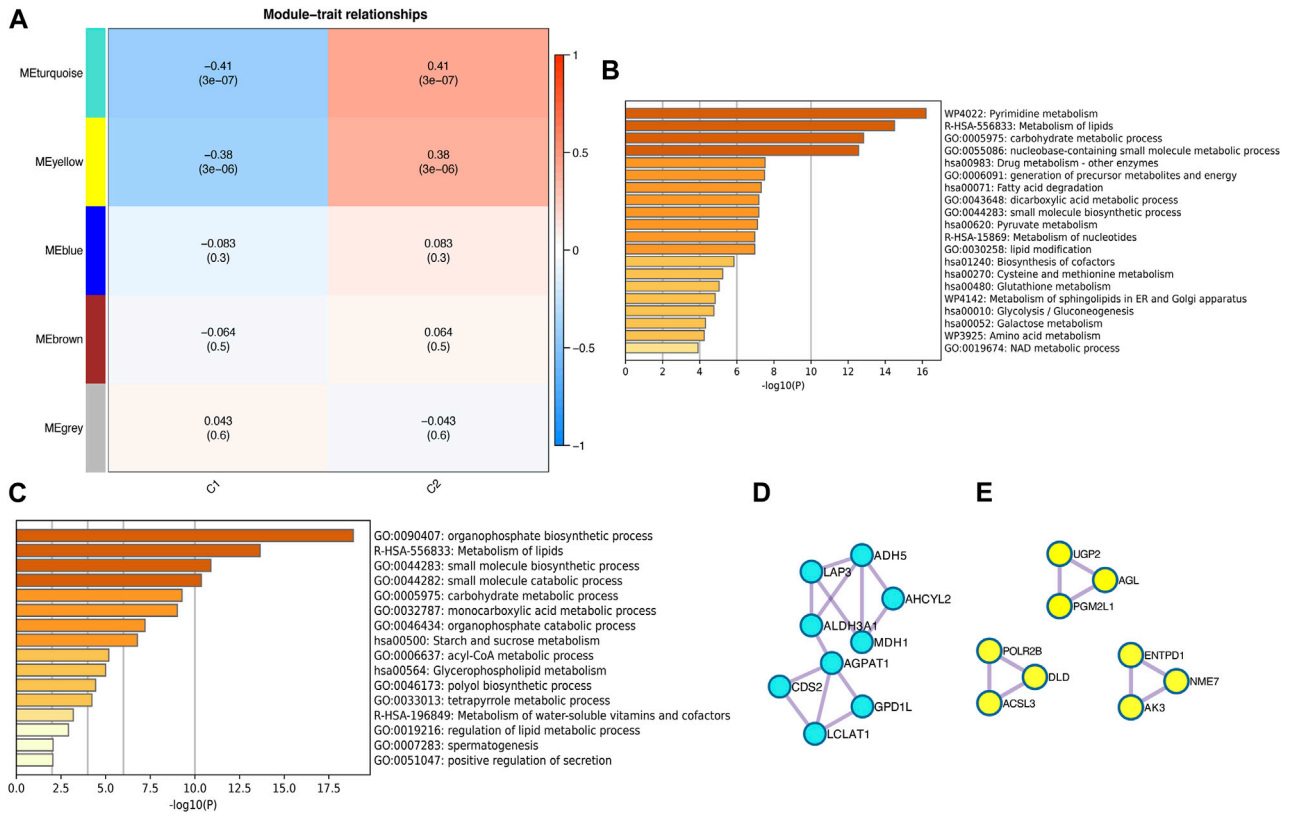

FIGURE 4
Identification of metabolism-related hub genes in IPF. **(A)** Heatmap of the correlation between modules and metabolism-related subtypes. **(B)** Enrichment analysis of the turquoise module. **(C)** Enrichment analysis of the yellow module. **(D)** Hub genes in the turquoise module. **(E)** Hub genes in the yellow module.

ALDH3A1, LAP3, ADH5, AHCYL2, and MDH1 in turquoise and PGM2L1, UGP2, AGL, AK3, ENTPD1, NME7, POLR2B, ACSL3, and DLD in yellow. These hub genes might play pivotal roles in the metabolic microenvironment of IPF and could be potential biomarkers for distinguishing the two subtypes of IPF.

3.4 Diagnostic efficiency of hub genes

We used the identified hub genes to efficiently diagnose the metabolism-related subtypes. To simplify the diagnosis, we selected the hub genes in the turquoise module, which were more closely related, for further analysis. We constructed a diagnostic model based on nine genes in the turquoise module to distinguish between subtypes C1 and C2. We evaluated the discriminatory ability of the model by generating a ROC curve (Figures 5A,B). The AUCs were 0.82 and 0.73 in the training and validation cohorts, respectively, indicating that the model can efficiently discriminate the two subtypes. Additionally, we constructed a calibration curve to evaluate the accuracy of the model (Figures 5C,D). The calibration curves in the training and validation cohorts revealed good predictive accuracy, with a p-value >0.05 for HL tests. Furthermore, we performed DCA to analyze the clinical benefits of the model (Figures 5E,F). As shown in the figures, the model could identify the positive benefits of clinical intervention. Collectively, the model constructed using hub genes could be an effective tool for distinguishing the different subtypes of IPF.

3.5 Drug probe of different subtypes

Since there are limited treatment options available for IPF, we screened drug probes for the metabolism-related subtypes using CMap. We identified 30 compounds targeting 30 molecular pathways and 30 compounds targeting 28 pathways for subtypes C1 and C2, respectively (Figures 6A,B). No molecular pathways were shared between the two subtypes for drug probes. Notably, some mechanisms of action involved more than one compound, such as an adenosine receptor agonist and a calcium channel blocker for subtype C1. Conversely, topoisomerase inhibitors exhibited a potent mechanism of action against subtype C2. Therefore, these findings indicate that the drugs suitable for the two subtypes may differ and may require further consideration for future treatment.

4 Discussion

In our study, we identified two subtypes based on 41 metabolism-related pathways that showed significant differences in prognosis between the training and validation

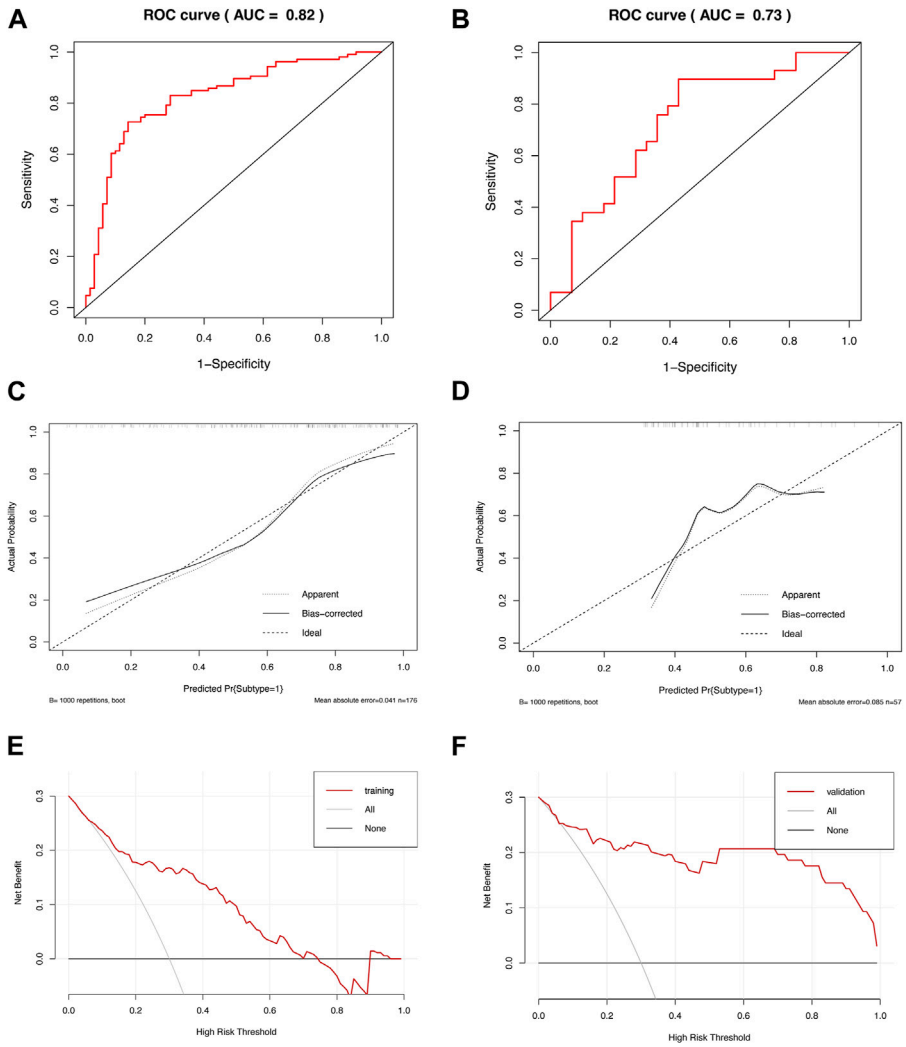

FIGURE 5
Diagnostic efficiency of the model based on hub genes. ROC curves of the diagnostic model in the **(A)** training and **(B)** validation cohorts. Calibration curves of the diagnostic model in the **(C)** training (HL test, $p = 0.228$) and **(D)** validation cohorts (HL test, $p = 0.109$). DCA of the diagnostic model in the **(E)** training and **(F)** validation cohorts.

cohorts. Furthermore, nine genes (CDS2, LCLAT1, GPD1L, AGPAT1, ALDH3A1, LAP3, ADH5, AHCYL2, and MDH1) were investigated to construct a model to distinguish between the two subtypes, with good discrimination and calibration. Notably, subtype C1, which displayed a low metabolic level, demonstrated a shorter survival time than subtype C2, which exhibited a high metabolic level. These findings suggest that metabolism-related pathways may help predict the prognosis of patients with IPF. To our knowledge, this is the first study to classify patients with IPF based on multiple metabolic pathways and screen potential treatments for each subtype.

Derricks et al. (2013) demonstrated that metabolic agents such as ascorbate could upregulate the synthesis of elastin and collagen, which could promote the deposition of the extracellular matrix (ECM). Lipid metabolism is a critical component in this process. In a mouse model, a lack of lipid synthesis increased endoplasmic reticular stress, which aggravated the remodeling of lung tissue (Romero et al., 2018). Similarly, dysfunction of apolipoprotein A could result in cholesterol deposition in alveolar macrophages, leading to the formation of foam cells, fibrosis, and remodeling of the lung tissue (Wygrecka et al., 2023). Ivanova et al. (2013) demonstrated promising results that liposomal prostaglandin E2 attenuated the extent of bleomycin-induced fibrosis in mice. Moreover, in clinical research, lipid metabolism-related products, such as amyloid A and adiponectin, are prognostic markers in clinical research (Vietri et al., 2019; d'Alessandro et al., 2020). Additionally, the activation of hypoxic response elements can modify glycolysis to promote the proliferation and differentiation of myofibroblasts during IPF progression (Dabral et al., 2019; Contreras-Lopez et al., 2020). Overall, subtyping based on metabolism-related pathways is an effective way of determining the prognosis of patients with IPF.

To determine the differences between the two subtypes, we performed an immune-related analysis. There was a negative

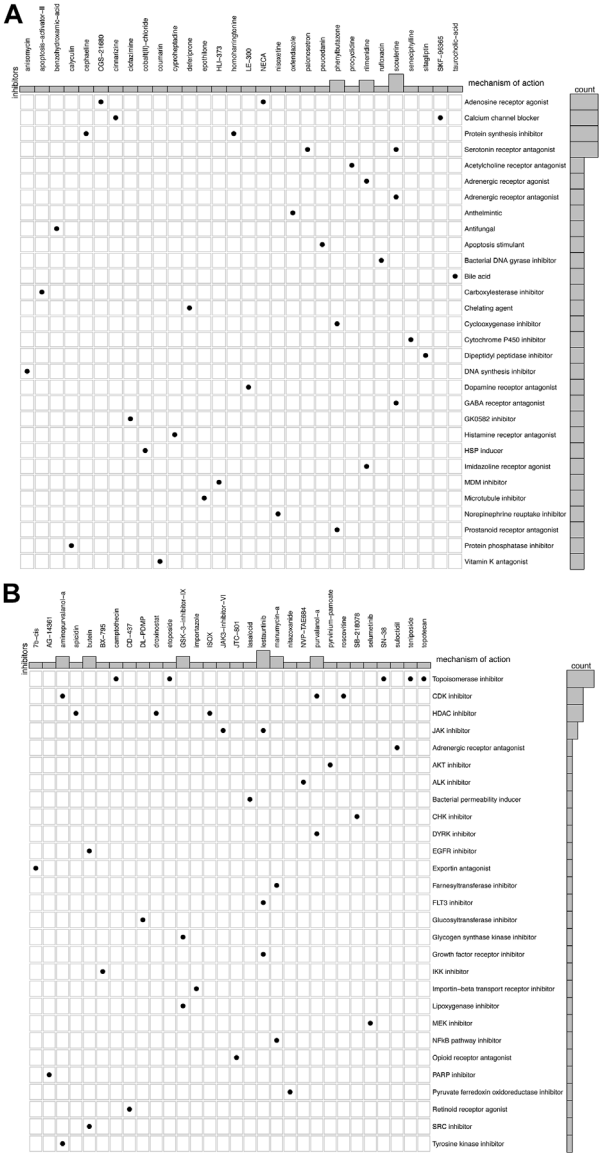

FIGURE 6
Candidate drugs and their mechanism in different subtypes of IPF. **(A)** 30 compounds and 30 molecular pathways in subtype C1. **(B)** 30 compounds and 28 molecular pathways in subtype C2.

correlation between metabolism and immunity in subtype C1. Owing to the low metabolism level in subtype C1, it may reach a more pronounced immune signature than subtype C2. This was demonstrated by the significant infiltration of immune cells and enrichment of immune pathways in subtype C1. Therefore, we hypothesized that metabolic dysregulation might correlate with immune status and promote pulmonary fibrosis by causing aberrative activation of immune cells. Researchers have previously used single-cell sequencing to identify an increase in CD8 effector memory T cells and alveolar macrophages with interferon-gamma (IFN-γ) enrichment in lung tissues affected by IPF, indicating the activation of adaptive immunity (Serezani et al., 2022). Additionally, monocyte-derived alveolar macrophages reportedly promote fibrosis, indicating the heterogeneity of macrophages in the IPF (Misharin et al., 2017). Furthermore, metabolic reprogramming in macrophages has been extensively studied, which contributes to the metabolic dysregulation of cholesterol and fatty acids (Batista-Gonzalez et al., 2019; Ahangari et al., 2023). Cholesterol deposition in macrophages results in the formation of foam cells. The accumulation of these leads to the activation of inflammatory response and increased oxidative stress in lung tissue, thereby promoting fibroblast differentiation and collagen deposition; this contributes to the progression of IPF (Wygrecka et al., 2023). The utilization and oxidation of fatty acids can provide energy for M2 macrophages to perform their biological functions, promoting fibrosis via TGF-β in IPF (Odegaard and Chawla, 2011; He et al., 2016; Rui et al., 2022). Meanwhile, a previous study found that M2 cells have glucose utilization properties, which can activate M2 polarization (Huang et al., 2016). Therefore, the aberrant metabolism-related pathway activation promotes fibrotic functions in macrophages. Neutrophils release neutrophil extracellular traps (NETs), which play a pro-fibrotic role in response to chronic inflammatory stimulation by activating the proliferation and differentiation of fibroblasts to promote collagen deposition (Chrysanthopoulou et al., 2014; Suzuki et al., 2020). Furthermore, mitochondrial inner membrane proteins, which participate in mitochondrial energy metabolism and maintain the stability of metabolic pathways, are essential for forming and releasing extracellular trapping nets from neutrophils (Amini et al., 2018). Thus, the relationship between metabolism and immunity may result in a high level of immunity in subtype C1, leading to the progression of pulmonary fibrosis and a poor prognosis.

We constructed a nine-gene diagnostic model to efficiently distinguish between the two subtypes. One of the genes in this model, CDS2, is involved in synthesizing phosphatidylinositol and plays a novel role in the progression of inflammation and fibrosis via mitochondrial dysfunction (Xu et al., 2022). Similarly, LCLAT1, which regulates linoleic acid levels, affects mitochondrial function and reactive oxygen species (ROS) generation, contributing to pulmonary fibrosis (Huang et al., 2014). Another gene, GPD1L, is involved in fibroblast proliferation and collagen synthesis in the atrium (Hao et al., 2022). Other genes, including AGPAT1, ALDH3A1, LAP3, and ADH5, have been shown to have different functions in fibrosis in various diseases (Tang et al., 2013; Niu et al., 2019; Irungbam et al., 2020; Talpan et al., 2023). Notably, we identified the novel role of AHCYL2 and MDH1 in IPF; however, further validation is required.

The nine-gene model demonstrated statistically robust results, with significant discrimination and calibration in both the training and validation cohorts, suggesting its potential clinical value. Furthermore, a drug probe was developed to distinguish between the two subtypes. It utilizes the gene expression signatures in different subtypes to connect with similar expression signatures in CMap, suggesting that the corresponding drugs that had caused these CMap signatures may confer related biological effects. Therefore, in this study, the corresponding CMap drug was the potential drug we explored for treating each IPF subtype. Drugs for subtype C1 focus on adenosine receptor activation, which can inhibit macrophage profibrotic function and abnormal metabolic activation (Csoka et al., 2014). Drugs for subtype C2, such as those targeting the inhibition of CDK, affect glucose and lactic acid

metabolism, which might be treatable for patients (Carvalhal et al., 2003). The drugs and mechanisms of action in the two subtypes suggest that different metabolism-related subtypes might have different treatable traits.

Our study has several limitations. First, the subtyping validation was performed in only one cohort, which might limit the generalizability of the results. Therefore, further validation using larger cohorts is required to increase the reliability of the results. Second, the lack of experimental verification in this study limits our understanding of the metabolic differences between the two subtypes. Thus, future studies should focus on verifying the metabolic levels in animal models and evaluating immune cell infiltration *in vivo* to further understand the biological mechanisms underlying IPF. Third, our study only identified markers for subtyping IPF; their efficiency in clinical practice still needs to be tested in human subjects. Therefore, further studies are needed to examine the efficiency of these markers and their value in clinical practice.

5 Conclusion

In conclusion, our findings confirmed that metabolic heterogeneity exists in patients with IPF. Furthermore, metabolic dysregulation contributes to the progression of pulmonary fibrosis, and different metabolic levels could result in different prognoses. Our diagnostic model, with two IPF prognosis-related subtypes based on 41 metabolism-related pathways, can aid clinicians in efficiently identifying patients with a poor prognosis, thereby facilitating individualized therapeutic management and shorter follow-up periods. Furthermore, the potential drugs identified in our study could aid in treating patients based on their distinctive subtypes. Further investigation is required to validate the clinical efficacy of the identified drugs and their potential to target metabolic pathways and treat IPF. Nonetheless, our findings provide novel insights into distinguishing patients with IPF based on metabolism-related pathways and developing individual treatment strategies for patients in different subtypes.

Data availability statement

The original contributions presented in the study are included in the article/Supplementary Material; further inquiries can be directed to the corresponding authors.

Author contributions

YW and JF contributed to the conception and design of the study. CY and GW performed the statistical analysis. CY and WZ wrote the first draft of the manuscript. CY, GW, and WZ wrote sections of the manuscript. All authors contributed to the manuscript revision and read and approved the submitted version. All authors listed have made a substantial, direct, and intellectual contribution to the work and approved it for publication.

Funding

This study was supported by the National Science and Technology Major Project of China (No. 2018ZX10305409001-001), the National Natural Science Foundation of China (81970083, 81270144, 81570084, and 30800507 to JF), the National Key Technology R&D Program, China (2015BAI12B00 to JF), and the Tianjin Key Medical Discipline (Specialty) Construction Project (TJYXZDXK-008A).

Acknowledgments

The authors would like to thank the GEO database for data collection and Metascape, Cytoscape, and Connectivity Map for data processing and customizable functions. The authors would like to thank Editage (www.editage.cn) for English language editing.

Conflict of interest

The authors declare that the research was conducted in the absence of any commercial or financial relationships that could be construed as a potential conflict of interest.

Publisher's note

Supplementary material

The Supplementary Material for this article can be found online at: https://www.frontiersin.org/articles/10.3389/fphar.2023.1173961/full#supplementary-material

References

Ahangari, F., Price, N. L., Malik, S., Chioccioli, M., Barnthaler, T., Adams, T. S., et al. (2023). microRNA-33 deficiency in macrophages enhances autophagy, improves mitochondrial homeostasis, and protects against lung fibrosis. *JCI Insight* 8, e158100. doi:10.1172/jci.insight.158100

Amati, F., Spagnolo, P., Oldham, J. M., Ryerson, C. J., Stainer, A., Gramegna, A., et al. (2023). Treatable traits in interstitial lung diseases: A call to action. *Lancet Respir. Med.* 11 (2), 125–128. doi:10.1016/S2213-2600(23)00002-4

Amini, P., Stojkov, D., Felser, A., Jackson, C. B., Courage, C., Schaller, A., et al. (2018). Neutrophil extracellular trap formation requires OPA1-dependent glycolytic ATP production. *Nat. Commun.* 9 (1), 2958. doi:10.1038/s41467-018-05387-y

Bader, G. D., and Hogue, C. W. (2003). An automated method for finding molecular complexes in large protein interaction networks. *BMC Bioinforma.* 4, 2. doi:10.1186/1471-2105-4-2

Barbie, D. A., Tamayo, P., Boehm, J. S., Kim, S. Y., Moody, S. E., Dunn, I. F., et al. (2009). Systematic RNA interference reveals that oncogenic KRAS-driven cancers require TBK1. *Nature* 462 (7269), 108–112. doi:10.1038/nature08460

Batista-Gonzalez, A., Vidal, R., Criollo, A., and Carreno, L. J. (2019). New insights on the role of lipid metabolism in the metabolic reprogramming of macrophages. *Front. Immunol.* 10, 2993. doi:10.3389/fimmu.2019.02993

Chung, K. P., Hsu, C. L., Fan, L. C., Huang, Z., Bhatia, D., Chen, Y. J., et al. (2019). Mitofusins regulate lipid metabolism to mediate the development of lung fibrosis. *Nat. Commun.* 10 (1), 3390. doi:10.1038/s41467-019-11327-1

Carvalhal, A. V., Marcelino, I., and Carrondo, M. J. (2003). Metabolic changes during cell growth inhibition by p27 overexpression. *Appl. Microbiol. Biotechnol.* 63 (2), 164–173. doi:10.1007/s00253-003-1385-5

Charoentong, P., Finotello, F., Angelova, M., Mayer, C., Efremova, M., Rieder, D., et al. (2017). Pan-cancer immunogenomic analyses reveal genotype-immunophenotype relationships and predictors of response to checkpoint blockade. *Cell Rep.* 18 (1), 248–262. doi:10.1016/j.celrep.2016.12.019

Chrysanthopoulou, A., Mitroulis, I., Apostolidou, E., Arelaki, S., Mikroulis, D., Konstantinidis, T., et al. (2014). Neutrophil extracellular traps promote differentiation and function of fibroblasts. *J. Pathol.* 233 (3), 294–307. doi:10.1002/path.4359

Contreras-Lopez, R., Elizondo-Vega, R., Paredes, M. J., Luque-Campos, N., Torres, M. J., Tejedor, G., et al. (2020). HIF1α-dependent metabolic reprogramming governs mesenchymal stem/stromal cell immunoregulatory functions. *FASEB J.* 34 (6), 8250–8264. doi:10.1096/fj.201902232R

Csoka, B., Koscso, B., Toro, G., Kokai, E., Virag, L., Nemeth, Z. H., et al. (2014). A2B adenosine receptors prevent insulin resistance by inhibiting adipose tissue inflammation via maintaining alternative macrophage activation. *Diabetes* 63 (3), 850–866. doi:10.2337/db13-0573

d'Alessandro, M., Bergantini, L., Refini, R. M., Cameli, P., Perillo, F., Landi, C., et al. (2020). Adiponectin and leptin levels in idiopathic pulmonary fibrosis: A new method for bal and serum assessment. *Immunobiology* 225 (5), 151997. doi:10.1016/j.imbio.2020.151997

Dabral, S., Muecke, C., Valasarajan, C., Schmoranzer, M., Wietelmann, A., Semenza, G. L., et al. (2019). A RASSF1A-HIF1α loop drives Warburg effect in cancer and pulmonary hypertension. *Nat. Commun.* 10 (1), 2130. doi:10.1038/s41467-019-10044-z

Derricks, K. E., Rich, C. B., Buczek-Thomas, J. A., and Nugent, M. A. (2013). Ascorbate enhances elastin synthesis in 3D tissue-engineered pulmonary fibroblasts constructs. *Tissue Cell* 45 (4), 253–260. doi:10.1016/j.tice.2013.03.001

Gonzalez-Garcia, K., Lopez-Martinez, A., Velazquez-Enriquez, J. M., Zertuche-Martinez, C., Carrasco-Torres, G., Sanchez-Navarro, L. M., et al. (2022). 3'5-Dimaleamylbenzoic acid attenuates bleomycin-induced pulmonary fibrosis in mice. *Int. J. Mol. Sci.* 23 (14), 7943. doi:10.3390/ijms23147943

Hao, H., Yan, S., Zhao, X., Han, X., Fang, N., Zhang, Y., et al. (2022). Atrial myocyte-derived exosomal microRNA contributes to atrial fibrosis in atrial fibrillation. *J. Transl. Med.* 20 (1), 407. doi:10.1186/s12967-022-03617-y

He, C., Larson-Casey, J. L., Gu, L., Ryan, A. J., Murthy, S., and Carter, A. B. (2016). Cu,Zn-Superoxide dismutase-mediated redox regulation of jumonji domain containing 3 modulates macrophage polarization and pulmonary fibrosis. *Am. J. Respir. Cell Mol. Biol.* 55 (1), 58–71. doi:10.1165/rcmb.2015-0183OC

Huang, L. S., Mathew, B., Li, H., Zhao, Y., Ma, S. F., Noth, I., et al. (2014). The mitochondrial cardiolipin remodeling enzyme lysocardiolipin acyltransferase is a novel target in pulmonary fibrosis. *Am. J. Respir. Crit. Care Med.* 189 (11), 1402–1415. doi:10.1164/rccm.201310-1917OC

Huang, S. C., Smith, A. M., Everts, B., Colonna, M., Pearce, E. L., Schilling, J. D., et al. (2016). Metabolic reprogramming mediated by the mTORC2-IRF4 signaling Axis is essential for macrophage alternative activation. *Immunity* 45 (4), 817–830. doi:10.1016/j.immuni.2016.09.016

Hutchinson, J. P., McKeever, T. M., Fogarty, A. W., Navaratnam, V., and Hubbard, R. B. (2014). Increasing global mortality from idiopathic pulmonary fibrosis in the twenty-first century. *Ann. Am. Thorac. Soc.* 11 (8), 1176–1185. doi:10.1513/AnnalsATS.201404-145OC

Irungbam, K., Roderfeld, M., Glimm, H., Hempel, F., Schneider, F., Hehr, L., et al. (2020). Cholestasis impairs hepatic lipid storage via AMPK and CREB signaling in Hepatitis B virus surface protein transgenic mice. *Lab. Invest.* 100 (11), 1411–1424. doi:10.1038/s41374-020-0457-9

Ivanova, V., Garbuzenko, O. B., Reuhl, K. R., Reimer, D. C., Pozharov, V. P., and Minko, T. (2013). Inhalation treatment of pulmonary fibrosis by liposomal prostaglandin E2. *Eur. J. Pharm. Biopharm.* 84 (2), 335–344. doi:10.1016/j.ejpb.2012.11.023

Johnson, W. E., Li, C., and Rabinovic, A. (2007). Adjusting batch effects in microarray expression data using empirical Bayes methods. *Biostatistics* 8 (1), 118–127. doi:10.1093/biostatistics/kxj037

Kang, Y. P., Lee, S. B., Lee, J. M., Kim, H. M., Hong, J. Y., Lee, W. J., et al. (2016). Metabolic profiling regarding pathogenesis of idiopathic pulmonary fibrosis. *J. Proteome Res.* 15 (5), 1717–1724. doi:10.1021/acs.jproteome.6b00156

Khor, Y. H., Ng, Y., Barnes, H., Goh, N. S. L., McDonald, C. F., and Holland, A. E. (2020). Prognosis of idiopathic pulmonary fibrosis without anti-fibrotic therapy: A systematic review. *Eur. Respir. Rev.* 29 (157), 190158. doi:10.1183/16000617.0158-2019

Langfelder, P., and Horvath, S. (2012). Fast R functions for robust correlations and hierarchical clustering. *J. Stat. Softw.* 46 (11), i11. doi:10.18637/jss.v046.i11

Langfelder, P., and Horvath, S. (2008). Wgcna: an R package for weighted correlation network analysis. *BMC Bioinforma.* 9, 559. doi:10.1186/1471-2105-9-559

Lederer, D. J., and Martinez, F. J. (2018). Idiopathic pulmonary fibrosis. *N. Engl. J. Med.* 378 (19), 1811–1823. doi:10.1056/NEJMra1705751

Maher, T. M., Bendstrup, E., Dron, L., Langley, J., Smith, G., Khalid, J. M., et al. (2021). Global incidence and prevalence of idiopathic pulmonary fibrosis. *Respir. Res.* 22 (1), 197. doi:10.1186/s12931-021-01791-z

Misharin, A. V., Morales-Nebreda, L., Reyfman, P. A., Cuda, C. M., Walter, J. M., McQuattie-Pimentel, A. C., et al. (2017). Monocyte-derived alveolar macrophages drive lung fibrosis and persist in the lung over the life span. *J. Exp. Med.* 214 (8), 2387–2404. doi:10.1084/jem.20162152

Mootha, V. K., Lindgren, C. M., Eriksson, K. F., Subramanian, A., Sihag, S., Lehar, J., et al. (2003). PGC-1alpha-responsive genes involved in oxidative phosphorylation are coordinately downregulated in human diabetes. *Nat. Genet.* 34 (3), 267–273. doi:10.1038/ng1180

Niu, L., Geyer, P. E., Wewer Albrechtsen, N. J., Gluud, L. L., Santos, A., Doll, S., et al. (2019). Plasma proteome profiling discovers novel proteins associated with non-alcoholic fatty liver disease. *Mol. Syst. Biol.* 15 (3), e8793. doi:10.15252/msb.20188793

Odegaard, J. I., and Chawla, A. (2011). Alternative macrophage activation and metabolism. *Annu. Rev. Pathol.* 6, 275–297. doi:10.1146/annurev-pathol-011110-130138

Richeldi, L., Collard, H. R., and Jones, M. G. (2017). Idiopathic pulmonary fibrosis. *Lancet* 389 (10082), 1941–1952. doi:10.1016/s0140-6736(17)30866-8

Rindlisbacher, B., Schmid, C., Geiser, T., Bovet, C., and Funke-Chambour, M. (2018). Serum metabolic profiling identified a distinct metabolic signature in patients with idiopathic pulmonary fibrosis - a potential biomarker role for LysoPC. *Respir. Res.* 19 (1), 7. doi:10.1186/s12931-018-0714-2

Romero, F., Hong, X., Shah, D., Kallen, C. B., Rosas, I., Guo, Z., et al. (2018). Lipid synthesis is required to resolve endoplasmic reticulum stress and limit fibrotic responses in the lung. *Am. J. Respir. Cell Mol. Biol.* 59 (2), 225–236. doi:10.1165/rcmb.2017-0340OC

Roque, W., and Romero, F. (2021). Cellular metabolomics of pulmonary fibrosis, from amino acids to lipids. *Am. J. Physiol. Cell Physiol.* 320 (5), C689–C695. doi:10.1152/ajpcell.00586.2020

Rui, Y., Han, X., Jiang, A., Hu, J., Li, M., Liu, B., et al. (2022). Eucalyptol prevents bleomycin-induced pulmonary fibrosis and M2 macrophage polarization. *Eur. J. Pharmacol.* 931, 175184. doi:10.1016/j.ejphar.2022.175184

Subramanian, A., Tamayo, P., Mootha, V. K., Mukherjee, S., Ebert, B. L., Gillette, M. A., et al. (2005). Gene set enrichment analysis: A knowledge-based approach for interpreting genome-wide expression profiles. *Proc. Natl. Acad. Sci. U. S. A.* 102 (43), 15545–15550. doi:10.1073/pnas.0506580102

Serezani, A. P. M., Pascoalino, B. D., Bazzano, J. M. R., Vowell, K. N., Tanjore, H., Taylor, C. J., et al. (2022). Multiplatform single-cell analysis identifies immune cell types enhanced in pulmonary fibrosis. *Am. J. Respir. Cell Mol. Biol.* 67 (1), 50–60. doi:10.1165/rcmb.2021-0418OC

Shannon, P., Markiel, A., Ozier, O., Baliga, N. S., Wang, J. T., Ramage, D., et al. (2003). Cytoscape: A software environment for integrated models of biomolecular interaction networks. *Genome Res.* 13 (11), 2498–2504. doi:10.1101/gr.1239303

Shenderov, K., Collins, S. L., Powell, J. D., and Horton, M. R. (2021). Immune dysregulation as a driver of idiopathic pulmonary fibrosis. *J. Clin. Invest.* 131 (2), e143226. doi:10.1172/JCI143226

Sing, T., Sander, O., Beerenwinkel, N., and Lengauer, T. (2005). Rocr: Visualizing classifier performance in R. *Bioinformatics* 21 (20), 3940–3941. doi:10.1093/bioinformatics/bti623

Subramanian, A., Narayan, R., Corsello, S. M., Peck, D. D., Natoli, T. E., Lu, X., et al. (2017). A next generation connectivity Map: L1000 platform and the first 1,000,000 profiles. *Cell* 171 (6), 1437–1452. doi:10.1016/j.cell.2017.10.049

Surendran, P., Stewart, I. D., Au Yeung, V. P. W., Pietzner, M., Raffler, J., Worheide, M. A., et al. (2022). Rare and common genetic determinants of metabolic individuality and their effects on human health. *Nat. Med.* 28 (11), 2321–2332. doi:10.1038/s41591-022-02046-0

Suzuki, M., Ikari, J., Anazawa, R., Tanaka, N., Katsumata, Y., Shimada, A., et al. (2020). PAD4 deficiency improves bleomycin-induced neutrophil extracellular traps

and fibrosis in mouse lung. *Am. J. Respir. Cell Mol. Biol.* 63 (6), 806–818. doi:10.1165/rcmb.2019-0433OC

Talpan, D., Salla, S., Seidelmann, N., Walter, P., and Fuest, M. (2023). Antifibrotic effects of caffeine, curcumin and pirfenidone in primary human keratocytes. *Int. J. Mol. Sci.* 24 (2), 1461. doi:10.3390/ijms24021461

Tang, C. H., Seeley, E. J., Huang, X., Wolters, P. J., and Liu, L. (2013). Increased susceptibility to Klebsiella pneumonia and mortality in GSNOR-deficient mice. *Biochem. Biophys. Res. Commun.* 442 (1-2), 122–126. doi:10.1016/j.bbrc.2013.11.028

Tanner, L., Single, A. B., Bhongir, R. K. V., Heusel, M., Mohanty, T., Karlsson, C. A. Q., et al. (2023). Small-molecule-mediated OGG1 inhibition attenuates pulmonary inflammation and lung fibrosis in a murine lung fibrosis model. *Nat. Commun.* 14 (1), 643. doi:10.1038/s41467-023-36314-5

Van Calster, B., McLernon, D. J., van Smeden, M., Wynants, L., and Steyerberg, E. W. (2019). Calibration: The achilles heel of predictive analytics. *BMC Med.* 17 (1), 230. doi:10.1186/s12916-019-1466-7

Vickers, A. J., and Elkin, E. B. (2006). Decision curve analysis: A novel method for evaluating prediction models. *Med. Decis. Mak.* 26 (6), 565–574. doi:10.1177/0272989X06295361

Vietri, L., Bennett, D., Cameli, P., Bergantini, L., Cillis, G., Sestini, P., et al. (2019). Serum amyloid A in patients with idiopathic pulmonary fibrosis. *Respir. Investig.* 57 (5), 430–434. doi:10.1016/j.resinv.2019.03.010

Wilkerson, M. D., and Hayes, D. N. (2010). ConsensusClusterPlus: A class discovery tool with confidence assessments and item tracking. *Bioinformatics* 26 (12), 1572–1573. doi:10.1093/bioinformatics/btq170

Wygrecka, M., Alexopoulos, I., Potaczek, D. P., and Schaefer, L. (2023). Diverse functions of apolipoprotein A-I in lung fibrosis. *Am. J. Physiol. Cell Physiol.* 324 (2), C438–C446. doi:10.1152/ajpcell.00491.2022

Xie, N., Tan, Z., Banerjee, S., Cui, H., Ge, J., Liu, R. M., et al. (2015). Glycolytic reprogramming in myofibroblast differentiation and lung fibrosis. *Am. J. Respir. Crit. Care Med.* 192 (12), 1462–1474. doi:10.1164/rccm.201504-0780OC

Xu, J., Chen, S., Wang, W., Man Lam, S., Xu, Y., Zhang, S., et al. (2022). Hepatic CDP-diacylglycerol synthase 2 deficiency causes mitochondrial dysfunction and promotes rapid progression of NASH and fibrosis. *Sci. Bull. (Beijing)* 67 (3), 299–314. doi:10.1016/j.scib.2021.10.014

Yan, F., Wen, Z., Wang, R., Luo, W., Du, Y., Wang, W., et al. (2017). Identification of the lipid biomarkers from plasma in idiopathic pulmonary fibrosis by Lipidomics. *BMC Pulm. Med.* 17 (1), 174. doi:10.1186/s12890-017-0513-4

Zhao, Y. D., Yin, L., Archer, S., Lu, C., Zhao, G., Yao, Y., et al. (2017). Metabolic heterogeneity of idiopathic pulmonary fibrosis: A metabolomic study. *BMJ Open Respir. Res.* 4 (1), e000183. doi:10.1136/bmjresp-2017-000183

Zhou, Y., Zhou, B., Pache, L., Chang, M., Khodabakhshi, A. H., Tanaseichuk, O., et al. (2019). Metascape provides a biologist-oriented resource for the analysis of systems-level datasets. *Nat. Commun.* 10 (1), 1523. doi:10.1038/s41467-019-09234-6

Zhu, Y., Chang, J., Tan, K., Huang, S. K., Liu, X., Wang, X., et al. (2021). Clioquinol attenuates pulmonary fibrosis through inactivation of fibroblasts via iron chelation. *Am. J. Respir. Cell Mol. Biol.* 65 (2), 189–200. doi:10.1165/rcmb.2020-0279OC

frontiers | Frontiers in Pharmacology

TYPE Original Research
PUBLISHED 09 June 2023
DOI 10.3389/fphar.2023.1167475

OPEN ACCESS

EDITED BY
Jie Liu,
Tongji University, China

REVIEWED BY
Sheng Song,
University of North Carolina at Chapel Hill, United States
Shih-Heng Chen,
National Institute of Environmental Health Sciences (NIH), United States
Amjad Kanj,
Mayo Clinic, United States

*CORRESPONDENCE
Yubao Wang,
yubaowang2020@hotmail.com
Jing Feng,
zyyhxkfj@126.com

RECEIVED 16 February 2023
ACCEPTED 30 May 2023
PUBLISHED 09 June 2023

CITATION
Yang L, Yang C, Wan N, Xie W, Tian Y, Xiao Y, Luo L, Chen E, Zhang J, Wang X, Xu L, Wang X, Zhou Y, Guo L, Zou J, Liu X, Wei X, Wang Y and Feng J (2023), Bronchoscopic instillation of amphotericin B is a safe and effective measure to treat pulmonary mycosis. *Front. Pharmacol.* 14:1167475. doi: 10.3389/fphar.2023.1167475

Bronchoscopic instillation of amphotericin B is a safe and effective measure to treat pulmonary mycosis

Lei Yang[1], Changqing Yang[1], Nansheng Wan[1], Wei Xie[1], Yu Tian[1], Yangbao Xiao[2], Li Luo[2], Enguo Chen[3], Jisong Zhang[3], Xiaoping Wang[4], Li Xu[4], Xingguang Wang[5], Yunzhi Zhou[6], Lu Guo[7], Jun Zou[7], Xingren Liu[7], Xuguang Wei[8], Yubao Wang[1]* and Jing Feng[1]*

[1]Department of Respiratory and Critical Care Medicine, Tianjin Medical University General Hospital, Tianjin, China, [2]Hunan Chest Hospital, Changsha, Hunan, China, [3]Department of Respiratory Therapy, Sir Run Run Shaw Hospital, Hangzhou, Zhejiang, China, [4]Shandong Public Health Clinical Center, Jinan, Shandong, China, [5]Shandong Provincial Hospital, Jinan, Shandong, China, [6]Emergency General Hospital, Beijing, China, [7]Sichuan Academy of Medical Sciences and Sichuan Provincial People's Hospital, Chengdu, Sichuan, China, [8]Hebei Provincial Shenzhou Hospital, Hengshui, Hebei, China

Background and objectives: In recent years, there has been a significant increase in the prevalence of pulmonary mycosis disease, and its mortality has increased. There are very few studies on treating pulmonary mycosiss with bronchoscopic instillation of amphotericin B. This study investigated the clinical efficacy and safety of bronchoscopic instillation of amphotericin B for treating pulmonary mycosiss.

Methods: This was a multi-centre, retrospective clinical study of 80 patients with pulmonary mycosiss who were treated with bronchoscopic instillation of amphotericin B. The efficacy and safety of this treatment were evaluated.

Results: Eighty patients were included {51 males; mean [standard deviation (SD)] age, 46 (15.9) years}. The most common underlying cause was haematological malignancy (73.75%). The mean number of bronchoscopic instillations of amphotericin B was 2.4 (SD 1.5). In terms of treatment success, 58 (72.5%) patients achieved complete or partial changes on imaging after treatment. A total of 62 (77.5%) patients achieved complete or partial changes on imaging and/or local limitation of the mycosis infection. Seventy-six (95%) patients achieved complete or partial changes on imaging and/or local limitation of mycosis infection and/or an immunotherapy time window. The efficacy rates for treatment of *Aspergillus* and *Mucor* infections in terms of the three treatment success criteria described above were 73.81% vs. 63.64%, 80.95% vs. 72.73%, and 92.86% vs. 90.91%, respectively.

Conclusion: Bronchoscopic instillation of amphotericin B is safe and effective for treatment of pulmonary mycosiss.

Abbreviations: CT, computed tomography; SD, standard deviation.

KEYWORDS
amphotericin B, *Mucor*, *Aspergillus*, fungal infection, intrabronchial

Introduction

In recent years, the prevalence of pulmonary mycosiss has significantly increased with an increase in the number of immunosuppressed high-risk susceptible groups. Even though early diagnosis of pulmonary mycosiss is possible given the continuous improvements in detection methods, and preventive and empirical treatments are used to treat the disease, the mortality rate is still as high as 50%–90% (Morgan et al., 2005). For the clinical treatment of deep fungal infections, commonly used antifungal drugs include polyenes (amphotericin B), triazoles (fluconazole, voriconazole, itraconazole), and echinocandins (caspofungin) (Walsh et al., 2008).

Pulmonary mycosiss, especially mycotic infections, are associated with the following characteristics: rapid dissemination, requiring timely drug intervention (Walsh et al., 2012); short-term tissue necrosis and local structural destruction of the lung; rapid formation of fibrous and granulation tissue encapsulation after control with effective antifungal drugs; and autoimmune limitation. These characteristics indicate the possible failure of transvenous pharmacologic interventions due to poor local blood flow.

Amphotericin B is a polyene antifungal drug with broad-spectrum effects. When administered intravenously, the drug concentration in the pleural fluid, ascites fluid, and synovial fluid is usually less than half of the blood concentration, and the drug concentration in bronchial secretions is even lower (Stone et al., 2016). However, in some cases, it is the only effective drug for treating acute deep fungal infections; it is highly water-soluble, absorbed less slowly through the airway mucosa, and causes no significant irritation to the airway mucosa. Based on these pharmacological and metabolic characteristics, local instillation of amphotericin B via bronchoscopy has irreplaceable advantages and is worthy of clinical promotion (Lass-Flörl et al., 1998; Polak, 1999).

For some lesions that do not communicate with the bronchi and have little contact with the bloodstream, this makes it difficult for antifungal agents to reach them through the blood. So we need new ways of treating these patients. J L Hargis et al., P Krakówka et al., G BROUET al., and M J Shapiro al. Proposing new treatment modalities (percutaneous instillation of intracavitary amphotericin B) (Brouet et al., 1964; Krakowka et al., 1970; Hargis et al., 1980; Shapiro et al., 1988). Kravitz et al. (2013) retrospectively reviewed 23 patients admitted to our institution for aspergilloma-associated hemoptysis over an 8-year period and underwent percutaneous intracavitary instillation of amphotericin B (ICAB); and identified ICAB as A form of short-term treatment. Takeda et al. (2014); Parikh et al. (2017) respectively, report a case of pulmonary aspergillosis treated with bronchoscopic instillation of amphotericin B. There are few articles on the treatment of such patients above, and the sample size of the published articles is small, or it is a case report or a relatively early study. There are even fewer articles on the bronchoscopic instillation of amphotericin B. There are also variations in the clinical efficacy of bronchoscopic instillation of amphotericin B (Lang et al., 2020). Endoscopic injections have demonstrated good therapeutic effects in multiple case reports and clinical studies (Hargis et al., 1980; Kravitz et al., 2013). However, because the total number of patients is small and most have serious comorbidities, it is difficult to balance the basic conditions among the research groups; it is difficult to implement large-scale multi-centre clinical studies. Therefore, to date, there are no recognised relevant clinical data or specific indicators or parameters for evaluating the benefits to patients.

Accordingly, we designed this "clinical study on the local application of amphotericin B via bronchoscopic instillation in pulmonary lesions" By collecting the clinical data of patients with pulmonary mycosis who met the inclusion criteria and performing statistical analysis, the clinical efficacy and safety of bronchoscopic instillation of amphotericin B in the treatment of pulmonary mycosiss were revealed.

Methods

Study design

The operational flow of the whole study is shown in Figure 1. This is a retrospective study of a multicentre clinical treatment trial of patients diagnosed with pulmonary mycosis based on the European Organization for Research and Treatment of Cancer/Mycoses Study Group criteria (Donnelly et al., 2020). The patients enrolled in this study were divided into the following three categories:

1. Recurrent haemoptysis and no bleeding tendency. (If surgical resection was not an option to control recurrent haemoptysis (possible meaning: lesion communicates with the airway, some solution must re-entry into the airway), then in patients without bleeding tendency, bronchoscopic instillation of antifungal drugs may be considered).
2. Systemic use of fungal drugs that was ineffective or involved adverse events that could not be tolerated. Systemic antifungal therapy is considered ineffective if any one or more of these criteria are met (Sanguinetti et al., 2019; Donnelly et al., 2020; Zhang and Zhu, 2020; Alexander et al., 2021; Acet-Öztürk et al., 2022; Fisher et al., 2022). 1) Lack of clinical improvement: the patient does not show any clinical improvement in their symptoms or condition despite receiving systemic antifungal therapy for a sufficient duration of time. 2) Persistence of radiographic abnormalities: radiographic abnormalities, such as pulmonary infiltrates or nodules, persist or worsen despite systemic antifungal therapy. 3) Continuous fungal culture positivity: fungal cultures from respiratory specimens continue to be positive despite systemic antifungal therapy. 4) Lack of serum biomarker response: serum biomarkers, such as galactomannan or beta-D-glucan, do not improve or continue to be positive despite systemic antifungal therapy. 5) Development of antifungal resistance: fungi developed resistance to the systemic antifungal agents.
3. Immunodeficiency. Every immunocompromised patient with pulmonary mycosis should receive treatment, with a few exceptions, especially those with elevated inflammatory markers, such as C-reactive protein. The main indication for

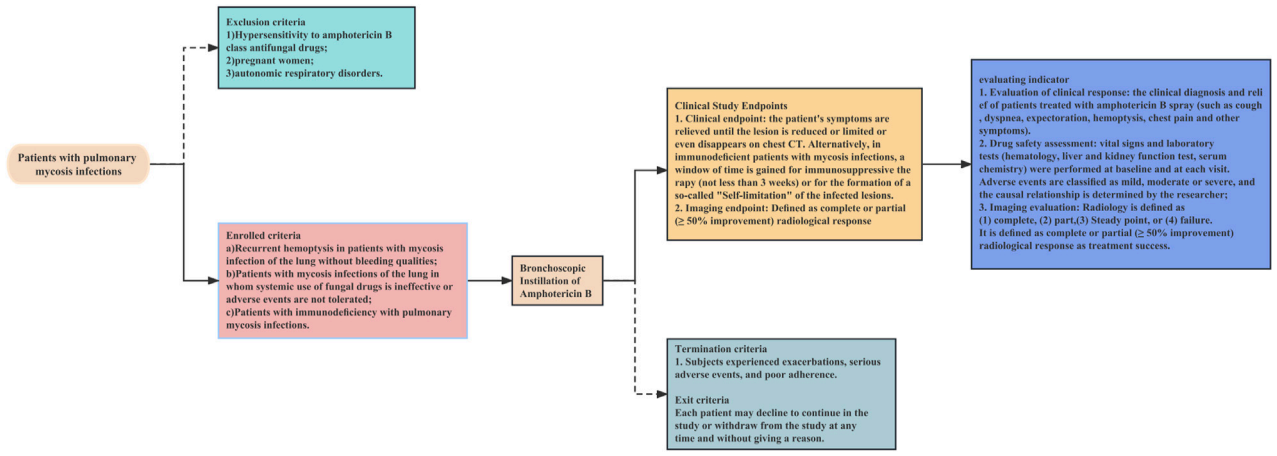

FIGURE 1
Flow chart of the clinical study of bronchoscopic instillation of amphotericin B.

endoscopic drug injection is that the patient suffers from the trachea, bronchi and/or pulmonary mycosis, and the pulmonary mycosis lesions have clear localized drainage bronchi on imaging.

The exclusion criteria were:

1. Hypersensitivity to amphotericin B class antifungal drugs
2. Pregnancy
3. Autonomic respiratory disorders

The termination criteria were:

1. Exacerbation of disease
2. Serious adverse events
3. Poor compliance

A decision to withdraw from the study was not subject to potential treatment constraints and did not affect the patient's medical care. Patients were permitted to withdraw from the study at any time without providing a reason.

Procedure for bronchoscopic instillation of amphotericin B

Before the intrabronchial instillation of the drug, the patient's condition will be assessed to ensure patient safety. An absolute contraindication to bronchoscopy is severe refractory hypoxia that cannot maintain adequate oxygenation during the procedure due to the patient's disease (Severe hypoxemia is defined as resting arterial oxygen partial pressure (PaO2) < 60 mmHg or blood oxygen saturation (SpO2) < 90%). After providing written informed consent, all patients were administered amphotericin B via bronchoscopy under local or general anaesthesia. During the instillation operation under the bronchoscope, oxygen inhalation or high-frequency ventilation is given, and the patient's vital signs are monitored by ECG monitoring. Five ml of water was added to each of the two 5-mg ampoules of amphotericin B deoxycholate and shaken thoroughly to dissolve for injection with a 10-mL syringe. Ten ml of completely dissolved amphotericin B deoxycholate solution was drawn from the two ampoules with a 20-mL syringe, and then 5 mL of air was drawn for propulsion to make a total of 15 mL (10 mL of a solution containing 10 mg of amphotericin B deoxycholate). For bronchoscopic instillation of amphotericin B, the bronchoscope was wedged into the segmental or subsegmental bronchus based on prior computed tomography (CT) thoracic lumen localisation or virtual navigation bronchoscopy; if a definite lesion was visible on bronchoscopy, the bronchoscope was wedged into the lumen. For two focal targets, a total dose of amphotericin B deoxycholate of 10–15 mg was recommended, and for multiple focal targets, the total quantity of amphotericin B deoxycholate was increased to 15–20 mg, and the amount of solvent (water for injection) was increased appropriately, divided into multiple syringes. Precise local injection was carried out visually or using guidance, with ultra-fine endoscopy for each of the target treatment sites. Try to push the bronchoscope front end into the target bronchus or probe into the lesion, and inject it directly; or insert the injection tube or spray tube (such as the unique injection tube or spray tube for bronchoscope) deep into the distal end of the target bronchus, or even directly insert the injection tube, The spray tube is placed in the lesion, and then injected (Figure 2). Each target treatment site received more than 2.5 mg of amphotericin B deoxycholate at each target site, and more than 5 mg of the drug was dispensed at important focal targets. In order to ensure local retention of the drug in the lesion, this can be achieved by using the front end of the endoscope for blocking, with posing and other methods.

Clinical study endpoints

After initiating amphotericin B treatment via bronchoscopic instillation, the patient's symptoms were relieved until the lesion was reduced, limited, or disappeared on chest CT. Alternatively, in immunodeficient patients with mycosis infections, a window of

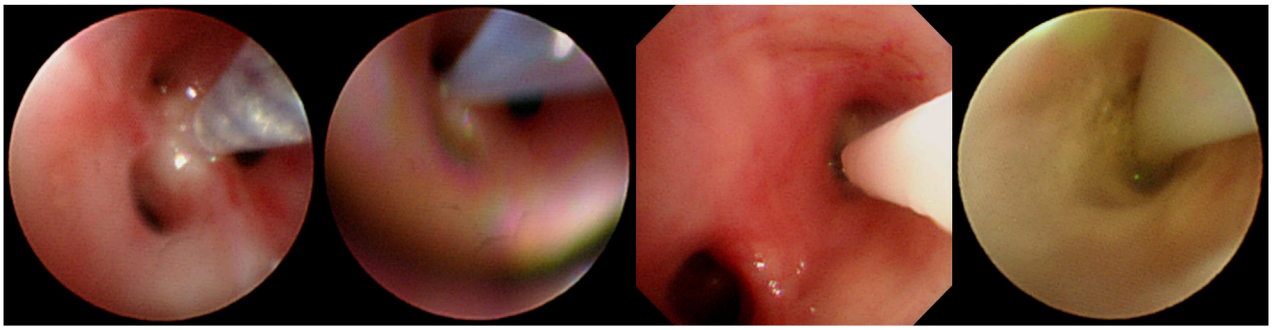

FIGURE 2
Operation procedure of instilling amphotericin B under bronchoscope.

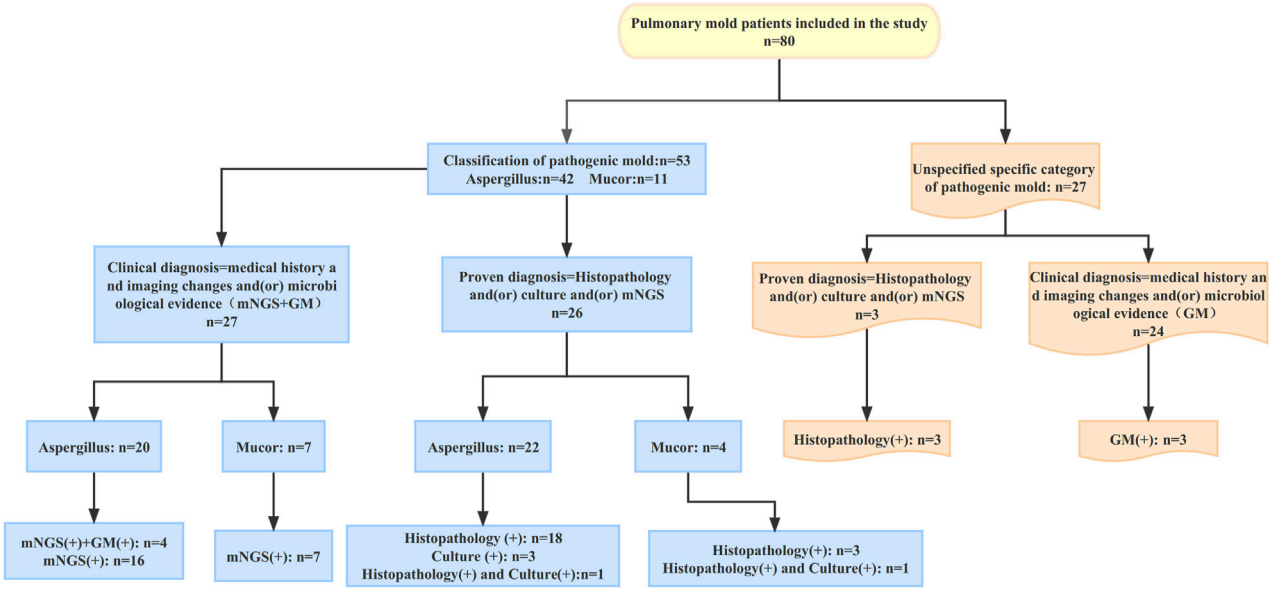

FIGURE 3
Diagnosis process of 80 patients with pulmonary mold infection Changes in the patient's chest CT after treatment with intrabronchial amphotericin B instillation.

time was achieved for immunosuppressive therapy (not less than 3 weeks) or for the development of self-limitation of infected lesions (clearly defined fibrous, mechanised encapsulation around the lesion that has been stable for 3 months) Figure 3.

Efficacy assessment

CT scans before and after bronchoscopic drug instillation were compared by an independent radiologist who was blinded to the patient information. A radiological response was defined as follows (Cadranel et al., 2012): 1) Complete: complete absorption of the chest CT lesion, 2) Partial: ≥50% reduction in the sum of all measurable lesions on chest tomography, 3) Stable: slight (<50%) or no improvement, or 4) Failure: deterioration of the condition (Cadranel et al., 2012). Treatment success was defined as a complete or partial (≥50% improvement) radiological response, achievement of a window of time (not less than 3 weeks) for immunosuppressive therapy in patients with immunodeficiency with mycosis infections or for the development of self-limitation of infected lesions.

Statistical analysis

Continuous variables are expressed as mean [SD (standard deviation)]. The discrete variables are expressed as frequency and rate. A histogram was used to compare the differences in the efficacy rates of *Aspergillus* and *Mucor* after instillation treatment.

TABLE 1 Baseline patient characteristics.

Variables	Patients [*n* (%)]
Age (y)	46 ± 15.93
Sex	
Male	51 (63.75%)
Female	29 (36.25%)
Underlying Disease	
Hematological malignancies	59
Tuberculosis	5
Lung cancer	2
Chronic obstructive pulmonary disease	1
Non-tuberculosis mycobacteria	1
Diabetes	5
Others	7
Status of systemic antifungal therapy before instillation of amphotericin B	
Yes	58 (72.5%)
No	22 (27.5%)

TABLE 2 Treatment with bronchoscopic instillation of amphotericin B.

Variables	*n* (%)
Patient's chest CT features	
Unilateral	63 (77.75)
Bilateral or multiple	17 (21.25)
Lung lobe involvement	
Right upper lobe	32
Right middle lobe	7
Right lower lobe	10
Left upper lobe	26
Left lower lobe	16
Imaging changes	
Consolidation	61
Nodules	47
Ground-glass opacity	42
Cavities	24
No. Sessions of intrabronchial amphotericin B instillation	2.4 ± 1.5
1 session	27
2 sessions	22
3 sessions	12
4 sessions	13
5 sessions	4
6 sessions	2
Successful treatment with intrabronchial amphotericin B instillation Imaging response (Complete + Partial)	58 (72.5%)
Imaging response (Complete + Partial)+ self-limitation	62 (77.5%)
Imaging response (Complete + Partial)+ self-limitation + Immunotherapy time window	76 (95%)

Results

Patient characteristics

The demographics of all patients are shown in Table 1 and Supplementary Table S1. In this multi-centre study, 80 patients underwent bronchoscopic amphotericin B instillation. Of these, 51 (63.75%) were male and the mean (SD) age of the total study population was 46 (15.93) years. In this study, most patients (59/77, 73.75%) had haematological malignancies, five had tuberculosis as their underlying disease, five had diabetes, and two had lung cancer. A total of 58 (72.5%) patients received the systemic antifungal therapy followed by the bronchoscopic instillation of amphotericin B due to ineffectiveness of the systemic antifungal therapy. And the rest 22 patients (27.5%) simultaneously received the systemic antifungal therapy and the bronchoscopic instillation therapy.

According to the EORTC/MSG consensus criteria, all patients had a proven or clinical diagnosis of pulmonary mold infection. The criteria for proven diagnosis are mainly positive histopathology and/or positive culture; the criteria for clinical diagnosis are the medical history and typical imaging changes and/or microbiological evidence (mNGS and GM). In this study, a total of 42 patients with pulmonary Aspergillus infection were identified by histopathology and (or) culture and (or) mNGS to identify the specific pathogenic fungi. Of the 42 patients with pulmonary Aspergillus infection, 22 were proven diagnoses; the other 20 were clinical diagnoses. In 11 patients with pulmonary mucor infection, the specific pathogenic fungi were identified by histopathology and (or) culture and (or) mNGS. Among these 11 patients, four were proven diagnoses; the remaining seven were clinical diagnoses. Except for the above 53 patients whose specific pathogenic fungi were identified, the other 27 mold patients failed to identify the specific pathogenic fungi. Among the 27 patients, 3 were proven diagnoses and 24 were clinical diagnoses.

Efficacy analyses

The clinical characteristics and operative information of all patients are shown in Table 2. Sixty-three (77.75%) had unilateral involvement. The sites of pulmonary abnormalities on chest HRCT included the right upper lobe for 32 patients, the right middle lobe for 7 patients, the right lower lobe for 10 patients, the left upper lobe for 26 patients, and the left lower lobe for 16 patients. Chest HRCT showed consolidations in 61 patients, nodules in 47 patients, ground-glass opacities in 42 patients, and cavities in

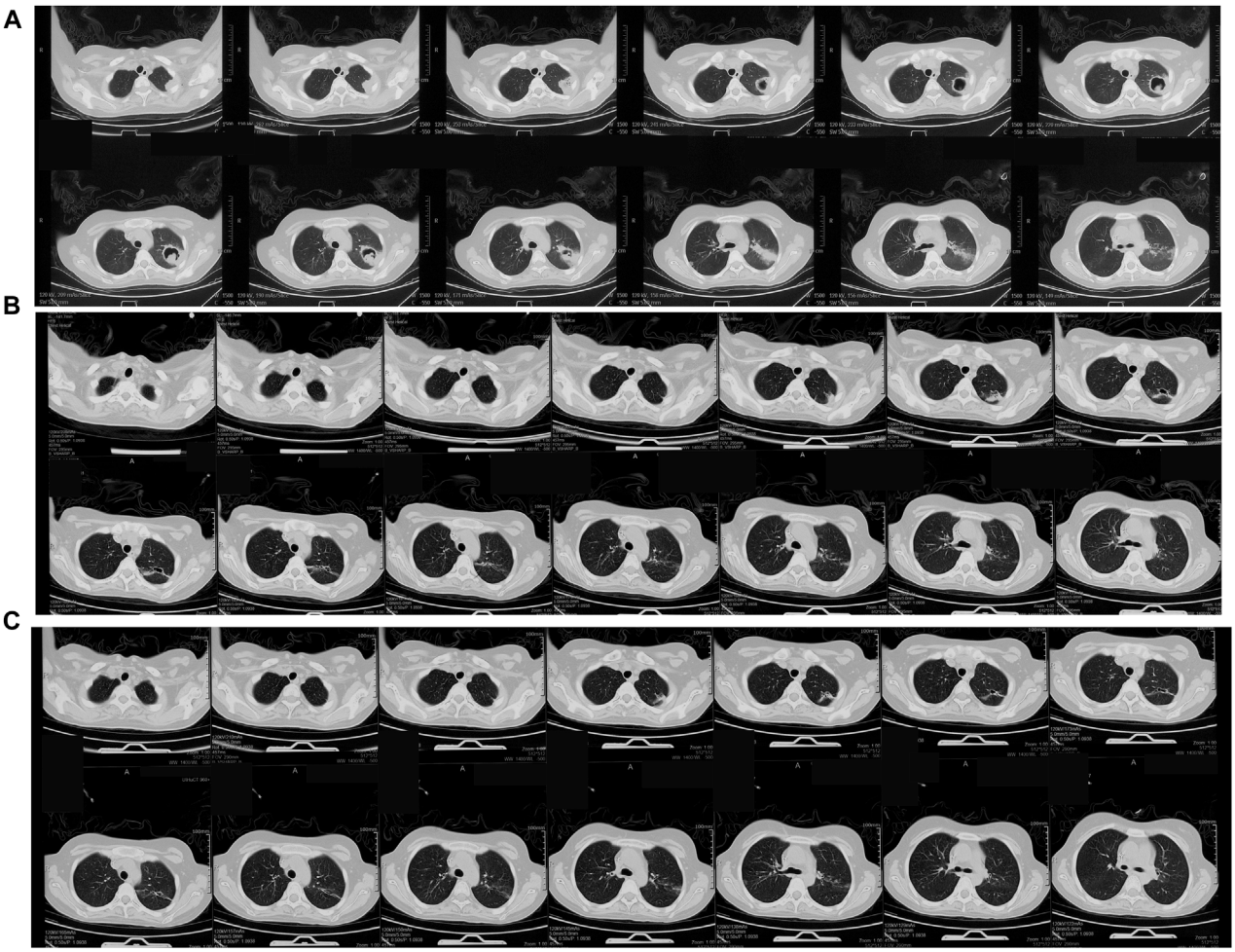

FIGURE 4
(A) Before treatment of bronchoscopic instillation, chest CT shows a solid left upper lobe shadow with cavity formation visible within it. **(B)** 55 days after treatment, chest CT shows that the solid shadow in the upper lobe of the left lung is reduced, and the cavity is further reduced. **(C)** 88 days after treatment, chest CT shows further reduction of solid shadow in the upper lobe of the left lung. Comparison of efficacy between Aspergillus and Mycor patients.

24 patients. The mean number of intrabronchial amphotericin B instillations was 2.4 (1.5). Twenty-seven patients underwent one session, 21 patients underwent two sessions, 12 patients underwent three sessions, 13 patients underwent four sessions, and six patients underwent more than five sessions of intrabronchial amphotericin B instillation. A total of 58 (72.5%) patients achieved complete or partial changes on imaging after bronchoscopic instillation of amphotericin B treatment, 62 (77.5%) patients achieved complete or partial changes on imaging and the formation of self-limitation of infected lesions, and 76 (95%) patients achieved complete or partial specimens in imaging and self-limitation and immunotherapy time windows.

Typical imaging response

In this study, patient no. 36, who had been diagnosed with acute lymphoblastic leukaemia 3 months prior, was admitted with "intermittent fever for 1 month, cough, and sputum for 1 week". Before treatment with respiratory endoscopy, chest CT suggested a solid shadow in the upper lobe of the left lung with cavity formation (Figure 4A). After bronchoscopy, a final clinical diagnosis of a pulmonary mycosis was made. After respiratory endoscopy, the patient was treated with amphotericin B (10 mg) in the sub-subsegment of the ascending apical segment of the left upper lobe, posterior segment of the ascending apical segment of the left upper lobe, and posterior segment of the ascending apical segment of the left upper lobe. After two instillations, the patient's chest CT lesion was significantly more absorbed than before and the patient's clinical symptoms were significantly relieved (Figures 4B, C).

Evaluation of the efficacy of intrabronchial amphotericin B instillation in the treatment of pulmonary mycosiss caused by different fungal species.

In this study, 42 patients were infected with *Aspergillus* and 11 patients were infected with *Mucor*. A total of 31 patients with *Aspergillus* infection achieved complete or partial improvement on chest imaging after bronchoscopic instillation of amphotericin B. A

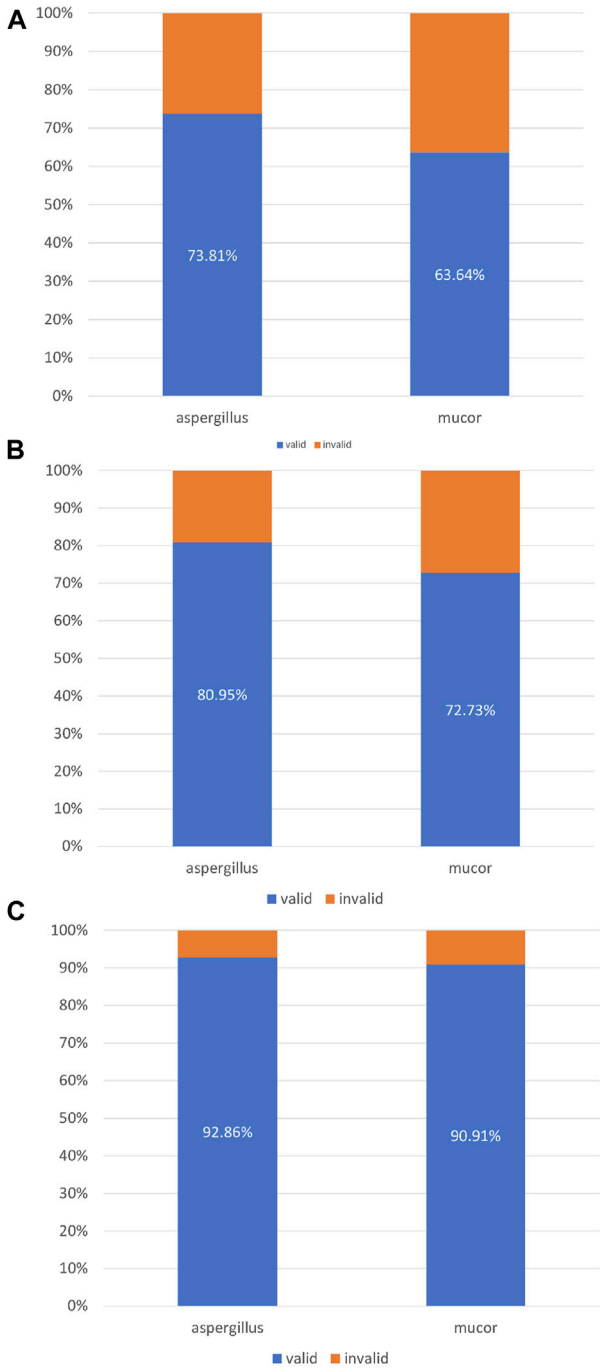

FIGURE 5
(A) Imaging response (complete + partial). **(B)** Imaging response (complete + partial) + self-limitation. **(C)** Imaging response (complete + partial) + self-limitation + immunotherapy time window.

total of 7 patients with *Mucor* infections achieved complete or partial progress on chest imaging after intrabronchial amphotericin B instillation (Figure 5A). Among the patients with *Aspergillus* infection, 34 patients showed complete or partial improvement and "self-limitation" changes on imaging. Among the patients with *Mucor* infection, eight patients showed complete or partial improvement and "self-limitation" changes on imaging (Figure 5B). Thirty-nine patients with *Aspergillus* infection achieved (complete or partial) improvement on imaging after bronchoscopic instillation, with "self-limitation" and a time window for immunotherapy. Ten patients with *Mucor* infection performed (complete or partial) improvement on imaging after bronchoscopic instillation, "self-limitation" and a time window for immunotherapy (Figure 5C).

Safety analysis

Seven of the 80 patients (7.5%) experienced adverse reactions, including one patient who developed a sore throat after the first bronchoscopic instillation, which was tolerated by the patient. It was not treated symptomatically and did not require withdrawal from the next bronchoscopic operation. The patient's sore throat was most likely related to the bronchoscopic operation and was not directly related to the intrabronchial amphotericin B instillation. The patient developed severe dyspnoea after the second bronchoscopic instillation and was intubated and treated symptomatically, and finally, the patient withdrew from the study. Six patients developed drug fever after bronchoscopic instillation and were administered symptomatic treatment; no other symptoms were observed. Of the 80 patients treated with bronchoscopic instillation, none showed any significant deviation from baseline in terms of blood, liver, and kidney function. Eighty patients were treated with bronchoscopic instillation; one had a sore throat, which was considered to be related to the bronchoscopic operation. The remaining patients did not have any complications such as fatal haemoptysis, pneumothorax, arrhythmia, or death.

Discussion

Pulmonary mycosis spreads rapidly and requires drugs and intervention; In the short term, it can cause tissue necrosis and structural damage to local lung tissues. After corresponding treatment, fibrous and granulation tissue parcels can be formed rapidly. Due to the above characteristics, intravenous drug intervention may hardly achieve the desired clinical outcome due to ischemia. Bronchoscopic instillation of antifungal drugs can provide precise local treatment of target lesions. Studies on the bronchoscopic instillation of antifungal drugs are scarce. Based on animal studies demonstrating the safety of nebulised amphotericin B-administered endobronchial therapy, Ramirez reported the first series of such therapies in humans in 1964 (Lang et al., 2020). The results were impressive, as all three patients showed significant clinical improvement and clearance of the fungal infection. Several subsequent studies also reported success with endobronchial therapy using amphotericin B, ketoconazole, fluconazole, and miconazole (Hamamoto et al., 1983; Yamada et al., 1993; Hinerman et al., 2002). Although all patients showed symptomatic improvement, only six of nine patients showed complete clearance of the fungal balls. Two case reports demonstrated the effectiveness of bronchoscopic instillation of amphotericin B in the treatment of pulmonary mucor and aspergillus infections (Alfageme et al., 2009; Morales et al., 2009). Bronchoscopic instillation of antifungal drugs can effectively control the hemoptysis caused by pulmonary aspergilloma and reduce the severity of hemoptysis caused by inoperable pulmonary

aspergilloma (Mohan et al., 2017a; Hadda et al., 2022). The lesions did not change significantly during systemic antifungal therapy alone. However, lesion size was significantly reduced after additional bronchoscopic instillation of amphotericin B (Winkler et al., 2007).

Compared with previous studies, the current study included 80 patients and was multi-centre. Under virtual navigation guidance, injecting drugs with an ultrafine endoscope allows precise local treatment of the target lesions. However, these drugs are not generally used to prevent pulmonary mycosis. Therapeutic drugs can be directly sprayed into the local drainage bronchus of the lesion, in the lesion, or the superior drainage bronchus, forming a long-term high-concentration drug solution environment in or around the target lesion to directly "remove the pathogen", "reduce the pathogen", or limit the lesion expansion. Bronchoscopic instillation of amphotericin B can achieve partial or complete remission on imaging or microbiology as well as localisation and stabilisation of lesions. It can also be used to determine a time window for immunosuppressive therapy and to control repeated haemoptysis. Another study included 82 patients. After voriconazole titration, haemoptysis resolved significantly in 25 patients (30.5%) after the first treatment and 52 patients (68.3%) after the second treatment. Transient postoperative cough (n = 38, 46.3%) was the most common procedure-related adverse event. Follow-up CT (n = 47) showed a 54% reduction in varicose tumour size, whereas 40.4% remained unchanged. The median (IQR) haemoptysis-free period was 12 months (IQR, 9 15.5 months). During a median follow-up of 14.5 months (IQR, 9–18 months), 24 (29.3%) patients showed significant haemoptysis, ultimately concluding that endobronchial voriconazole titration is a safe and effective method for controlling pulmonary aspergilloma hemoptysis (Mohan et al., 2017b). In this study, a total of 58 (72.5%) patients achieved complete or partial changes on imaging after treatment with bronchoscopic instillation of amphotericin B. A total of 62 (77.5%) patients achieved complete or partial modifications on imaging, and/or local limitation of the mycosis infection. A total of 76 (95%) patients achieved complete or partial changes on imaging, and/or local limitation of mycosis infection, and/or achieved an immunotherapy time window. It can also be seen from the above data in this study that bronchoscopic instillation of amphotericin B is an effective way to treat pulmonary mycosiss.

Regarding the effectiveness of bronchoscopic instillation of amphotericin B, we must strictly adhere to the indications. Pulmonary mycosis often forms a wrapped pus cavity in the lesion, and the concentration of antifungal agents in the lung tissue by the systemic administration is usually too low to produce therapeutic effects (Lass-Flörl et al., 1998; Polak, 1999). Therefore, to make sure the accurate bronchoscopic instillation of amphotericin B in the pulmonary lesion is crucial for the effectiveness. In our study, according to the patient's chest CT positioning or under virtual navigation, the front end of the bronchoscope is inserted deep into the lesion segment or subsegmental bronchus. Amphotericin B is directly injected into the lesion accurately and locally, ensuring the concentration of the drug at the lesion site. The skilled physicians performing the bronchoscopic instillation of amphotericin B are essential for not only safety but also effectiveness.

With the rapid cytological evaluation technology of respiratory endoscopic intervention, clinicians can perform endoscopic drug injection at the same time as the diagnosis of tracheal, bronchial, and/or pulmonary mycosis. Integrating clinical information and pathogenic microorganism test results to make an accurate diagnosis, even for microbial species, can optimise drug selection for systemic treatment. This study compared the efficacy of respiratory endoscopic nebulisation with amphotericin B for the treatment of *Aspergillus* and *Mucor*. The efficacy rates for the three treatment success criteria were 73.81% vs. 63.64%, 80.95% vs. 72.73%, and 92.86% vs. 90.91%.

Concerning the safety of the treatment, first of all, we must strictly adhere to the indications of the patient and evaluate whether the patient has any disease that may cause difficulty in maintaining sufficient oxygenation during the operation before instillation under the bronchoscope. The aerosol inhalation of amphotericin B was used as the main pre-induction, to prevent severe adverse reactions such as allergy and wheezing during instillation. Again, the bronchoscopic instillation of amphotericin B deoxycholate in this study was performed by the experienced physicians. Finally, during the treatment process, some unnecessary invasive operations should be reduced to avoid the unwarranted risks, such as bleeding.

Compared to systemic drugs, the systemic absorption of drugs through respiratory endoscopy is lower, and the side effects are relatively few. And the adverse reactions are also related to the lung lesions of the patients. Before the respiratory endoscopic spray treatment, aerosol inhalation of amphotericin B is generally performed for induction before endoscopic injection. The purpose is to prevent severe adverse reactions such as allergy and wheezing during injection, and to gradually adapt the patient's airway to amphotericin B. Complications and adverse reactions of endoscopic drug injection include: fever, cough, expectoration, wheezing (other underlying diseases such as asthma and chronic obstructive pulmonary disease should be dealt with separately), chest pain (pleural irritation due to amphotericin B), and a small amount of pneumothorax, more purulent secretion drainage, or allergic reaction (Ramirez, 1964; Ikemoto, 1965; Krakowka et al., 1970; Yamada et al., 1993). In this study, seven out of 80 patients (7.5%) had adverse reactions, one patient withdrew from the study due to obvious dyspnoea, six patients developed fever, and all patients returned to normal after anti-thermal treatment. No fatal haemoptysis, pneumothorax, arrhythmia, death, or other complications occurred.

Compared with the percutaneous intraluminal instillation of antifungal drugs, the endobronchial technique allows frequent examination of local adverse effects or disease progression, avoids the risk of pneumothorax associated with percutaneous needle puncture and allows for a more precise injection of amphotericin B drops into the lesion site with the aid of advanced virtual navigation technology.

Nebulized inhalation has less systemic absorption and toxicity. In a wide range of ventilable areas, including airways and alveoli at all levels, an antifungal drug environment with a concentration higher than the minimum inhibitory concentration can be maintained for a long time, and this can be useful for prevention as well as treatment. However, nebulising inhalation has certain disadvantages. Atomised and inhaled antifungal drugs can only reach areas with acceptable ventilation. Lesions with poor local ventilation, such as consolidation or cavitation, can only limit the progression and expansion of lesions, and direct treatment has a limited effect.

This shows the advantages of bronchoscopic instillation of amphotericin B; however, this treatment method has certain shortcomings. One disadvantage of endoscopic injection is that it is less effective for multiple lesions. However, endoscopic drug

injections are invasive. According to the degree of the patient's condition, the patient will experience pain and poor compliance after drug injection. In addition, owing to the condition of the patient's lesion, intraoperative and postoperative haemorrhages may also occur. The appearance of the abovementioned changes is also related to the patient's condition.

Our study has some limitations. First, our study was a retrospective study, and some cases were clinically diagnosed, which may also affect the accuracy of this study. Second, further studies with larger sample sizes are needed to prospectively explore the potential of bronchoscopic instillation of amphotericin B in the treatment of fungal infections of the lung.

In summary, for patients with cavitation (single or multiple), bronchopulmonary fistulas, consolidation, and other target lesions in poorly ventilated areas, a sufficient amount of effective antifungal drug should be administered systemically together with bronchoscopic instillation. And bronchoscopic instillation of amphotericin B is a safe and effective form of treatment.

Data availability statement

The original contributions presented in the study are included in the article/Supplementary Material, further inquiries can be directed to the corresponding authors.

Ethics statement

The studies involving human participants were reviewed and approved by Medical Ethics Committee of Tianjin Medical University General Hospital. The patients/participants provided their written informed consent to participate in this study. Written informed consent was obtained from the individual(s) for the publication of any potentially identifiable images or data included in this article.

Author contributions

YW and JF contributed to conception and design of the study. NW, WX, YT, YX, LL, EC, JiZ, XpW, LX, XgW, YZ, LG, JuZ, XL, and XuW organized the database. CY and LY performed the statistical analysis. LY wrote the first draft of the manuscript. CY and LY wrote sections of the manuscript. All authors contributed to the article and approved the submitted version.

Funding

This work was funded by National Natural Science Foundation of China (82170097, 81970083, 81270144, 81570084, and 30800507 to JF) and the Tianjin Key Medical Discipline (Specialty) Construction Project.

Acknowledgments

We would like to thank Editage (www.editage.cn) for English language editing.

Conflict of interest

The authors declare that the research was conducted in the absence of any commercial or financial relationships that could be construed as a potential conflict of interest.

Publisher's note

All claims expressed in this article are solely those of the authors and do not necessarily represent those of their affiliated organizations, or those of the publisher, the editors and the reviewers. Any product that may be evaluated in this article, or claim that may be made by its manufacturer, is not guaranteed or endorsed by the publisher.

Supplementary material

The Supplementary Material for this article can be found online at: https://www.frontiersin.org/articles/10.3389/fphar.2023.1167475/full#supplementary-material

References

Acet-Öztürk, N. A., Ömer-Topçu, D., Vurat-Acar, K., Aydın-Güçlü, Ö., Pınar, İ. E., Demirdöğen, E., et al. (2022). Impact of revised EORTC/MSGERC 2020 criteria on diagnosis and prognosis of invasive pulmonary aspergillosis in patients with hematological malignancies undergoing bronchoscopy. *J. Mycol. Med.* 32, 101304. doi:10.1016/j.mycmed.2022.101304

Alexander, B. D., Lamoth, F., Heussel, C. P., Prokop, C. S., Desai, S. R., Morrissey, C. O., et al. (2021). Guidance on imaging for invasive pulmonary aspergillosis and mucormycosis: From the imaging working group for the revision and update of the consensus definitions of fungal disease from the EORTC/MSGERC. *Clin. Infect. Dis.* 72, S79–S88. doi:10.1093/cid/ciaa1855

Alfageme, I., Reina, A., Gallego, J., Reyes, N., and Torres, A. (2009). Endobronchial instillations of amphotericin B: Complementary treatment for pulmonary mucormycosis. *J. Bronchology & Interventional Pulmonol.* 16, 214–215. doi:10.1097/LBR.0b013e3181aa2583

Brouet, G., Liot, F., Demange, J., and Nevot, P. (1964). Local treatment of pulmonary aspergilloma with transparietal injections of amphotericin B. *J. Fr. Med. Chir. Thorac.* 18, 789–798.

Cadranel, J., Philippe, B., Hennequin, C., Bergeron, A., Bergot, E., Bourdin, A., et al. (2012). Voriconazole for chronic pulmonary aspergillosis: A prospective multicenter trial. *Eur. J. Clin. Microbiol.* 31, 3231–3239. doi:10.1007/s10096-012-1690-y

Donnelly, J. P., Chen, S. C., Kauffman, C. A., Steinbach, W. J., Baddley, J. W., Verweij, P. E., et al. (2020). Revision and update of the consensus definitions of invasive fungal disease from the European organization for research and treatment of cancer and the mycoses study group education and research consortium. *Clin. Infect. Dis.* 71, 1367–1376. doi:10.1093/cid/ciz1008

Fisher, M. C., Alastruey-Izquierdo, A., Berman, J., Bicanic, T., Bignell, E. M., Bowyer, P., et al. (2022). Tackling the emerging threat of antifungal resistance to human health. *Nat. Rev. Microbiol.* 20, 557–571. doi:10.1038/s41579-022-00720-1

Hadda, V., Doddamani, S., Mittal, S., Tiwari, P., Madan, K., Mohan, A., et al. (2022). Efficacy of intrabronchial voriconazole instillation for inoperable pulmonary aspergilloma: A pilot randomized controlled trial. *Respiration* 101, 833–840. doi:10.1159/000525376

Hamamoto, T., Watanabe, K., and Ikemoto, H. (1983). Endobronchial miconazole for pulmonary aspergilloma. *Ann. Intern Med.* 98, 1030. doi:10.7326/0003-4819-98-6-1030_1

Hargis, J. L., Bone, R. C., Stewart, J., Rector, N., and Hiller, F. C. (1980). Intracavitary amphotereicin B in the treatment of symptomatic pulmonary aspergillomas. *Am. J. Med.* 68, 389–394. doi:10.1016/0002-9343(80)90109-6

Hinerman, R., Alvarez, F., Singh, A., and Keller, C. (2002). Treatment of endobronchial mucormycosis with amphotericin B via flexible bronchoscopy. *J. Bronchology* 9, 294–297. doi:10.1097/00128594-200210000-00007

Ikemoto, H. (1965). Treatment of pulmonary aspergilloma with amphotericin B. *Arch. Intern Med.* 115, 598–601. doi:10.1001/archinte.1960.03860170080017

Krakowka, P., Traczyk, K., Walczak, J., Halweg, H., Elsner, Z., and Pawlicka, L. (1970). Local treatment of aspergilloma of the lung with a paste containing nystatin or amphotericin B. *Tubercle* 51, 184–191. doi:10.1016/0041-3879(70)90071-1

Kravitz, J. N., Berry, M. W., Schabel, S. I., and Judson, M. A. (2013). A modern series of percutaneous intracavitary instillation of amphotericin B for the treatment of severe hemoptysis from pulmonary aspergilloma. *Chest* 143, 1414–1421. doi:10.1378/chest.12-1784

Lang, M., Lang, A. L., Chauhan, N., and Gill, A. (2020). Non-surgical treatment options for pulmonary aspergilloma. *Respir. Med.* 164, 105903. doi:10.1016/j.rmed.2020.105903

Lass-Flörl, C., Kofler, G., Kropshofer, G., Hermans, J., Kreczy, A., Dierich, M. P., et al. (1998). *In-vitro* testing of susceptibility to amphotericin B is a reliable predictor of clinical outcome in invasive aspergillosis. *J. Antimicrob. Chemother.* 42, 497–502. doi:10.1093/jac/42.4.497

Mohan, A., Tiwari, P., Madan, K., Hadda, V., Poulose, R., Bhalla, A. S., et al. (2017a). Intrabronchial voriconazole is a safe and effective measure for hemoptysis control in pulmonary aspergilloma. *J. Bronchology Interv. Pulmonol.* 24, 29–34. doi:10.1097/LBR.0000000000000321

Mohan, A., Tiwari, P., Madan, K., Hadda, V., Poulose, R., Bhalla, A. S., et al. (2017b). Intrabronchial voriconazole is a safe and effective measure for hemoptysis control in pulmonary aspergilloma. *J. Bronchology & Interventional Pulmonol.* 24, 29–34. doi:10.1097/LBR.0000000000000321

Morales, P., Galán, G., Sanmartín, E., Monte, E., Tarrazona, V., and Santos, M. (2009). Intrabronchial instillation of amphotericin B lipid complex: A case report. *Transpl. Proc.* 41, 2223–2224. doi:10.1016/j.transproceed.2009.06.017

Morgan, J., Wannemuehler, K. A., Marr, K. A., Hadley, S., Kontoyiannis, D. P., Walsh, T. J., et al. (2005). Incidence of invasive aspergillosis following hematopoietic stem cell and solid organ transplantation: Interim results of a prospective multicenter surveillance program. *Med. Mycol.* 43 (1), S49–S58. doi:10.1080/13693780400020113

Parikh, M. S., Seeley, E., Nguyen-Tran, E., and Krishna, G. (2017). Endobronchial ultrasound-guided transbronchial needle injection of liposomal amphotericin B for the treatment of symptomatic aspergilloma. *J. Bronchology & Interventional Pulmonol.* 24, 330–333. doi:10.1097/LBR.0000000000000383

Polak, A. (1999). The past, present and future of antimycotic combination therapy. *Mycoses* 42, 355–370. doi:10.1046/j.1439-0507.1999.00475.x

Ramirez, J. (1964). Pulmonary aspergilloma: Endobronchial treatment. *N. Engl. J. Med.* 271, 1281–1285. doi:10.1056/NEJM196412172712502

Sanguinetti, M., Posteraro, B., Beigelman-Aubry, C., Lamoth, F., Dunet, V., Slavin, M., et al. (2019). Diagnosis and treatment of invasive fungal infections: Looking ahead. *J. Antimicrob. Chemother.* 74, ii27–ii37. doi:10.1093/jac/dkz041

Shapiro, M. J., Albelda, S. M., Mayock, R. L., and McLean, G. K. (1988). Severe hemoptysis associated with pulmonary aspergilloma: Percutaneous intracavitary treatment. *Chest* 94, 1225–1231. doi:10.1378/chest.94.6.1225

Stone, N. R., Bicanic, T., Salim, R., and Hope, W. (2016). Liposomal amphotericin B (AmBisome®): A review of the pharmacokinetics, pharmacodynamics, clinical experience and future directions. *Drugs* 76, 485–500. doi:10.1007/s40265-016-0538-7

Takeda, T., Itano, H., Kakehashi, R., Fukita, S., Saitoh, M., and Takeda, S. (2014). Direct transbronchial administration of liposomal amphotericin B into a pulmonary aspergilloma. *Respir. Med. Case Rep.* 11, 7–11. doi:10.1016/j.rmcr.2013.12.003

Walsh, T. J., Anaissie, E. J., Denning, D. W., Herbrecht, R., Kontoyiannis, D. P., Marr, K. A., et al. (2008). Treatment of aspergillosis: Clinical practice guidelines of the infectious diseases society of America. *Clin. Infect. Dis.* 46, 327–360. doi:10.1086/525258

Walsh, T. J., Gamaletsou, M. N., McGinnis, M. R., Hayden, R. T., and Kontoyiannis, D. P. (2012). Early clinical and laboratory diagnosis of invasive pulmonary, extrapulmonary, and disseminated mucormycosis (zygomycosis). *Clin. Infect. Dis.* 54, S55–S60. doi:10.1093/cid/cir868

Winkler, J., Müller, U., Nenoff, P., Seyfarth, H.-J., Vogtmann, M., Borte, G., et al. (2007). Treatment of invasive pulmonary aspergillosis in neutropenic patients by additional bronchoscopic amphotericin B instillation. *Respiration* 74, 663–673. doi:10.1159/000105385

Yamada, H., Kohno, S., Koga, H., Maesaki, S., and Kaku, M. (1993). Topical treatment of pulmonary aspergilloma by antifungals. Relationship between duration of the disease and efficacy of therapy. *Chest* 103, 1421–1425. doi:10.1378/chest.103.5.1421

Zhang, H., and Zhu, A. (2020). Emerging invasive fungal infections: Clinical features and controversies in diagnosis and treatment processes. *Infect. Drug Resist* 13, 607–615. doi:10.2147/IDR.S237815

frontiers | Frontiers in Pharmacology

TYPE Original Research
PUBLISHED 19 June 2023
DOI 10.3389/fphar.2023.1200110

OPEN ACCESS

EDITED BY
Na Wang,
Tongji University, China

REVIEWED BY
Hong Bihong,
Ministry of Natural Resources, China
Yimin Mao,
The First Affiliated Hospital of Henan University of Science and Technology, China

*CORRESPONDENCE
Baicun Li,
lbc19890303@126.com
Meijuan Fang,
fangmj@xmu.edu.cn
Ting Yang,
dryangting@qq.com

RECEIVED 04 April 2023
ACCEPTED 26 May 2023
PUBLISHED 19 June 2023

CITATION
Chang C, He F, Ao M, Chen J, Yu T, Li W, Li B, Fang M and Yang T (2023), Inhibition of Nur77 expression and translocation by compound B6 reduces ER stress and alleviates cigarette smoke-induced inflammation and injury in bronchial epithelial cells.
Front. Pharmacol. 14:1200110.
doi: 10.3389/fphar.2023.1200110

Inhibition of Nur77 expression and translocation by compound B6 reduces ER stress and alleviates cigarette smoke-induced inflammation and injury in bronchial epithelial cells

Chenli Chang[1], Fengming He[2], Mingtao Ao[3], Jun Chen[2], Tao Yu[1], Weiyu Li[1], Baicun Li[1]*, Meijuan Fang[2]* and Ting Yang[1]*

[1]China-Japan Friendship Hospital, Center of Respiratory Medicine, National Center for Respiratory Medicine, National Clinical Research Center for Respiratory Diseases, Institute of Respiratory Medicine, Chinese Academy of Medical Sciences, Beijing, China, [2]School of Pharmaceutical Sciences, Xiamen University, Xiamen, China, [3]College of Pharmacy, Hubei University of Science and Technology, Xianning, China

Chronic obstructive pulmonary disease (COPD) is a leading cause of death worldwide with inflammation and injury in airway epithelial cells. However, few treatment options effectively reduce severity. We previously found that Nur77 is involved in lipopolysaccharide-induced inflammation and injury of lung tissue. Here, we established an *in vitro* model of COPD-related inflammation and injury in 16-HBE cells induced by cigarette smoke extract (CSE). In these cells, Nur77 expression and localization to the endoplasmic reticulum (ER) increased following CSE treatment, as did ER stress marker (BIP, ATF4, CHOP) expression, inflammatory cytokine expression, and apoptosis. The flavonoid derivative, named B6, which was shown to be a modulator of Nur77 in previous screen, molecular dynamics simulation revealed that B6 binds strongly to Nur77 through hydrogen bonding and hydrophobic interactions. Treating CSE-stimulated 16-HBE cells with B6 resulted in a reduction of both inflammatory cytokine expression and secretion, as well as attenuated apoptosis. Furthermore, B6 treatment resulted in a decrease in Nur77 expression and translocation to the ER, which was accompanied by a concentration-dependent reduction in the expression of ER stress markers. Meanwhile, B6 played a similar role in CSE-treated BEAS-2B cells. These combined effects suggest that B6 could inhibit inflammation and apoptosis in airway epithelial cells after cigarette smoke stimulation, and support its further development as a candidate intervention for treating COPD-related airway inflammation.

KEYWORDS

Nur77, airway epithelial cells, inflammation, apoptosis, small molecule derivative of flavonoid

Introduction

Chronic obstructive pulmonary disease (COPD), a common chronic respiratory disease, was the third leading cause of death worldwide in 2019, caused by a complex set of environmental factors, primarily including inhalation of particulate matter, cigarette smoke, and air pollutants, along with genetic, developmental, and social factors (Christenson et al., 2022). According to large-scale epidemiological studies such as BOLD and others, the estimated global prevalence of COPD is 10.3% (Adeloye et al., 2015; Adeloye et al., 2022), and its prevalence increases yearly (Venkatesan, 2023). COPD is a heterogeneous disease, characterized by persistent respiratory symptoms and airflow restriction due to abnormalities in the distal airway (Barnes et al., 2015). Its pathological manifestations include varying degrees of chronic bronchitis and damage to the pulmonary parenchyma (Calverley and Walker, 2003).

Cigarette smoke (CS) is known to contain more than 7,000 harmful substances (Soleimani et al., 2022), which can lead to oxidative stress, squamous metaplasia, mucus hypersecretion, ciliary shedding in the airway epithelium, cytokine secretion and subsequent recruitment of immune cells, which cumulatively result in limiting airflow (Yoshida et al., 2019; Dang et al., 2020; Zhou et al., 2020). At the cellular level, exposure to CS compromises the integrity or leads to loss of tight junctions between epithelial cells, resulting in the development of emphysema and subsequent pathogenesis of COPD (Tatsuta et al., 2019). However, the mechanism through which CS exposure leads to COPD development remains unclear.

Nur77, also known as NR4A1, is reportedly involved in asthma and acute lung injury through the activation of inflammatory response *via* regulation of NF-κB signaling (Kurakula et al., 2015; Jiang et al., 2016). Similarly, Nur77 $^{-/-}$ mice were found to exhibit increased sensitivity to bleomycin and higher susceptibility to pulmonary fibrosis (Palumbo-Zerr et al., 2015). Although the absence of endogenous ligands has led to its annotation as an orphan receptor (Safe et al., 2021), Nur77 is nevertheless widely expressed in different tissues and known to participate in a variety of processes as a transcriptional regulator in the nucleus or interaction partner modulating the function of other proteins (Chen et al., 2019; Niu et al., 2021). In particular, Nur77 has been shown to play roles in inflammatory response, cellular proliferation and differentiation, apoptosis, and autophagy (Koenis et al., 2018; Peng et al., 2021; Ye et al., 2021). Nur77 was also found to contribute to pathological inflammatory responses in diseases such as atherosclerosis, obesity, diabetes, arthritis, inflammatory bowel disease, acute liver inflammation, neuroinflammation, tumor inflammation, and respiratory diseases (Hanna et al., 2012; Wu et al., 2016; Li et al., 2020; Li et al., 2022; Ahuja et al., 2023). These studies collectively highlight the role of Nur77 in disease development and suggest that Nur77 may be an effective target for developing anti-inflammatory drugs. However, the function and mechanism of Nur77 in COPD have been largely overlooked.

Approximately one-third of the proteins in eukaryotic cells are secreted or membrane proteins that depend on the endoplasmic reticulum (ER) for biosynthesis, folding, and post-translational modification (Borges and Lake, 2014). In general, cells maintain a dynamic balance between protein biosynthesis and folding, a process known as ER homeostasis (Schinzel et al., 2019). Endoplasmic reticulum stress (ER stress) is induced by the aberrant accumulation of unfolded proteins in the ER due to the disruption of ER homeostasis by pathological factors such as oxidative stress, nutrient deprivation, ischemia, hypoxia, glucose deprivation, viral infection, or loss of calcium homeostasis. The development of ER stress involves the IRE1, PERK (PEK), and ATF6 pathways, and can result in programmed cell death or injury via apoptosis, autophagy, or ferroptosis (Wang et al., 2021; Zhang et al., 2021). In addition, ER stress can lead to cellular inflammation mediated by the MAPK, NF-κB, and other signaling pathways, which has been shown to contribute to the pathogenesis of several diseases (Zhang et al., 2018; Chen et al., 2022).

In previous work, we found that the flavonoid derivative, B6, could inhibit the development of lipopolysaccharide (LPS)-induced acute lung injury by targeting Nur77 (Ao et al., 2022). However, the effects of B6 on the subcellular localization of Nur77 and downstream ER stress in airway epithelial cells characteristic of COPD-related airway inflammation have not been explored. In this study, we found that Nur77 expression and translocation to the ER is increased in airway epithelial cells following exposure to cigarette smoke extract *in vitro*. These aberrant patterns of expression and localization lead to downstream induction of ER stress, which consequently promotes inflammation and apoptosis in airway epithelial cells. However, treatment with B6 results in decreased Nur77 expression and translocation to the ER, subsequently alleviating inflammation and reducing apoptosis in bronchial epithelial cells exposed to cigarette smoke extract. Molecular dynamics (MD) simulations suggest that B6 directly interacts with Nur77 and support its further exploration for possible application in the treatment of CSE-related inflammation.

Methods

Molecular docking

The crystal structure of the Nur77-3NB complex utilized in this study was sourced from the PDB database and had a resolution of 2.18 Å (PDB ID: 4WHG). The protein structure was prepared using the default parameters of the Protein Preparation Wizard panel of the Schrödinger Suite (version 2021-2). The preparation steps involved adding hydrogen atoms, deleting water molecules, adding charges, removing crystal solvents, completing missing residue side chains and loops utilizing the Prime module (Jacobson et al., 2002; Jacobson et al., 2004), optimizing hydrogen bond networks, and performing restrained energy minimization of the protein structure utilizing the OPLS4 force field (Lu et al., 2021). The small molecule ligand was prepared by subjecting it to the LigPrep (LigPrep, Schrödinger, LLC, New York, NY, 2021) tool of Schrödinger with default parameters, thereby converting its 2D structure to a 3D structure. Thereafter, molecular docking was conducted using the Induced Fit Docking panel (Induced Fit Docking, Schrödinger, LLC, New York, NY, 2021) of Schrödinger. The native ligand 3NB served as the docking box center, and default parameters were applied under the standard protocol. The top-ranking docking conformation was selected based

on the binding mode and docking score for subsequent MD simulations.

Binding pose metadynamics simulation

Before conducting the all-atom MD simulation, we performed a 10 × 10 ns binding pose metadynamics (BPMD) stimulation to evaluate the binding stability of B6 and Nur77. We utilized the Binding Pose Metadynamics panel of Schrödinger with default parameters, which involved selecting the Nur77-B6 complex as the structure type and setting the number of trials per pose to 10. The time series plot of the collective variable root-mean-square deviation (CV RMSD) was then obtained to analyze the reliability of the selected docking pose.

Molecular dynamics simulation

The B6/Nur77 complex was subjected to an all-atom MD simulation with periodic boundary conditions utilizing the OPLS4 force field (Lu et al., 2021) within the Desmond software (Desmond, Schrödinger, LLC, New York, NY, 2021) (Bowers et al., 2006; Desmond, 2021). The simulation system was constructed using the System Builder module of Desmond and solvated within a periodic cubic box. The distance between the box boundary and the complex was maintained at a minimum of 10 Å. The simulation system employed the predefined TIP3P water model and was neutralized by the inclusion of K^+ and Cl^- ions. Sufficient K^+ and Cl^- ions were added to achieve a KCl salt concentration of 0.15 M in the simulation system. Prior to the final simulation, a sequence of restrained minimization and MD simulations were executed to equilibrate the system (He et al., 2023). The final MD production was executed in the NPT (constant number of atoms *N*, pressure *P*, and temperature *T*) ensemble. The Nose-Hoover chain thermostat and Martyna-Tobias-Klein barostat were utilized to maintain a constant temperature of 310 K and a pressure of 1.01325 bar, respectively. The trajectory was recorded every 100 ps, and the simulation lasted for 100 ns. The Simulation Interaction Diagram tool was employed to analyze the simulation trajectory, including the RMSD of protein backbone atoms and small molecule ligand heavy atoms, and the analysis of ligand-protein interactions. The binding free energy between B6 and Nur77 was computed the obtained trajectory using the thermal_mmgbsa.py script within Schrödinger. PyMOL (The PyMOL Molecular Graphics System, Version 2.3 Schrödinger, LLC) was used to render overlay plots of the MD trajectory.

Surface plasmon resonance (SPR)

Following the same procedure in our previous study (Ao et al., 2022). A BIAcore T200 instrument (GE Healthcare) was used in the SPR study. The binding kinetics of Nur77-LBD and B6 were analyzed using the BIAcore T200 (GE Healthcare) at 25°C. The screening concentration was from 0.28 to 10 μM. The negative control was phosphate-buffered saline (PBS). Nur77-LBD proteins were diluted to 0.4 mg/mL in NaOAc (pH 4.5) and immobilized using amine coupling at 6,000 receptor units (RU) on a CM5 sensor chip (GE Healthcare). B6 was injected into the flow wells in running buffer (PBS, 0.1% DMSO) at a flow rate of 30 mL/min for 120 s of association, then dissociated for 420 s. The data was analyzed using the BIAcore T200 Evaluation Software 2.0. The dissociation constant (K_D) was calculated using kinetic data from gradient concentrations fitted to a 1:1 interaction model.

Fluorescence quenching assay

Different concentrations of B6 were added to Nur77-LBD proteins, and fluorescence quenching was monitored at 25°C with 10 nm slit widths for excitation and 10 nm slit widths for emission. A wavelength of 284 nm was used for excitation, and a wavelength of 450 nm was used for emission. A binding affinity was estimated by measuring fluorescence intensities at 332 nm as quencher concentration increased, and in accordance with the standard formula, the values of K_D were calculated.

CSE preparation

CSE was prepared as previously described (Xu et al., 2018). Briefly, a vacuum suction device was used to draw smoke from Marlborough cigarettes (Philip Morris, United States) into glass tubes containing 10 mL of room-temperature Dulbecco's Modified Eagle Medium (DMEM) (Gibco, United States) at a constant speed. Each cigarette was continuously aspirated for 5 min. The resulting CSE solution was added to a 96-well Costar plate (200 mL of solution per well) and the absorbance was measured at 320 nm with a microplate reader (Spark®, Tecan, Mannedorf, Switzerland). The optical density of the CSE was adjusted to 1.0 in DMEM, and the resultant CSE solution was considered as 100% CSE. The diluted solution was then sterilized with a 0.22 μm pore filter (Millipore, United States). The sterilized solution was further diluted in serum-free medium to the concentrations required for the experiments described below. Dilutions occurred within 1 h of sterilization.

Cell culture and treatment

The 16-HBE and BEAS-2B cells were cultured in DMEM supplemented with 10% fetal bovine serum (Procell Technology), 2 mM L-glutamine (Gibco), 100 U/mL penicillin (Gibco), and 100 μg/mL streptomycin (Gibco) at 37°C in ambient air supplemented with 5% CO_2. The cells were incubated with 2% CSE for 24 h to detect the effects of CSE on Nur77 concentrations, ER stress markers, and inflammatory cytokine levels. Other cells were stimulated with 5% CSE, then apoptosis was measured by CCK-8 assay and flow cytometry. To investigate the effects of B6, several concentrations (1, 2, 3, and 5 μM) were added to separate samples at 1 h after CSE stimulation. The assays described above were then conducted after 24 h of co-treatment.

Quantitative reverse transcription-PCR (RT-qPCR)

16-HBE and BEAS-2B cells were inoculated into 24-well plates and co-treated with CSE and B6. The supernatant was removed and cells

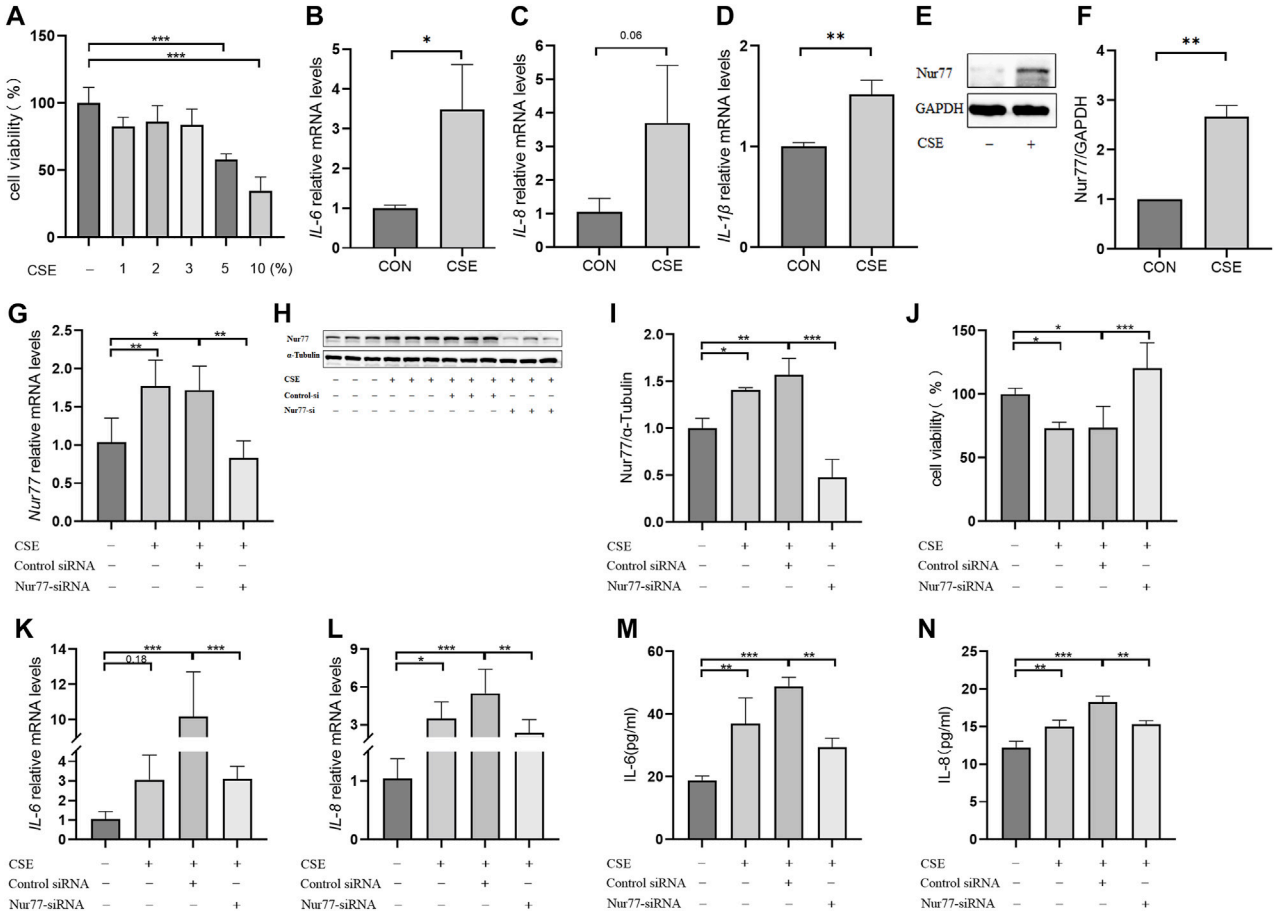

FIGURE 1
Nur77 plays an important role in cigarette smoke-induced epithelial cell inflammation and injury **(A)** Evaluation of 16-HBE cell viability after stimulation with several concentrations of cigarette smoke extract (CSE). Cell viability was measured with a Cell Counting Kit-8 (CCK8) bioassay. **(B–D)** mRNA levels of *IL-6* **(B)**, *IL-8* **(C)**, and *IL-1β* **(D)** after 2% CSE stimulation as determined with reverse transcription (RT)-qPCR. **(E, F)** Nur77 protein levels after 2% CSE stimulation as detected with western blot (WB). **(G–I)** Transfection efficiency of Nur77 short interfering (si)RNA in 16-HBE cells as determined with RT-PCR **(G)** and WB **(H, I)**. **(J)** Effects of 5% CSE on 16-HBE cell viability after transfection with Nur77 siRNA as determined with a CCK8 bioassay. **(K, L)** mRNA levels of *IL-6* **(K)** and *IL-8* **(L)** in 16-HBE cells transfected with Nur77 siRNA after 2% CSE stimulation as determined with RT-PCR. **(M, N)** Levels of IL-6 **(M)** and IL-8 **(N)** secreted by 16-HBE cells transfected with Nur77 siRNA after stimulation with 2% CSE as determined with enzyme-linked immunosorbent assay (ELISA). Data are presented as the least squares mean ± standard deviation. $^{*}p < 0.05$, $^{**}p < 0.01$, $^{***}p < 0.001$ (one-way analysis of variance).

were washed three times with PBS. TRIzol reagent (Takara Biomedical Technology, Beijing) was added to each well (1 mL each) and the plates were incubated at room temperature for 5 min. Chloroform (0.2 mL per well) was added and the plates were shaken vigorously. After incubation for 15 min on ice, cells were centrifuged at 12,000 rpm to extract RNA from the aqueous phase. The upper liquid containing RNA was isolated and mixed with an equal volume of isopropyl alcohol, then incubated on ice for 10 min. After centrifugation, the supernatant was discarded. The resulting RNA was washed with 1 mL 75% anhydrous ethanol and resuspended in 20 mL RNase-free water. RNA concentrations were measured with a NanoDrop One (Thermo Fisher Scientific, United States), and RNA quality was assessed using the A260/280 ratio, which was between 1.8 and 2.0 for each sample. RNA samples were stored at -80°C or used as cDNA template using a reverse transcription kit following the manufacturer's instructions (PrimeScript™ RT Master Mix, Takara Biomedical Technology, Beijing). RT-qPCR was performed with an real time PCR kit as instructed by the manufacturer to detect mRNA levels of *IL-6*, *IL-8*, *IL-1β*, and *TNFα* (TB Green® Premix Ex Taq™, Takara Biomedical Technology, Beijing).

Western blot

Cell lysates were prepared in radioimmunoprecipitation assay (RIPA) buffer containing 50 mM Tris (pH 8.0), 150 mM NaCl, 1% Triton X-100, 1 mM EDTA, 0.5% sodium deoxycholate, and 0.1% sodium dodecyl sulfate (SDS) (Solarbio, Beijing). The supernatant and precipitation fractions were obtained via centrifugation. The proteins were then separated with 10% SDS-polyacrylamide gel electrophoresis (PAGE) (Shanghai Epizyme Biomedical Technology) and transferred to a PVDF membrane (Merck KGaA, Darmstadt, Germany). The

10.3389/fphar.2023.1200110

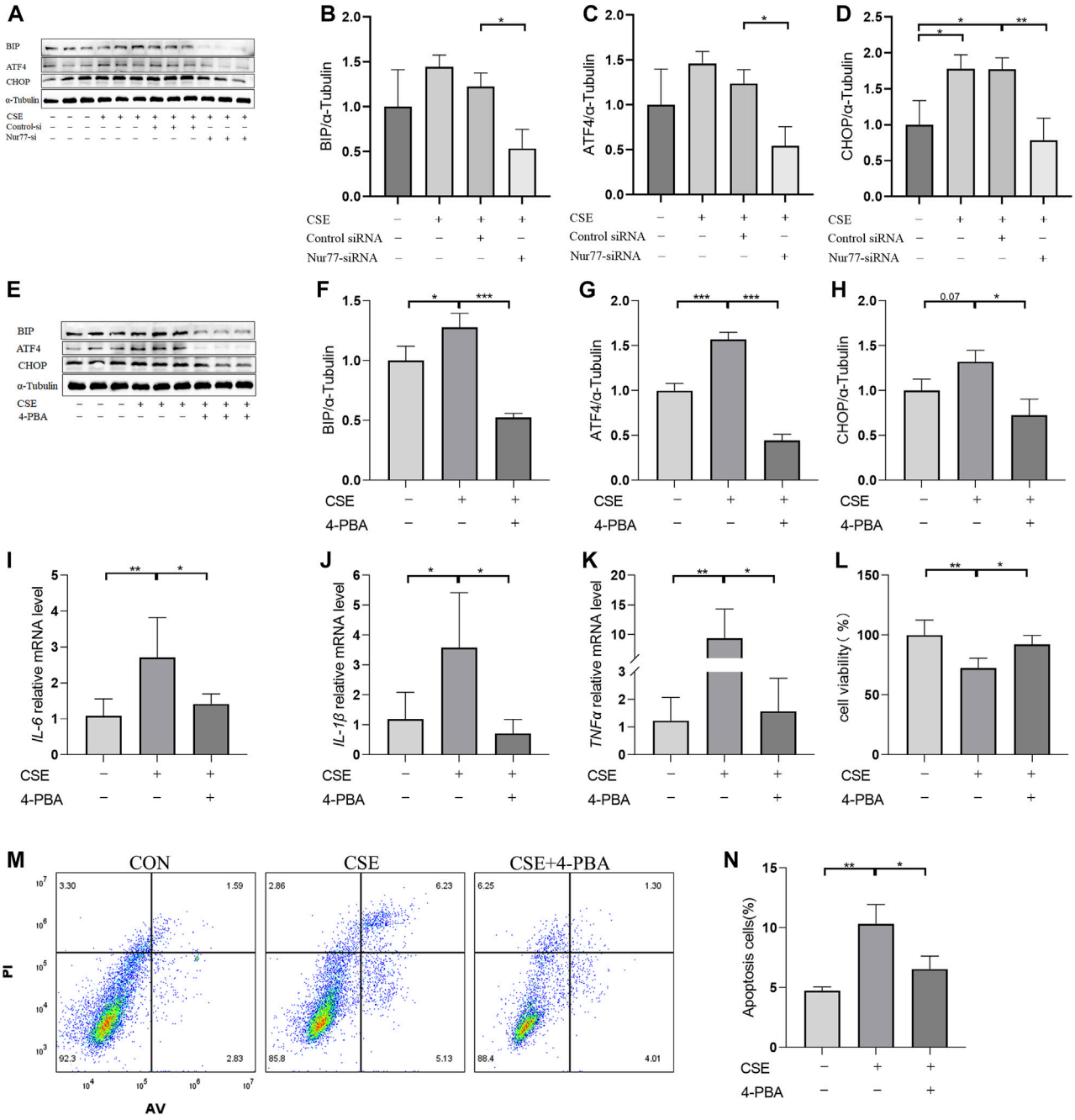

FIGURE 2
Endoplasmic reticulum stress, activated by Nur77, plays an important role in apoptosis and inflammation of airway epithelial cells **(A–D)** Protein expression levels of BIP (A, quantified in **(B)**, ATF4 (A, quantified in **(C)**, and CHOP (A, quantified in **(D)** in cells transfected with Nur77 short interfering (si) RNA after 2% cigarette smoke extract (CSE) stimulation as detected with western blot. **(E–H)** Protein expression levels of BIP (E, quantified in **(F)**, ATF4 (E, quantified in **(G)**, and CHOP (E, quantified in **(H)** in 16-HBE cells treated with 2% CSE and 4-PBA as detected with western blot. **(I–K)** mRNA expression levels of *IL-6* **(I)**, *IL-1β* **(J)**, and *TNF-α* **(K)** after treatment with 2% CSE and 4-PBA as detected with reverse transcription (RT)-PCR. **(L)** Viability of 16-HBE cells after treatment with 5% CSE and 4-PBA as measured with a CCK8 bioassay. **(M, N)** Apoptosis rates among 16-HBE cells after treatment with 5% CSE and 4-PBA as determined with flow cytometry. Data are presented as the least squares mean ± standard deviation. $^{*}p < 0.05$, $^{**}p < 0.01$, $^{***}p < 0.001$ (one-way analysis of variance).

following primary antibodies were used: anti-Nur77 (CST, 3960, 1:1000), anti-CHOP (CST, 2895, 1:1000), anti-BIP (CST, 3177, 1:1000), anti-ATF4 (Proteintech, 10835-1-AP, 1:1000) and anti-cleaved caspase3 (Immunoway, YC0006, 1:1000). The membrane was incubated with primary antibodies overnight at 4°C, then with secondary antibodies for 1 h at room temperature. Protein bands were visualized with an enhanced chemiluminescence kit on a ChemiDoc Chemiluminescent Gel Imaging System (Bio-Rad, United States). Individual protein band intensities were quantified with ImageJ software (NIH, United States).

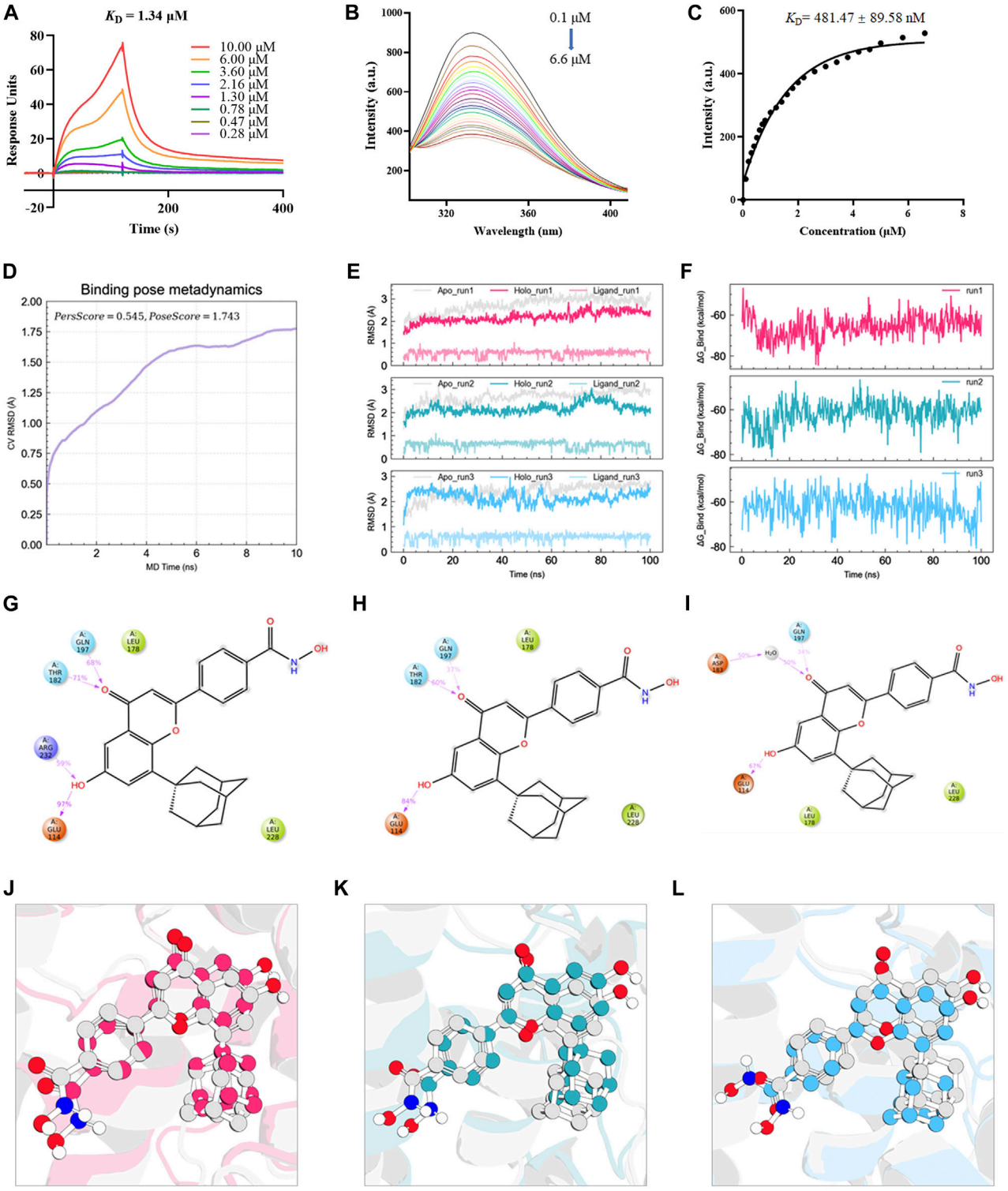

FIGURE 3
B6 exhibits high binding affinity with the NUR77-LBD through hydrogen bonding and hydrophobic interactions **(A)** An SPR experiment with purified Nur77-LBD showed binding of B6 to Nur77. **(B, C)** Fluorescence titration curve of Nur77-LBD with B6. The inhibitor concentration was increased from 0.1 μM to 6.6 μM at 0.1 μM intervals. **(D)** Binding pose metadynamics simulation. **(E)** Time series analysis of RMSD of protein backbone and ligand heavy atoms (three independent replicates). **(F)** Variation of the binding free energy between B6 and Nur77 over time. **(G–I)** Schematic representation of the interaction between B6 and Nur77 during the 100 ns MD simulation (three independent replicates). The percentage value indicates the ability to form hydrogen bond interactions during the simulation time. **(J–L)**. Superposition of the initial conformation and final conformation of the MD trajectory (three independent replicates). The initial conformation of B6 is depicted as a silver ball-and-sticks, while the last frames of the MD trajectory are represented as magenta (run1), cyan (run2), and sky-blue (run3) ball-and-sticks.

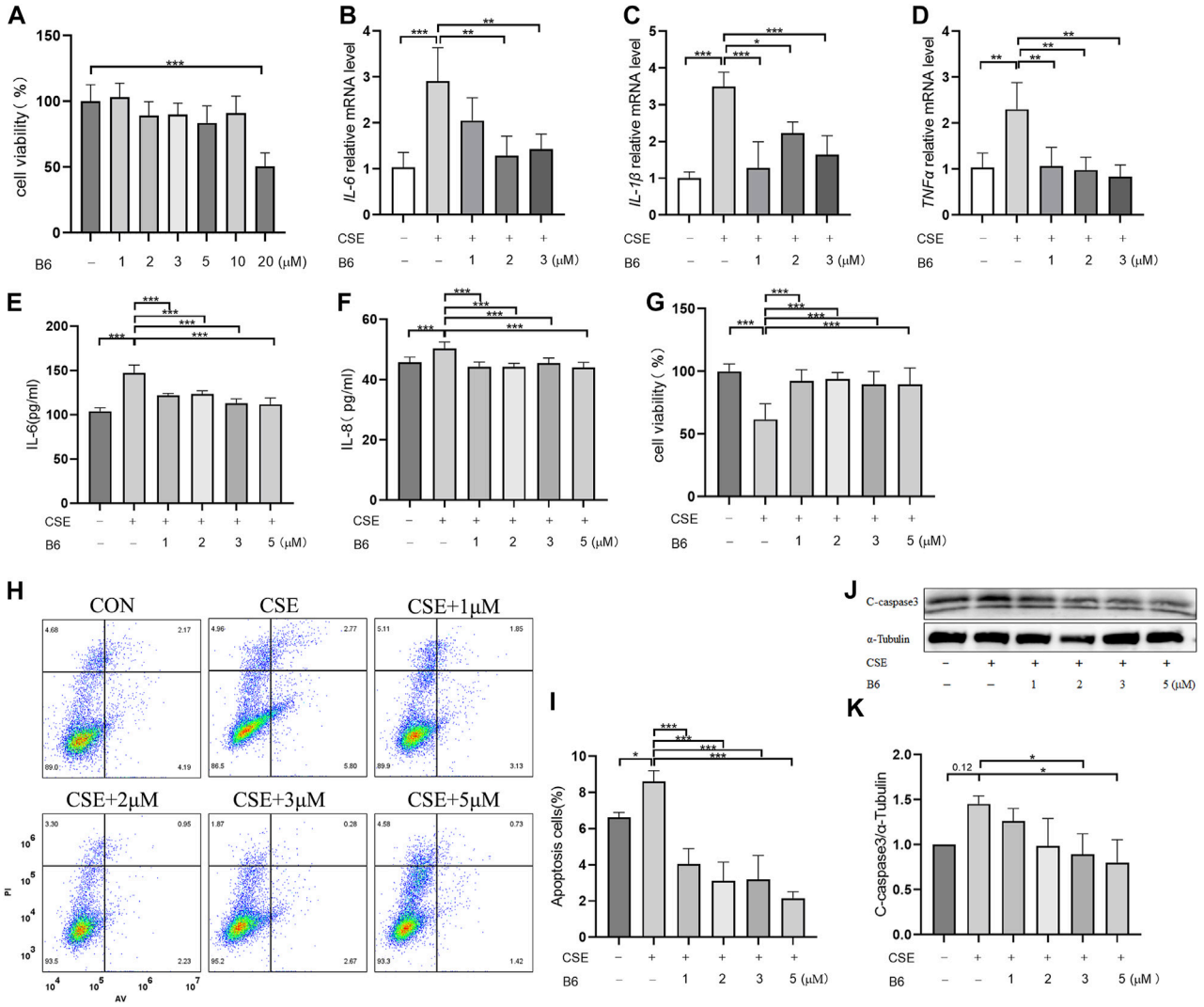

FIGURE 4
B6 significantly reduces the cellular inflammation and injury caused by cigarette smoke exposure **(A)** Effects of B6 on the viability of 16-HBE cells *in vitro* as determined with a CCK8 bioassay. **(B–D)** rt-PCR was used to detect the mRNA levels of inflammatory cytokines after 2% CSE stimulation with different concentrations of B6 in 16-HBE cells. **(E, F)** ELISA was used to detect the levels of inflammatory cytokines IL-6 **(E)** and IL-8 **(F)** in the medium of 16- HBE cells after 2% CSE stimulation with different concentrations of B6. **(G)** CCK8 was used to determine the viability of 16-HBE cells stimulated by 2% CSE with different concentrations of B6. **(H, I)** Flow cytometry was used to detect the apoptosis percentages of 16-HBE cells after 5% CSE stimulation with different concentrations of B6. **(J, K)** Western Blot was used to detect the protein levels of C-caspase3 [**(J)**, quantified in **(K)**] in 16-HBE cells after the intervention of B6 with different concentrations and CSE. Data are least squares means ± standard errors. *$p < 0.05$; **$p < 0.01$,***$p < 0.001$.

Enzyme-linked immunosorbent assay (ELISA)

The supernatant was collected from cultured 16-HBE cells after 24 h CSE stimulation. Levels of secreted IL-6 and IL-8 were measured in the collected culture medium using the Human Interleukin 6 (IL-6) ELISA Kit and the Human Interleukin 8 (IL-8) ELISA Kit (Invitrogen, Thermo Fisher Scientific, United States) following the manufacturer's instructions. After reaction termination, sample absorbances were detected at 450 nm using a microplate reader (Spark®, Tecan, Mannedorf, Switzerland). The standard curve was generated using the concentrations of the standards and the associated OD values. Finally, IL-6 and IL-8 concentrations in the samples were calculated using the standard curve.

Immunofluorescence

Equal numbers of 16-HBE cells were seeded on 14-mm glass coverslips pretreated with TC (Tissue culturetreated) (NEST, Jiangsu). After culturing for 24 h to reach 90% confluency, cells were treated with vehicle or test compounds for 24 h. The supernatant was discarded, then cells were washed with PBS. Cells were fixed in 4% paraformaldehyde for 15 min, which was followed by three consecutive washes with PBS. Cells were permeabilized with 0.1% Triton X-100 in PBS for 20 min, washed three times with PBS, and incubated with 10% goat serum for 1 h. These steps were conducted at room temperature. Cells were then incubated with 10% goat serum containing a 1:200 dilution of Nur77 primary antibody at 4°C

overnight, then washed three times with PBS for 5 min each. Cells were incubated with the red-labeled antibody IFKine™ Red Donkey Anti-Rabbit IgG (1:200, Abbkine Scientific Co., United States) for 2 h at room temperature. Cells were then incubated with a 1:200 dilution of the green-labeled ER-tracker (Beyotime, C1042) at 37°C for 30 min so the ER membranes could be visualized. After washing 3 times with PBS, cells were stained with DAPI (C1005) (1:1,000) for 5 min so the cell nuclei could be visualized. Glass coverslips were removed from the dishes, then cells were inverted on glass slides and mounted with antifading mounting medium (S2100, Solarbio). Images were captured with an image microscope (Nikon, Japan).

Flow cytometry

Six-well plates (Corning, New York, United States) were seeded with 16-HBE cells at a concentration of 2×10^5 cells per well. At 24 h after seeding, cells were treated with vehicle or test compounds and incubated for 24 h. Cells were then digested with trypsin to prepare single-cell suspensions. The digests were centrifuged and resuspended in antibody-binding buffer, then the cells were counted. Annexin V-FITC (4A biotech, Suzhou) (5 mL per sample) was added to each sample of 1×10^5 resuspended cells and mixed gently. Samples were incubated for 10 min in the dark at room temperature. After centrifugation, the supernatant was discarded, and cells were resuspended in 100 mL of antibody binding buffer. Propidium iodide staining solution (4A biotech, Suzhou) (10 mL) was added to each sample and gently mixed well, then staining was immediately halted by adding PBS. Flow cytometry was performed immediately (Beckman Coulter, United States).

Cell viability assay

Cell viability assays were conducted for 16-HBE and BEAS-2B cells using CCK8 bioassay. Briefly, 5×10^3 cells per well were seeded into 96-well plates to adhere overnight. Vehicle or test compounds were added and incubated for 24 h, after which 100 mL of complete medium with 10 mL CCK solution was added to each well and incubated for 1–4 h according to the appropriate OD value. Finally, absorption values were measured at 450 nm with a spectrophotometer (Spark®, Tecan, Mannedorf, Switzerland). Cell viability rates were calculated as follows:

$$\text{viability rate (\%)} = \text{OD(experimental group} - \text{blank well / control group} - \text{blank well)} \times 100\%$$

Statistical analysis

For each experiment, the mean values and standard deviation were calculated from at least three independent replicates. Differences between groups were analyzed with one-way analysis of variance (ANOVA). Differences were considered statistically significant at $p < 0.05$. All statistical analyses were performed in GraphPad Prism 9. $^*p < 0.05$, $^{**}p < 0.01$, $^{***}p < 0.001$.

Results

Nur77 is involved in cigarette smoke-induced injury and inflammation in epithelial cells

In order to better understand the role of Nur77 in cigarette smoke-related injury in human bronchial epithelial cells, we measured the viability of cultured 16-HBE cells treated with different concentrations (1%, 2%, 3%, 5%, or 10%) of cigarette smoke extract (CSE) *in vitro* by CCK8 assays. While viability was significantly decreased in the 5% and 10% treatment groups, cells treated with 1%, 2%, or 3% CSE showed a non-significant decreasing trend in the proportion of viable cells compared to controls (Figure 1A). In light of the above data, we selected 2% CSE to examine the transcriptional effects of CSE without inducing cell death in a significant proportion of our cultures (Maremanda et al., 2021). Following 24 h incubation with 2% CSE, we used RT-qPCR to measure mRNA levels of the inflammatory factors *IL-6* (Figure 1B), *IL-8* (Figure 1C) and *IL-1*β (Figure 1D), all of which were increased after CSE stimulation compared with that in untreated controls. Previous study of Nur77 in acute lung injury confirmed that Nur77 plays an important role in airway inflammation (Ao et al., 2022), we examined Nur77 expression in these 16-HBE cells after CSE stimulation. Western blotting showed that Nur77 protein accumulated to significantly higher levels after CSE treatment than that in untreated control cells (Figure 1E, quantified in Figure 1F).

To investigate the potential role of *Nur77* in cigarette smoke-induced inflammation in epithelial cells, we synthesized siRNAs targeting Nur77 and non-targeted RNA scramble controls, and transfected 16-HBE cells with 50 nM siNur77 or RNA scramble controls at a cell confluency of 50%. The medium was removed at 6 hours post-transfection and cells were stimulated with 2% CSE. RT-qPCR assays showed that the CSE-induced increase in *Nur77* mRNA levels was abolished in the si-Nur77 transfected cells, with transcript levels lower than that in untreated control cells (Figure 1G), which was verified by Western blot detection of Nur77 protein (Figure 1H, quantified in 1I). CCK8 assays further indicated that Nur77 knockdown (KD) could attenuate the CSE-induced reduction in cell viability (Figure 1J), While RT-qPCR and ELISA assays indicated that both transcriptional expression and secretion of inflammatory factors were inhibited in Nur77 KD cells (Figures 1K–N). These results suggested that Nur77 participates in cigarette smoke-induced inflammation and injury of bronchial epithelial cells.

Nur77-activated ER stress leads to apoptosis and inflammatory processes in airway epithelial cells

Previous studies have confirmed that ER stress plays an important role in inflammation and apoptosis (Choi et al., 2020). Therefore, we investigated whether the upregulation of Nur77 in

TABLE 1 IC_{50} values of B6 against different epithelial cell lines.

Cell lines	IC_{50} (μmol/L)
16-HBE	19.63 ± 2.46
BEAS-2B	18.05 ± 1.86
MLE-12	10.25 ± 0.98

[1]IC_{50} values were determined in triplicate (n = 6) and expressed as mean ± standard deviation (SD), meaning that the concentration at which B6 inhibited cell viability to 50% was measured using the CCK8 assay.

airway epithelial cells following CSE exposure also contributed to ER stress and further supported the role of ER stress in CSE-induced airway inflammation and injury via a specific inhibitor of ER stress, 4-PBA. Western blot analysis showed that treatment with 2% CSE resulted in significantly higher protein levels of the ER stress marker proteins, BIP (Figure 2A, quantified in Figure 2B), ATF4 (Figure 2A, quantified in Figure 2C)and CHOP (Figure 2A, quantified in Figure 2D), but not in the siNur77 cells, suggesting that Nur77 was also involved in CSE-induced ER stress. Next, we pretreated 16-HBE cells with 4-PBA for 2 h and then stimulated them with CSE to detect the indicators of ER stress. Western blotting indicated that BIP (Figure 2E, quantified in Figure 2F), ATF4 (Figure 2E, quantified in Figure 2G), and CHOP (Figure 2E, quantified in Figure 2H) protein levels were significantly lower in CSE-exposed cells pretreated with 4-PBA compared to that in CSE-stimulated without ER stress inhibitor. In addition, mRNA expression of the inflammatory factors *IL-6* (Figure 2I), *IL-1β* (Figure 2J), and *TNFα* (Figure 2K) was significantly lower in CSE-treated 16-HBE cells pre-treated with 4-PBA compared to their expression under CSE stimulation alone, suggesting that blocking ER stress could alleviate CSE-induced inflammation. To further investigate whether ER stress led to apoptosis in CSE-treated cells, we evaluated the effects of 4-PBA on apoptosis after CSE treatment using CCK8 assays (Figure 2L) and flow cytometry (Figures 2M,N). Both experiments showed that 4-PBA could reduce the proportion of apoptotic 16-HBE cells induced by CSE. These collective results supported the likelihood that cigarette smoke exposure could activate ER stress through Nur77 upregulation, resulting in airway inflammation and apoptosis in bronchial epithelial cells, and thus suggesting a role in the pathogenesis of COPD.

Hydrogen bonding and hydrophobic interactions mediate the high binding affinity of B6 with the Nur77 ligand binding domain

Based on a previous screen of candidate Nur77 modulators (Ao et al., 2022), we next examined the effects of the small molecule flavonoid derivative, B6, on cell inflammation and apoptosis following CSE exposure. To this end, we synthesized B6, characterized its binding affinity to Nur77, and evaluated its potential cytoxicity. To confirm that B6 could physically bind to the Nur77-LBD, we performed SPR experiments *in vitro*. The results showed that B6 could indeed bind the Nur77-LBD in a dose-dependent manner, with a dissociation constant (K_D) value of 1.34 μM, and relatively fast association/dissociation reaction kinetics (Figure 3A). Furthermore, the intrinsic fluorescence intensity of the Nur77-LBD (284 nm excitation/332 nm emission) was significantly reduced in the presence of B6 (Figure 3B) in a dose-dependent manner, with a calculated K_D value of 481.47 ± 89.58 nM (Figure 3C). These results supported that the flavonoid derivative B6 could directly and efficiently bind to Nur77-LBD *in vitro*.

We utilized molecular docking and MD simulations to investigate the interaction between B6 and Nur77. Initially, the induced-fit docking method was used to dock B6 to the active site of Nur77's ligand-binding domain (Nur77-LBD), and the top-ranked docking conformation was selected for subsequent MD analysis. To evaluate the stability of ligand-protein binding in aqueous solution during short MD simulations, we conducted BPMD simulation, a variant of metadynamics. It is considered that a PersScore ≥0.6 as an indicator of stable and sustained hydrogen bond interactions between the ligand and the protein in aqueous environment, and a PoseScore ≤2 as an indicator of stable ligand-protein binding in aqueous solution. The BPMD simulation results of B6/Nur77 complex demonstrated stable binding of B6 to the active site of Nur77 in aqueous environment (PoseScore = 1.743) with relatively persistent hydrogen bond interactions with the amino acid residues around the binding site, with a PersScore of 0.545 (Figure 3D). In addition, we performed three independent 100 ns all-atom MD simulations to confirm the stability of the B6/Nur77 complex. Figure 3E shows that the RMSD of protein backbone atoms in the simulation system with B6 bound (Holo) was smaller than that without ligand (Apo), and the RMSD of heavy atoms of B6 was relatively stable, fluctuating around 0.6 Å. The binding free energies between B6 and Nur77-LBD in three independent MD simulation runs were −65.86 ± 5.46, −59.94 ± 5.38, and −60.30 ± 5.99 kcal/mol (average of -62 kcal/mol), indicating a high binding affinity between B6 and Nur77 (Figure 3F).

Through analysis of the simulation trajectories, it was observed that B6 mainly forms hydrogen bond and hydrophobic interactions with key residues in the active site of Nur77. Figures 3G–I demonstrates that B6 can form stable and strong hydrogen bond interactions with the THR182, GUN197, GLU114 and ARG232. Notably, B6 can form hydrogen bond interactions with GLU114 and GUN197 for more than 30% of the simulation time in all three independent simulations, indicating the stability and importance of these hydrogen bonds. Moreover, the phenyl ring and adamantane of B6 can form hydrophobic interactions with LEU178 and LEU228, further stabilizing the binding of the small molecule to the protein. Finally, we overlaid the initial and final conformations of the MD trajectories to visually study the conformational changes of the small molecule during the MD simulations. Figures 3J–L shows that after 100 ns MD simulation, B6 can stably bind to Nur77-LBD and interact strongly with key residues through non-covalent bonds, with an RMSD of heavy atoms of B6 in run1, 2, and 3 systems of 0.8488, 1.1609, and 1.2450 Å, respectively.

B6 significantly reduces cigarette smoke extract-induced inflammation and apoptosis *in vitro*

Based on the above interactions between B6 and Nur77, we next examined the effects of various concentrations of B6 on 16-HBE

10.3389/fphar.2023.1200110

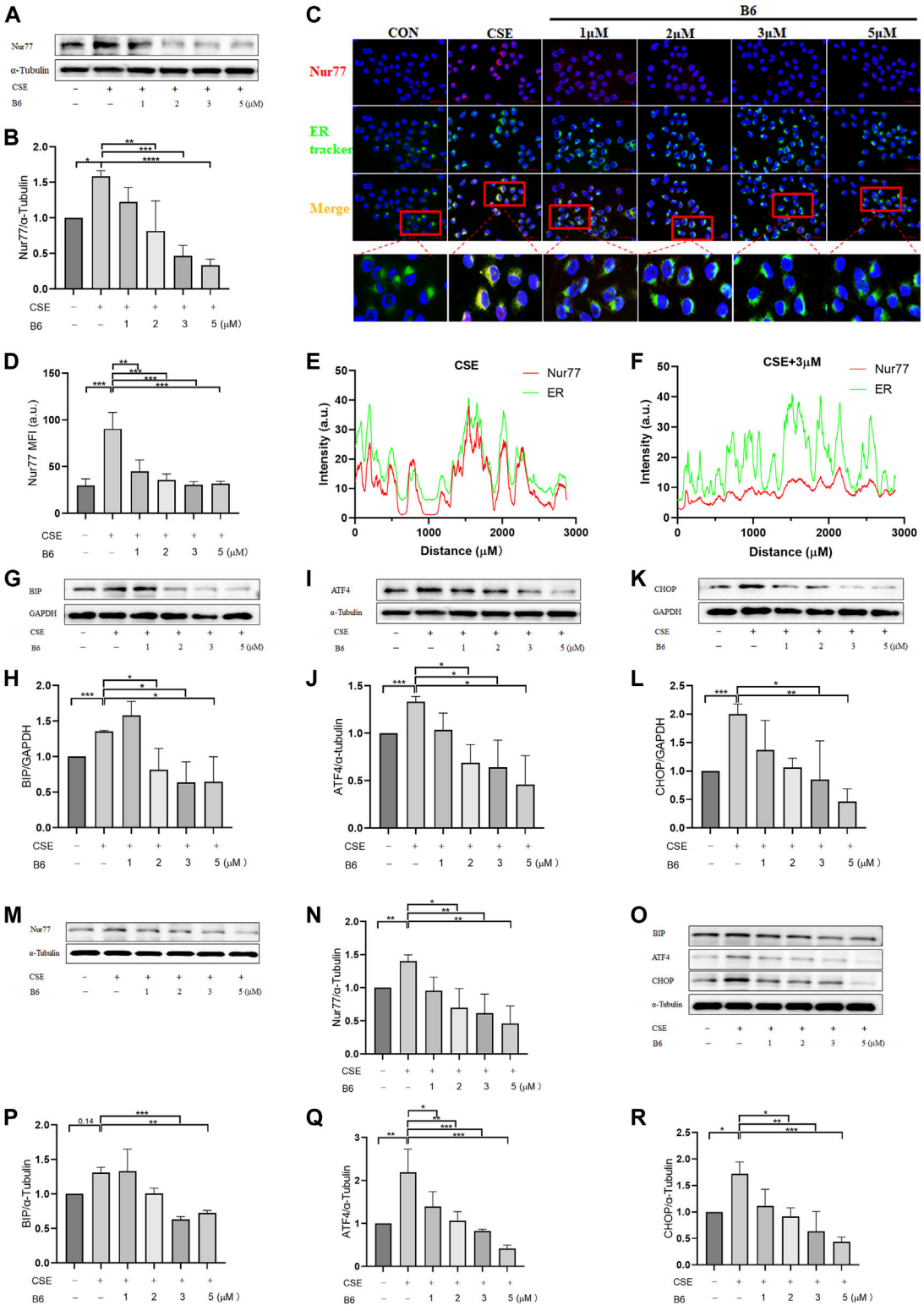

FIGURE 5
B6 plays a role in the production and subcellular localization of Nur77 under CSE stimulation **(A, B)** Western Blotting was used to detect the protein levels of Nur77 after the intervention of B6 with different concentrations and 2%CSE. **(C)** The co-localization of Nur77 (red) and ER tracker (green) was determined by immunofluorescence; **(D)** Statistical analysis of average fluorescence intensity of Nur77 in different groups; **(E, F)** Statistical analysis of colocalization between Nur77 (red) and ER tracker (green). Western Blotting was used to detect the BIP **(G, H)**, ATF4 **(I, J)** and CHOP **(K, L)** protein level in 16-HBE cells after the stimulation of 2% CSE with different concentrations of B6. **(M, N)** Protein expression levels of Nur77 [**(M)**, quantified in **(N)**] in BEAS-2B cells treated with 2% CSE and different concentrations of B6 as detected with Western blot. **(O–R)** Western blot was used to detect the protein expression of BIP [**(O)**, quantified in **(P)**], ATF4 [**(O)**, quantified in **(Q)**] and CHOP [**(O)**, quantified in **(R)**] in BEAS-2B cells stimulated by 2% CSE and different concentrations of B6. Data are least squares means ± standard errors. $*p < 0.05$; $**p < 0.01$,$***p < 0.001$.

airway epithelial cell viability using CCK8 bioassays. Calculation of IC_{50} values showed that viability was not significantly reduced compared to untreated controls at concentrations of ≤10 mM (Figure 4A; Table 1). To further evaluate whether B6 might be an effective intervention for COPD, we examined the effects of various concentrations of B6, from 1 to 3 μM, in 16-HBE cells at 1 h after CSE stimulation. Relative expression assays using RT-qPCR to quantify *IL-6* (Figure 4B), *IL-1*β (Figure 4C) and *TNF*-α (Figure 4D) transcription showed that treatment with B6 resulted in significantly lower expression following CSE treatment, while ELISA assays indicated that IL-6 (Figure 4E) and IL-8 (Figure 4F) levels were also reduced in cells stimulated with ≥1 μM B6. Moreover, CCK8 assays indicated that the decline in cell viability decline induced by CSE could be rescued by treatment with B6 (Figure 4G), while flow cytometry the proportion of 16-HBE cells with CSE-induced apoptosis was also markedly reduced in cells treated with B6 (Figures 4H,I). In addition, as a typical marker of apoptosis, we used Western blot to detect the protein level of cleaved-caspase3 in 16-HBE cells, as shown in Figures 4J,K, a significant increase in cleaved-caspase3 was observed after CSE stimulation, indicating increased apoptosis. B6 significantly inhibits the expression of cleavage-caspase3, consistent with the flow cytometry results, further supporting the inhibitory effect of B6 on CSE-stimulated apoptosis in 16-HBE cells. These results cumulatively supported that B6 could reduce CSE-induced inflammation and apoptosis.

B6 inhibits ER stress by affecting Nur77 production and ER localization

To further investigate the mechanism by which B6 affected cell inflammation and apoptosis, we examined Nur77 expression and localization following CSE stimulation in 16-HBE cells treated or not with B6. Western blot analysis indicated that Nur77 protein levels were significantly lower in CSE-stimulated cells treated with B6 compared to that in cells with CSE stimulation alone (Figure 5A, quantified in Figure 5B). Immunofluorescence staining experiments examining the subcellular localization of Nur77 showed an obvious increase in Nur77 signal and strong co-localization with a probe for ER following CSE treatment (Figure 5C), both of which were partially but significantly reduced in cells treated with B6 (Figures 5D–F). These results indicated that the flavonoid derivative, B6, could inhibit Nur77 expression and function, potentially alleviating inflammation and apoptosis by inhibiting Nur77 translocation to the ER.

We then explored the effects of B6 on ER stress through Western blot analysis of BIP, ATF4 and CHOP protein levels. The results showed that BIP (Figure 5G, quantified in Figure 5H), ATF4 (Figure 5I, quantified in Figure 5J), and CHOP (Figure 5K, quantified in Figure 5L) protein accumulation was lower in cells treated with both CSE and B6 than that in cells stimulated only with CSE. These results suggested that B6 acted as modulator of Nur77 to attenuate ER stress. Further, we detected the time-dependent effects of B6 combined with 2% CSE on the protein level of Nur77 and ER stress indicators at 6, 12, 18, and 24 h time points by Western blot. The results showed that Nur77 (Supplementary Figures S1A, B) increased gradually with time after CSE stimulation, as well as CHOP (Supplementary Figures S1A, C), BIP (Supplementary Figures S1D, E) and ATF4 (Supplementary Figures S1D, F). The protein levels of these indexes were suppressed after the addition of B6 in a time-dependent manner. In addition, cell viability was measured by CCK8 bioassay, and it was found that cell viability decreased significantly at both 6 h (Supplementary Figure S1G) and 12 h (Supplementary Figure S1H) after CSE stimulation, while the inhibitory effect of B6 on apoptosis was significant at 12 h (Supplementary Figure S1H). These results indicate that B6 may have a time-dependent role. To confirm that the effect of B6 on 16-HBE cells was not a special case, we cultured BEAS-2B cells, another common human bronchial epithelial cell line. After CSE and different concentrations of B6 were combined to stimulate BEAS-2B cells, Western Blot was used to detect the effects of CSE and B6 on protein level of Nur77 and ER stress indicators. Consistent with the findings in 16-HBE cells, CSE stimulation significantly increased the protein levels of Nur77 (Figures 5M, N), BIP (Figures 5O, P), ATF4 (Figures 5O, Q) and CHOP (Figures 5O, R), which were significantly inhibited by B6 in a dose-dependent manner. As we found, B6 can inhibit the transcriptional level of Nur77 (Supplementary Figure S2A), inflammatory cytokines (Supplementary Figures S2B–E) in BEAS-2B cells after CSE stimulation. Meanwhile, CCK8 assay showed that B6 can rescue the injury of CSE for BEAS-2B cells (Supplementary Figures S2F). The above results in BEAS-2B cells suggest a universal effect of B6 on airway epithelial cells. Combined with our above results, these experiments indicated that B6 inhibits Nu77 translocation into the ER, suppressing the downstream induction of ER stress, and thereby inhibiting the progression of cigarette smoke-related inflammation and apoptosis in airway epithelial cells.

Discussion

In the present study, we established an *in vitro* cell model of CSE-associated inflammation and injury in the airway by exposing bronchial epithelial cells to CSE. We then investigate the role of Nur77 in the process of CSE-induced cell injury and inflammatory response. We found that CSE exposure increases the overall expression of Nur77 and as well as its translocation to the ER, subsequently activating endoplasmic reticulum stress, which thus contributes to the inflammation and apoptosis in airway epithelium. A screen of small molecules in previous work identified flavonoid derivative B6, as a potential modulator of inflammation. We confirmed this effect and further found through molecular dynamics simulations that B6 can bind with Nur77. Finally, we found that treatment with B6 resulted in lower Nur77 levels, less translocation to the ER, and reduced ER stress in bronchial epithelial cells, supporting that B6 could reduce CSE-related airway inflammation and injury.

As a nuclear receptor, Nur77 has been shown to participate in the regulation of a variety of inflammatory diseases, and is differentially expressed in organs and tissues with chronic inflammation in both humans and animal models *in vivo*, and changes in its expression have been associated with different disease outcomes in various inflammatory disease models (Lith and de Vries, 2021). Some studies have reported that Nur77 can exert inhibitory effects on inflammation *via* transcriptional regulation of NF-κB signaling in the nucleus (Li et al., 2015). However, we found that Nur77 exerts pro-inflammatory and pro-apoptotic effects through ER translocation and subsequently activation

of ER stress after exposure to CSE. These results suggest that the subcellular localization of Nur77 is essential for its function, that increased localization of Nur77 in ER may be a reflection of its increased localization out of the nucleus, where it might indeed play an inhibitory role in NF-KB transcription, which is align well with its purported role. Previous studies of Nur77 translocation also demonstrated that Nur77 can induce apoptosis of tumor cells, cardiomyocytes, and other cells via binding to Bcl-2 on mitochondria (Lin et al., 2004; Liu et al., 2008). However, its role in inflammation and apoptosis of airway epithelial cell during COPD development has not been documented. Airway epithelial cells represent the first barrier against environmental damage, such as that caused by inhaling cigarette smoke, and inflammatory and apoptotic processes in these cells play a critical role in the pathogenesis of COPD (Roscioli et al., 2018). Thus, identifying the relevant signaling pathways and potentially druggable targets involved in these pathological processes is an essential step in the effective treatment of COPD-related airway inflammation and injury.

Findings in this study support that ER stress is activated by treatment with CSE *in vitro*, which in turn promotes cell inflammation and apoptosis in bronchial epithelial cells. Moreover, the ER stress activation process involves Nur77 translocation to the ER, which is reduced, along with ER stress, following treatment with B6. B6, a flavonoid derivative, has been shown to play a therapeutic role in ALI disease by binding with Nur77-LBD *in vivo* and *in vitro*. Our study confirms that B6, which exhibits low toxicity to airway epithelial cells, has an inhibitory effect on inflammation and injury of airway epithelial cells after CSE stimulation, suggesting the promise of its clinical application in airway diseases.

These results provide mechanistic insight into the role of Nur77 in CSE-related inflammation and apoptosis, and the possible application of B6 in the treatment of COPD. However, there are some shortcomings of our research that should be addressed. First, as a respiratory disease, it would be better to explore the efficacy of candidate drugs in animal models of COPD, which is focus of our ongoing and future research. Second, we have not investigated the regulatory and transport mechanisms responsible for determining the subcellular localization of Nur77, which are both necessary to fully understand the role of B6 in modulating Nur77 nuclear and ER localization processes. To address this issue, future studies will experimentally investigate the details of Nur77-B6 interactions.

Conclusion

This study provides robust evidence supporting the role of Nur77 in COPD-related airway inflammation and apoptosis. Our findings demonstrate that increased expression and translocation of Nur77 to the ER leads to ER stress, inflammatory response, and activation of apoptosis in human bronchial epithelial cells exposed to cigarette smoke extract *in vitro*. Moreover, we identified B6, a flavonoid derivative, as a modulator of Nur77 accumulation and ER translocation in CSE-treated airway epithelial cells. These results underscore the potential of B6 as a therapeutic candidate for airway inflammation and injury, and suggest that it may represent an effective therapeutic option for alleviating the severity of COPD. Further studies are warranted to fully elucidate the therapeutic potential of B6 in COPD management.

Data availability statement

The original contributions presented in the study are included in the article/Supplementary Material, further inquiries can be directed to the corresponding authors.

Author contributions

BL, MF, and TY designed the experiments. CC, FH, JC, MA, TY, and WL performed the experiments. CC, TY, and FH contributed to literature review and data analysis. CC and BL contributed to the article writing. BL, MF, and TY revised the manuscript. All authors contributed to the article and approved the submitted version.

Funding

This work was supported by grants from the National Natural Science Foundation of China (Grant Nos. 81970043, 82270038), National Key Research and Development Program of China (2022YFF0710803, 2022YFF0710800), CAMS Innovation Fund for Medical Sciences (CIFMS) (No.2021-I2M-1-049).

Conflict of interest

The authors declare that the research was conducted in the absence of any commercial or financial relationships that could be construed as a potential conflict of interest.

Publisher's note

Supplementary material

The Supplementary Material for this article can be found online at: https://www.frontiersin.org/articles/10.3389/fphar.2023.1200110/full#supplementary-material

SUPPLEMENTARY FIGURE S1
The time-dependent effect of B6 in 16-HBE cells. **(A–C)** Western Blot was used to detect the protein levels of Nur77 [**(A)**, quantified in **(B)**] and CHOP [**(A)**, quantified in **(C)**] after the treatment of B6 combined with 2% CSE at different time points. **(D–F)** Detecting the protein levels of BIP [**(D)**, quantified in **(E)**] and ATF4 [**(D)**, quantified in **(F)**] after the treatment of B6 combined with 2% CSE at different time points by Western Blot. **(G–H)** CCK8 was used to determine the

viability of 16-HBE cells stimulated by 5% CSE with B6 at 6 h **(G)** or 12 h **(H)**. Data are least squares means ± standard errors. *$p < 0.05$; **$p < 0.01$,***$p < 0.001$.

SUPPLEMENTARY FIGURE S2
Effects of B6 on inflammation and apoptosis in BEAS-2B cells stimulated by CSE.**(A)** rt-PCR was used to detect the mRNA levels of *Nur77* after 2% CSE stimulation with different concentrations of B6 in BEAS-2B cells. **(B–E)** The mRNA levels of *IL-6* **(B)**, *IL-8* **(C)**, *IL-1b* **(D)** and *TNFa* **(E)** in BEAS-2B cells stimulated by CSE with different concentrations of B6. **(F)** CCK8 was used to determine the viability of BEAS-2B cells stimulated by 5% CSE with different concentrations of B6. Data are least squares means ± standard errors. *$p < 0.05$; **$p < 0.01$,***$p < 0.001$.

References

Adeloye, D., Chua, S., Lee, C., Basquill, C., Papana, A., Theodoratou, E., et al. (2015). Global and regional estimates of COPD prevalence: Systematic review and meta-analysis. *J. Glob. Health* 5 (2), 020415. doi:10.7189/jogh.05.020415

Adeloye, D., Song, P., Zhu, Y., Campbell, H., Sheikh, A., Rudan, I., et al. (2022). Global, regional, and national prevalence of, and risk factors for, chronic obstructive pulmonary disease (COPD) in 2019: A systematic review and modelling analysis. *Lancet Respir. Med.* 10 (5), 447–458. doi:10.1016/S2213-2600(21)00511-7

Ahuja, P., Bi, X., Ng, C. F., Tse, M. C. L., Hang, M., Pang, B. P. S., et al. (2023). Src homology 3 domain binding kinase 1 protects against hepatic steatosis and insulin resistance through the Nur77-FGF21 pathway. *Hepatology* 77 (1), 213–229. doi:10.1002/hep.32501

Ao, M., Zhang, J., Qian, Y., Li, B., Wang, X., Chen, J., et al. (2022). Design and synthesis of adamantyl-substituted flavonoid derivatives as anti-inflammatory Nur77 modulators: Compound B7 targets Nur77 and improves LPS-induced inflammation *in vitro* and *in vivo*. *Bioorg Chem.* 120, 105645. doi:10.1016/j.bioorg.2022.105645

Barnes, P. J., Burney, P. G., Silverman, E. K., Celli, B. R., Vestbo, J., Wedzicha, J. A., et al. (2015). Chronic obstructive pulmonary disease. *Nat. Rev. Dis. Prim.* 1, 15076. doi:10.1038/nrdp.2015.76

Borges, C. R., and Lake, D. F. (2014). Oxidative protein folding: nature's knotty challenge. *Antioxid. Redox Signal* 21 (3), 392–395. doi:10.1089/ars.2014.5946

Bowers, K. J., Chow, D. E., Xu, H., Dror, R. O., Eastwood, M. P., Gregersen, B. A., et al. (2006). "Scalable algorithms for molecular dynamics simulations on commodity clusters," in *SC '06: Proceedings of the 2006 ACM/IEEE conference on supercomputing*, 43.

Calverley, P. M. A., and Walker, P. (2003). Chronic obstructive pulmonary disease. *Lancet (London, Engl.* 362 (9389), 1053–1061. doi:10.1016/s0140-6736(03)14416-9

Chen, J., López-Moyado, I. F., Seo, H., Lio, C-W. J., Hempleman, L. J., Sekiya, T., et al. (2019). NR4A transcription factors limit CAR T cell function in solid tumours. *Nature* 567 (7749), 530–534. doi:10.1038/s41586-019-0985-x

Chen, Y., Yang, J., Huang, Z., Yin, B., Umar, T., Yang, C., et al. (2022). Vitexin mitigates Staphylococcus aureus-induced mastitis via regulation of ROS/ER stress/NF-κB/MAPK pathway. *Oxid. Med. Cell Longev.* 2022, 7977433. doi:10.1155/2022/7977433

Choi, S. S., Lee, S. K., Kim, J. K., Park, H-K., Lee, E., Jang, J., et al. (2020). Flightless-1 inhibits ER stress-induced apoptosis in colorectal cancer cells by regulating Ca2+ homeostasis. *Exp. Mol. Med.* 52 (6), 940–950. doi:10.1038/s12276-020-0448-3

Christenson, S. A., Smith, B. M., Bafadhel, M., and Putcha, N. (2022). Chronic obstructive pulmonary disease. *Lancet (London, Engl.* 399 (10342), 2227–2242. doi:10.1016/S0140-6736(22)00470-6

Dang, X., He, B., Ning, Q., Liu, Y., Guo, J., Niu, G., et al. (2020). Alantolactone suppresses inflammation, apoptosis and oxidative stress in cigarette smoke-induced human bronchial epithelial cells through activation of Nrf2/HO-1 and inhibition of the NF-κB pathways. *Respir. Res.* 21 (1), 95. doi:10.1186/s12931-020-01358-4

Desmond (2021). *Desmond molecular dynamics system, D. E. Shaw research, New York, NY, 2021*. New York, NY: Maestro-Desmond Interoperability Tools, Schrödinger, 2021.

Hanna, R. N., Shaked, I., Hubbeling, H. G., Punt, J. A., Wu, R., Herrley, E., et al. (2012). NR4A1 (Nur77) deletion polarizes macrophages toward an inflammatory phenotype and increases atherosclerosis. *Circ. Res.* 110 (3), 416–427. doi:10.1161/CIRCRESAHA.111.253377

He, F., Wang, X., Wu, Q., Liu, S., Cao, Y., Guo, X., et al. (2023). Identification of potential ATP-competitive cyclin-dependent kinase 1 inhibitors: De novo drug generation, molecular docking, and molecular dynamics simulation. *Comput. Biol. Med.* 155, 106645. doi:10.1016/j.compbiomed.2023.106645

Jacobson, M. P., Friesner, R. A., Xiang, Z., and Honig, B. (2002). On the role of the crystal environment in determining protein side-chain conformations. *J. Mol. Biol.* 320 (3), 597–608. doi:10.1016/s0022-2836(02)00470-9

Jacobson, M. P., Pincus, D. L., Rapp, C. S., Day, T. J. F., Honig, B., Shaw, D. E., et al. (2004). A hierarchical approach to all-atom protein loop prediction. *Proteins* 55 (2), 351–367. doi:10.1002/prot.10613

Jiang, Y., Zeng, Y., Huang, X., Qin, Y., Luo, W., Xiang, S., et al. (2016). Nur77 attenuates endothelin-1 expression via downregulation of NF-κB and p38 MAPK in A549 cells and in an ARDS rat model. *Am. J. Physiol. Lung Cell Mol. Physiol.* 311 (6), L1023–L35. doi:10.1152/ajplung.00043.2016

Koenis, D. S., Medzikovic, L., van Loenen, P. B., van Weeghel, M., Huveneers, S., Vos, M., et al. (2018). Nuclear receptor Nur77 limits the macrophage inflammatory response through transcriptional reprogramming of mitochondrial metabolism. *Cell Rep.* 24 (8), 2127–2140. doi:10.1016/j.celrep.2018.07.065

Kurakula, K., Vos, M., Logiantara, A., Roelofs, J. J., Nieuwenhuis, M. A., Koppelman, G. H., et al. (2015). Nuclear receptor Nur77 attenuates airway inflammation in mice by suppressing NF-κB activity in lung epithelial cells. *J. Immunol.* 195 (4), 1388–1398. doi:10.4049/jimmunol.1401714

Li, B., Huang, J., Liu, J., He, F., Wen, F., Yang, C., et al. (2022). Discovery of a Nur77-mediated cytoplasmic vacuolation and paraptosis inducer (4-PQBH) for the treatment of hepatocellular carcinoma. *Bioorg Chem.* 121, 105651. doi:10.1016/j.bioorg.2022.105651

Li, B., Yao, J., Guo, K., He, F., Chen, K., Lin, Z., et al. (2020). Design, synthesis, and biological evaluation of 5-((8-methoxy-2-methylquinolin-4-yl)amino)-1H-indole-2-carbohydrazide derivatives as novel Nur77 modulators. *Eur. J. Med. Chem.* 204, 112608. doi:10.1016/j.ejmech.2020.112608

Li, L., Liu, Y., Chen, H-Z., Li, F-W., Wu, J-F., Zhang, H-K., et al. (2015). Impeding the interaction between Nur77 and p38 reduces LPS-induced inflammation. *Nat. Chem. Biol.* 11 (5), 339–346. doi:10.1038/nchembio.1788

Lin, B., Kolluri, S. K., Lin, F., Liu, W., Han, Y-H., Cao, X., et al. (2004). Conversion of Bcl-2 from protector to killer by interaction with nuclear orphan receptor Nur77/TR3. *Cell* 116 (4), 527–540. doi:10.1016/s0092-8674(04)00162-x

Lith, S. C., and de Vries, C. J. M. (2021). Nuclear receptor Nur77: Its role in chronic inflammatory diseases. *Essays Biochem.* 65 (6), 927–939. doi:10.1042/EBC20210004

Liu, J., Zhou, W., Li, S-S., Sun, Z., Lin, B., Lang, Y-Y., et al. (2008). Modulation of orphan nuclear receptor Nur77-mediated apoptotic pathway by acetylshikonin and analogues. *Cancer Res.* 68 (21), 8871–8880. doi:10.1158/0008-5472.CAN-08-1972

Lu, C., Wu, C., Ghoreishi, D., Chen, W., Wang, L., Damm, W., et al. (2021). OPLS4: Improving force field accuracy on challenging regimes of chemical space. *J. Chem. Theory Comput.* 17 (7), 4291–4300. doi:10.1021/acs.jctc.1c00302

Maremanda, K. P., Sundar, I. K., and Rahman, I. (2021). Role of inner mitochondrial protein OPA1 in mitochondrial dysfunction by tobacco smoking and in the pathogenesis of COPD. *Redox Biol.* 45, 102055. doi:10.1016/j.redox.2021.102055

Niu, B., Liu, J., Lv, B., Lin, J., Li, X., Wu, C., et al. (2021). Interplay between transforming growth factor-β and Nur77 in dual regulations of inhibitor of differentiation 1 for colonic tumorigenesis. *Nat. Commun.* 12 (1), 2809. doi:10.1038/s41467-021-23048-5

Palumbo-Zerr, K., Zerr, P., Distler, A., Fliehr, J., Mancuso, R., Huang, J., et al. (2015). Orphan nuclear receptor NR4A1 regulates transforming growth factor-β signaling and fibrosis. *Nat. Med.* 21 (2), 150–158. doi:10.1038/nm.3777

Peng, S-Z., Chen, X-H., Chen, S-J., Zhang, J., Wang, C-Y., Liu, W-R., et al. (2021). Phase separation of Nur77 mediates celastrol-induced mitophagy by promoting the liquidity of p62/SQSTM1 condensates. *Nat. Commun.* 12 (1), 5989. doi:10.1038/s41467-021-26295-8

Roscioli, E., Hamon, R., Lester, S. E., Jersmann, H. P. A., Reynolds, P. N., and Hodge, S. (2018). Airway epithelial cells exposed to wildfire smoke extract exhibit dysregulated autophagy and barrier dysfunction consistent with COPD. *Respir. Res.* 19 (1), 234. doi:10.1186/s12931-018-0945-2

Safe, S., Shrestha, R., and Mohankumar, K. (2021). Orphan nuclear receptor 4A1 (NR4A1) and novel ligands. *Essays Biochem.* 65 (6), 877–886. doi:10.1042/EBC20200164

Schinzel, R. T., Higuchi-Sanabria, R., Shalem, O., Moehle, E. A., Webster, B. M., Joe, L., et al. (2019). The hyaluronidase, TMEM2, promotes ER homeostasis and longevity independent of the UPRER. *Cell* 179 (6), 1306–1318. doi:10.1016/j.cell.2019.10.018

Soleimani, F., Dobaradaran, S., De-la-Torre, G. E., Schmidt, T. C., and Saeedi, R. (2022). Content of toxic components of cigarette, cigarette smoke vs cigarette butts: A comprehensive systematic review. *Sci. Total Environ.* 813, 152667. doi:10.1016/j.scitotenv.2021.152667

Tatsuta, M., Kan, -O. K., Ishii, Y., Yamamoto, N., Ogawa, T., Fukuyama, S., et al. (2019). Effects of cigarette smoke on barrier function and tight junction proteins in the bronchial epithelium: Protective role of cathelicidin LL-37. *Respir. Res.* 20 (1), 251. doi:10.1186/s12931-019-1226-4

Venkatesan, P. (2023). GOLD COPD report: 2023 update. *Lancet Respir. Med.* 11 (1), 18. doi:10.1016/S2213-2600(22)00494-5

Wang, P., Yang, Y., Pang, G., Zhang, C., Wei, C., Tao, X., et al. (2021). Hepatocyte-derived MANF is protective for rifampicin-induced cholestatic hepatic injury via inhibiting ATF4-CHOP signal activation. *Free Radic. Biol. Med.* 162, 283–297. doi:10.1016/j.freeradbiomed.2020.10.028

Wu, H., Li, X-M., Wang, J-R., Gan, W-J., Jiang, F-Q., Liu, Y., et al. (2016). NUR77 exerts a protective effect against inflammatory bowel disease by negatively regulating the TRAF6/TLR-IL-1R signalling axis. *J. Pathol.* 238 (3), 457–469. doi:10.1002/path.4670

Xu, H., Ling, M., Xue, J., Dai, X., Sun, Q., Chen, C., et al. (2018). Exosomal microRNA-21 derived from bronchial epithelial cells is involved in aberrant epithelium-fibroblast cross-talk in COPD induced by cigarette smoking. *Theranostics* 8 (19), 5419–5433. doi:10.7150/thno.27876

Ye, Z., Zhuo, Q., Hu, Q., Xu, X., Mengqi, L., Zhang, Z., et al. (2021). FBW7-NRA41-SCD1 axis synchronously regulates apoptosis and ferroptosis in pancreatic cancer cells. *Redox Biol.* 38, 101807. doi:10.1016/j.redox.2020.101807

Yoshida, M., Minagawa, S., Araya, J., Sakamoto, T., Hara, H., Tsubouchi, K., et al. (2019). Involvement of cigarette smoke-induced epithelial cell ferroptosis in COPD pathogenesis. *Nat. Commun.* 10 (1), 3145. doi:10.1038/s41467-019-10991-7

Zhang, L., Bao, D., Li, P., Lu, Z., Pang, L., Chen, Z., et al. (2018). Particle-induced SIRT1 downregulation promotes osteoclastogenesis and osteolysis through ER stress regulation. *Biomed. Pharmacother.* 104, 300–306. doi:10.1016/j.biopha.2018.05.030

Zhang, Q., Zhang, Q., Li, H., Zhao, X., and Zhang, H. (2021). LiCl induces apoptosis via CHOP/NOXA/Mcl-1 axis in human choroidal melanoma cells. *Cancer Cell Int.* 21 (1), 96. doi:10.1186/s12935-021-01778-2

Zhou, J-S., Li, Z-Y., Xu, X-C., Zhao, Y., Wang, Y., Chen, H-P., et al. (2020). Cigarette smoke-initiated autoimmunity facilitates sensitisation to elastin-induced COPD-like pathologies in mice. *Eur. Respir. J.* 56 (3), 2000404. doi:10.1183/13993003.00404-2020

frontiers | Frontiers in Pharmacology

TYPE Original Research
PUBLISHED 04 July 2023
DOI 10.3389/fphar.2023.1203033

OPEN ACCESS

EDITED BY
Peiran Yang,
Chinese Academy of Medical Sciences and Peking Union Medical College, China

REVIEWED BY
Ayyanar Sivanantham,
Boston Medical Center, United States
Darrell Pilling,
Texas A&M University, United States

*CORRESPONDENCE
Yun-Sil Lee,
yslee0425@ewha.ac.kr

†PRESENT ADDRESS
Seulgi Jeon,
Inhalation Toxicology Research Group, Korea Institute of Toxicology, Jeongeup-si, South Korea

RECEIVED 10 April 2023
ACCEPTED 22 June 2023
PUBLISHED 04 July 2023

CITATION
Yoo YJ, Jeon S, Jin H, Won HY, Jeong MG, Cho Y, Hwang ES, Na Y, Cho J and Lee Y-S (2023), Drug like HSP27 cross linkers with chromenone structure ameliorates pulmonary fibrosis. *Front. Pharmacol.* 14:1203033. doi: 10.3389/fphar.2023.1203033

Drug like HSP27 cross linkers with chromenone structure ameliorates pulmonary fibrosis

Young Jo Yoo[1], Seulgi Jeon[1†], Hee Jin[1], Hee Yeon Won[1], Mi Gyeong Jeong[1], Yeseul Cho[1], Eun Sook Hwang[1], Younghwa Na[2], Jaeho Cho[3] and Yun-Sil Lee[1*]

[1]Graduate School of Pharmaceutical Sciences, Ewha Womans University, Seoul, Republic of Korea, [2]College of Pharmacy, CHA University, Pocheon-si, Gyeonggi-do, Republic of Korea, [3]Department of Radiation Oncology, Yonsei University Health System, Seoul, Republic of Korea

Background: Pulmonary fibrosis (PF) is a progressive lung disease characterized by fibroblast accumulation and collagen deposition, resulting in lung scarring and impaired gas exchange. Current treatments for idiopathic pulmonary fibrosis (IPF) have limited efficacy and significant side effects. Heat shock protein 27 (HSP27) has emerged as a potential therapeutic target for PF due to its involvement in fibrotic processes. However, effective HSP27 inhibitors for PF treatment are still lacking.

Methods: To assess the anti-fibrotic effects of NA49, we utilized murine PF models induced by radiation (IR) or bleomycin (BLM). We administered NA49 to the PF mice and evaluated its impact on lung fibrosis progression. We also investigated the molecular mechanisms underlying NA49's effects, focusing on its inhibition of EMT-related signaling pathways.

Results: In our study, we evaluated the potential of a novel HSP27 inhibitor, NA49, in preclinical models of PF. NA49 effectively suppressed PF development in radiation and bleomycin-induced PF models. It reduced fibrosis, inhibited NFkB signaling, and downregulated EMT-related molecules. Importantly, we evaluated the safety profile of NA49 by assessing its impact on DNA strand breakage. Compared to previous HSP27 inhibitors, NA49 showed lower levels of DNA damage in human lung epithelial cells, and suggests that NA49 may have reduced toxicity compared to other HSP27 inhibitors. Overall, our results demonstrate that NA49 effectively inhibits PF development in preclinical models. It reduces lung fibrosis, inhibits EMT-related signaling pathways, and exhibits improved safety profiles. These findings highlight the potential of NA49 as a promising candidate for the treatment of PF.

Conclusion: NA49 exhibited significant anti-fibrotic effects, inhibiting fibrosis development and EMT-related signaling pathways. Moreover, NA49 showed improved safety profiles compared to previous HSP27 inhibitors.

KEYWORDS

heat shock protein 27, cross linking inhibitors, NA49, pulmonary fibrosis, radiation, bleomycin

Introduction

Pulmonary fibrosis (PF), which includes idiopathic pulmonary fibrosis (IPF), primarily affects older individuals, with a typical age of diagnosis in the mid-60s (Raghu et al., 2006). The underlying mechanism of PF is believed to involve repeated micro injuries to the alveolar epithelium and a severely disrupted injury-repair response. This leads to the accumulation of fibroblasts and collagen, resulting in lung scarring and impaired gas exchange (Wilson and Wynn, 2009). The prevailing theory is that fibrosis in PF follows a pathway comparable to the normal process of wound healing (Wynn, 2011). Instead of concluding the reparative process with the elimination of fibroblasts during the maturation phase, a continuous fibrotic response ensues, sustained by a positive feedback mechanism involving the proliferation and activation of fibroblasts, production of extracellular matrix (ECM), and inhibition of fibroblast apoptosis (Wynn, 2011; White and Mantovani, 2013).

Three pharmacological treatments for IPF, pirfenidone (PFD), nintedanib (NTD), and N-acetylcysteine (NAC) are currently commercially available. PFD, by inhibiting TGFβ, has demonstrated its ability to prevent the accumulation of hydroxyproline, procollagen I and III, inflammatory cells, and TGFβ1 in bronchoalveolar lavage and/or lung tissue (Westergren-Thorsson et al., 1993; Iyer et al., 1999a; Iyer et al., 1999b; Oku et al., 2008; Carter, 2011; Myllärniemi and Kaarteenaho, 2015). In mouse models of PF, PFD has exhibited the ability to reduce the population of fibrocytes and inhibit their migration (Inomata et al., 2014). Nintedanib (NTD), a pan-tyrosine kinase receptor inhibitor, was serendipitously discovered as a byproduct during extensive screening assays originally intended for targeting cyclin-dependent kinase (Roth et al., 2015). However, conclusive evidence establishing its clinical efficacy in the treatment of PF is currently lacking. Although these drugs have shown effectiveness in slowing the decline in lung function and reducing the risk of acute respiratory deterioration, they are associated with a substantial occurrence of morbidity and mortality. Notably, individual clinical trials have not demonstrated a reduction in mortality (Roth et al., 2015). Furthermore, both therapies commonly exhibit side effects, primarily affecting the gastrointestinal system (Richeldi et al., 2014).

Heat shock protein 27 (HSP27), known as HSP27 in humans and HSP25 in mice, is an ATP-independent molecular chaperone that exhibits significant upregulation in response to various cellular stresses (Ferns et al., 2006). HSP27 promotes the migration and invasion of cancer cells and facilitates the process of epithelial-to-mesenchymal transition (EMT) (Shiota et al., 2013). It also induces EMT during fibrosis, including IPF (Hill et al., 2019). HSP27 overexpression has been reported in patients diagnosed with IPF (Park et al., 2016). Elevated levels of HSP27 play a significant role in the development of myofibroblasts and may serve as a potential therapeutic target for fibrotic disorders. The suppression of the HSP27 gene using OGX-427, a second-generation antisense oligonucleotide, has been shown to decrease PF induced by bleomycin (BLM) and inhibit EMT through the degradation of Snail (Wettstein et al., 2013). In addition, we identified HPS27 as a molecular target for PF and functional inhibition of HSP27 using a small molecule J2, a HSP27 cross-linker (Choi et al., 2017; Hwang et al., 2017), ameliorated PF. The activation of IkBα-NFκB signaling, facilitated by the direct interaction between IkBα and HSP27, plays a crucial role in the process of EMT, which is closely associated with the development of PF (Kim et al., 2019). As a consequence, HSP27 inhibition is an appealing treatment option, even though HSP27, unlike HSP90 and HSP70, lacks an ATP-binding site, thus to date, no effective inhibitors targeting HSP27 have been identified.

Previously, we have been working on the development of different HSP27 inhibitors that induce cross-linking of HSP27 by inserting themselves between the disulfide bonds of HSP27. Some examples of these inhibitors include zerumbone, which was derived from a natural product, SW15, a synthetic xanthone compound (Kim et al., 2016), and J2, a chromenone compound (Choi et al., 2017; Hwang et al., 2017) However, these compounds faced the challenges in terms of their poor drugability or toxicity. Therefore, we developed NA49, a J2 derivative, which showed better drugability in absorption, distribution, metabolism, excretion, and toxicity (ADME/Tox) (Yoo et al., 2021).

In the current study, we investigated the potential of NA49 as a more effective HSP27 inhibitor for the treatment of PF. To assess its antifibrotic effects, we used murine PF models induced by radiation (IR) or BLM and NA49 may be a good drug candidate for overcoming PF by blocking the EMT stage.

Materials and methods

For a comprehensive description of the Materials and methods, please refer to the Supplementary Material.

Chemicals

J2 (Choi et al., 2017; Hwang et al., 2017) and NA49 (Yoo et al., 2021) were chemically synthesized and previously described.

IR and BLM induced PF models

All experimental procedures were granted approval by the Animal Care and Use Committees of Ewha Womans University (IACUC 18–064) and Yonsei University Medical School (2015–0267) and were conducted in strict adherence to the applicable guidelines. C57BL/6N mice (male, 6 weeks old, with a minimum of three mice per group) were obtained from JOA bio Inc. (Seoul, Korea). The mice were either irradiated with a single dose of 75 Gy using the X-RAD 320 platform as described previously (Jin et al., 2017) or received a single intratracheal instillation of 2.5 mg/kg BLM (Santacruz Biotechnology, Dallas, TX, United States). NA49 and J2 (3 mg/kg) were intraperitoneally injected every other day for 6 weeks or 2 weeks after IR or BLM treatment, respectively. C57BL/6N wild-type (WT) mice and HSP25 transgenic (TG) mice were generated and housed under pathogen-free conditions at Macrogen, Inc. (Kim et al., 2019).

Cell culture and immunoblotting

The L132 cell line (human normal lung epithelial cell line) was obtained from the ATCC (RPMI media) and the KCLB (Korean Cell Lines Bank) (DMEM media). The cells were cultured in media (Gibco) supplemented with 10% FBS (Gibco) and maintained in a 37°C incubator with 5% CO_2. To ensure the absence of *Mycoplasma* contamination, the cell lines were tested using the BioMycoX *Mycoplasma* PCR Detection Kit (JCBIO Co., Ltd.). The L132 cells were extracted using RIPA lysis buffer, and the cell extracts were subjected to SDS-polyacrylamide gel electrophoresis under reducing conditions and subsequently transferred onto a nitrocellulose membrane. After incubation with primary antibodies, the protein blot was next probed with the appropriate secondary antibodies that had been conjugated to HRP. The ECL detection technology was used in order to see the protein bands (GE Healthcare, Freiburg, Germany). At least three separate immunoblots were used to provide the quantitative protein analysis that was achieved. After being normalized to β-actin, the quantification of the detected intensities of the protein bands was then performed using the ImageJ program. The antibodies that were tested for this investigation may be found listed in Supplementary Table S1.

Quantitative RT-PCR

Total RNA was extracted from the cells or tissues using TRIzol reagent (Qiazen, Valencia, CA, United States). A Nanodrop was used to evaluate RNA purity and concentration. According to the manufacturer's instructions, RNA was reverse transcribed using the ReverTra Ace® qPCR RT Kit (TOYOBO, Osaka, Japan). For quantitative RT-PCR, the THUNDERBIRD SYBR qPCR Mix (TOYOBO, Osaka, Japan), and the Step One Plus RT-PCR machine (Applied Biosystems, Carlsbad, CA, United States) were used. After normalization using the Ct values of the GAPDH gene, the relative transcript levels of genes were determined. The primers used are detailed in Supplementary Table S2.

Preparation of lung tissues for immunohistochemistry and immunofluorescence staining

Lung tissue was removed from IR or BLM-treated mice, fixed in 10% (v/v) neutral buffered formalin and paraffin embedding was performed to prepare the samples. The paraffin-embedded sections were deparaffinized and subsequently stained using hematoxylin and eosin (H&E, Sigma-Aldrich) as well as a Masson's trichrome (MT) staining kit (Sigma-Aldrich). Additionally, immunohistochemistry, and immunofluorescence staining were carried out. Images were acquired using a Zeiss Apotome microscope (Carl Zeiss) installed at the Ewha Drug Development Research Core Center. All antibodies used in the study were listed in Supplementary Table S3.

Irradiation

The cells in this study were subjected to IR with a single dose of either 5 or 10 Gy. The IR was generated using a ^{137}Cs gamma-ray source (Elan 3000, Atomic Energy of Canada, Mississauga, Canada) at a dose rate of 3.81 Gy/min. To ensure radiation safety, radiation workers underwent annual radiation safety management training conducted by the Korea Foundation of Nuclear Safety (KoFONS).

Micro-CT analysis

Micro-CT analysis was performed as described previously (Kim et al., 2017). High-resolution micro-computed tomography (CT) images were obtained using a volumetric CT scanner (NFR Polaris-G90MVC: NanoFocusRay, Iksan, South Korea) operating at 50 kVp, 180 μA, and 150 mGy. The scanning parameters included 700 views and a frame rate of 142 ms. The images were reconstructed using volumetric cone-beam reconstruction with the Feldkamp-Davis-Kress method. The reconstructed images had a size of 1,232 × 1,120 pixels and consisted of 512 slices. For the analysis, ImageJ software was utilized for volumetric measurements. To ensure consistent measurements across specimens, the same level settings were applied to all images during the analysis.

Alkaline comet assay

At 37°C, 1×10^5 cells/mL L132 suspended in PBS were combined with low-melting agarose in a 1:10 (v/v) ratio. The combination was applied to a CometSlide (Trevigen Inc., Maryland, United States, #4250-200-03). After the agarose had solidified, the slides were submerged in a lysis solution for 1 h. They were then placed in an alkaline unwinding solution comprising 200 mM NaOH and 200 mM EDTA (pH 13) and incubated at room temperature for 20 min. At 4°C, an electrical field (25 V) was administered for 30 min. After being stored at 4°C for 1 h to overnight, the slides were stained with 70 μL of ×1 SYBR Gold (Thermo Fisher Scientific, #S11494) and the comet photos were acquired using a Zeiss confocal microscope. The Komet 5.5 software application was used to examine the datasets.

Statistical analysis

One-way ANOVA was used to determine the statistical significance among and between conditions by Tukey's test or using GraphPad Prism Software version 9.0. All data were obtained from a minimum of three independent experiments. Data are reported as the mean ± SEM.

Results

Inhibition of EMT by NA49, a druggable HSP27 cross-linker

A previous study demonstrated that J2 induces the cross-linking of HSP27, leading to the formation of altered dimers. These altered dimers result in the functional inhibition of HSP27, ultimately leading to the inhibition of PF (Kim et al., 2019). However, due to the inadequate solubility and short *in vivo* circulation time of J2, we have developed a

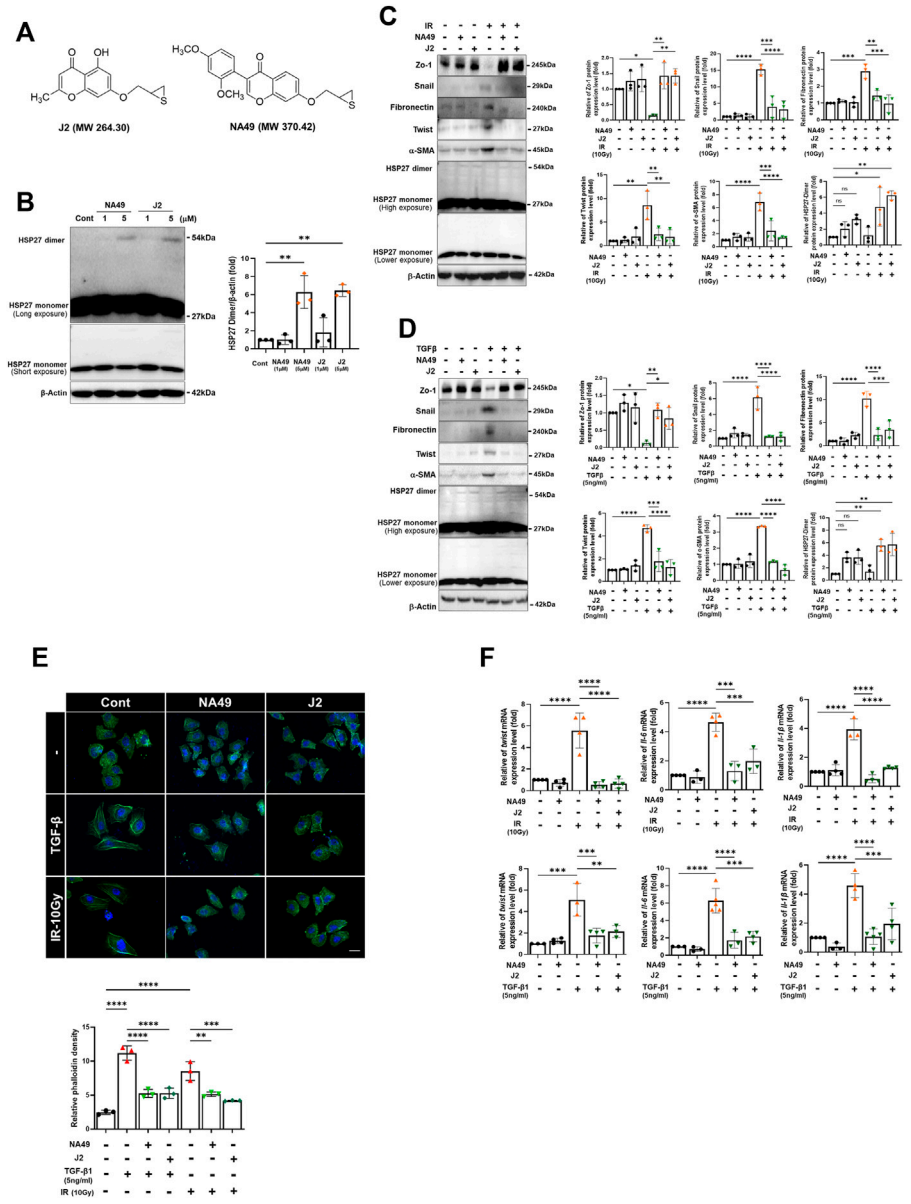

FIGURE 1
HSP27 cross-linker NA49 inhibits EMT in lung cell lines. **(A)** Chemical structures of NA49 and J2. **(B)** The protein expression levels after treatment of HSP27 cross-linkers NA49 and J2 (1 or 5 μM) for 9 h were verified by immunoblot analysis. The intensity band was quantified by ImageJ software, and the data were normalized to β-actin. **(C,D)** Immunoblot analysis using cell lysates of L132 cells at 24 and 48 h of 10 Gy irradiation (IR) or 5 ng/mL TGFβ treatment with or without NA49 and J2 (0.5 μM) pretreatment were performed. The intensity band was quantified by ImageJ software, and the data were normalized to β-actin. **(E)** L132 cells were pre-treated with 0.5 μM NA49 or J2 for 2 h and then exposed to IR of 10 Gy. At 48 h post-irradiation, the levels of phalloidin (green) and DAPI (blue) were evaluated using immunofluorescence staining. Magnification at ×400. **(F)** Cell lysate of L132 cells were irradiated with 10 Gy IR after pretreatment of NA49 or J2 (0.5 μM) and after 24 h, quantitative RT-PCR analysis was performed. Data are expressed as mean ±SEM; Scale bar: Magnification, ×400; Scale bar: 50 μm $*p < 0.05$ $**p < 0.01$ $***p < 0.001$ and $****p < 0.0001$ (p-valued by ANOVA).

more druggable compound, NA49 (Figure 1A). In comparison to J2, NA49 exhibited a superior pharmacokinetic profile and did not display any observable toxicity (Yoo et al., 2021). NA49 induced HSP27 cross-linking and abnormal dimerization in L132 lung epithelial cells (Figure 1B). The IC_{50} value of NA49 in cellular cytotoxicity was similar to that of J2 in L132 cells (J2; 17.8 ± 0.75 μM and NA49; 11.4 ± 0.42 μM) (Supplementary Figure S1A). IR and TGFβ-mediated EMT, which was represented by increased expression of Twist, Snail, Fibronectin and α-SMA, as well as decreased expression of Zo-1, was dramatically reversed by 3 h pretreatment with NA49 (Figures 1C, D). Because J2 was previously reported to inhibit IR-induced morphologic changes, as well as the expression of IL-6, IL-1β and Twist, which are involved in inhibition of IR-mediated PF (Kim et al., 2019), we tested these phenomena using NA49 after treatment with IR or TGFβ. The L132 cells had a round or polygonal shape and had very close cell–cell contact, while the treatment with IR or TGFβ caused the cells to undergo a transformation, adopting a spindle-shaped morphology reminiscent of cellular tight junctions. However, cells pretreated with NA49 showed

10.3389/fphar.2023.1203033

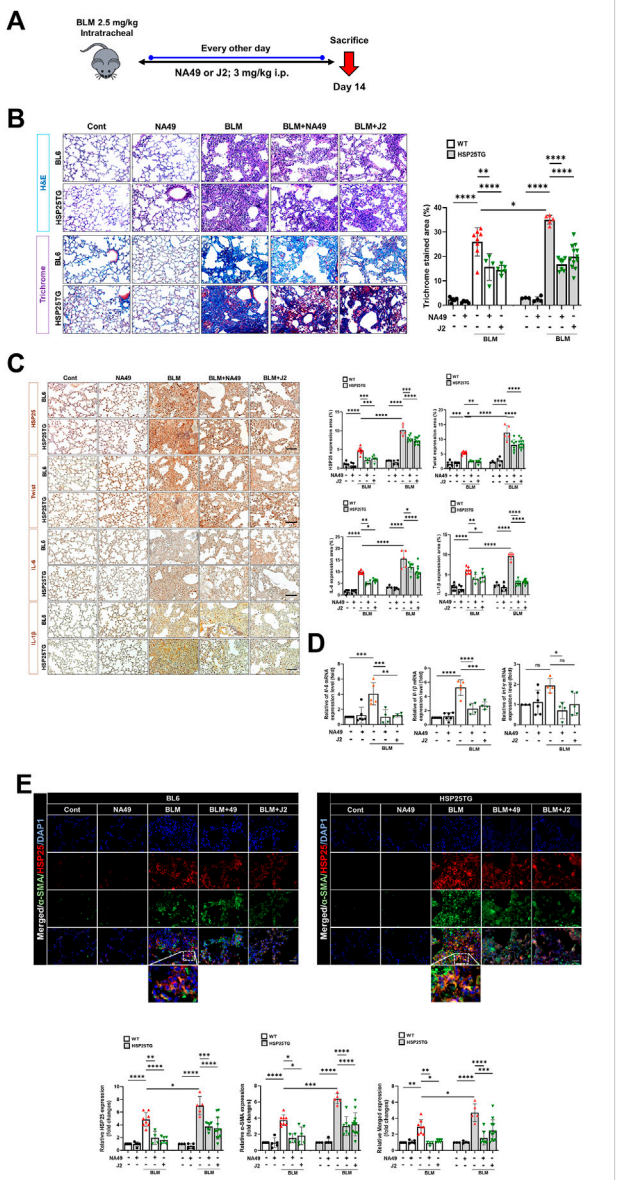

FIGURE 2
HSP27 cross linker NA49 attenuates BLM-induced in PF. NA49 and J2 (3 mg/kg) were intraperitoneally administered every other day after BLM treatment and lungs of BL6 and HSP25TG mice were harvested on day 14. **(A)** *In vivo* scheme of BLM-induced PF. **(B)** Represented images showed H&E and MT staining of lung tissue and **(C)** Immunostaining of HSP25, Twist, IL-6, and IL-1β. **(D)** BL6 mice were injected with BLM and additionally administered NA49 or J2. After 6 weeks of BLM treatment, lungs were analyzed for quantitative RT-PCR analysis. **(E)** Immunofluorescence (IF) staining was performed to identify the area co-stained with HSP25 (red) and α-SMA (green). Magnification, ×400. Quantitative analysis of staining intensity using ImageJ software. Data are expressed as mean ± SEM (n ≥ 3 per groups). **(B,C)** Bar plot of Trichrome area and protein area (%). *p < 0.05** p < 0.01 ***p < 0.001, and ****p < 0.0001 (p-valued by ANOVA). Magnification; ×200 (H&E and MT), ×400 (IF); Scale bar: 50 μm.

inhibition of these IR or TGFβ-induced morphologic features, and the restoration efficiency of morphology was similar in NA49 and J2 (Figure 1E). We next examined whether NA49 treatment modulated IR or TGFβ-induced *twist1*, *il-6*, and *il-1β* mRNAs. Quantitative RT-PCR analysis of L132 cells demonstrated that the upregulation of *twist1*, *il-6*, and *il-1β* genes induced by IR or TGFβ was effectively suppressed by NA49. The suppressive effect of NA49 was comparable to or even more potent than that of J2 (Figure 1F).

NA49 inhibited BLM-induced PF in mice

To elucidate whether NA49 can inhibit BLM-induced PF in mice, we compared the alterations in lung surface morphology between the control group and the group treated with BLMs. We also investigated the effects of NA49 on BLM-induced PF in HSP25TG mice. J2 was treated to compare the effects of NA49 (Figure 2A). The H&E staining data indicated that intraperitoneal administration of NA49 resulted in less tissue injury compared to mice treated with BLM alone. In the BLM group, there was a notable increase in alveolar infiltration of inflammatory cells and the formation of alveolar hyaline membranes, which was significantly higher compared to the control group. However, mice treated with NA49 showed a decrease in tissue damage. HSP25TG mice were also compared, and NA49 treatment reduced the inflammation scores. MT staining revealed a significant increase in collagen accumulation in the BLM-exposed group compared to the control group. However, treatment with NA49 effectively reversed the deposition of collagen. Two weeks following BLM treatment, the lungs exhibited ground-glass opacities and consolidation. In contrast, NA49-treated mice showed a reduction in these effects. The recovery effects for PF were similar between J2 and NA49 treated mice. We also compared the inhibitory effects of collagen deposition in HSP25TG mice. TG mice showed more aggravated lung injury grossly and histologically after BLM treatment than BL6 mice, which was also attenuated by NA49 treatment. Similar to BL6 mice, the inhibitory effects were similar in J2 or NA49 treated TG mice (Figure 2B). Immunohistochemical analysis revealed that HSP25 protein expression in lung tissues increased as PF progressed. The levels of IL-6, IL-1β and Twist, which were identified as genes modulated by J2 in BLM- or IR-induced PF (Kim et al., 2019) and were more prominent in HSP25TG mice, were also inhibited by NA49 treatment in both normal BL6 and HSP25TG mice with similar potency between J2 and NA49 (Figure 2C). The mRNA levels of *il-6*, *il-1β* and *twist* which were increased in BLM-induced lung tissues, were also declined by treatment of J2 or NA49 (Figure 2D). The co-localization of HSP25 and α-SMA was investigated, and the double-stained HSP27+/α-SMA+ area was increased in the BLM-induced PF model, and this portion was inhibited by the treatment with NA49. The amount of double-stained HSP27+/α-SMA+ after treatment with BLM was greater in HSP25TG mice than in normal BL6 mice, and NA49 also significantly inhibited this area with similar potency J2 (Figure 2E).

NA49 inhibited IR-induced PF in mice

We also investigated NA49 effects using another PF model, the IR-induced PF model (Figure 3A). Irradiated mice displayed a notable white, ring-like appearance in their lungs, which was partially restored

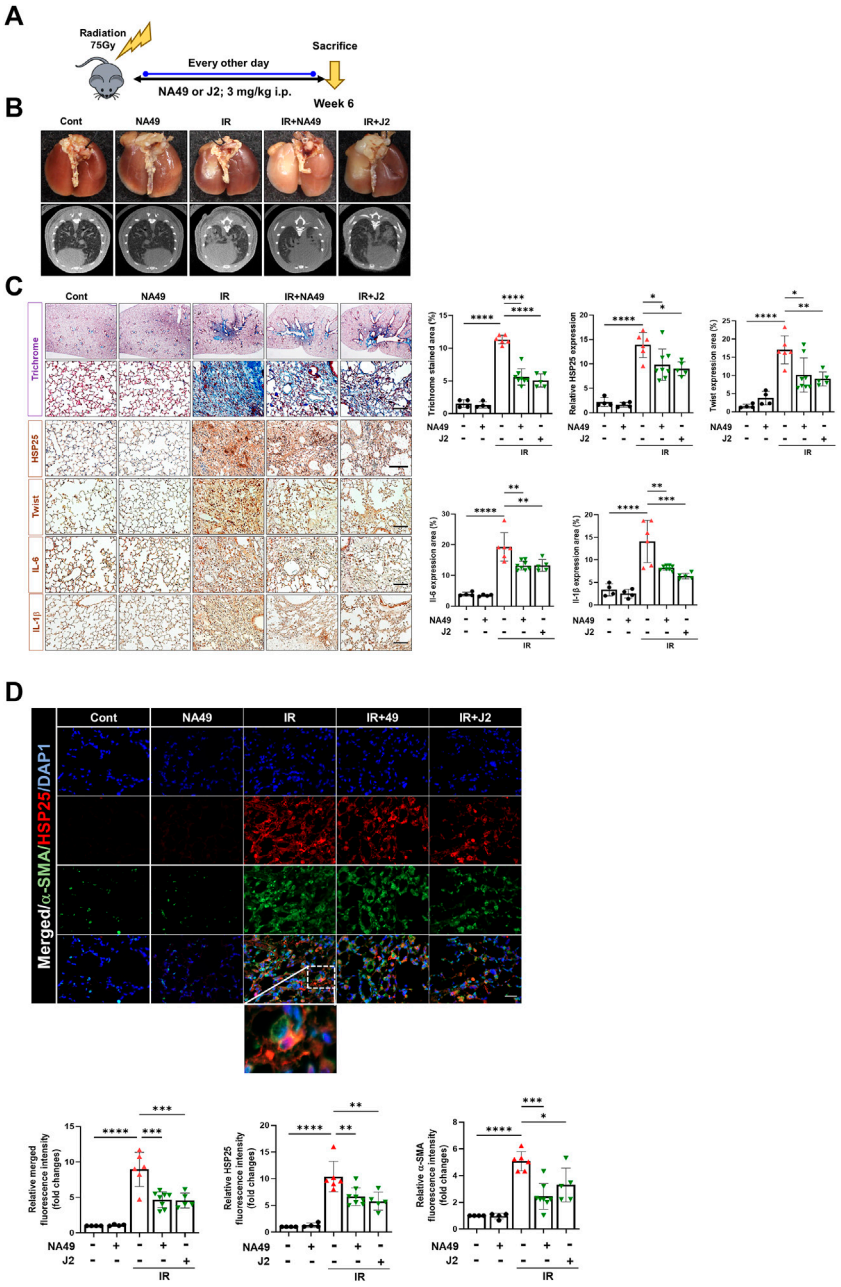

FIGURE 3
HSP25 cross linker NA49 attenuates IR-induced PF. NA49 and J2 (3 mg/kg) were intraperitoneally administered every other day after high dose radiation (75 Gy) and lungs were harvested on week 6. **(A)** *In vivo* scheme of IR-induced PF. **(B)** Lung was photographed after complete fixation, horizontal images acquired at 6 weeks after IR. **(C)** Represented images showed MT staining of lung tissue and immunostaining of HSP25, Twist, IL-6, and IL-1β. Bar plot of Trichrome area and protein area (%). **(D)** Immunofluorescence staining was performed to identify the area co-stained with HSP25 (red) and α-SMA (green). Magnification, ×400. Quantitative analysis of staining intensity using ImageJ software. Data are expressed as mean ± SEM (n ≥ 3 per groups); *$p < 0.05$ **, $p < 0.01$ ***$p < 0.001$ and ****$p < 0.0001$ (p-valued by ANOVA). Magnification; ×200 (H&E and MT), 400X (IF); Scale bar: 50 μm.

by the administration of NA49 treatment. Six weeks after IR, the typical micro-CT manifestations of lung injury were observed in the irradiated left lung. However, treatment with NA49 also mitigated these manifestations (Figure 3B). Infiltration of inflammatory cells in the alveolar region and the formation of hyaline membranes within the alveoli were significantly increased in the IR group compared to the control group. MT staining indicated that the IR group had much more collagen deposition than the control group, which was dramatically ameliorated by NA49 treatment. Immunohistochemical staining data also suggested that the increased expression of HSP27, Twist, IL-1β, and IL-6 was reduced by NA49 (Figure 3C). The co-localization of HSP25 and α-SMA was studied, and similar to the BLM-induced PF model, the double-stained HSP27+/-SMA+ region became more in the IR-induced PF model, and that region was considerably decreased by NA49 treatment (Figure 3D). The inhibition rate of PF by NA49 or J2 was almost similar.

10.3389/fphar.2023.1203033

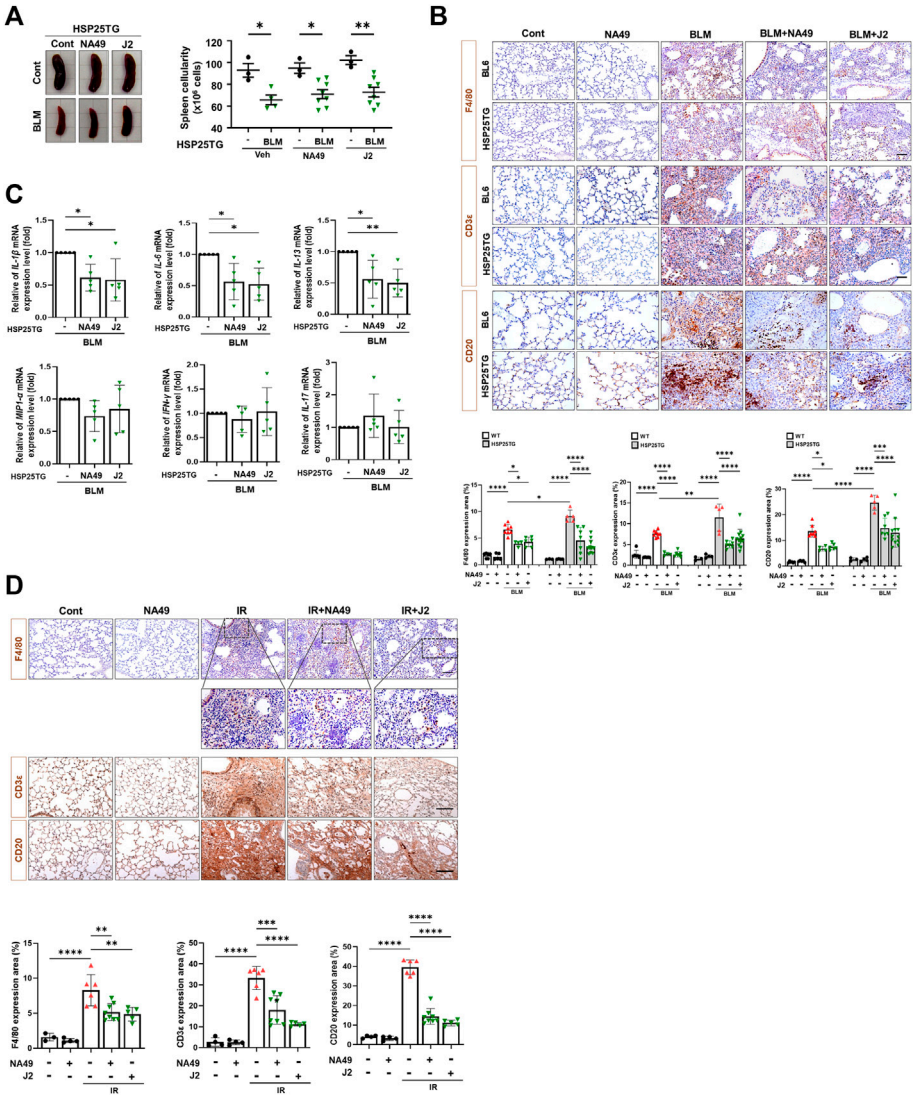

FIGURE 4
Attenuation of systemic and lung inflammation by NA49 in B6 and HSP25TG mice. **(A)** HSP25TG mice were injected with either PBS (veh, n = 3) or BLM together with Cont (n = 4), NA49 (n = 8) or J2 (n = 8). Spleen cellularity was determined by trypan blue exclusion assay. *p < 0.05. **(B)** Decreased pro-inflammatory cytokines by NA49 and J2 in BLM-treated HSP25TG mice. HSP25TG mice were injected with BLM and additionally administered Cont (n = 5), NA49 (n = 5) or J2 (n = 5) and spleen was obtained for the cytokine analysis. Relative cytokine gene expression was determined after normalization with actin level. *p < 0.05; **p < 0.005. Represented images showed immunostaining of CD3ε, CD20, and F4/80 in HSP25TG mice in BLM **(C)** or IR **(D)** induced fibrosis model (75 Gy). Quantitative analysis of staining intensity using ImageJ software. Bar plot of Protein area (%). Data are expressed as mean ± SEM (n ≥ 3 per groups); *p < 0.05 ** p < 0.01 ***p < 0.001 and ****p < 0.0001 (p-valued by ANOVA). Magnification, ×200; Scale bar: 50 μm.

NA49 reduced lung inflammation

Since HSP25 induction in lung tissue aggravates IR-induced lung fibrosis, and the elevated infiltration of macrophages, B cells, and T cells was significantly reduced by J2 treatment in HSP25TG mice (Oh et al., 2021), in this study, we aimed to investigate the effects of NA49 on immune cells from splenocytes after treatment of BLM in HSP25TG mice, comparing its efficacy with that of J2. BLM injection caused splenopathy in HSP25TG mice, as evidenced by decreased splenic cellularity (Figure 4A). Treatment with NA49 had no effect on splenic cellularity of HSP25TG mice in the case of untreated BLM mice. Since fibrosis is triggered and promoted by inflammatory cytokines, such as macrophage-associated IL-1β, IL-6, and MIP1α, Th2-related IL-13, and Th17 cell-derived IL-17, we examined the effects of NA49 on the production of inflammatory cytokines. Quantitative RT-PCR analysis revealed that NA49 significantly reduced the expression of pro-inflammatory cytokines IL-1β, IL-6, and IL-13 in HSP25TG mice. However, NA49 did not have an effect on the expression of MIP1α, IFN-γ, and IL-17 (Figure 4B). Next, we conducted an investigation to assess the effects of HSP27 inhibitors on airway inflammation induced by IR and BLM in control B6 WT and HSP25TG mice. Moreover, consistent with expectations, both BLM and IR led to an elevation in immune cell infiltration in the lungs of WT mice. Moreover,

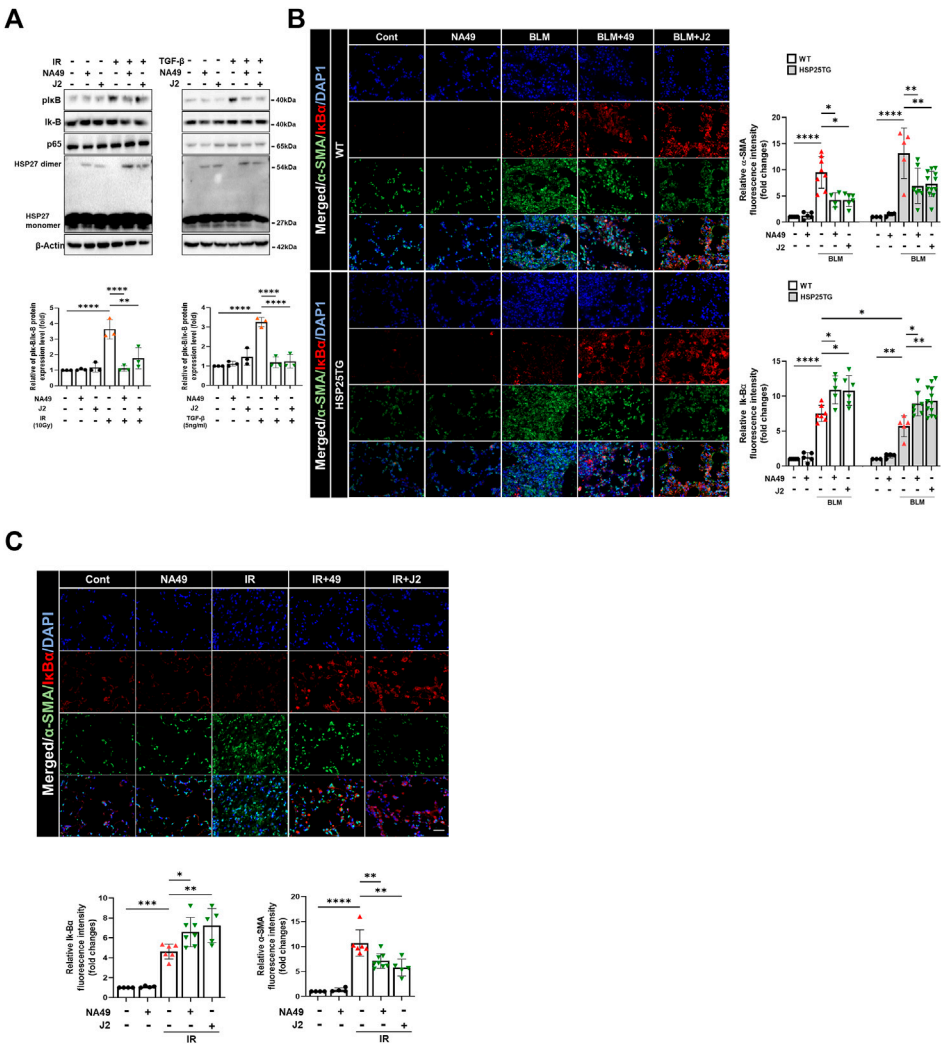

FIGURE 5
NA49 inhibits NFκB pathway in lung cell line. **(A)** Using L132 cells, the protein expression levels after 3 h treatment of 10 Gy irradiation (IR) or 5 ng/mL TGFβ with or without NA49 and J2 (0.5 μM) pretreatment were verified by immunoblot analysis. The intensity band was quantified by ImageJ software, and the data were normalized to β-actin. **(B, C)** Immunofluorescence staining was performed to identify the area co-stained with IkB (red) and α-SMA (green). Magnification, ×400; Scale bar: 50 μm. Quantitative analysis of staining intensity using ImageJ software. Data are expressed as mean ± SEM (n ≥3 per groups); *$p < 0.05$ **, $p < 0.01$ ***$p < 0.001$ and ****$p < 0.0001$ (p-valued by ANOVA).

immune cell infiltration was notably intensified in the lungs of HSP25TG mice. NA49 injection significantly reduced the infiltration of macrophages (F4/80 positive), T cells (CD3ε positive), and B cells (CD20 positive) stimulated by BLM or IR treatment in both WT and HSP25TG mice (Figures 4C, D). These findings indicate that NA49 has immunomodulatory action similar to J2 and may similarly contribute to the prevention of PF through the reduction of pro-inflammatory cytokines, which is mediated via immune cell regulation.

NA49 inhibited HSP27-mediated NFkB activation

A latest study revealed that focused irradiation upregulated *twist1*, *il-6*, and *il-1β* genes through NFkB activation via HSP27 overexpression, while J2 reversed these effects (Kim et al., 2019). Therefore, we investigated whether NA49 can also inhibit BLM- or IR-mediated NFkB activation, which is represented by the inhibition of IkBα phosphorylation. After 3 h of IR or TGFβ1 treatment in L132 cells, NA49 dramatically inhibited IkBα phosphorylation (Figure 5A). Furthermore, NFkB activation in the fibrotic region of the BLM or IR-induced PF mouse model, as reflected by IkBα degradation, was greater in HSP25TG mice, and these phenomena were reduced by NA49 treatment when detected by immunofluorescence analysis (Figure 5B), indicating that IkBα expression was lower in fibrotic lungs compared to control mice and NA49 treatment increased the intensity of IkBα fluorescence. NA49 also showed similar effects in the case of IR-induced PF model (Figure 5C). The inhibition rate of NFkB activation by NA49 or J2 was almost similar.

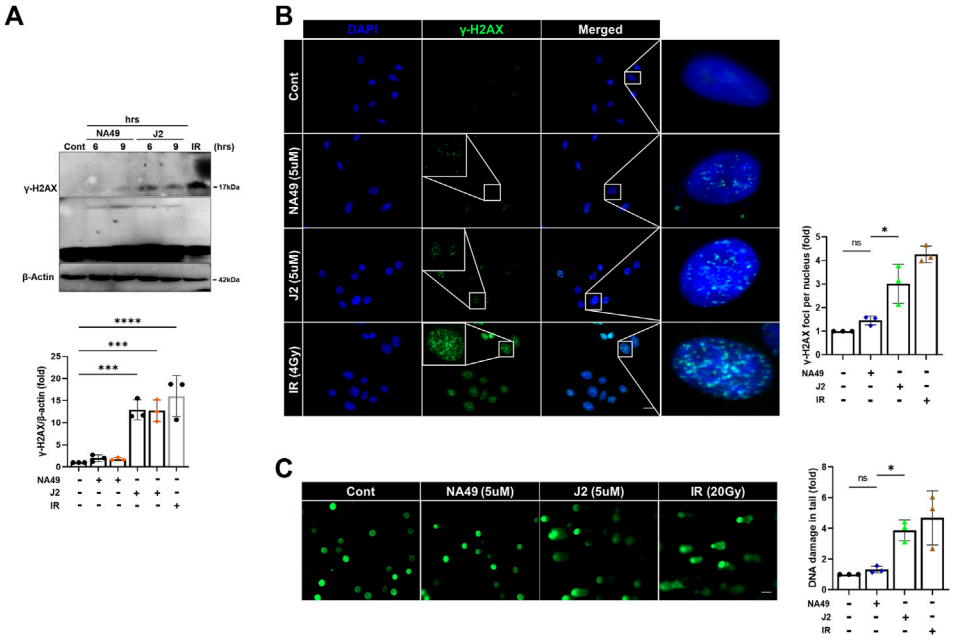

FIGURE 6
NA49 does not induce DNA damage toxicity, unlike J2. **(A)** L132 cells were treated with 6 and 9 h of 5 μM NA49 or J2 and protein expression was verified using immunoblots. IR (1 Gy) was used as a positive control. The intensity band was quantified by ImageJ software, and the data were normalized to β-actin. **(B)** L132 cells were treated with 5 μM NA49 or J2 for 1 h. Immunofluorescence staining was performed to identify the area co-stained with DAPI (blue) and γ-H2AX (green). IR 4 Gy was also applied. γ-H2AX foci number was quantified using ImageJ software. **(C)** L132 cells were treated with 5 μM NA49 or J2 for 24 h, and the alkaline comet assay was conducted, and representative photos are included. IR 20 Gy was used as a positive control. The olive tail moment was determined using Comet 5.5 software. The data represent the mean ± SD. Magnification: ×5; Scale bar: 50 μm. **(C)** Data are expressed as mean ±SEM; Scale bar: Magnification, ×400; Scale bar: 50 μm $*p < 0.05$ $**p < 0.01$ $***p < 0.001$ and $****p < 0.0001$ (p-valued by ANOVA).

NA49 showed less DNA stand break damage than J2

Due to the limited solubility and short *in vivo* circulation time of J2, NA49 was developed as a more druggable compound. NA49 exhibits a superior pharmacokinetic profile compared to J2, showing improved characteristics such as enhanced bioavailability, longer circulation time, and negligible toxicity (Yoo et al., 2021). Furthermore, the exposure to J2 at a concentration of 40 μg/plate for 48 h led to a significant increase in bacterial reverse mutation in the Ames test, utilizing *Salmonella typhimurium* strains TA98 and TA100, compared to the control vehicle group. In contrast, treatment with 200 μg/plate of NA49 for 48 h did not show a significant increase in the number of relevant colonies (Yoo et al., 2021). Therefore, to elucidate whether NA49 or J2 also differentially affect DNA strand break damage, we examined γ-H2AX expression and comet tail moments. J2 increased γ-H2AX expression at a concentration of 5 μM; however, in the case of NA49, γ-H2AX induction was not observed at the same concentration (Figure 6A). Immunofluorescence of γ-H2AX foci, an indicator of the DNA strand breaks, also suggested that NA49 only slightly, but no significantly induced γ-H2AX foci in the cells, while J2 dramatically induced γ-H2AX foci. The nucleus was stained with DAPI (blue) (Figure 6B). Similarly, alkaline comet tail moments were significantly induced by J2 treatment; however, NA49 did not show any significant induction of comet tail moments (Figure 6C). IR exposure to the cells was used as a positive control.

Discussion

In this study, we proposed NA49, a small molecule HSP27 inhibitor, as a potential therapeutic agent for PF. NA49, which shares a structural similarity with the chromenone compound J2, exhibited comparable levels of altered HSP27 cross-linking as J2. However, NA49 demonstrated improved druggability and comparable potency for PF, along with superior toxicity profiles, making it a promising candidate for further development. Moreover, unlike J2, NA49 did not show any DNA strand break damage at the same concentration.

Previously, we have demonstrated the novel mechanisms of HSP27 in the development of PF and proposed HSP27 as a potential therapeutic target for treating PF. We observed HSP27 upregulation during the development of PF. Additional evidence of HSP27 overexpression in PF comes from proteomics studies, which have shown the upregulation of HSP27 in lung fibroblast cell lines following treatment with TGFβ1 (Malmström et al., 2004) and in IPF lung tissues (Kim et al., 2019). Recent studies have reported the successful mitigation of BLM-induced

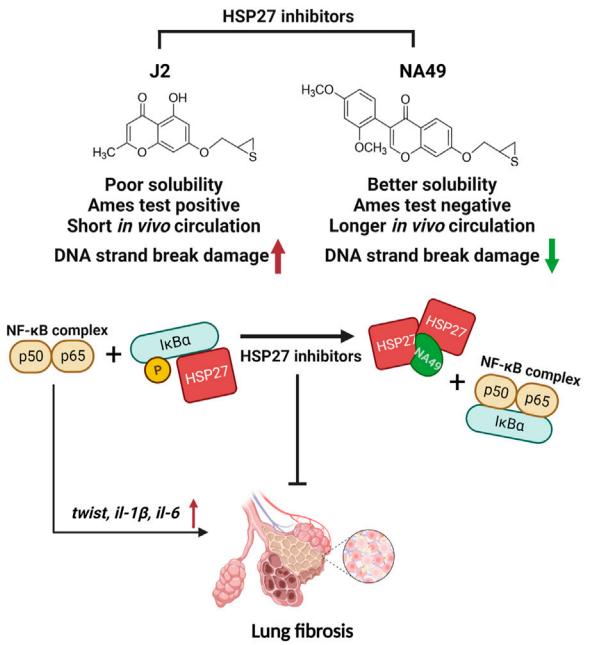

FIGURE 7
The graphic illustration of the pathway of NA49 protecting against PF. NA49, a small molecule HSP27 inhibitor, induces the abnormal dimerization of HSP27 and maintains the binding of NF-kB and IkBα, thereby effectively inhibiting the transcriptional activity of NF-kB, which provides the evidence for the alleviation of PF. NA49 exhibiting higher solubility than J2 and negative results in the AMES test while also displaying improved pharmacokinetic parameters, shows relatively lower DNA strand break damage. Figure 7 was created with BioRender.com accessed on 8 June 2023.

PF in mice through the administration of HSP27 siRNAs via the airway by downregulation of myofibroblast-related proteins, including fibronectin and type 1 collagen (Park et al., 2016). In addition, the effectiveness of HSP27 antisense oligonucleotide in suppressing subpleural fibrosis induced by adenovirus-expressing TGFβ1 in rats has been demonstrated. Furthermore, HSP27 has been found to prevent Snail degradation through the proteasomal system (Hagiwara et al., 2007). Elevated HSP27 levels have been found to exacerbate NF-κB signaling pathways, leading to increased EMT. However, the use of HSP27 inhibitors, such as J2, has been shown to effectively prevent PF during the inflammation or EMT. We also looked at the impact of delaying J2 medication till late in the fibrosis process (Jeon et al., 2023). Therefore, HSP27 inhibition at EMT stage is likely to give a useful medical care option for PF, which presently has few viable treatment alternatives.

PF is a progressive fibrotic disease with pathophysiological characteristics of TGFβ and reactive oxygen species-induced excessive EMT and ECM deposition. Several research studies have highlighted the involvement of various types of cells, such as epithelial cells, macrophages, and fibroblasts, in the progression of PF (Wynn, 2011). According to current understanding, it is widely believed that epithelial cells contribute to the formation of myofibroblasts through the process of EMT (Radisky et al., 2007). EMT has the capability to trigger transcription factors, release cell surface proteins and cytokines associated with fibrosis, and enhance the accumulation of EMT (Di Gregorio et al., 2020). The conversion of fibroblasts into myofibroblasts is a key characteristic of fibrotic conditions, resulting in the excessive production and accumulation of ECM components such as collagen, fibronectin, and elastin (Sun, 2021). Therefore, the inhibition of EMT, inflammatory cascade activation, and fibroblast stimulation emerge as potential strategies for mitigating PF (Kendall and Feghali-Bostwick, 2014).

Another important inhibitory mechanism of HSP27 on IR- or BLM-induced PF was due to the modulation of inflammatory immune systems. HSP27 is implicated in the infiltration and activation of macrophages, B cells, and T cells, which potentiated the inflammatory cytokine production (Oh et al., 2021). Although relationship between immune cell modulation and EMT process by HSP27 is not known exactly, it is clear that PF is improved by various complex mechanisms by HSP27 inhibition by a drug like compound, NA49.

Despite the fact that presently authorized IPF treatments, such as PFD and NTD, are clinically accessible, there are certain limits in terms of side effects and efficacy. As a result, an alternative method is required to meet the unmet therapeutic need for PF, and the discovery and clinical use of novel HSP27 inhibitors will provide an additional therapeutic option for overcoming IPF. However, unlike HSP90 and HSP70, HSP27 does not have an active site or an ATP-binding pocket. As a result, only two HSP27 inhibitors are currently in clinical studies. Nevertheless, the restricted intracellular delivery of OGX427 is attributed to its small molecular size and the lack of a mechanism targeting HSP27 specifically in the case of RP101 (Bartis et al., 2014). Apart from RP101, there have been no other small molecules developed as inhibitors of HSP27, and the existing clinical trial data for RP101 is not promising. While approved treatments like PFD and NTD are currently available for PF, there is a pressing need for an alternative approach to address the unmet therapeutic requirements of PF.

Previously, small molecule HSP27 inhibitors, such as ZER, SW15, and J2, have been shown to induce the formation of abnormal HSP27 dimers, were developed, and J2 showed inhibition of PF in various mouse models (Kim et al., 2019; Yoo et al., 2021; Jeon et al., 2023). A drug's chemical structure impacts its physicochemical properties of a drug are directly influenced by its chemical structure, and these properties, in turn, impact the drug's ADME/Tox characteristics, ultimately determining its pharmacological effectiveness. Therefore, our focus was on creating drug-like molecules with potentially favorable ADME/Tox properties. In pursuit of this objective, we conducted studies using J2, an effective HSP27 cross linker that is a synthetic chromenone derivative. However, J2 exhibits limitations such as poor solubility and a short *in vivo* circulation time, and positive Ames test results, we aimed to identify more druggable compounds that exhibit similar or superior efficacy to J2. Among these compounds, NA49, which is also a chromenone compound, demonstrated the desired effects. NA49 exhibited comparable levels of HSP27 cross-linking to J2. NA49 demonstrates lower toxicity and a superior pharmacokinetic profile in comparison to J2, even without mutation toxicity (Yoo et al., 2021), and showed similar effects on PF inhibition induced by BLM or IR. Moreover, NA49 did not show a DNA strand break in normal lung epithelial cells, unlike J2 (Figure 7).

In summary, our data demonstrate that a druggable HSP27 inhibitor with minimal toxicity, NA49 efficiently ameliorates PF progression by suppressing EMT and

inflammation. Our study indicates that NA49 may serve as a clinically available drug for the treatment of PF.

Data availability statement

The original contributions presented in the study are included in the article/Supplementary Material, further inquiries can be directed to the corresponding author.

Ethics statement

The animal study was reviewed and approved by Committee of Ewha Womans University (IACUC 18-064). Written informed consent was obtained from the owners for the participation of their animals in this study.

Author contributions

Y-SL conceived the study concept, experimental design and supervision. YY, HW, MJ, and YC carried out the experiments and analyzed data. SJ and HJ conceived the experimental design. YN synthesized the small molecules. EH and JC provide intellectual input, edited the manuscript and performed the data analysis. All authors reviewed and edited the manuscript. All authors contributed to the article and approved the submitted version.

Funding

This work was supported by a grant from the National Research Foundation of Korea (NRF) grants (NRF-2018R1A5A2025286 and 2020M2D9A2093974), funded by the Korean government (Ministry of Science and ICT).

Conflict of interest

The authors declare that the research was conducted in the absence of any commercial or financial relationships that could be construed as a potential conflict of interest.

Publisher's note

All claims expressed in this article are solely those of the authors and do not necessarily represent those of their affiliated organizations, or those of the publisher, the editors and the reviewers. Any product that may be evaluated in this article, or claim that may be made by its manufacturer, is not guaranteed or endorsed by the publisher.

Supplementary material

The Supplementary Material for this article can be found online at: https://www.frontiersin.org/articles/10.3389/fphar.2023.1203033/full#supplementary-material

References

Bartis, D., Mise, N., Mahida, R. Y., Eickelberg, O., and Thickett, D. R. (2014). Epithelial-mesenchymal transition in lung development and disease: Does it exist and is it important? *Thorax* 69, 760–765. doi:10.1136/thoraxjnl-2013-204608

Carter, N. J. (2011). Pirfenidone: In idiopathic pulmonary fibrosis. *Drugs* 71, 1721–1732. doi:10.2165/11207710-000000000-00000

Choi, B., Choi, S. K., Park, Y. N., Kwak, S. Y., Lee, H. J., Kwon, Y., et al. (2017). Sensitization of lung cancer cells by altered dimerization of HSP27. *Oncotarget* 8, 105372–105382. doi:10.18632/oncotarget.22192

Di Gregorio, J., Robuffo, I., Spalletta, S., Giambuzzi, G., De Iuliis, V., Toniato, E., et al. (2020). The epithelial-to-mesenchymal transition as a possible therapeutic target in fibrotic disorders. *Front. Cell Dev. Biol.* 8, 607483. doi:10.3389/fcell.2020.607483

Ferns, G., Shams, S., and Shafi, S. (2006). Heat shock protein 27: Its potential role in vascular disease. *Int. J. Exp. Pathol.* 87, 253–274. doi:10.1111/j.1365-2613.2006.00484.x

Hagiwara, S., Iwasaka, H., Matsumoto, S., and Noguchi, T. (2007). Antisense oligonucleotide inhibition of heat shock protein (HSP) 47 improves bleomycin-induced pulmonary fibrosis in rats. *Respir. Res.* 8, 37. doi:10.1186/1465-9921-8-37

Hill, C., Jones, M. G., Davies, D. E., and Wang, Y. (2019). Epithelial-mesenchymal transition contributes to pulmonary fibrosis via aberrant epithelial/fibroblastic cross-talk. *J. Lung Health Dis.* 3, 31–35. doi:10.29245/2689-999x/2019/2.1149

Hwang, S. Y., Kwak, S. Y., Kwon, Y., Lee, Y. S., and Na, Y. (2017). Synthesis and biological effect of chrom-4-one derivatives as functional inhibitors of heat shock protein 27. *Eur. J. Med. Chem.* 139, 892–900. doi:10.1016/j.ejmech.2017.08.065

Inomata, M., Kamio, K., Azuma, A., Matsuda, K., Kokuho, N., Miura, Y., et al. (2014). Pirfenidone inhibits fibrocyte accumulation in the lungs in bleomycin-induced murine pulmonary fibrosis. *Respir. Res.* 15, 16. doi:10.1186/1465-9921-15-16

Iyer, S. N., Gurujeyalakshmi, G., and Giri, S. N. (1999a). Effects of pirfenidone on procollagen gene expression at the transcriptional level in bleomycin hamster model of lung fibrosis. *J. Pharmacol. Exp. Ther.* 289, 211–218.

Iyer, S. N., Gurujeyalakshmi, G., and Giri, S. N. (1999b). Effects of pirfenidone on transforming growth factor-beta gene expression at the transcriptional level in bleomycin hamster model of lung fibrosis. *J. Pharmacol. Exp. Ther.* 291, 367–373.

Jeon, S., Jin, H., Kim, J.-M., Hur, Y., Song, E. J., Lee, Y.-J., et al. (2023). The miR-15b-Smurf2-HSP27 axis promotes pulmonary fibrosis. *J. Biomed. Sci.* 30, 2. doi:10.1186/s12929-023-00896-5

Jin, H., Jeon, S., Kang, G. Y., Lee, H. J., Cho, J., and Lee, Y. S. (2017). Identification of radiation response genes and proteins from mouse pulmonary tissues after high-dose per fraction irradiation of limited lung volumes. *Int. J. Radiat. Biol.* 93, 184–193. doi:10.1080/09553002.2017.1235297

Kendall, R. T., and Feghali-Bostwick, C. A. (2014). Fibroblasts in fibrosis: Novel roles and mediators. *Front. Pharmacol.* 5, 123. doi:10.3389/fphar.2014.00123

Kim, J. H., Jung, Y. J., Choi, B., Lee, N. L., Lee, H. J., Kwak, S. Y., et al. (2016). Overcoming HSP27-mediated resistance by altered dimerization of HSP27 using small molecules. *Oncotarget* 7, 53178–53190. doi:10.18632/oncotarget.10629

Kim, J. Y., Jeon, S., Yoo, Y. J., Jin, H., Won, H. Y., Yoon, K., et al. (2019). The hsp27-mediated IkBα-nf?b signaling Axis promotes radiation-induced lung fibrosis. *Clin. Cancer Res.* 25, 5364–5375. doi:10.1158/1078-0432.CCR-18-3900

Kim, J. Y., Shin, D., Lee, G., Kim, J. M., Kim, D., An, Y. M., et al. (2017). Standardized herbal formula PM014 inhibits radiation-induced pulmonary inflammation in mice. *Sci. Rep.* 7, 45001. doi:10.1038/srep45001

Malmström, J., Lindberg, H., Lindberg, C., Bratt, C., Wieslander, E., Delander, E. L., et al. (2004). Transforming growth factor-beta 1 specifically induce proteins involved in the myofibroblast contractile apparatus. *Mol. Cell Proteomics* 3, 466–477. doi:10.1074/mcp.M300108-MCP200

Myllärniemi, M., and Kaarteenaho, R. (2015). Pharmacological treatment of idiopathic pulmonary fibrosis - preclinical and clinical studies of pirfenidone, nintedanib, and N-acetylcysteine. *Eur. Clin. Respir. J.* 2, 26385. doi:10.3402/ecrj.v2.26385

Oh, A., Jeon, S., Jeong, M. G., Kim, H. K., Kang, J., Lee, Y. S., et al. (2021). HSPB1 inhibitor J2 attenuates lung inflammation through direct modulation of Ym1 production and paracrine signaling. *Biomed. Pharmacother.* 143, 112225. doi:10.1016/j.biopha.2021.112225

Oku, H., Shimizu, T., Kawabata, T., Nagira, M., Hikita, I., Ueyama, A., et al. (2008). Antifibrotic action of pirfenidone and prednisolone: Different effects on pulmonary

cytokines and growth factors in bleomycin-induced murine pulmonary fibrosis. *Eur. J. Pharmacol.* 590, 400–408. doi:10.1016/j.ejphar.2008.06.046

Park, A. M., Kanai, K., Itoh, T., Sato, T., Tsukui, T., Inagaki, Y., et al. (2016). Heat shock protein 27 plays a pivotal role in myofibroblast differentiation and in the development of bleomycin-induced pulmonary fibrosis. *PLoS One* 11, e0148998. doi:10.1371/journal.pone.0148998

Radisky, D. C., Kenny, P. A., and Bissell, M. J. (2007). Fibrosis and cancer: Do myofibroblasts come also from epithelial cells via EMT? *J. Cell Biochem.* 101, 830–839. doi:10.1002/jcb.21186

Raghu, G., Weycker, D., Edelsberg, J., Bradford, W. Z., and Oster, G. (2006). Incidence and prevalence of idiopathic pulmonary fibrosis. *Am. J. Respir. Crit. Care Med.* 174, 810–816. doi:10.1164/rccm.200602-163OC

Richeldi, L., Du Bois, R. M., Raghu, G., Azuma, A., Brown, K. K., Costabel, U., et al. (2014). Efficacy and safety of nintedanib in idiopathic pulmonary fibrosis. *N. Engl. J. Med.* 370, 2071–2082. doi:10.1056/NEJMoa1402584

Roth, G. J., Binder, R., Colbatzky, F., Dallinger, C., Schlenker-Herceg, R., Hilberg, F., et al. (2015). Nintedanib: From discovery to the clinic. *J. Med. Chem.* 58, 1053–1063. doi:10.1021/jm501562a

Shiota, M., Bishop, J. L., Nip, K. M., Zardan, A., Takeuchi, A., Cordonnier, T., et al. (2013). Hsp27 regulates epithelial mesenchymal transition, metastasis, and circulating tumor cells in prostate cancer. *Cancer Res.* 73, 3109–3119. doi:10.1158/0008-5472.CAN-12-3979

Sun, B. (2021). The mechanics of fibrillar collagen extracellular matrix. *Cell Rep. Phys. Sci.* 2, 100515. doi:10.1016/j.xcrp.2021.100515

Westergren-Thorsson, G., Hernnäs, J., Särnstrand, B., Oldberg, A., Heinegård, D., and Malmström, A. (1993). Altered expression of small proteoglycans, collagen, and transforming growth factor-beta 1 in developing bleomycin-induced pulmonary fibrosis in rats. *J. Clin. Invest.* 92, 632–637. doi:10.1172/JCI116631

Wettstein, G., Bellaye, P. S., Kolb, M., Hammann, A., Crestani, B., Soler, P., et al. (2013). Inhibition of HSP27 blocks fibrosis development and EMT features by promoting Snail degradation. *Faseb J.* 27, 1549–1560. doi:10.1096/fj.12-220053

White, E. S., and Mantovani, A. R. (2013). Inflammation, wound repair, and fibrosis: Reassessing the spectrum of tissue injury and resolution. *J. Pathol.* 229, 141–144. doi:10.1002/path.4126

Wilson, M. S., and Wynn, T. A. (2009). Pulmonary fibrosis: Pathogenesis, etiology and regulation. *Mucosal Immunol.* 2, 103–121. doi:10.1038/mi.2008.85

Wynn, T. A. (2011). Integrating mechanisms of pulmonary fibrosis. *J. Exp. Med.* 208, 1339–1350. doi:10.1084/jem.20110551

Yoo, H., Choi, S. K., Lee, J., Park, S. H., Park, Y. N., Hwang, S. Y., et al. (2021). Drug-like small molecule HSP27 functional inhibitor sensitizes lung cancer cells to gefitinib or cisplatin by inducing altered cross-linked Hsp27 dimers. *Pharmaceutics* 13, 630. doi:10.3390/pharmaceutics13050630

frontiers | Frontiers in Pharmacology

TYPE Review
PUBLISHED 07 August 2023
DOI 10.3389/fphar.2023.1205948

OPEN ACCESS

EDITED BY
Haiyang Tang,
University of Arizona, United States

REVIEWED BY
Timothy N. Perkins,
University of Pittsburgh, United States
Xiang Tong,
Sichuan University, China

*CORRESPONDENCE
Yulan Zeng,
1989LY0551@hust.edu.cn

RECEIVED 14 April 2023
ACCEPTED 28 July 2023
PUBLISHED 07 August 2023

CITATION
Guo H, Sun J, Zhang S, Nie Y, Zhou S and Zeng Y (2023), Progress in understanding and treating idiopathic pulmonary fibrosis: recent insights and emerging therapies.
Front. Pharmacol. 14:1205948.
doi: 10.3389/fphar.2023.1205948

Progress in understanding and treating idiopathic pulmonary fibrosis: recent insights and emerging therapies

Hehua Guo, Jiazheng Sun, Siyu Zhang, Yalan Nie, Sirui Zhou and Yulan Zeng*

Department of Respiratory Medicine, Liyuan Hospital, Tongji Medical College, Huazhong University of Science and Technology, Wuhan, China

Idiopathic pulmonary fibrosis (IPF) is a long-lasting, continuously advancing, and irrevocable interstitial lung disorder with an obscure origin and inadequately comprehended pathological mechanisms. Despite the intricate and uncharted causes and pathways of IPF, the scholarly consensus upholds that the transformation of fibroblasts into myofibroblasts—instigated by injury to the alveolar epithelial cells—and the disproportionate accumulation of extracellular matrix (ECM) components, such as collagen, are integral to IPF's progression. The introduction of two novel anti-fibrotic medications, pirfenidone and nintedanib, have exhibited efficacy in decelerating the ongoing degradation of lung function, lessening hospitalization risk, and postponing exacerbations among IPF patients. Nonetheless, these pharmacological interventions do not present a definitive solution to IPF, positioning lung transplantation as the solitary potential curative measure in contemporary medical practice. A host of innovative therapeutic strategies are presently under rigorous scrutiny. This comprehensive review encapsulates the recent advancements in IPF research, spanning from diagnosis and etiology to pathological mechanisms, and introduces a discussion on nascent therapeutic methodologies currently in the pipeline.

KEYWORDS

idiopathic pulmonary fibrosis, etiology, pathogenesis, treatment, progress

1 Introduction

Idiopathic pulmonary fibrosis (IPF) is a pervasive chronic pulmonary ailment marked by irreversible lung function loss and structural disfigurement attributable to an overproduction of extracellular matrix deposition (Mei et al., 2021), compounded by progressive scarring of lung tissue and interstitial lung disease (Qian et al., 2021). The disease is predominantly observed in middle-aged to elderly men, and its global prevalence is estimated to exceed 3 million people, with an annual incidence rate between 2 and 9 per 100,000 individuals and an escalating trend (He et al., 2021a). The mean survival time post-diagnosis is a mere 3–5 years (Lambert et al., 2021), and clinically, IPF is associated with dyspnea, a relentless decline in lung function, a dismal prognosis, and disease trajectories that span from gradual deterioration to swift collapse, culminating in mortality due to respiratory failure (Zhang et al., 2022).

The exact origins and progression mechanisms of IPF remain ambiguous, with aging recognized as the most considerable risk factor (Roque et al., 2020a). Additional contributing factors include genetics, environmental exposure, smoking habits, viral infections, gastroesophageal reflux disease, and fibrogenesis, all playing roles in IPF manifestation (Mostafaei et al., 2021). Therapeutic interventions are currently limited, with only two FDA-endorsed pharmaceuticals in the United States, namely, pirfenidone and nintedanib (Shenderov et al., 2021). While both drugs mitigate the pace of IPF progression and lung function degradation, they fall short of reversing the lung damage inflicted by the disease (Ma et al., 2022). Pirfenidone, a small molecule pyridine, possesses anti-fibrotic, anti-inflammatory, and antioxidant properties (Aimo et al., 2020), acting to inhibit fibrotic processes via the suppression of the cytokine TGF-β (Petnak et al., 2021). Nintedanib is a small molecule tyrosine kinase inhibitor that targets receptors, leading to a broad inhibition of downstream signaling pathways in fibroblasts and myofibroblasts (Wind et al., 2019). Both drugs function to curb fibroblast proliferation, obstruct collagen production, and diminish fibrogenic mediator production (Tanaka et al., 2022).

Presently, lung transplantation stands as the sole clinically validated effective treatment strategy (Han et al., 2022), yet it is encumbered by high costs, a dearth of compatible donors, and post-operative rejection risks, significantly constraining its clinical utility. The principal objective of IPF management is to alleviate symptoms, enhance patient health and quality of life, and maintain lung function as a means to extend survival (Olson et al., 2018). The importance of a profound comprehension of IPF's etiology and pathogenesis for early diagnosis and efficacious treatment has been underscored through long-term clinical practice. The past two decades have witnessed significant strides in basic and clinical research on IPF, both domestically and internationally. This review is intended to compile and present the advancements in understanding the etiology, pathogenesis, and therapeutic approaches of idiopathic pulmonary fibrosis.

2 Etiology

2.1 Genetic

Genetic constituents serve as fundamental drivers in the initiation and evolution of IPF (Ballester et al., 2019). A growing body of evidence indicates that susceptibility to IPF is linked to a complex interplay of genetic variations and alterations in transcriptional activity (Wolters et al., 2018). Mutations in the mucin 5B gene have emerged as one of the most influential risk factors for IPF (Wang et al., 2022). A pivotal study unveiled a prevalent single nucleotide polymorphism in the promoter domain of the MUC5B gene on chromosome 11 (Stainer et al., 2021), predominantly associated with pulmonary fibrosis (Biondini et al., 2021). Telomeres, non-coding, repetitive nucleotide sequences situated at chromosome extremities, shield chromosomes from progressive attrition during typical cellular replication (Drakopanagiotakis et al., 2018). Rare aberrations in genes associated with telomere homeostasis have been strongly implicated in pulmonary fibrosis (Wells et al., 2018). It has been observed that nearly all sporadic IPF patients present shortened telomeres in alveolar epithelial cells (Sgalla et al., 2018). Furthermore, both acute and chronic fibrotic lung diseases transpire in patients with mutations in pulmonary surfactant apolipoprotein and lipid transporter (Plantier et al., 2018), insinuating a significant role of surfactant composition or metabolic alterations in IPF.

2.2 Environmental exposure

Frequently, particulate matter, fibers, and dust constitute the primary environmental contributors to IPF onset (Phan et al., 2021). A noteworthy surge in IPF incidence is observable among individuals with exposure to animal dust, chemical fumes, metal dust (including lead and steel), and other pollutants (Walters, 2020). These contaminants are identified as precipitators of oxidative stress, epithelial damage, and airway inflammation (Sack and Raghu, 2019). Studies suggest that air pollution may incite epigenetic modifications in the lung, enhancing pathogenicity in synergy with other antigens (Park et al., 2021), and potentially initiating or fostering disruptions in alveolar damage and repair mechanisms. Post-mortem examinations of IPF patients have detected inorganic particles in lung lymph nodes (Collins et al., 2018), further corroborating the environmental exposure etiology.

2.3 Lung microbiota

Recent investigations underscore the crucial role of microbiota in inciting and exacerbating pulmonary fibrosis in animal models, thereby elucidating the association between microbiota and pulmonary fibrosis (Spagnolo et al., 2019). Contemporary characterizations of the respiratory microbiota in IPF suggest that an escalated bacterial burden and the presence of specific organisms may be instrumental in disease onset (Molyneaux et al., 2014). Some viruses have also been implicated in initiating, promoting, or intensifying IPF (Phan et al., 2021). Bacteria and viruses can inflict damage on airway epithelial cells directly or indirectly through the activation of immune responses to infection (Sack and Raghu, 2019). Evidence indicates that extracellular vesicles generated by certain Gram-negative bacteria, resulting from lung microbiota dysregulation, instigate the expression of pro-inflammatory and pro-fibrotic genes across a variety of cell types. Additionally, IL-17B and TNF-a secreted by these extracellular vesicles interact to construct an inflammatory network system conducive to pulmonary fibrosis (Yang et al., 2019). Research conducted by David and colleagues unveiled a significant correlation between the lung microbiota burden and IPF progression (O'Dwyer et al., 2019). Furthermore, it has been reported that the mortality risk in IPF escalates with the increasing bacterial burden in the lung (Molyneaux et al., 2014).

2.4 Smoking

Recognized as a principal risk factor for chronic respiratory diseases such as COPD (Aghapour et al., 2018), smoking also has a significant role in precipitating pulmonary fibrosis. A potent

correlation exists between smoking and IPF, which amplifies with the escalation in dosage, especially evident in habitual smokers or those who have smoked over extended periods (Bellou et al., 2021). Cigarette smoke can inflict damage on all lung cell types, particularly alveolar epithelial cells, giving rise to diffuse infiltration and parenchymal fibrosis (Kumar et al., 2018). One investigation indicated that IPF patients with a long-term smoking history exhibited lower overall cell density, albeit higher alveolar cell density and more severe damage (Zhang et al., 2021). One study established that cigarette smoking correlates with an augmented risk of IPF, with ever-smokers facing a 60% elevated risk (Bae et al., 2022).

2.5 Gastroesophageal reflux disease

The pronounced incidence of gastroesophageal reflux disease (GERD) in IPF suggests a pathogenic role for microaspiration attributable to GERD (Bedard Methot et al., 2019). Chronic microaspiration stemming from GERD is deemed a likely precursor to IPF (King and Nathan, 2017). For individuals predisposed to IPF, chronic microaspiration induced by gastric reflux can inflict enduring, recurrent damage to lung tissue, increasing lung epithelial cell permeability, continually stimulating pulmonary fibrosis proliferation, and eventually contributing to the manifestation of pulmonary fibrosis (Ghisa et al., 2019). Several cell biology experiments and preclinical studies indicate that gastric reflux constituents, such as acid and proteases, can elicit adverse effects such as immune response stimulation, enhanced cell membrane permeability, severe airway inflammation, and lung tissue structure alteration (Nelkine et al., 2020). Evidence supporting this hypothesis emerges from descriptive studies conducted in both experimental animal models and humans (Chen et al., 2019; Reynolds et al., 2023).

2.6 Aging

The mechanism by which aging leads to pulmonary fibrosis remains unclear. Cellular senescence can disrupt various cellular biological activities in the body, manifesting as telomere attrition, DNA damage, and mitochondrial dysfunction (Merkt et al., 2020). Research indicates that cellular senescence induced by telomere degradation primarily afflicts alveolar epithelial type II cells, which is intricately linked to IPF pathogenesis (Stuart et al., 2014; Selman et al., 2019). Repeated microdamage to senescent epithelial cells in genetically susceptible individuals can trigger abnormal fibroblast activation, culminating in ECM accumulation and fibrosis (Pardo and Selman, 2016). Multiple murine models of pulmonary fibrosis display evidence of various cellular senescence markers, including heightened aging-associated β-galactosidase in lysosomes, an increased BCL-2/Bax ratio of apoptosis-involved proteins in mitochondria, and amplified DNA damage in the nucleus (Schafer et al., 2017; Blokland et al., 2020), all coupled with robust pro-fibrotic effects, such as TGF-β (Rana et al., 2020). Aging can impede stem cell turnover functionality, obstructing the repair and regeneration of alveolar epithelial cells in damaged lungs (Mei et al., 2021). Aging has been implicated in promoting fibrosis by thwarting blood vessel regeneration (Chen et al., 2021). IPF prevalence and incidence continue to rise in individuals over 65 years and remain exceedingly rare in those under 50 years old (Raghu et al., 2018), reinforcing the classification of IPF as an aging-related disease.

3 Pathogenesis

The pathogenesis of IPF is multifaceted and, as of yet, not wholly comprehended. Nevertheless, several pivotal factors have been pinpointed as significant contributors to the disease's inception and evolution. Herein is a synopsis of our current understanding of IPF pathogenesis.

3.1 Transforming growth factor (TGF)

TGF-β is considered a central component among the diverse factors contributing to pulmonary fibrosis development (Chanda et al., 2019). Released in response to epithelial cell injury, TGF-β acts as a key upstream pro-fibrotic growth factor propelling the disease's pathophysiology (Shimbori et al., 2019; He et al., 2021b). As a multifunctional cytokine, TGF-β fosters pulmonary fibrosis through a range of mechanisms (Nolte and Margadant, 2020). Primarily, it incites the proliferation and differentiation of epithelial cells and fibroblasts (Ghavami et al., 2018), spurs myofibroblasts to generate the extracellular matrix, catalyzes epithelial-mesenchymal transition, expedites epithelial apoptosis and cell migration, and provokes the production of connective tissue growth factor among other mediators (Phan et al., 2021). TGF-β not only choreographs the congregation of fibroblasts at injury sites but also facilitates their metamorphosis into myofibroblasts (Ye and Hu, 2021). Moreover, TGF-β distinguishes itself as the most efficacious extracellular matrix production stimulant and is considered the strongest chemoattractant for immune cells, including monocytes and macrophages (Kinoshita and Goto, 2019).

3.2 Insulin-like growth factor (IGF)

The insulin-like growth factor has a significant role in pulmonary fibrosis progression (Kheirollahi et al., 2022). Composed of 70 amino acids, IGF-1 chiefly mediates a range of biological functions, including cell division, differentiation, apoptosis, and metabolism (Jensen-Cody and Potthoff, 2021; Jiang et al., 2023). IGF-1 is postulated to facilitate fibroblast proliferation, migration, and differentiation, augmenting the ability of fibroblasts to synthesize fibronectin and collagen, thereby boosting ECM deposition (Renaud et al., 2020). This leads to scarring, resulting in stiffness, the loss of standard lung architecture, and, ultimately, compromised lung function. Epithelial-mesenchymal transition (EMT) plays a pivotal role in the development of pulmonary fibrosis by contributing to myofibroblast generation. Studies indicate that IGF promotes the pro-fibrotic milieu chiefly through IGF1R signaling pathways, by suppressing matrix metalloproteinases, up-regulating TGFβ, and secreting tissue metalloproteinase inhibitors (Garrett et al., 2019).

Further research has shown that TGF-β is crucial for IGF-1 induction in myofibroblasts, and increased levels of IGF-1 in IPF tissues are associated with diminished lung function during disease progression (Hernandez et al., 2020). Mice with bleomycin-induced lung fibrosis and human IPF lung tissue have exhibited elevated IGF-1 levels (Sun et al., 2021). IGF-1 invigorates fibroblast proliferation, protects myofibroblasts from apoptosis, and advocates ECM accumulation, all of which are integral processes in pulmonary fibrosis. Hence, IGF-1 occupies a vital role in the onset and/or proliferation of pulmonary fibrosis.

3.3 Connective tissue growth factor (CTGF)

CTGF, or CCN2, is recognized as a prolific instigator of chronic fibrosis hyperplasia (Sgalla et al., 2020a; Effendi and Nagano, 2022). As a cysteine-rich stromal cell protein, it exerts influence over numerous biological processes, including cell proliferation, differentiation, adhesion, angiogenesis, and multiple pathological processes such as tumorigenesis and tissue fibrosis (Ungvari et al., 2017). CTGF is a primary mediator of TGF-β-induced pulmonary fibrosis (Yanagihara et al., 2022). The activation mediated by TGF-β response elements within the CTGF promoter instigates CTGF production, thereby affirming it as a principal arbitrator of TGF-β-induced pulmonary fibrosis (Nguyen et al., 2018). Frequently expressed in mesenchymal cell lines, CTGF often directs tissue regeneration and pathological fibrosis formation via ECM deposition, fibroblast proliferation, and matrix generation (Ramazani et al., 2018). Indeed, the utilization of anti-CTGF antibodies in fibrotic animal models attenuates ECM component expression, enhances survival post-radiation-induced lung injury, and conserves the morphology of alveolar epithelial cells (Bickelhaupt et al., 2017). In IPF patients, CTGF expression is elevated in alveolar cells and mesenchymal fibroblasts (Kasam et al., 2020).

3.4 Matrix metalloproteinases (MMPs)

MMPs are proactive contributors to pulmonary fibrosis (Todd et al., 2020). This family of endopeptidases, including MMP-3, MMP-7, and MMP-8, is integral to regulating EMT degradation in IPF (Roque et al., 2020b; Bormann et al., 2022). EMT activation in the lungs is believed to be one of the mechanisms associated with the loss of alveolar cells and the formation of pulmonary fibrosis. These MMPs facilitate pulmonary fibrosis development via several mechanisms: 1. Fostering epithelial-mesenchymal transition (Liu et al., 2020); 2. Inducing m acrophage polarization (Le et al., 2020); 3. Propelling fibroblast migration (Menou et al., 2018); 4. Encouraging abnormal epithelial cell migration and other irregular repair processes (Drankowska et al., 2019). MMP-7 expression is enhanced in both human IPF and mouse fibrosis models (Mahalanobish et al., 2020; Probst et al., 2020). Research has demonstrated that mice with MMP-3 deletion or MMP-7 knockout are safeguarded from bleomycin-induced fibrosis (Mahalanobish et al., 2020). IPF patients exhibit elevated MMP levels in alveolar lavage fluid and blood (Inoue et al., 2020; Espindola et al., 2021). Clinical data suggest an association between elevated MMP-7 levels and an increased risk of mortality and disease progression (Khan et al., 2022).

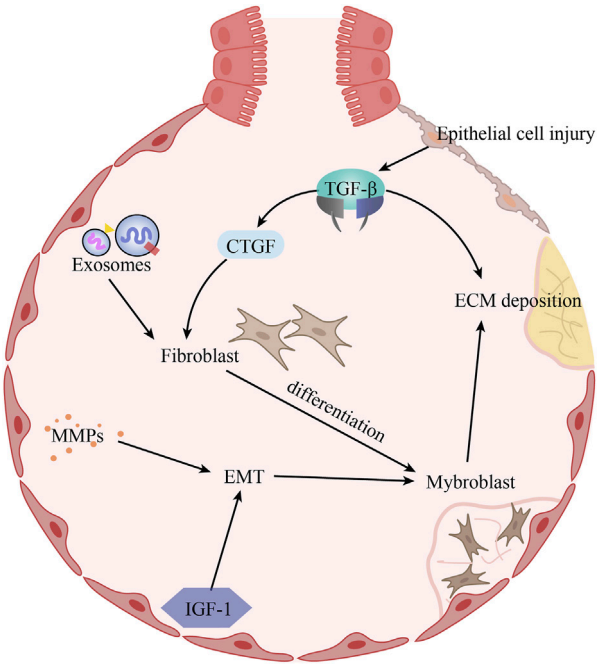

FIGURE 1
The pathogenesis of idiopathic pulmonary fibrosis. Alveolar epithelial cell injury induces increased TGF-β expression, which promotes ECM deposition and CTGF expression. Under the combined effect of CTGF and exosomes, fibroblasts proliferate and differentiate into myogenic cells. In addition, increased expression of MMPs and IGF-1 in IPF promotes EMT, which in turn affects myogenic cells. The increase in the number of myogenic cells further aggravates ECM deposition.

3.5 Exosomes

Exosomes are phospholipid bilayer membranous vesicles, measuring between 30 and 150 nm (Negrete-Garcia et al., 2022). Continuously secreted by a variety of cell types, they transport biologically active substances such as proteins, lipids, and genetic material (DNA, mRNA, miRNAs, and lncRNAs) (Yang et al., 2022). Bronchial epithelial cells primarily generate exosomes in the lungs, which activate fibroblasts, stimulate their differentiation into myofibroblasts, and catalyze excessive extracellular matrix component deposition (Abreu et al., 2021). By delivering miRNA to recipient cells, exosomes regulate diverse inflammatory and angiogenic pathways, playing an instrumental role in inflammation, tissue repair, and fibrogenesis (Rasaei et al., 2022). A multitude of studies underscore the significance of exosomes in IPF pathogenesis, particularly regarding epithelial phenotypes and fibroproliferative responses (d'Alessandro et al., 2021a; Martin-Medina et al., 2018; Parimon et al., 2019). Studies indicate an upregulation of miR-21 in exosomes in mouse pulmonary fibrosis models and human IPF patient serum, correlating with disease progression and mortality (Pastor et al., 2021). A recent study reported an elevated number of Wnt5a-carrying exosomes in

IPF patients. These lung fibroblast-derived exosomes exert an autocrine effect, stimulating *in vitro* fibroblast proliferation (Baarsma and Konigshoff, 2017).

To summarize, the pathogenesis of idiopathic pulmonary fibrosis is complex, with specific mechanisms appearing to intersect with each other, as outlined in this paper, is depicted in Figure 1.

4 Treatment

Currently, conventional medications approved for the clinical treatment of idiopathic pulmonary fibrosis (IPF), such as pirfenidone and nintedanib, only alleviate symptoms without reversing pulmonary fibrosis to facilitate a curative outcome. Consequently, the development of new therapeutic options is imperative. Innovations include investigating novel effects of existing drugs, developing new drugs, and exploring treatments such as stem cell transplantation for IPF. Many drugs are currently under clinical trials, with some advancing to phase 3, thereby expanding the therapeutic arsenal for IPF.

4.1 Glucocorticoids and immunosuppressants

Historically, chronic inflammation, seemingly uncontrollable, was perceived as the primary driver of progressive parenchymal fibrosis development (Behr, 2013). Systemic steroids, due to a dearth of effective alternatives, served as the standard treatment for IPF (Raghu et al., 2015). Combinatorial immunosuppressants, including prednisone, azathioprine, cyclophosphamide, and acetylcysteine, were similarly efficacious (Walter et al., 2006). Glucocorticoids and immunosuppressants are usually used for empirical treatment of acute exacerbation of idiopathic pulmonary fibrosis (Naccache et al., 2022). Some studies have shown that the combination of them is beneficial in prolonging the survival of acute patients (Yamazoe and Tomioka, 2018). However, there is currently insufficient evidence to support their routine use. An increasing number of clinical trials have shown that anti-inflammatory therapy and immunosuppressive agents are not effective in conventional treatment of IPF (Ryu et al., 2014; Barratt et al., 2018), leading to the discontinuation of their recommendation for the routine treatment of IPF.

4.2 Pirfenidone

Pirfenidone, the inaugural oral antifibrotic drug to receive approval, is a pyridine derivative widely recognized for the treatment of IPF (Vancheri et al., 2018). Its mechanism of action, while multifaceted, remains incompletely understood. Pirfenidone exhibits anti-inflammatory, anti-oxidative, and anti-fibrotic properties, thereby reducing collagen synthesis and deposition in the lungs (Saito et al., 2019). By inhibiting the cytokine TGF-β, it curtails the proliferation, differentiation, and collagen secretion of human lung fibroblasts, decelerates the fibrotic process, and attenuates the decline rate of forced vital capacity (FVC) (Aimo et al., 2022). Several animal model studies in recent years have corroborated the antifibrotic characteristics of pirfenidone (Carrington et al., 2018). It can enhance the prognosis of IPF, reduce mortality, and prolong progression-free survival (Nathan et al., 2017; Vancheri et al., 2018), as has been demonstrated in numerous randomized, placebo-controlled phase III trials (King et al., 2014; Noble et al., 2016). In IPF treatment, pirfenidone demonstrates not only tolerability but also a desirable safety profile (Veit et al., 2019). Therefore, pirfenidone presents a promising treatment avenue for IPF.

4.3 Nintedanib

Nintedanib, another approved oral antifibrotic drug, operates as an orally active triple tyrosine kinase receptor inhibitor (Molina-Molina, 2019). Originally conceived as an anti-cancer drug, it later displayed antifibrotic effects and received approval for IPF treatment (d'Alessandro et al., 2021b). Nintedanib effectively impairs the activity of platelet-derived growth factor receptor kinase, fibroblast growth factor receptor kinase, and vascular endothelial growth factor receptor kinase (Hilberg et al., 2008). It suppresses the release of pro-inflammatory and pro-fibrotic mediators, inhibits fibroblast migration and differentiation, and contributes to the blockade of extracellular matrix deposition (Wollin et al., 2015). In bleomycin-induced animal pulmonary fibrosis models, nintedanib exhibited antifibrotic, anti-inflammatory, and vascular remodeling activities (Ackermann et al., 2017). Phase 3 clinical trials demonstrated that, compared to a placebo, nintedanib significantly attenuates the decline rate of forceful lung volume following mild to moderate lung function impairment in IPF patients (Collins and Raghu, 2019). Nintedanib significantly mitigated the risk of disease progression and also demonstrated a mortality-reducing benefit (Richeldi et al., 2014). Moreover, nintedanib exhibited a manageable safety and tolerability profile in clinical trials involving patients (Seibold et al., 2020).

4.4 Lung transplantation

Lung transplantation presents itself as the sole treatment alternative that can enhance the quality of life and augment survival rates when previous treatments have failed to yield positive outcomes (Balestro et al., 2019). This life-saving procedure serves as the ultimate solution for advanced stages of IPF. After the diagnosis of IPF, the lung transplantation should be actively evaluated to start the early implantation of transplantation concept. Candidates typically considered for lung transplantation are those with limited treatment alternatives and face a death risk exceeding 50% within 2 years without the transplantation (George et al., 2019). The survival rate post-transplantation has shown consistent improvement over the years, with recent statistics indicating a 1-year survival rate of 88.8% and a 5-year survival rate of 59.2% (Valapour et al., 2021). Despite the continual enhancement in the overall prognosis of lung transplantation, it remains a complex procedure for IPF laden with potential complications. Limitations in the procedure's application arise from the scarcity of donor organs, the possibility of acute graft-

versus-host disease, and the risk of infection (Kapnadak and Raghu, 2021).

4.5 Potential therapeutic strategies

4.5.1 Monoclonal antibodies

Pamrevlumab, a humanized monoclonal antibody, targets CTGF, a fibroblast and endothelial cell-secreted glycoprotein pivotal in the pathogenesis of fibrosis (Di Martino et al., 2021). Investigations have demonstrated that pamrevlumab permeates tissues, diminishing effective CTGF levels, which in turn leads to a decline in profibrotic factors, reestablishes the equilibrium between secretion and processing of the extracellular matrix (ECM), and restores tissue homeostasis (Raghu et al., 2016). In a mouse model simulating radiation-induced pulmonary fibrosis, pamrevlumab treatment reversed established lung remodeling and reinstated lung function (Bickelhaupt et al., 2017). Some clinical trials have showcased promising results with pamrevlumab significantly reducing FVC deterioration and slowing disease progression, exhibiting comparable efficacy to pirfenidone and nintedanib (Sgalla et al., 2020a; Richeldi et al., 2020). Data derived from a phase 2 study underscored a favorable safety and tolerability profile for pamrevlumab among the IPF patients participating in the study (Raghu et al., 2016). Pamrevlumab is presently under investigation in a Phase 3 randomized, double-blind, controlled, multicenter trial (Sgalla et al., 2020b). It holds potential as an innovative, safe, and efficacious treatment modality for idiopathic pulmonary fibrosis. Some other monoclonal antibodies, including Atezolizumab, Garadacimab, and Vixarelimab, traditionally employed in the treatment of various other diseases, have also demonstrated therapeutic potential in the clinical management of IPF.

4.5.2 Metformin

Metformin, a time-honored hypoglycemic agent clinically employed in the treatment of type 2 diabetes mellitus, is increasingly recognized for its antifibrotic properties, as corroborated by numerous preclinical investigations (Choi et al., 2016; Rangarajan et al., 2018; Foretz et al., 2019). Metformin was identified to exert pronounced antifibrotic effects by modulating metabolic pathways, impeding transforming growth factor-beta, inhibiting collagen formation, and inducing adipogenic differentiation of lung fibroblasts in IPF patients (Kheirollahi et al., 2019). In the bleomycin-induced pulmonary fibrosis model, metformin mitigated pulmonary fibrosis through the inhibition of TGF-β via the activation of adenosine monophosphate-activated protein kinase. This activation fast-tracked the removal of established fibrosis by promoting myofibroblast inactivation and apoptosis (Choi et al., 2016; Sato et al., 2016). In one particular study, metformin was found to attenuate bleomycin-induced pulmonary fibrosis via the Insulin-like Growth Factor 1 pathway, demonstrating antifibrotic efficacy comparable to that of pirfenidone (Xiao et al., 2020). A retrospective clinical examination of IPF patients with concurrent diabetes revealed that the group treated with metformin exhibited lower all-cause mortality and hospitalization rates compared to the control group (Teague et al., 2022). The robust antifibrotic action of metformin, its low adverse effect profile, and affordability underscore its potential as an antifibrotic therapeutic candidate.

4.5.3 Proton pump inhibitors (PPIs)

PPIs are currently under investigation as potential therapeutic agents for IPF due to the frequent coexistence of gastroesophageal reflux disease and IPF in clinical scenarios (Tran et al., 2021). The antifibrotic potential of PPIs is theorized to stem from their effective inhibition of fibroblast proliferation and downregulation of TGFβ receptor (Ghebremariam et al., 2015). A dose-dependent inhibition of the gene expression of profibrotic markers, such as collagen 1, fibronectin 1, and matrix metalloproteinase 7, by PPIs has also been documented (Nelson et al., 2017). PPIs are further recognized to exhibit antifibrotic effects by upregulating the cytoprotective enzyme heme oxygenase 1 (Ghebre and Raghu, 2016). Anti-fibrotic impacts of PPIs were evident in lung injury models induced by carbon tetrachloride, a liver fibrosis model (Eltahir and Nazmy, 2018). Preclinical *in vivo* studies demonstrated that oral esomeprazole mitigated inflammation and fibrosis in rodent models of bleomycin-induced lung injury, with approximately 50% reduction in each parameter (Ghebremariam et al., 2015). Several studies generally vouch for the beneficial effects of PPI therapy in managing IPF, where PPIs could decelerate lung function deterioration and enhance patient survival (Lee et al., 2011; Lee et al., 2013). Furthermore, a longer duration of PPI use was significantly associated with lower IPF-related mortality in both univariate and multivariate Cox regression analyses (Lee et al., 2016). Given the influence of GERD on IPF progression, proton pump inhibitors are recommended for the management of this disease and have been incorporated into international IPF treatment guidelines (Tran and Suissa, 2021). Lansoprazole, a proton pump inhibitor, is currently undergoing a Phase 3 clinical trial against pulmonary fibrosis, the outcomes of which hold promising prospects.

4.5.4 Stem cell therapy

The exploitation of embryonic stem cells for lung regeneration or repair has gained notable momentum in recent years. Stem cells, essentially immature cells that proliferate and metamorphose into adult cells, demonstrate anti-inflammatory and anti-fibrotic traits, rendering them as a potent potential therapy for fibrotic diseases (Kletukhina et al., 2022). Mesenchymal stem cells (MSCs), pluripotent cells endowed with immunomodulatory and tissue repair capabilities, emerge as a prospective therapeutic avenue for IPF (Yang S. et al., 2022). The potential engagement of MSCs in pulmonary fibrosis hinges on their capacity to generate a plethora of biologically active substances with anti-inflammatory, immunosuppressive, and angiogenic attributes, alongside their ability to minimize extracellular matrix and collagen deposition, thus fostering alveolar repair (Jiang et al., 2015). For instance, MSCs curtail TGF-β1 and tumor necrosis factor-alpha (TNF-α) levels by secreting prostaglandin E2 (PGE2) and hepatocyte growth factor (Dong et al., 2015). Lung spheroid cells (LSCs), forming a distinct spherical structure in culture, comprise stem and support cells native to the lungs that can be reliably cultured from biopsied lung tissue (Surolia et al., 2017). A study revealed that LSC treatment can attenuate and resolve bleomycin-induced fibrosis by reconstructing normal alveolar structure, curtailing collagen accumulation, and myofibroblast proliferation (Henry et al., 2015). When administered intravenously into a mouse model of pulmonary fibrosis, a majority of the cells localized in the animal's lungs, with the lung spheroid cells demonstrating potent regenerative properties (Dinh et al., 2017). Rats with pulmonary fibrosis treated with spheroid cells manifested healthier lung cells overall and exhibited

10.3389/fphar.2023.1205948

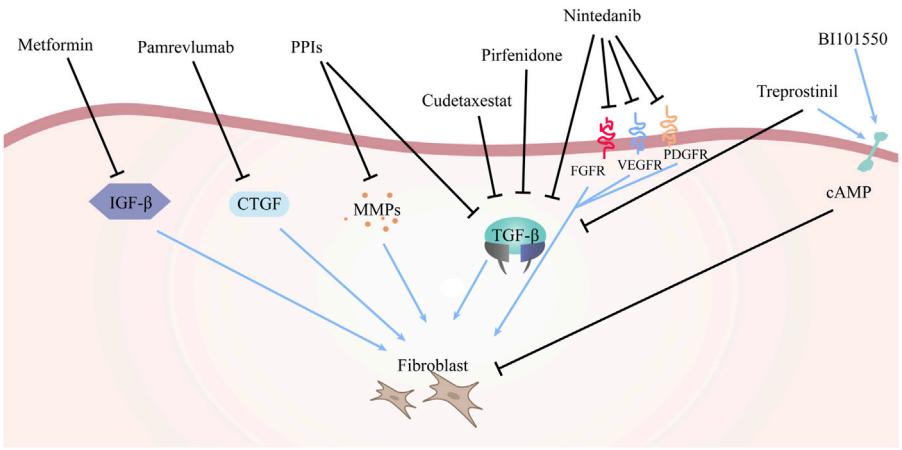

FIGURE 2
The mechanism of drugs for the treatment of IPF. The arrows in the figure represent the activating effect and the black lines represent the inhibiting effect. The different drugs mentioned above have different principles of action, but the ultimate goal of all drugs is to inhibit fibroblast production and reduce or even block the deposition of ECM.

TABLE 1 A few representative ongoing clinical trials for IPF.

Therapeutic measures	Mechanism	Phase	Status	Trial identifier
Pamrevlumab	CTGF inhibitor	3	Active, not recruiting	NCT03955146
Treprostinil	DP1/EP2 agonist	3	Recruiting	NCT05255991
BI 1015550	PDE4B inhibitor	3	Recruiting	NCT05321069
Lansoprazole	PPIs	3	Recruiting	NCT04965298
Cudetaxestat	Autotaxin inhibitor	2	Active, not recruiting	NCT05373914
Garadacimab	FXIIa mAb	2	Recruiting	NCT05130970
Autoantibody Reductive Therapy	Immunologic Factors	2	Recruiting	NCT03286556
Fipaxalparant	LPA1 antagonist	2	Recruiting	NCT05032066
Orvepitant	NK-1 Receptor Antagonist	2	Recruiting	NCT05185089
Setanaxib	NOX1/4 Inhibitor	2	Recruiting	NCT03865927
Vixarelimab	OSMR-β inhibitor	2	Recruiting	NCT05785624
Bersiporocin	PRS inhibitor	2	Recruiting	NCT05389215
RXC007	ROCK2 inhibitor	2	Recruiting	NCT05570058
Taladegib	Smo inhibitor	2	Recruiting	NCT04968574
TTI-101	STAT3 inhibitor	2	Recruiting	NCT05671835
Bexotegrast	αvβ6 integrin inhibitor	2	Active, not recruiting	NCT04396756
ORIN1001	IRE1a inhibitor	1	Active, not recruiting	NCT04643769
Atezolizumab	PD-L1 inhibitor	1	Recruiting	NCT05515627
ARO-MMP7	RNAi	1	Recruiting	NCT05537025
Human Umbilical Cord MSC	Stem cells	1	Recruiting	NCT05468502
Lung Spheroid Stem Cells	Stem cells	1	Recruiting	NCT04262167
Mesenchymal Stem Cell	Stem cells	1	Recruiting	NCT05016817

substantially less lung inflammation and fibrosis (Dinh et al., 2020). In certain clinical studies of IPF, queries regarding the efficacy and safety of stem cell therapy have been addressed. In terms of efficacy, patients receiving the treatment displayed significant improvement in FVC compared to the placebo group (Ntolios et al., 2018; Fishman et al., 2019; Averyanov et al., 2020), with these results being considerably encouraging. No major adverse events were reported, thereby alleviating the majority of concerns (Glassberg et al., 2017; Zhang et al., 2017; Campo et al., 2021). Presently, several Phase I clinical trials of stem cell therapy for IPF are in progress, seeking to fully appraise the safety and feasibility of stem cell therapy. Hence, stem cells' employment in the treatment of pulmonary fibrosis is deemed a promising therapeutic strategy.

4.5.5 Other potential therapies

Additional therapeutic drugs and methods are undergoing investigation, and although the specific mechanisms remain to be thoroughly scrutinized, it does not impede the advancement of exploratory efforts in IPF treatment strategies. Currently, treprostinil and BI 1015550, which are in Phase 3 clinical trials, are under consideration. Treprostinil is a stable prostacyclin analog, a PGI2 receptor agonist, promoting vasodilation and inhibiting platelet aggregation (Nathan et al., 2022). Certain studies reveal that treprostinil influences cell adhesion and differentiation by inhibiting extracellular regulated kinase signaling, thereby impeding fibroblast proliferation (Blumer et al., 2021). It also demonstrates dose-dependent prevention of fibroblast proliferation to decrease extracellular matrix composition via TGF-beta1 in human peripheral lung fibroblasts (Lambers et al., 2018). BI 1015550, a preferential Phosphodiesterase 4 (PDE4) inhibitor, has been developed for the treatment of IPF and other forms of progressive pulmonary fibrosis (Sgalla et al., 2023). PDE4 inhibition is renowned for its anti-inflammatory and antifibrotic properties (Richeldi et al., 2022). Several experiments have established the inhibition of pulmonary fibrosis by PDE4 inhibitors (Kim et al., 2016; Herrmann et al., 2022). BI 1015550 has been recently evaluated in a phase 2, randomized, double-blind, multi-center, placebo-controlled trial that demonstrated a beneficial treatment effect with an acceptable safety and tolerability profile. Autotaxin, an enzyme involved in lysophosphatidic acid production, is upregulated in IPF patients, thereby constituting a potential target for novel IPF therapeutics. Cudetaxestat is an autotaxin inhibitor, and ARO-MMP7 is an investigational RNA-interfering drug designed to reduce the expression of MMP7 to combat pulmonary fibrosis. Autoantibody Reductive Therapy is mechanistically aimed at ameliorating autoantibody-mediated pulmonary injury.

In addition, smoking patients are advised to quit smoking and given appropriate traditional Chinese medicine adjuvant therapy, which is helpful to improve the quality of life of patients. At the same time, active pulmonary rehabilitation and oxygenotherapy if necessary, which also play a great role in improving the function of the body and stabilizing or slowing down the development of the disease.

Various drugs employed to manage idiopathic pulmonary fibrosis are enumerated above, with their mechanisms of action delineated in Figure 2.

While most of these therapies are in their nascent stages of research, they provide substantial reassurance, and it is hoped that they receive expedited approval for the clinical benefit of IPF patients. Research into IPF treatment strategies, buoyed by the introduction of innovative therapeutic agents and treatments, has witnessed a burgeoning number of clinical trials. Some ongoing clinical trials are succinctly presented in Table 1.

5 Conclusion

Despite substantial strides in comprehending IPF and formulating innovative treatment strategies, the labyrinthine nature of this disease continues to mandate further exploration. The contemporary perspectives on IPF treatment can be encapsulated as follows.

1 Early Diagnosis and Intervention: The importance of early IPF diagnosis cannot be overstated for administering treatment prior to extensive lung damage. Strategies may encompass heightened awareness and education for healthcare professionals, biomarker utilization, and the creation of avant-garde imaging techniques for early disease detection.

2 Personalized Medicine: As our grasp of the molecular mechanisms underpinning IPF becomes more sophisticated, opportunities may arise to devise personalized treatment strategies aimed at specific pathways or genetic factors in individual patients. This could culminate in more efficacious, customized therapies with diminished side effects.

3 Combination Therapies: Owing to IPF's multifaceted nature, it is improbable that a single treatment would entirely stymie the disease's progression. Therefore, combination therapies targeting multiple facets of the disease, including inflammation, fibrosis, and oxidative stress, might enhance IPF management.

4 Regenerative Medicine: Delving into regenerative medicine, inclusive of stem cell therapy and tissue engineering, offers potential for novel IPF treatment strategies. The ultimate aim would be to mend or substitute damaged lung tissue, potentially reversing the disease's effects.

5 Improved Support and Symptom Management: While a definitive cure for IPF currently eludes us, optimizing symptom management and providing comprehensive support to patients and their families remain paramount. This entails pulmonary rehabilitation, oxygen therapy, and psychological support to assist patients in grappling with the physical and emotional tribulations associated with IPF.

6 Enhanced Collaboration and Research: Sustained collaboration among researchers, clinicians, and pharmaceutical companies is indispensable to catalyze innovation and engender new treatment options for IPF. This calls for a collaborative spirit that encourages data, resource, and knowledge sharing across disciplines to expedite the discovery of new therapeutic targets and augment our understanding of the disease.

In summary, although IPF persists as a formidable and intricate disease, the landscape appears promising with the advent of novel treatment options and research advancements.

With an emphasis on early diagnosis, personalized medicine, combination therapies, regenerative medicine, improved support and symptom management, and enhanced collaboration and research, the field stands poised to make substantial progress in the foreseeable future.

Author contributions

HG conceived and drafted the manuscript. JS, SZ, YN, and SZ discussed the concepts of the manuscript. JS created the figures. HG and YZ reviewed and revised the manuscript. All authors contributed to the article and approved the submitted version.

Conflict of interest

The authors declare that the research was conducted in the absence of any commercial or financial relationships that could be construed as a potential conflict of interest.

Publisher's note

References

Abreu, S. C., Lopes-Pacheco, M., Weiss, D. J., and Rocco, P. R. M. (2021). Mesenchymal stromal cell-derived extracellular vesicles in lung diseases: Current status and perspectives. *Front. Cell Dev. Biol.* 9, 600711. doi:10.3389/fcell.2021.600711

Ackermann, M., Kim, Y. O., Wagner, W. L., Schuppan, D., Valenzuela, C. D., Mentzer, S. J., et al. (2017). Effects of nintedanib on the microvascular architecture in a lung fibrosis model. *Angiogenesis* 20 (3), 359–372. doi:10.1007/s10456-017-9543-z

Aghapour, M., Raee, P., Moghaddam, S. J., Hiemstra, P. S., and Heijink, I. H. (2018). Airway epithelial barrier dysfunction in chronic obstructive pulmonary disease: Role of cigarette smoke exposure. *Am. J. Respir. Cell Mol. Biol.* 58 (2), 157–169. doi:10.1165/rcmb.2017-0200TR

Aimo, A., Cerbai, E., Bartolucci, G., Adamo, L., Barison, A., Lo Surdo, G., et al. (2020). Pirfenidone is a cardioprotective drug: Mechanisms of action and preclinical evidence. *Pharmacol. Res.* 155, 104694. doi:10.1016/j.phrs.2020.104694

Aimo, A., Spitaleri, G., Nieri, D., Tavanti, L. M., Meschi, C., Panichella, G., et al. (2022). Pirfenidone for idiopathic pulmonary fibrosis and beyond. *Card. Fail Rev.* 8, e12. doi:10.15420/cfr.2021.30

Averyanov, A., Koroleva, I., Konoplyannikov, M., Revkova, V., Lesnyak, V., Kalsin, V., et al. (2020). First-in-human high-cumulative-dose stem cell therapy in idiopathic pulmonary fibrosis with rapid lung function decline. *Stem Cells Transl. Med.* 9 (1), 6–16. doi:10.1002/sctm.19-0037

Baarsma, H. A., and Konigshoff, M. (2017). 'WNT-er is coming': WNT signalling in chronic lung diseases. *Thorax* 72 (8), 746–759. doi:10.1136/thoraxjnl-2016-209753

Bae, W., Lee, C. H., Lee, J., Kim, Y. W., Han, K., and Choi, S. M. (2022). Impact of smoking on the development of idiopathic pulmonary fibrosis: Results from a nationwide population-based cohort study. *Thorax* 77 (5), 470–476. doi:10.1136/thoraxjnl-2020-215386

Balestro, E., Cocconcelli, E., Tinè, M., Biondini, D., Faccioli, E., Saetta, M., et al. (2019). Idiopathic pulmonary fibrosis and lung transplantation: When it is feasible. *Medicina* 55 (10), 702. doi:10.3390/medicina55100702

Ballester, B., Milara, J., and Cortijo, J. (2019). Idiopathic pulmonary fibrosis and lung cancer: Mechanisms and molecular targets. *Int. J. Mol. Sci.* 20 (3), 593. doi:10.3390/ijms20030593

Barratt, S., Creamer, A., Hayton, C., and Chaudhuri, N. (2018). Idiopathic pulmonary fibrosis (IPF): An overview. *J. Clin. Med.* 7 (8), 201. doi:10.3390/jcm7080201

Bedard Methot, D., Leblanc, E., and Lacasse, Y. (2019). Meta-analysis of gastroesophageal reflux disease and idiopathic pulmonary fibrosis. *Chest* 155 (1), 33–43. doi:10.1016/j.chest.2018.07.038

Behr, J. (2013). The diagnosis and treatment of idiopathic pulmonary fibrosis. *Dtsch. Arztebl Int.* 110 (51-52), 875–881. doi:10.3238/arztebl.2013.0875

Bellou, V., Belbasis, L., and Evangelou, E. (2021). Tobacco smoking and risk for pulmonary fibrosis: A prospective cohort study from the UK biobank. *Chest* 160 (3), 983–993. doi:10.1016/j.chest.2021.04.035

Bickelhaupt, S., Erbel, C., Timke, C., Wirkner, U., Dadrich, M., Flechsig, P., et al. (2017). Effects of CTGF blockade on attenuation and reversal of radiation-induced pulmonary fibrosis. *J. Natl. Cancer Inst.* 109 (8). doi:10.1093/jnci/djw339

Biondini, D., Cocconcelli, E., Bernardinello, N., Lorenzoni, G., Rigobello, C., Lococo, S., et al. (2021). Prognostic role of MUC5B rs35705950 genotype in patients with idiopathic pulmonary fibrosis (IPF) on antifibrotic treatment. *Respir. Res.* 22 (1), 98. doi:10.1186/s12931-021-01694-z

Blokland, K. E. C., Pouwels, S. D., Schuliga, M., Knight, D. A., and Burgess, J. K. (2020). Regulation of cellular senescence by extracellular matrix during chronic fibrotic diseases. *Clin. Sci. (Lond)* 134 (20), 2681–2706. doi:10.1042/CS20190893

Blumer, S., Fang, L., Chen, W-C., Khan, P., Hostettler, K., Tamm, M., et al. (2021). IPF-fibroblast erk1/2 activity is independent from microRNA cluster 17-92 but can Be inhibited by treprostinil through DUSP1. *Cells* 10 (11), 2836. doi:10.3390/cells10112836

Bormann, T., Maus, R., Stolper, J., Tort Tarrés, M., Brandenberger, C., Wedekind, D., et al. (2022). Role of matrix metalloprotease-2 and MMP-9 in experimental lung fibrosis in mice. *Respir. Res.* 23 (1), 180. doi:10.1186/s12931-022-02105-7

Campo, A., González-Ruiz, J. M., Andreu, E., Alcaide, A. B., Ocón, M. M., De-Torres, J., et al. (2021). Endobronchial autologous bone marrow-mesenchymal stromal cells in idiopathic pulmonary fibrosis: a phase I trial. *ERJ Open Res.* 7 (2), 00773-2020. doi:10.1183/23120541.00773-2020

Carrington, R., Jordan, S., Pitchford, S. C., and Page, C. P. (2018). Use of animal models in IPF research. *Pulm. Pharmacol. Ther.* 51, 73–78. doi:10.1016/j.pupt.2018.07.002

Chanda, D., Otoupalova, E., Smith, S. R., Volckaert, T., De Langhe, S. P., and Thannickal, V. J. (2019). Developmental pathways in the pathogenesis of lung fibrosis. *Mol. Asp. Med.* 65, 56–69. doi:10.1016/j.mam.2018.08.004

Chen, S., Chen, H., Cheng, Y., Wei, Y., Zhou, X., Li, T., et al. (2019). Gastric acid and pepsin work together in simulated gastric acid inhalation leading to pulmonary fibrosis in rats. *Med. Sci. Monit.* 25, 6153–6164. doi:10.12659/MSM.915628

Chen, Y., Pu, Q., Ma, Y., Zhang, H., Zhao, C., et al. (2021). Aging reprograms the hematopoietic-vascular niche to impede regeneration and promote fibrosis. *Cell Metab.* 33 (2), 395–410 e4. doi:10.1016/j.cmet.2020.11.019

Choi, S. M., Jang, A. H., Kim, H., Lee, K. H., and Kim, Y. W. (2016). Metformin reduces bleomycin-induced pulmonary fibrosis in mice. *J. Korean Med. Sci.* 31 (9), 1419–1425. doi:10.3346/jkms.2016.31.9.1419

Collins, B. F., McClelland, R. L., Ho, L. A., Mikacenic, C. R., Hayes, J., Spada, C., et al. (2018). Sarcoidosis and IPF in the same patient-a coincidence, an association or a phenotype? [j]. *Respir. Med.* 144S, S20–S27. doi:10.1016/j.rmed.2018.08.008

Collins, B. F., and Raghu, G. (2019). Antifibrotic therapy for fibrotic lung disease beyond idiopathic pulmonary fibrosis. *Eur. Respir. Rev.* 28 (153), 190022. doi:10.1183/16000617.0022-2019

d'Alessandro, M., Bergantini, L., Cameli, P., Pieroni, M., Refini, R. M., Sestini, P., et al. (2021b). Serum concentrations of KL-6 in patients with IPF and lung cancer and serial measurements of KL-6 in IPF patients treated with antifibrotic therapy. *J. Cancers (Basel)* 13 (4), 689. doi:10.3390/cancers13040689

d'Alessandro, M., Soccio, P., Bergantini, L., Cameli, P., Scioscia, G., Foschino Barbaro, M. P., et al. (2021a). Extracellular vesicle surface signatures in IPF patients: A multiplex bead-based flow cytometry approach. *J. Cells* 10 (5), 1045. doi:10.3390/cells10051045

Di Martino, E., Provenzani, A., Vitulo, P., and Polidori, P. (2021). Systematic review and meta-analysis of pirfenidone, nintedanib, and pamrevlumab for the treatment of idiopathic pulmonary fibrosis. *Ann. Pharmacother.* 55 (6), 723–731. doi:10.1177/1060028020964451

Dinh, P. C., Cores, J., Hensley, M. T., Vandergriff, A. C., Tang, J., Allen, T. A., et al. (2017). Derivation of therapeutic lung spheroid cells from minimally invasive transbronchial pulmonary biopsies. *Respir. Res.* 18 (1), 132. doi:10.1186/s12931-017-0611-0

Dinh, P. C., Paudel, D., Brochu, H., Popowski, K. D., Gracieux, M. C., Cores, J., et al. (2020). Inhalation of lung spheroid cell secretome and exosomes promotes lung repair in pulmonary fibrosis. *Nat. Commun.* 11 (1), 1064. doi:10.1038/s41467-020-14344-7

Dong, L. H., Jiang, Y. Y., Liu, Y. J., Cui, S., Xia, C. C., Qu, C., et al. (2015). The anti-fibrotic effects of mesenchymal stem cells on irradiated lungs via stimulating endogenous secretion of HGF and PGE2. *Sci. Rep.* 5, 8713. doi:10.1038/srep08713

Drakopanagiotakis, F., Wujak, L., Wygrecka, M., and Markart, P. (2018). Biomarkers in idiopathic pulmonary fibrosis. *Matrix Biol.* 68-69, 404–421. doi:10.1016/j.matbio.2018.01.023

Drankowska, J., Kos, M., Kosciuk, A., Marzęda, P., Boguszewska-Czubara, A., Tylus, M., et al. (2019). MMP targeting in the battle for vision: Recent developments and future prospects in the treatment of diabetic retinopathy. *Life Sci.* 229, 149–156. doi:10.1016/j.lfs.2019.05.038

Effendi, W. I., and Nagano, T. (2022). Connective tissue growth factor in idiopathic pulmonary fibrosis: Breaking the bridge. *Int. J. Mol. Sci.* 23 (11), 6064. doi:10.3390/ijms23116064

Eltahir, H. M., and Nazmy, M. H. (2018). Esomeprazole ameliorates CCl4 induced liver fibrosis in rats via modulating oxidative stress, inflammatory, fibrogenic and apoptotic markers. *Biomed. Pharmacother.* 97, 1356–1365. doi:10.1016/j.biopha.2017.11.028

Espindola, M. S., Habiel, D. M., Coelho, A. L., Stripp, B., Parks, W. C., Oldham, J., et al. (2021). Differential responses to targeting matrix metalloproteinase 9 in idiopathic pulmonary fibrosis. *Am. J. Respir. Crit. Care Med.* 203 (4), 458–470. doi:10.1164/rccm.201910-1977OC

Fishman, J. E., Kim, G. H. J., Kyeong, N. Y., Goldin, J. G., and Glassberg, M. K. (2019). Intravenous stem cell dose and changes in quantitative lung fibrosis and DLCO in the AETHER trial: A pilot study. *Eur. Rev. Med. Pharmacol. Sci.* 23 (17), 7568–7572. doi:10.26355/eurrev_201909_18877

Foretz, M., Guigas, B., and Viollet, B. (2019). Understanding the glucoregulatory mechanisms of metformin in type 2 diabetes mellitus. *Nat. Rev. Endocrinol.* 15 (10), 569–589. doi:10.1038/s41574-019-0242-2

Garrett, S. M., Hsu, E., Thomas, J. M., Pilewski, J. M., and Feghali-Bostwick, C. (2019). Insulin-like growth factor (IGF)-II- mediated fibrosis in pathogenic lung conditions. *PLoS One* 14 (11), e0225422. doi:10.1371/journal.pone.0225422

George, P. M., Patterson, C. M., Reed, A. K., and Thillai, M. (2019). Lung transplantation for idiopathic pulmonary fibrosis. *Lancet Respir. Med.* 7 (3), 271–282. doi:10.1016/S2213-2600(18)30502-2

Ghavami, S., Yeganeh, B., Zeki, A. A., Shojaei, S., Kenyon, N. J., Ott, S., et al. (2018). Autophagy and the unfolded protein response promote profibrotic effects of TGF-β_1 in human lung fibroblasts. *Am. J. Physiol. Lung Cell Mol. Physiol.* 314 (3), L493–L504. doi:10.1152/ajplung.00372.2017

Ghebre, Y. T., and Raghu, G. (2016). Idiopathic pulmonary fibrosis: Novel concepts of proton pump inhibitors as antifibrotic drugs. *Am. J. Respir. Crit. Care Med.* 193 (12), 1345–1352. doi:10.1164/rccm.201512-2316PP

Ghebremariam, Y. T., Cooke, J. P., Gerhart, W., Griego, C., Brower, J. B., Doyle-Eisele, M., et al. (2015). Pleiotropic effect of the proton pump inhibitor esomeprazole leading to suppression of lung inflammation and fibrosis. *J. Transl. Med.* 13, 249. doi:10.1186/s12967-015-0614-x

Ghisa, M., Marinelli, C., Savarino, V., and Savarino, E. (2019). Idiopathic pulmonary fibrosis and GERD: Links and risks. *Ther. Clin. Risk Manag.* 15, 1081–1093. doi:10.2147/TCRM.S184291

Glassberg, M. K., Minkiewicz, J., Toonkel, R. L., Simonet, E. S., Rubio, G. A., DiFede, D., et al. (2017). Allogeneic human mesenchymal stem cells in patients with idiopathic pulmonary fibrosis via intravenous delivery (aether): A phase I safety clinical trial. *Chest* 151 (5), 971–981. doi:10.1016/j.chest.2016.10.061

Han, M., Song, Y., Liu, S., Lu, X., Su, L., Liu, M., et al. (2022). Engineering of stimulus-responsive pirfenidone liposomes for pulmonary delivery during treatment of idiopathic pulmonary fibrosis. *Front. Pharmacol.* 13, 882678. doi:10.3389/fphar.2022.882678

He, J., Du, Y., Li, G., Xiao, P., Sun, X., Song, W., et al. (2021b). Myeloid Fbxw7 prevents pulmonary fibrosis by suppressing TGF-β production. *Front. Immunol.* 12, 760138. doi:10.3389/fimmu.2021.760138

He, J., Li, X., and Yu, M. (2021a). Bioinformatics analysis identifies potential ferroptosis key genes in the pathogenesis of pulmonary fibrosis. *Front. Genet.* 12, 788417. doi:10.3389/fgene.2021.788417

Henry, E., Cores, J., Hensley, M. T., Anthony, S., Vandergriff, A., de Andrade, J. B. M., et al. (2015). Adult lung spheroid cells contain progenitor cells and mediate regeneration in rodents with bleomycin-induced pulmonary fibrosis. *Stem Cells Transl. Med.* 4 (11), 1265–1274. doi:10.5966/sctm.2015-0062

Hernandez, D. M., Kang, J. H., Choudhury, M., Andrianifahanana, M., Yin, X., Limper, A. H., et al. (2020). IPF pathogenesis is dependent upon TGFβ induction of IGF-1. *FASEB J.* 34 (4), 5363–5388. doi:10.1096/fj.201901719RR

Herrmann, F. E., Hesslinger, C., Wollin, L., and Nickolaus, P. (2022). BI 1015550 is a PDE4B inhibitor and a clinical drug candidate for the oral treatment of idiopathic pulmonary fibrosis. *Front. Pharmacol.* 13, 838449. doi:10.3389/fphar.2022.838449

Hilberg, F., Roth, G. J., Krssak, M., Kautschitsch, S., Sommergruber, W., Tontsch-Grunt, U., et al. (2008). BIBF 1120: Triple angiokinase inhibitor with sustained receptor blockade and good antitumor efficacy. *Cancer Res.* 68 (12), 4774–4782. doi:10.1158/0008-5472.CAN-07-6307

Inoue, Y., Kaner, R. J., Guiot, J., Maher, T. M., Tomassetti, S., Moiseev, S., et al. (2020). Diagnostic and prognostic biomarkers for chronic fibrosing interstitial lung diseases with a progressive phenotype. *Chest* 158 (2), 646–659. doi:10.1016/j.chest.2020.03.037

Jensen-Cody, S. O., and Potthoff, M. J. (2021). Hepatokines and metabolism: Deciphering communication from the liver. *Mol. Metab.* 44, 101138. doi:10.1016/j.molmet.2020.101138

Jiang, H., Zhang, J., Zhang, Z., Ren, S., and Zhang, C. (2015). Effect of transplanted adipose-derived stem cells in mice exhibiting idiopathic pulmonary fibrosis. *Mol. Med. Rep.* 12 (4), 5933–5938. doi:10.3892/mmr.2015.4178

Jiang, S., Xu, Z., Shi, Y., Liang, S., Jiang, X., Xiao, M., et al. (2023). Circulating insulin-like growth factor-1 and risk of lung diseases: A mendelian randomization analysis. *Front. Endocrinol.* 14, 1126397. doi:10.3389/fendo.2023.1126397

Kapnadak, S. G., and Raghu, G. (2021). Lung transplantation for interstitial lung disease. *Eur. Respir. Rev. Official J. Eur. Respir. Soc.* 30 (161), 210017. doi:10.1183/16000617.0017-2021

Kasam, R. K., Ghandikota, S., Soundararajan, D., Reddy, G. B., Huang, S. K., Jegga, A. G., et al. (2020). Inhibition of Aurora Kinase B attenuates fibroblast activation and pulmonary fibrosis. *EMBO Mol. Med.* 12 (9), e12131. doi:10.15252/emmm.202012131

Khan, F. A., Stewart, I., Saini, G., Robinson, K. A., and Jenkins, R. G. (2022). A systematic review of blood biomarkers with individual participant data meta-analysis of matrix metalloproteinase-7 in idiopathic pulmonary fibrosis. *Eur. Respir. J.* 59 (4), 2101612. doi:10.1183/13993003.01612-2021

Kheirollahi, V., Khadim, A., Kiliaris, G., Korfei, M., Barroso, M. M., Alexopoulos, I., et al. (2022). Transcriptional profiling of insulin-like growth factor signaling components in embryonic lung development and idiopathic pulmonary fibrosis. *J. Cells* 11 (12), 1973. doi:10.3390/cells11121973

Kheirollahi, V., Wasnick, R. M., Biasin, V., Vazquez-Armendariz, A. I., Chu, X., Moiseenko, A., et al. (2019). Metformin induces lipogenic differentiation in myofibroblasts to reverse lung fibrosis. *Nat. Commun.* 10 (1), 2987. doi:10.1038/s41467-019-10839-0

Kim, S. W., Lim, J. Y., Rhee, C. K., Kim, J. H., Park, C. K., Kim, T. J., et al. (2016). Effect of roflumilast, novel phosphodiesterase-4 inhibitor, on lung chronic graft-versus-host disease in mice. *Exp. Hematol.* 44 (5), 332–341. doi:10.1016/j.exphem.2016.02.002

King, C. S., and Nathan, S. D. (2017). Idiopathic pulmonary fibrosis: Effects and optimal management of comorbidities. *Lancet Respir. Med.* 5 (1), 72–84. doi:10.1016/S2213-2600(16)30222-3

King, T. E., Jr., Bradford, W. Z., Castro-Bernardini, S., Fagan, E. A., Glaspole, I., Glassberg, M. K., et al. (2014). A phase 3 trial of pirfenidone in patients with idiopathic pulmonary fibrosis. *N. Engl. J. Med.* 370 (22), 2083–2092. doi:10.1056/NEJMoa1402582

Kinoshita, T., and Goto, T. (2019). Molecular mechanisms of pulmonary fibrogenesis and its progression to lung cancer: A review. *Int. J. Mol. Sci.* 20 (6), 1461. doi:10.3390/ijms20061461

Kletukhina, S., Mutallapova, G., Titova, A., and Gomzikova, M. (2022). Role of mesenchymal stem cells and extracellular vesicles in idiopathic pulmonary fibrosis. *Int. J. Mol. Sci.* 23 (19), 11212. doi:10.3390/ijms231911212

Kumar, A., Cherian, S. V., Vassallo, R., Yi, E. S., and Ryu, J. H. (2018). Current concepts in pathogenesis, diagnosis, and management of smoking-related interstitial lung diseases. *Chest* 154 (2), 394–408. doi:10.1016/j.chest.2017.11.023

Lambers, C., Roth, M., Jaksch, P., Muraközy, G., Tamm, M., Klepetko, W., et al. (2018). Treprostinil inhibits proliferation and extracellular matrix deposition by fibroblasts through cAMP activation. *Sci. Rep.* 8 (1), 1087. doi:10.1038/s41598-018-19294-1

Lambert, E. L., Wuyts, W. A., Yserbyt, J., and De Sadeleer, L. J. (2021). Statins: Cause of fibrosis or the opposite? Effect of cardiovascular drugs in idiopathic pulmonary fibrosis [J]. *Respir. Med.* 176, 106259. doi:10.1016/j.rmed.2020.106259

Le, Y., Cao, W., Zhou, L., Fan, X., Liu, Q., Liu, F., et al. (2020). Infection of Mycobacterium tuberculosis promotes both M1/M2 polarization and MMP production in cigarette smoke-exposed macrophages. *Front. Immunol.*, 11. doi:10.3389/fimmu.2020.01902

Lee, C. M., Lee, D. H., Ahn, B. K., Hwang, J. J., Yoon, H., Shin, C. M., et al. (2016). Protective effect of proton pump inhibitor for survival in patients with gastroesophageal reflux disease and idiopathic pulmonary fibrosis. *J. Neurogastroenterol. Motil.* 22 (3), 444–451. doi:10.5056/jnm15192

Lee, J. S., Collard, H. R., Anstrom, K. J., Martinez, F. J., Noth, I., Roberts, R. S., et al. (2013). Anti-acid treatment and disease progression in idiopathic pulmonary fibrosis: An analysis of data from three randomised controlled trials. *Lancet Respir. Med.* 1 (5), 369–376. doi:10.1016/S2213-2600(13)70105-X

Lee, J. S., Ryu, J. H., Elicker, B. M., Lydell, C. P., Jones, K. D., Wolters, P. J., et al. (2011). Gastroesophageal reflux therapy is associated with longer survival in patients with idiopathic pulmonary fibrosis. *Am. J. Respir. Crit. Care Med.* 184 (12), 1390–1394. doi:10.1164/rccm.201101-0138OC

Liu, Y. N., Guan, Y., Shen, J., Jia, Y. L., Zhou, J. C., Sun, Y., et al. (2020). Shp2 positively regulates cigarette smoke-induced epithelial mesenchymal transition by mediating MMP-9 production. *Respir. Res.* 21 (1), 161. doi:10.1186/s12931-020-01426-9

Ma, H., Liu, S., Li, S., and Xia, Y. (2022). Targeting growth factor and cytokine pathways to treat idiopathic pulmonary fibrosis. *Front. Pharmacol.* 13, 918771. doi:10.3389/fphar.2022.918771

Mahalanobish, S., Saha, S., Dutta, S., and Sil, P. C. (2020). Matrix metalloproteinase: An upcoming therapeutic approach for idiopathic pulmonary fibrosis. *Pharmacol. Res.* 152, 104591. doi:10.1016/j.phrs.2019.104591

Martin-Medina, A., Lehmann, M., Burgy, O., Hermann, S., Baarsma, H. A., Wagner, D. E., et al. (2018). Increased extracellular vesicles mediate WNT5A signaling in idiopathic pulmonary fibrosis. *Am. J. Respir. Crit. Care Med.* 198 (12), 1527–1538. doi:10.1164/rccm.201708-1580OC

Mei, Q., Liu, Z., Zuo, H., Yang, Z., and Qu, J. (2021). Idiopathic pulmonary fibrosis: An update on pathogenesis. *Front. Pharmacol.* 12, 797292. doi:10.3389/fphar.2021.797292

Menou, A., Duitman, J., and Crestani, B. (2018). The impaired proteases and anti-proteases balance in Idiopathic Pulmonary Fibrosis. *Matrix Biol.* 68-69, 382–403. doi:10.1016/j.matbio.2018.03.001

Merkt, W., Bueno, M., Mora, A. L., and Lagares, D. (2020). Senotherapeutics: Targeting senescence in idiopathic pulmonary fibrosis. *Semin. Cell Dev. Biol.* 101, 104–110. doi:10.1016/j.semcdb.2019.12.008

Molina-Molina, M. (2019). The future of pharmacological treatment in idiopathic pulmonary fibrosis. *Arch. Bronconeumología (English Ed.* 55 (12), 642–647. doi:10.1016/j.arbres.2019.05.008

Molyneaux, P. L., Cox, M. J., Willis-Owen, S. A. G., Mallia, P., Russell, K. E., Russell, A. M., et al. (2014). The role of bacteria in the pathogenesis and progression of idiopathic pulmonary fibrosis. *Am. J. Respir. Crit. Care Med.* 190 (8), 906–913. doi:10.1164/rccm.201403-0541OC

Mostafaei, S., Sayad, B., Azar, M. E. F., Doroudian, M., Hadifar, S., Behrouzi, A., et al. (2021). The role of viral and bacterial infections in the pathogenesis of IPF: A systematic review and meta-analysis. *Respir. Res.* 22 (1), 53. doi:10.1186/s12931-021-01650-x

Naccache, J-M., Jouneau, S., Didier, M., Borie, R., Cachanado, M., Bourdin, A., et al. (2022). Cyclophosphamide added to glucocorticoids in acute exacerbation of idiopathic pulmonary fibrosis (EXAFIP): A randomised, double-blind, placebo-controlled, phase 3 trial. *Lancet Respir. Med.* 10 (1), 26–34. doi:10.1016/S2213-2600(21)00354-4

Nathan, S. D., Albera, C., Bradford, W. Z., Costabel, U., Glaspole, I., Glassberg, M. K., et al. (2017). Effect of pirfenidone on mortality: Pooled analyses and meta-analyses of clinical trials in idiopathic pulmonary fibrosis. *Lancet Respir. Med.* 5 (1), 33–41. doi:10.1016/S2213-2600(16)30326-5

Nathan, S. D., Behr, J., Cottin, V., Lancaster, L., Smith, P., Deng, C. Q., et al. (2022). Study design and rationale for the TETON phase 3, randomised, controlled clinical trials of inhaled treprostinil in the treatment of idiopathic pulmonary fibrosis. *BMJ Open Respir. Res.* 9 (1), e001310. doi:10.1136/bmjresp-2022-001310

Negrete-Garcia, M. C., de Jesus Ramos-Abundis, J., Alvarado-Vasquez, N., Montes-Martínez, E., Montaño, M., Ramos, C., et al. (2022). Exosomal micro-RNAs as intercellular communicators in idiopathic pulmonary fibrosis. *Int. J. Mol. Sci.* 23 (19), 11047. doi:10.3390/ijms231911047

Nelkine, L., Vrolijk, M. F., Drent, M., and Bast, A. (2020). Role of antioxidants in the treatment of gastroesophageal reflux disease-associated idiopathic pulmonary fibrosis. *Curr. Opin. Pulm. Med.* 26 (4), 363–371. doi:10.1097/MCP.0000000000000684

Nelson, C., Lee, J., Ko, K., Sikora, A. G., Bonnen, M. D., Enkhbaatar, P., et al. (2017). Therapeutic efficacy of esomeprazole in cotton smoke-induced lung injury model. *Front. Pharmacol.* 8, 16. doi:10.3389/fphar.2017.00016

Nguyen, X. X., Muhammad, L., Nietert, P. J., and Feghali-Bostwick, C. (2018). IGFBP-5 promotes fibrosis via increasing its own expression and that of other pro-fibrotic mediators. *Front. Endocrinol. (Lausanne)* 9, 601. doi:10.3389/fendo.2018.00601

Noble, P. W., Albera, C., Bradford, W. Z., Costabel, U., du Bois, R. M., Fagan, E. A., et al. (2016). Pirfenidone for idiopathic pulmonary fibrosis: Analysis of pooled data from three multinational phase 3 trials. *Eur. Respir. J.* 47 (1), 243–253. doi:10.1183/13993003.00026-2015

Nolte, M., and Margadant, C. (2020). Controlling immunity and inflammation through integrin-dependent regulation of TGF-β. *Trends Cell Biol.* 30 (1), 49–59. doi:10.1016/j.tcb.2019.10.002

Ntolios, P., Manoloudi, E., Tzouvelekis, A., Bouros, E., Steiropoulos, P., Anevlavis, S., et al. (2018). Longitudinal outcomes of patients enrolled in a phase Ib clinical trial of the adipose-derived stromal cells-stromal vascular fraction in idiopathic pulmonary fibrosis. *Clin. Respir. J.* 12 (6), 2084–2089. doi:10.1111/crj.12777

O'Dwyer, D. N., Ashley, S. L., Gurczynski, S. J., Xia, M., Wilke, C., Falkowski, N. R., et al. (2019). Lung microbiota contribute to pulmonary inflammation and disease progression in pulmonary fibrosis. *Am. J. Respir. Crit. Care Med.* 199 (9), 1127–1138. doi:10.1164/rccm.201809-1650OC

Olson, A. L., Gifford, A. H., Inase, N., Fernández Pérez, E. R., and Suda, T. (2018). The epidemiology of idiopathic pulmonary fibrosis and interstitial lung diseases at risk of a progressive-fibrosing phenotype. *Eur. Respir. Rev.* 27 (150), 180077. doi:10.1183/16000617.0077-2018

Pardo, A., and Selman, M. (2016). Lung fibroblasts, aging, and idiopathic pulmonary fibrosis. *Ann. Am. Thorac. Soc.* 13 (Suppl. 5), S417–S421. doi:10.1513/AnnalsATS.201605-341AW

Parimon, T., Yao, C., Habiel, D. M., Ge, L., Bora, S. A., Brauer, R., et al. (2019). Syndecan-1 promotes lung fibrosis by regulating epithelial reprogramming through extracellular vesicles. *JCI Insight* 5 (17), e129359. doi:10.1172/jci.insight.129359

Park, Y., Ahn, C., and Kim, T. H. (2021). Occupational and environmental risk factors of idiopathic pulmonary fibrosis: A systematic review and meta-analyses. *Sci. Rep.* 11 (1), 4318. doi:10.1038/s41598-021-81591-z

Pastor, L., Vera, E., Marin, J. M., and Sanz-Rubio, D. (2021). Extracellular vesicles from airway secretions: New insights in lung diseases. *Int. J. Mol. Sci.* 22 (2), 583. doi:10.3390/ijms22020583

Petnak, T., Lertjitbanjong, P., Thongprayoon, C., and Moua, T. (2021). Impact of antifibrotic therapy on mortality and acute exacerbation in idiopathic pulmonary fibrosis: A systematic review and meta-analysis. *Chest* 160 (5), 1751–1763. doi:10.1016/j.chest.2021.06.049

Phan, T. H. G., Paliogiannis, P., Nasrallah, G. K., Giordo, R., Eid, A. H., Fois, A. G., et al. (2021). Emerging cellular and molecular determinants of idiopathic pulmonary fibrosis. *Cell Mol. Life Sci.* 78 (5), 2031–2057. doi:10.1007/s00018-020-03693-7

Plantier, L., Cazes, A., Dinh-Xuan, A. T., Bancal, C., Marchand-Adam, S., and Crestani, B. (2018). Physiology of the lung in idiopathic pulmonary fibrosis. *Eur. Respir. Rev.* 27 (147), 170062. doi:10.1183/16000617.0062-2017

Probst, C. K., Montesi, S. B., Medoff, B. D., Shea, B. S., and Knipe, R. S. (2020). Vascular permeability in the fibrotic lung. *Eur. Respir. J.* 56 (1), 1900100. doi:10.1183/13993003.00100-2019

Qian, W., Cai, X., Qian, Q., and Zhang, X. (2021). Identification and validation of potential biomarkers and pathways for idiopathic pulmonary fibrosis by comprehensive bioinformatics analysis. *Biomed. Res. Int.* 2021, 5545312. doi:10.1155/2021/5545312

Raghu, G., Amatto, V. C., Behr, J., and Stowasser, S. (2015). Comorbidities in idiopathic pulmonary fibrosis patients: A systematic literature review. *Eur. Respir. J.* 46 (4), 1113–1130. doi:10.1183/13993003.02316-2014

Raghu, G., Remy-Jardin, M., Myers, J. L., Richeldi, L., Ryerson, C. J., Lederer, D. J., et al. (2018). Diagnosis of idiopathic pulmonary fibrosis. An official ATS/ERS/JRS/ALAT clinical practice guideline. *Am. J. Respir. Crit. Care Med.* 198 (5), e44–e68. doi:10.1164/rccm.201807-1255ST

Raghu, G., Scholand, M. B., de Andrade, J., Lancaster, L., Mageto, Y., Goldin, J., et al. (2016). FG-3019 anti-connective tissue growth factor monoclonal antibody: Results of an open-label clinical trial in idiopathic pulmonary fibrosis. *Eur. Respir. J.* 47 (5), 1481–1491. doi:10.1183/13993003.01030-2015

Ramazani, Y., Knops, N., Elmonem, M. A., Nguyen, T. Q., Arcolino, F. O., van den Heuvel, L., et al. (2018). Connective tissue growth factor (CTGF) from basics to clinics. *Matrix Biol.* 68-69, 44–66. doi:10.1016/j.matbio.2018.03.007

Rana, T., Jiang, C., Liu, G., Miyata, T., Antony, V., Thannickal, V. J., et al. (2020). PAI-1 regulation of TGF-β1-induced alveolar type II cell senescence, SASP secretion, and SASP-mediated activation of alveolar macrophages. *Am. J. Respir. Cell Mol. Biol.* 62 (3), 319–330. doi:10.1165/rcmb.2019-0071OC

Rangarajan, S., Bone, N. B., Zmijewska, A. A., Jiang, S., Park, D. W., Bernard, K., et al. (2018). Metformin reverses established lung fibrosis in a bleomycin model. *Nat. Med.* 24 (8), 1121–1127. doi:10.1038/s41591-018-0087-6

Rasaei, R., Tyagi, A., Rasaei, S., Lee, S. J., Yang, S. R., Kim, K. S., et al. (2022). Human pluripotent stem cell-derived macrophages and macrophage-derived exosomes: Therapeutic potential in pulmonary fibrosis. *Stem Cell Res. Ther.* 13 (1), 433. doi:10.1186/s13287-022-03136-z

Renaud, L., da Silveira, W. A., Takamura, N., Hardiman, G., and Feghali-Bostwick, C. (2020). Prominence of IL6, IGF, TLR, and bioenergetics pathway perturbation in lung tissues of scleroderma patients with pulmonary fibrosis. *Front. Immunol.* 11, 383. doi:10.3389/fimmu.2020.00383

Reynolds, C. J., Del Greco, M. F., Allen, R. J., Flores, C., Jenkins, R. G., Maher, T. M., et al. (2023). The causal relationship between gastro-oesophageal reflux disease and idiopathic pulmonary fibrosis: A bidirectional two-sample mendelian randomisation study. *Eur. Respir. J.* 61 (5), 2201585. doi:10.1183/13993003.01585-2022

Richeldi, L., Azuma, A., Cottin, V., Hesslinger, C., Stowasser, S., Valenzuela, C., et al. (2022). Trial of a preferential phosphodiesterase 4B inhibitor for idiopathic pulmonary fibrosis. *N. Engl. J. Med.* 386 (23), 2178–2187. doi:10.1056/NEJMoa2201737

Richeldi, L., du Bois, R. M., Raghu, G., Azuma, A., Brown, K. K., Costabel, U., et al. (2014). Efficacy and safety of nintedanib in idiopathic pulmonary fibrosis. *N. Engl. J. Med.* 370 (22), 2071–2082. doi:10.1056/NEJMoa1402584

Richeldi, L., Fernandez Perez, E. R., Costabel, U., Albera, C., Lederer, D. J., Flaherty, K. R., et al. (2020). Pamrevlumab, an anti-connective tissue growth factor therapy, for idiopathic pulmonary fibrosis (PRAISE): A phase 2, randomised, double-blind, placebo-controlled trial. *Lancet Respir. Med.* 8 (1), 25–33. doi:10.1016/S2213-2600(19)30262-0

Roque, W., Boni, A., Martinez-Manzano, J., and Romero, F. (2020b). A tale of two proteolytic machines: Matrix metalloproteinases and the ubiquitin-proteasome system in pulmonary fibrosis. *Int. J. Mol. Sci.* 21 (11), 3878. doi:10.3390/ijms21113878

Roque, W., Cuevas-Mora, K., and Romero, F. (2020a). Mitochondrial quality control in age-related pulmonary fibrosis. *Int. J. Mol. Sci.* 21 (2), 643. doi:10.3390/ijms21020643

Ryu, J. H., Moua, T., Daniels, C. E., Hartman, T. E., Yi, E. S., Utz, J. P., et al. (2014). Idiopathic pulmonary fibrosis: Evolving concepts. *Mayo Clin. Proc.* 89 (8), 1130–1142. doi:10.1016/j.mayocp.2014.03.016

Sack, C., and Raghu, G. (2019). Idiopathic pulmonary fibrosis: Unmasking cryptogenic environmental factors. *Eur. Respir. J.* 53 (2), 1801699. doi:10.1183/13993003.01699-2018

Saito, S., Alkhatib, A., Kolls, J. K., Kondoh, Y., and Lasky, J. A. (2019). Pharmacotherapy and adjunctive treatment for idiopathic pulmonary fibrosis (IPF). *J. Thorac. Dis.* 11 (Suppl. 14), S1740–S1754. doi:10.21037/jtd.2019.04.62

Sato, N., Takasaka, N., Yoshida, M., Tsubouchi, K., Minagawa, S., Araya, J., et al. (2016). Metformin attenuates lung fibrosis development via NOX4 suppression. *Respir. Res.* 17 (1), 107. doi:10.1186/s12931-016-0420-x

Schafer, M. J., White, T. A., Iijima, K., Haak, A. J., Ligresti, G., Atkinson, E. J., et al. (2017). Cellular senescence mediates fibrotic pulmonary disease. *Nat. Commun.* 8, 14532. doi:10.1038/ncomms14532

Seibold, J. R., Maher, T. M., Highland, K. B., Assassi, S., Azuma, A., Hummers, L. K., et al. (2020). Safety and tolerability of nintedanib in patients with systemic sclerosis-associated interstitial lung disease: Data from the SENSCIS trial. *Ann. Rheum. Dis.* 79 (11), 1478–1484. doi:10.1136/annrheumdis-2020-217331

Selman, M., Martinez, F. J., and Pardo, A. (2019). Why does an aging smoker's lung develop idiopathic pulmonary fibrosis and not chronic obstructive pulmonary disease? *[J]. Am. J. Respir. Crit. Care Med.* 199 (3), 279–285. doi:10.1164/rccm.201806-1166PP

Sgalla, G., Flore, M., Siciliano, M., and Richeldi, L. (2020b). Antibody-based therapies for idiopathic pulmonary fibrosis. *Expert Opin. Biol. Ther.* 20 (7), 779–786. doi:10.1080/14712598.2020.1735346

Sgalla, G., Franciosa, C., Simonetti, J., and Richeldi, L. (2020a). Pamrevlumab for the treatment of idiopathic pulmonary fibrosis. *Expert Opin. Investig. Drugs* 29 (8), 771–777. doi:10.1080/13543784.2020.1773790

Sgalla, G., Iovene, B., Calvello, M., Ori, M., Varone, F., and Richeldi, L. (2018). Idiopathic pulmonary fibrosis: Pathogenesis and management. *Respir. Res.* 19 (1), 32. doi:10.1186/s12931-018-0730-2

Sgalla, G., Simonetti, J., Cortese, S., and Richeldi, L. (2023). BI 1015550: An investigational phosphodiesterase 4B (PDE4B) inhibitor for lung function decline in idiopathic pulmonary fibrosis (IPF). *Expert Opin. Investigational Drugs* 32 (1), 17–23. doi:10.1080/13543784.2023.2173061

Shenderov, K., Collins, S. L., Powell, J. D., and Horton, M. R. (2021). Immune dysregulation as a driver of idiopathic pulmonary fibrosis. *J. Clin. Invest.* 131 (2), e143226. doi:10.1172/JCI143226

Shimbori, C., Upagupta, C., Bellaye, P-S., Ayaub, E. A., Sato, S., Yanagihara, T., et al. (2019). Mechanical stress-induced mast cell degranulation activates TGF-β1 signalling pathway in pulmonary fibrosis. *Thorax* 74 (5), 455–465. doi:10.1136/thoraxjnl-2018-211516

Spagnolo, P., Molyneaux, P. L., Bernardinello, N., Cocconcelli, E., Biondini, D., Fracasso, F., et al. (2019). The role of the lung's microbiome in the pathogenesis and progression of idiopathic pulmonary fibrosis. *Int. J. Mol. Sci.* 20 (22), 5618. doi:10.3390/ijms20225618

Stainer, A., Faverio, P., Busnelli, S., Catalano, M., Della Zoppa, M., Marruchella, A., et al. (2021). Molecular biomarkers in idiopathic pulmonary fibrosis: State of the art and future directions. *Int. J. Mol. Sci.* 22 (12), 6255. doi:10.3390/ijms22126255

Stuart, B. D., Lee, J. S., Kozlitina, J., Noth, I., Devine, M. S., Glazer, C. S., et al. (2014). Effect of telomere length on survival in patients with idiopathic pulmonary fibrosis: An observational cohort study with independent validation. *Lancet Respir. Med.* 2 (7), 557–565. doi:10.1016/S2213-2600(14)70124-9

Sun, W., Jing, X., Yang, X., Huang, H., Luo, Q., Xia, S., et al. (2021). Regulation of the IGF1 signaling pathway is involved in idiopathic pulmonary fibrosis induced by alveolar epithelial cell senescence and core fucosylation. *J. Aging (Albany NY)* 13 (14), 18852–18869. doi:10.18632/aging.203335

Surolia, R., Li, F. J., Wang, Z., Li, H., Liu, G., Zhou, Y., et al. (2017). 3D pulmospheres serve as a personalized and predictive multicellular model for assessment of antifibrotic drugs. *JCI Insight* 2 (2), e91377. doi:10.1172/jci.insight.91377

Tanaka, K. I., Shimoda, M., Sugizaki, T., Ikeda, M., Takafuji, A., Kawahara, M., et al. (2022). Therapeutic effects of eperisone on pulmonary fibrosis via preferential suppression of fibroblast activity. *Cell Death Discov.* 8 (1), 52. doi:10.1038/s41420-022-00851-7

Teague, T. T., Payne, S. R., Kelly, B. T., Dempsey, T. M., McCoy, R. G., Sangaralingham, L. R., et al. (2022). Evaluation for clinical benefit of metformin in patients with idiopathic pulmonary fibrosis and type 2 diabetes mellitus: A national claims-based cohort analysis. *Respir. Res.* 23 (1), 91. doi:10.1186/s12931-022-02001-0

Todd, J. L., Vinisko, R., Liu, Y., Neely, M. L., Overton, R., Flaherty, K. R., et al. (2020). Circulating matrix metalloproteinases and tissue metalloproteinase inhibitors in patients with idiopathic pulmonary fibrosis in the multicenter IPF-PRO Registry cohort. *BMC Pulm. Med.* 20 (1), 64. doi:10.1186/s12890-020-1103-4

Tran, T., Assayag, D., Ernst, P., and Suissa, S. (2021). Effectiveness of proton pump inhibitors in idiopathic pulmonary fibrosis: A population-based cohort study. *Chest* 159 (2), 673–682. doi:10.1016/j.chest.2020.08.2080

Tran, T., and Suissa, S. (2021). Comparing new-user cohort designs: The example of proton pump inhibitor effectiveness in idiopathic pulmonary fibrosis. *Am. J. Epidemiol.* 190 (5), 928–938. doi:10.1093/aje/kwaa242

Ungvari, Z., Valcarcel-Ares, M. N., Tarantini, S., Yabluchanskiy, A., Fülöp, G. A., Kiss, T., et al. (2017). Connective tissue growth factor (CTGF) in age-related vascular pathologies. *Geroscience* 39 (5-6), 491–498. doi:10.1007/s11357-017-9995-5

Valapour, M., Lehr, C. J., Skeans, M. A., Smith, J. M., Miller, E., Goff, R., et al. (2021). OPTN/SRTR 2019 annual data report: Lung. *Am. J. Transplant. Official J. Am. Soc. Transplant. Am. Soc. Transpl. Surg.* 21 (Suppl. 2), 441–520. doi:10.1111/ajt.16495

Vancheri, C., Kreuter, M., Richeldi, L., Ryerson, C. J., Valeyre, D., Grutters, J. C., et al. (2018). Nintedanib with add-on pirfenidone in idiopathic pulmonary fibrosis. Results of the INJOURNEY trial. *Am. J. Respir. Crit. Care Med.* 197 (3), 356–363. doi:10.1164/rccm.201706-1301OC

Veit, T., Leuschner, G., Sisic, A., Ceelen, F., Munker, D., Schmitzer, M., et al. (2019). Pirfenidone exerts beneficial effects in patients with IPF undergoing single lung transplantation. *Am. J. Transpl.* 19 (8), 2358–2365. doi:10.1111/ajt.15378

Walter, N., Collard, H. R., and King, T. E., Jr (2006). Current perspectives on the treatment of idiopathic pulmonary fibrosis. *Proc. Am. Thorac. Soc.* 3 (4), 330–338. doi:10.1513/pats.200602-016TK

Walters, G. I. (2020). Occupational exposures and idiopathic pulmonary fibrosis. *Curr. Opin. Allergy Clin. Immunol.* 20 (2), 103–111. doi:10.1097/ACI.0000000000000610

Wang, J., Hu, K., Cai, X., Yang, B., He, Q., et al. (2022). Targeting PI3K/AKT signaling for treatment of idiopathic pulmonary fibrosis. *Acta Pharm. Sin. B* 12 (1), 18–32. doi:10.1016/j.apsb.2021.07.023

Wells, A. U., Brown, K. K., Flaherty, K. R., Kolb, M., and Thannickal, V. J.IPF Consensus Working Group (2018). What's in a name? That which we call IPF, by any other name would act the same [J]. *Eur. Respir. J.* 51 (5), 1800692. doi:10.1183/13993003.00692-2018

Wind, S., Schmid, U., Freiwald, M., Marzin, K., Lotz, R., Ebner, T., et al. (2019). Clinical pharmacokinetics and pharmacodynamics of nintedanib. *Clin. Pharmacokinet.* 58 (9), 1131–1147. doi:10.1007/s40262-019-00766-0

Wollin, L., Wex, E., Pautsch, A., Schnapp, G., Hostettler, K. E., Stowasser, S., et al. (2015). Mode of action of nintedanib in the treatment of idiopathic pulmonary fibrosis. *Eur. Respir. J.* 45 (5), 1434–1445. doi:10.1183/09031936.00174914

Wolters, P. J., Blackwell, T. S., Eickelberg, O., Loyd, J. E., Kaminski, N., Jenkins, G., et al. (2018). Time for a change: Is idiopathic pulmonary fibrosis still idiopathic and only fibrotic? [J]. *Lancet Respir. Med.* 6 (2), 154–160. doi:10.1016/S2213-2600(18)30007-9

Xiao, H., Huang, X., Wang, S., Liu, Z., Dong, R., Song, D., et al. (2020). Metformin ameliorates bleomycin-induced pulmonary fibrosis in mice by suppressing IGF-1. *Am. J. Transl. Res.* 12 (3), 940–949.

Yamazoe, M., and Tomioka, H. (2018). Acute exacerbation of idiopathic pulmonary fibrosis: A 10-year single-centre retrospective study. *BMJ Open Respir. Res.* 5 (1), e000342. doi:10.1136/bmjresp-2018-000342

Yanagihara, T., Tsubouchi, K., Gholiof, M., Chong, S. G., Lipson, K. E., Zhou, Q., et al. (2022). Connective-tissue growth factor contributes to TGF-β1-induced lung fibrosis. *Am. J. Respir. Cell Mol. Biol.* 66 (3), 260–270. doi:10.1165/rcmb.2020-0504OC

Yang, D., Chen, X., Wang, J., Lou, Q., Lou, Y., Li, L., et al. (2019). Dysregulated lung commensal bacteria drive interleukin-17B production to promote pulmonary fibrosis through their outer membrane vesicles. *Immunity* 50 (3), 692–706. doi:10.1016/j.immuni.2019.02.001

Yang, S., Liu, P., Gao, T., Song, D., Zhao, X., Li, Y., et al. (2022b). Every road leads to rome: Therapeutic effect and mechanism of the extracellular vesicles of human embryonic stem cell-derived immune and matrix regulatory cells administered to mouse models of pulmonary fibrosis through different routes. *Stem Cell Res. Ther.* 13 (1), 163. doi:10.1186/s13287-022-02839-7

Yang, Y., Liu, Y., Chai, Y., Liu, K., Hu, W., Zhao, K., et al. (2022a). Exosomes in pathogenesis, diagnosis, and treatment of pulmonary fibrosis. *Front. Pharmacol.* 13, 927653. doi:10.3389/fphar.2022.927653

Ye, Z., and Hu, Y. (2021). TGF-β1: Gentlemanly orchestrator in idiopathic pulmonary fibrosis (Review). *Int. J. Mol. Med.* 48 (1), 132. doi:10.3892/ijmm.2021.4965

Zhang, A., Zou, Y., Xu, Q., Tian, S., Wang, J., Li, Y., et al. (2022). Investigation of the pharmacological effect and mechanism of jinbei oral liquid in the treatment of idiopathic pulmonary fibrosis using network Pharmacology and experimental validation. *Front. Pharmacol.* 13, 919388. doi:10.3389/fphar.2022.919388

Zhang, C., Yin, X., Zhang, J., Ao, Q., Gu, Y., and Liu, Y. (2017). Clinical observation of umbilical cord mesenchymal stem cell treatment of severe idiopathic pulmonary fibrosis: A case report. *Exp. Ther. Med.* 13 (5), 1922–1926. doi:10.3892/etm.2017.4222

Zhang, Y., Huang, W., Zheng, Z., Wang, W., Yuan, Y., Hong, Q., et al. (2021). Cigarette smoke-inactivated SIRT1 promotes autophagy-dependent senescence of alveolar epithelial type 2 cells to induce pulmonary fibrosis. *Free Radic. Biol. Med.* 166, 116–127. doi:10.1016/j.freeradbiomed.2021.02.013

Frontiers in Pharmacology

Explores the interactions between chemicals and living beings

The most cited journal in its field, which advances access to pharmacological discoveries to prevent and treat human disease.

Discover the latest Research Topics

See more →

Frontiers

Avenue du Tribunal-Fédéral 34
1005 Lausanne, Switzerland
frontiersin.org

Contact us

+41 (0)21 510 17 00
frontiersin.org/about/contact